

PURDUE UNIVERSITY
GRADUATE SCHOOL
Thesis/Dissertation Acceptance

This is to certify that the thesis/dissertation prepared

By Garrison L. Birch

Entitled
LIPIDOMIC PROFILING OF DICTYOSTELIUM DISCOIDEUM

For the degree of Master of Science

Is approved by the final examining committee:

Robert E. Minto

Chair

Brenda J. Blacklock

Michael J. McLeish

To the best of my knowledge and as understood by the student in the *Research Integrity and Copyright Disclaimer (Graduate School Form 20)*, this thesis/dissertation adheres to the provisions of Purdue University's "Policy on Integrity in Research" and the use of copyrighted material.

Approved by Major Professor(s): Robert E. Minto

Approved by: Martin J. O'Donnell

Head of the Graduate Program

11/14/2011

Date

**PURDUE UNIVERSITY
GRADUATE SCHOOL**

Research Integrity and Copyright Disclaimer

Title of Thesis/Dissertation:

LIPIDOMIC PROFILING OF DICTYOSTELIUM DISCOIDEUM

For the degree of Master of Science

I certify that in the preparation of this thesis, I have observed the provisions of *Purdue University Executive Memorandum No. C-22, September 6, 1991, Policy on Integrity in Research*.*

Further, I certify that this work is free of plagiarism and all materials appearing in this thesis/dissertation have been properly quoted and attributed.

I certify that all copyrighted material incorporated into this thesis/dissertation is in compliance with the United States' copyright law and that I have received written permission from the copyright owners for my use of their work, which is beyond the scope of the law. I agree to indemnify and save harmless Purdue University from any and all claims that may be asserted or that may arise from any copyright violation.

Garrison L. Birch

Printed Name and Signature of Candidate

11/14/2011

Date (month/day/year)

*Located at http://www.purdue.edu/policies/pages/teach_res_outreach/c_22.html

LIPIDOMIC PROFILING OF *DICTYOSTELIUM DISCOIDEUM*

A Thesis

Submitted to the Faculty

of

Purdue University

by

Garrison L. Birch

In Partial Fulfillment of the

Requirements for the Degree

of

Master of Science

December 2011

Purdue University

Indianapolis, Indiana

ACKNOWLEDGMENTS

I am very grateful to the many people that encouraged and helped me along the journey of pursuing this degree. I would especially like to thank my advisor Dr. Brenda Blacklock for her wisdom and guidance. I also had the great pleasure of working with Dr. Robert Minto, who allowed me to collaborate on his research and gave me sound advice and support throughout my graduate career. I would also like to thank my committee members for their willingness to see me through this challenging process. Dr. Karl Dria and Mr. Cary Pritchard have been invaluable assets throughout my career. I would like to thank my lab co-workers, and particularly Michael Shepard, for their help, advice, and friendship.

TABLE OF CONTENTS

	Page
LIST OF TABLES	v
LIST OF FIGURES	vi
LIST OF ABBREVIATIONS	x
ABSTRACT	xiii
CHAPTER 1. INTRODUCTION	1
1.1. Fatty acid elongation and <i>Dictyostelium discoideum</i>	1
1.2. Fatty acid biosynthesis and degradation	6
1.2.1. Fatty Acid Biosynthesis	7
1.2.2. Fatty Acid Degradation	11
1.3. Sphingolipids.....	14
1.3.1. Sphingolipid Biosynthesis.....	17
CHAPTER 2. FATTY ACID PROFILING OF <i>DICTYOSTELIUM</i> <i>DISCOIDEUM</i>	22
2.1. Introduction	22
2.2. Methods and materials.....	23
2.2.1. Maintenance and growth of <i>Dictyostelium discoideum</i>	24
2.2.2. Preparation and Analysis of Derivatives	24
2.3. Results and discussion	26
2.3.1. Synthesis of authentic fatty acid standards	26
2.3.2. The fatty acid profile of <i>D. discoideum</i>	31
CHAPTER 3. FATTY ACID METABOLISM IN <i>DICTYOSTELIUM</i> <i>DISCOIDEUM</i>	41
3.1. Introduction	41
3.2. Methods and materials.....	43
3.2.1. Calculation of incorporation levels	43
3.2.2. Statistical analysis	45
3.3. Results and discussion	46
3.3.1. Synthesis of deuterium-labeled fatty acids	46
3.3.2. <i>In vivo</i> feeding studies	52

	Page
CHAPTER 4. SPHINGOLIPID CHARACTERIZATION IN <i>DICTYOSTELIUM DISCOIDEUM</i>	74
4.1. Introduction	74
4.2. Methods and materials	74
4.2.1. Culturing of <i>D. discoideum</i> and <i>S. cerevisiae</i>	75
4.2.2. Ba(OH) ₂ hydrolysis	75
4.2.3. Dinitrophenyl derivatization of LCBs.....	76
4.2.4. Total lipid extraction.....	76
4.2.5. Mild alkaline hydrolysis.....	77
4.2.6. Lithiation of sphingolipids	77
4.2.7. LC-MS analysis of lipids	78
4.3. Results and discussion	82
4.3.1. Identification of sphingolipid long chain bases in <i>D. discoideum</i>	82
4.3.2. Isolation of sphingolipids for characterization	93
4.3.3. Sphingolipid characterization for <i>D. discoideum</i>	98
4.3.4. Closing Remarks	113
 CHAPTER 5. EXPERIMENTAL DETAILS OF THE SYNTHESIS OF FATTY ACIDS	 115
5.1. General experimental information	115
5.2. Synthetic standards for characterization of fatty acid profile	116
5.2.1. Synthesis of 18:2 ^{5,9} (35)	116
5.3. Production of ² H-labeled fatty acids for <i>in vivo</i> studies.....	122
5.3.1. Synthesis of stearic acid-17,17,18,18,18- <i>d</i> ₅ (49).....	123
5.3.2. Synthesis of stearic acid-3,3,4,4- <i>d</i> ₄ (55).....	127
5.3.3. Synthesis of octadec-5-enoic acid-16,16,17,17,18,18,18- <i>d</i> ₇ (74)	131
5.3.4. Synthesis of octadec-11-enoic acid-16,16,17,17,18,18,18- <i>d</i> ₇ (81) ..	137
5.4. Synthesis of ² H-labeled fatty acid stereoisomers	140
 REFERENCES	 152
 APPENDIX	 163

LIST OF TABLES

Table	Page
Table 1. Summary of alkylations and the resulting products.	29
Table 2. GC-MS retention time comparison of methyl ester and pyrrolidine-derivatized synthetic standards to the FAs found in <i>D. discoideum</i>	32
Table 3. Optimizer defined conditions for MRM.....	80
Table 4. Three long chain bases quantified by MRM as free LCBs.....	88
Table 5. The sphingolipids of <i>D. discoideum</i>	114

LIST OF FIGURES

Figure	Page
Figure 1. Relevant lipid structures; a monounsaturated C ₁₈ fatty acid, a phospholipid, and the sphingolipids sphingosine-1-phosphate, ceramide, and glycosylceramide.....	2
Figure 2. The positioning of <i>D. discoideum</i> on the eukaryotic phylogenetic tree	3
Figure 3. Composite electron micrograph of the developmental stages of <i>D. discoideum</i> upon starvation.....	4
Figure 4. The synthesis of saturated fatty acids in plants and mammals.....	8
Figure 5. The primary fatty acid elongation pathway of eukaryotes.....	9
Figure 6. Desaturation of stearoyl-CoA	10
Figure 7. Examples of β -oxidation for saturated and unsaturated fatty acids	12
Figure 8. α -Oxidation of a β -substituted fatty acid	14
Figure 9. The most commonly observed sphingolipid long chain bases in plants, animals, and yeast	15
Figure 10. The biosynthesis of long chain bases and ceramides	18
Figure 11. The building blocks of ceramide, ceramide-1-phosphate, glycosylceramide, and inositolphosphoryl ceramide complex sphingolipids.....	20
Figure 12. Common GSL carbohydrate head groups	21
Figure 13. The mass spectrum of the pyrrolidine derivative of 18:2 ^{5c,11c}	23
Figure 14. The GC oven methods for FAME and FAPY analysis	25
Figure 15. Generic fatty acid reaction scheme	26
Figure 16. The synthesis of dioxolanes 3 and 6	28
Figure 17. The intermediary diacetylenes 7 , 8 and 9	29
Figure 18. Synthesis of specialized fatty acids	31
Figure 19. The TIC of the FAMES of <i>D. discoideum</i>	32
Figure 20. The investigative power of FAPYs in fragmentation-based analysis: contrasting 18:2 ^{5,11} (left) and 18:2 ^{7,11} (right).....	33
Figure 21. The percent composition of fatty acids of <i>D. discoideum</i>	34
Figure 22. The mass spectrum of the TMS derivative of 2-hydroxy eicosanoic acid (<i>h</i> 20:0) from <i>Dictyostelium</i>	35
Figure 23. The mass spectrum of the unknown species of <i>D. discoideum</i>	36
Figure 24. The mass spectrum of the unknown species with CD ₃ OD reacting solvent	37
Figure 25. The 16:0 acetal fragments.....	37

Figure	Page
Figure 26. The mechanisms of FAME and acetal formation.....	38
Figure 27. Example of an ether lipid	39
Figure 28. The mechanism of aldehyde release from a vinyl ether	39
Figure 29. The hypothetical fatty acid metabolic pathway for <i>D. discoideum</i>	42
Figure 30. The synthetic pathway for producing stearic acid- d_5 (49) and palmitic acid- d_5 (50)	46
Figure 31. The synthetic scheme of stearic acid-[3,3,4,4- d_4] (55).....	47
Figure 32. Mass spectrum of the 18:0- d_4 (55) FAME derivative using 10% palladium on carbon and D_2 for alkyne reduction; $[M^+]$ m/z 302	48
Figure 33. Mass spectrum of the 18:0- d_4 (55) FAME derivative using Wilkinson's catalyst and D_2 for alkyne reduction; $[M^+]$ m/z 302	49
Figure 34. The synthetic approach utilized to afford 18:1 ⁵ - d_7	51
Figure 35. The synthetic methodology for producing 18:1 ¹¹ - d_7	51
Figure 36. The total ion chromatogram (A) from supplementation with 18:0- d_5 and the mass spectrum of the resulting 16:0 FAME product (B).....	53
Figure 37. Time course of the percent incorporation of d_5 label into FA products after supplementation with 18:0- d_5 and 1% NP-40.	55
Figure 38. The mass spectrum of 16:1 ⁹ - d_5 FAPY	57
Figure 39. The percent composition of all d_5 -labeled fatty acids observed upon supplementation with 18:0- d_5	59
Figure 40. Time course of the percent incorporation of d_5 label into FA products after supplementation with 16:0- d_5 and 1% NP-40	61
Figure 41. The percent composition of all d_5 -labeled fatty acids observed upon supplementation with 16:0- d_5	63
Figure 42. The potential products of stearate- d_4 metabolism	64
Figure 43. The loss of deuterium during β -oxidation of stearate- d_4	65
Figure 44. The total ion chromatogram (A) from 24 h-supplementation with 18:0- d_4 and the mass spectrum of the 18:2 ^{5,11} FAME product (B).....	66
Figure 45. Time course of the percent incorporation of d_4 -label into FA products after supplementation with 18:0- d_4 and 1% NP-40	67
Figure 46. Mass spectrum of a background compound sharing the molecular weight of the 16:0- d_4 product (m/z 274)	68
Figure 47. Time course of the percent incorporation of d_2 -label into FA products after supplementation with 18:0- d_4 and 1% NP-40	69
Figure 48. The cell growth curves of the 16:0- d_5 , 18:0- d_5 , 18:0- d_4 , and control (NP-40) cultures during time courses.....	70
Figure 49. The summarized metabolic processes that yield the observed fatty acid profile in <i>D. discoideum</i>	72
Figure 50. Hydrolysis of <i>N</i> -acyl lipids with $Ba(OH)_2$	83
Figure 51. The psychosine formation from $Ba(OH)_2$ hydrolysis of a C_{12} GlcCer standard performed in replicate under identical conditions	84

Figure	Page
Figure 52. HPLC-UV chromatograms of DNP-derivatized LCB standards and biological samples	85
Figure 53. The structural fragmentation of the phytosphingosine backbone upon CID	87
Figure 54. Fragmentation patterns of additional <i>D. discoideum</i> long chain bases from Ba(OH) ₂ hydrolysate	89
Figure 55. The exact masses of long chain bases obtained via a quadrupole time-of-flight mass spectrometer	90
Figure 56. The percent composition of LCBs	91
Figure 57. Approach to obtaining and isolating complex lipids from cells	93
Figure 58. Efficiency of optimized total lipid extraction procedure, as illustrated with SL standards	95
Figure 59. The complex lipids of <i>S. cerevisiae</i> following total lipid extraction (A) and sphingolipids following methylamine hydrolysis (B)	96
Figure 60. Examples of the IPC and MIPC SLs in <i>S. cerevisiae</i>	97
Figure 61. The fragments resulting from CID at 50 eV of a prominent inositolphosphorylceramide (<i>m/z</i> 952.7) in yeast.....	98
Figure 62. MS2 scan of the <i>D. discoideum</i> total lipid extract (phospholipids).....	99
Figure 63. The collision-induced dissociation spectrum of 34:4 PC via tandem mass spectrometry	99
Figure 64. Mass spectrum of the enriched sphingolipid sample of <i>D. discoideum</i> following methylamine hydrolysis of phospholipids ..	100
Figure 65. The total ion chromatogram (A) from FAME analysis of a mild alkaline hydrolysate and the mass spectrum of an 18:2 ^{5,11} methyl amide (B).....	101
Figure 66. TIC of FAME analysis of a mild alkaline hydrolysate following hexane wash	102
Figure 67. TIC of TMS-FAME analysis of a mild alkaline hydrolysate following hexane wash.....	103
Figure 68. The CID mass spectrum of probable ceramide-1-phosphates in <i>D. discoideum</i> ; [M-H ⁺] <i>m/z</i> 698 (A) and <i>m/z</i> 700 (B)	104
Figure 69. The proposed structures of the ceramide-1-phosphates of <i>Dictyostelium</i> ; [M-H ⁺] <i>m/z</i> 698 and <i>m/z</i> 700.....	105
Figure 70. Collision-induced dissociation of <i>d</i> 18:1/16:0 ceramide-1-phosphate standard	106
Figure 71. The mass fragmentation of most prominent IPC sphingolipid of <i>D. discoideum</i> ; [M-H ⁺] <i>m/z</i> 868	107
Figure 72. <i>t</i> 18:0/ <i>h</i> 20:0 IPC, the most prominent inositolphosphoryl ceramide of <i>D. discoideum</i>	108
Figure 73. The CID mass spectrum of a sphingolipid of <i>D. discoideum</i> [M-H ⁺] <i>m/z</i> 1064.....	109
Figure 74. The CID mass spectrum of an MIPC from yeast; [M-H ⁺] <i>m/z</i> 1064.....	109

Figure	Page
Figure 75. The proposed structure for the sphingolipid of <i>D. discoideum</i> ; [M-H ⁺] <i>m/z</i> 1064.....	111
Figure 76. The CID mass spectrum of a sphingolipid of <i>D. discoideum</i> ; [M-H ⁺] <i>m/z</i> 1328.....	112
Figure 77. The abbreviated synthesis of 18:2 ^{9c,15c} and 18:2 ^{9c,15t}	112

LIST OF ABBREVIATIONS

ACC	acetyl-CoA carboxylase
ACN	acetonitrile
ACP	acyl carrier protein
APCI	atmospheric pressure chemical ionization
BSTFA	N,O-bis(trimethylsilyl) trifluoroacetamide
C1P	ceramide-1-phosphate
Cer	ceramide
CHO	aldehyde
CID	collision-induced dissociation
CoA	coenzyme A
DCM	dichloromethane
DIBAL-H	diisobutylaluminium hydride
DNP	dinitrophenyl
EI	electron impact
ELO	elongase
ER	endoplasmic reticulum
ESI	electrospray ionization
FA	fatty acid
FAMEs	fatty acid methyl esters
FAPys	fatty acid pyrrolidines
FAS	fatty acid synthase
GC-MS	gas chromatography-mass spectrometry
GlcCer	glucoceramide
GSL	glycosphingolipids

HMPA	hexamethylphosphoramide
HPLC	high pressure liquid chromatography
HRMS	high resolution mass spectrometry
IPC	inositol phosphorylceramides
IT-MS	ion trap mass spectrometer
KCS	3-ketoacyl-CoA synthase
KS	3-ketoacyl-ACP synthase
LC	liquid chromatography
LCB	long chain base
LCFA	long-chain fatty acid
LC-MS	liquid chromatography-mass spectrometry
MIPC	mannosyl inositol phosphorylceramides
MOM	methoxymethyl
MRM	multiple reaction monitoring
MS	mass spectrometry
<i>n</i> -BuLi	<i>n</i> -butyllithium
NMR	nuclear magnetic resonance
OSPC	1-oleoyl-2-stearoyl- <i>sn</i> -glycero-3-phosphocholine
PC	phosphotidylcholine
PE	phosphotidylethanolamine
PI	phosphatidylinositol
PS	phosphotidylserine
<i>p</i> -TsOH	para-toluenesulfonic acid
QQQ	triple quadrupole mass spectrometer
QTOF	quadrupole time-of-flight mass spectrometer
S1P	sphingosine-1-phosphate
SL	sphingolipid
TAG	triacylglycerol
TIC	total ion chromatogram
TLE	total lipid extract

TMS	trimethylsilyl
VLCFA	very-long chain fatty acid
YPD	yeast peptone dextrose

ABSTRACT

Birch, Garrison L. M.S., Purdue University, December 2011. Lipidomic Profiling in *Dictyostelium discoideum*. Major Professor: Robert E. Minto.

The lipid profile of *Dictyostelium discoideum*, a cellular slime mold found evolutionarily between plants and animals, has never been clearly defined. To address this, the fatty acid content of vegetative cells was analyzed by gas chromatography-mass spectrometry of fatty acid methyl esters and their identities verified with synthesized authentic standards. The synthetic scheme developed to produce the unusual fatty acids found in *D. discoideum* was engineered to afford the labeling of compounds (^2H) for use in feeding studies to elucidate the fatty acid elongation and desaturation pathways present in *D. discoideum*. After establishing the fatty acid profile and acyl metabolic pathway, an initial understanding the complex lipids present in *D. discoideum*, chiefly sphingolipids, was sought. Triple quadrupole and quadrupole time-of flight mass spectrometers equipped with electrospray ionization sources were used to identify these complex lipids.

CHAPTER 1. INTRODUCTION

1.1. Fatty acid elongation and *Dictyostelium discoideum*

It has long been understood that *de novo* fatty acids (FAs; Figure 1) are biosynthesized in animals and plants by Type I and II fatty acid synthases, respectively (3). However, it is becoming increasingly apparent that fatty acids produced from *de novo* synthesized FAs via elongation pathways exhibit extraordinary bioactive functionality, as elongated FAs have become known to be essential bioregulators through their incorporation into specialized lipids, such as sphingolipids (SLs; Figure 1) (4, 5). SLs constitute an emerging class of bioactive molecules, influencing such biological processes as signal transduction, metabolism and apoptosis (6, 7).

Fatty acid elongation, the lengthening of acyl-CoA chains by two carbon units, produces the long-chain fatty acids (LCFAs, C₁₄-C₂₀) and very long-chain fatty acids (VLCFAs, >C₂₀). These fatty acids are lengthened in a manner analogous to that mediated by fatty acid synthase, but are instead catalyzed by specialized enzymes known as elongases. The condensation reaction is catalyzed by two families of condensing enzymes; the 3-ketoacyl-CoA synthases (KCSs), which are characteristic of plants (8), and the ELO enzymes (for elongation), which are found in all eukaryotes that have been examined, including mammals, plants, algae and fungi (9). Both condensing enzyme families initiate elongation, then pass their product on to a 3-ketoacyl-CoA reductase of the elongation complex. With both alternative pathways ultimately arriving at the same end products, it is unclear why some organisms have both pathways, while many (such as animals) possess only one.

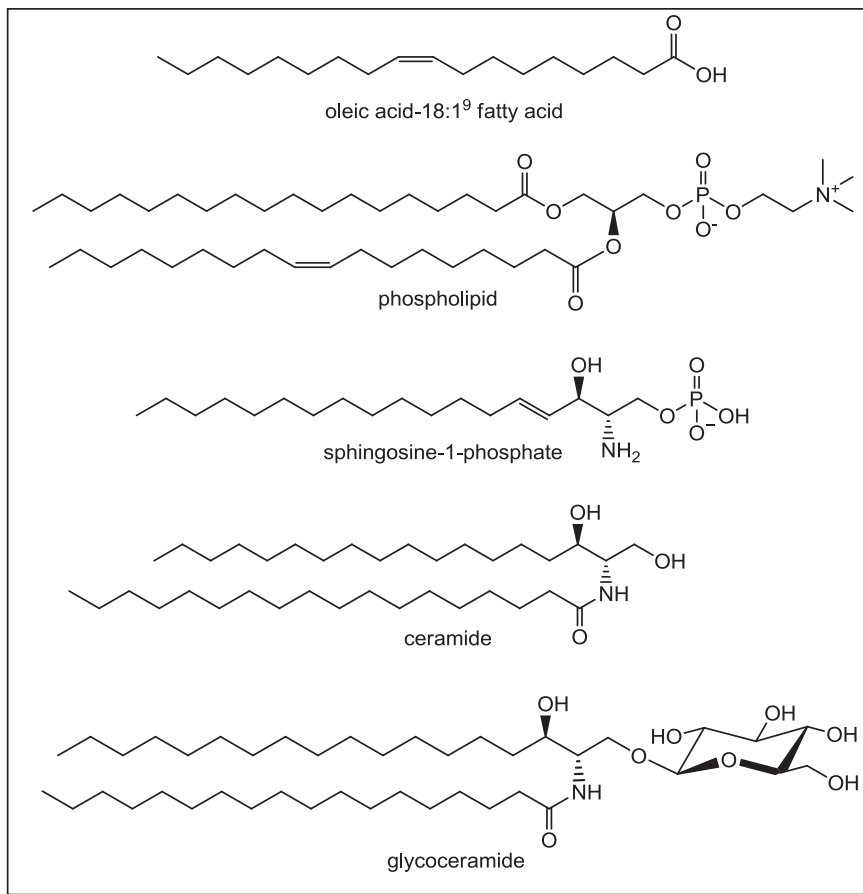


Figure 1. Relevant lipid structures; a monounsaturated C₁₈ fatty acid, a phospholipid, and the sphingolipids, sphingosine-1-phosphate, ceramide, and glycosphingolipid.

Dictyostelium discoideum, the free living cellular slime mold found evolutionarily between plants and animals, is an important model for understanding fatty acid elongation because it possesses examples of both condensing enzyme families; four ELO genes and one 3-ketoacyl-CoA synthase gene. Furthermore, *D. discoideum* has been shown to be active in the elongation of both saturated and unsaturated fatty acid substrates (10).

D. discoideum is an important model for understanding various signaling and developmental processes in higher eukaryotes, such as cell-to-cell communication, intracellular signaling, and cytoskeletal organization that have

been found to be conserved across eukaryotes (11, 12). The sequencing of the *D. discoideum* genome was published in 2005 (13). Comparison of its predicted proteome to other eukaryotes resulted in *D. discoideum*'s placement in the eukaryotic phylogeny (Figure 2) along the animal branch, diverging shortly after plants and before fungi (14). Despite the close proximity of *D. discoideum* to fungi, it is thought to have more in common with animals due to fungi's accelerated rate of divergence relative to plants and animals (14).

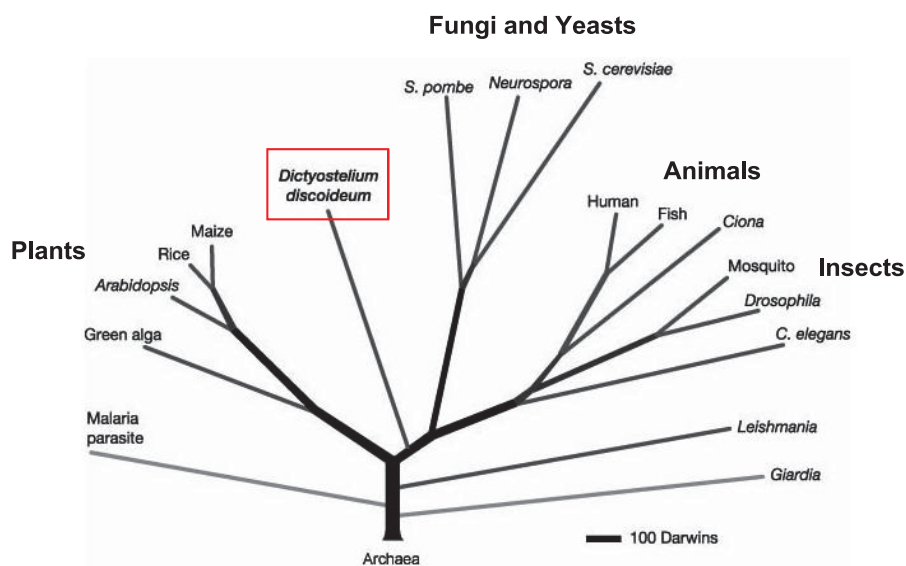


Figure 2. The positioning of *D. discoideum* on the eukaryotic phylogenetic tree (13).

Dictyostelium lives in an amoeboid or unicellular form in its natural habitat of decaying soil rich in bacteria, which is its main food source. However, when nutrients become scarce, cells aggregate and progress through a developmental program ultimately producing a multicellular fruiting body, composed of two main cell types: stalk and spore cells (Figure 3). Spore cells germinate once nutrition has been reestablished (12). During starvation, cells amass in response to cyclic adenosine monophosphate (cAMP) pulses, initially forming loose and tight mounds of cells (stages 1 and 2), which develop into a "finger" (stage 4) or migrating slug (stage 3). After a variable time period of phototaxis, a "Mexican

hat" emerges (stage 5), which culminates and ultimately forms the fruiting body (stage 6) (12). As such, *D. discoideum* is often referred to as a "social amoeba" because it forms a multicellular structure during famine. Some of the signaling pathways involved in this developmental program have been elucidated (11, 12, 15), and literature suggests that specific molecular species of sphingolipids may play particular roles in this development. Therefore, the practicality of *D. discoideum* as a model organism to interpret the relevance of VLCFAs is twofold. Not only is it applicable in terms of elongation studies, but sphingolipids, which often contain such VLCFAs, are believed to play a role in a unique developmental pathway that is observed when it is subjected to starvation.

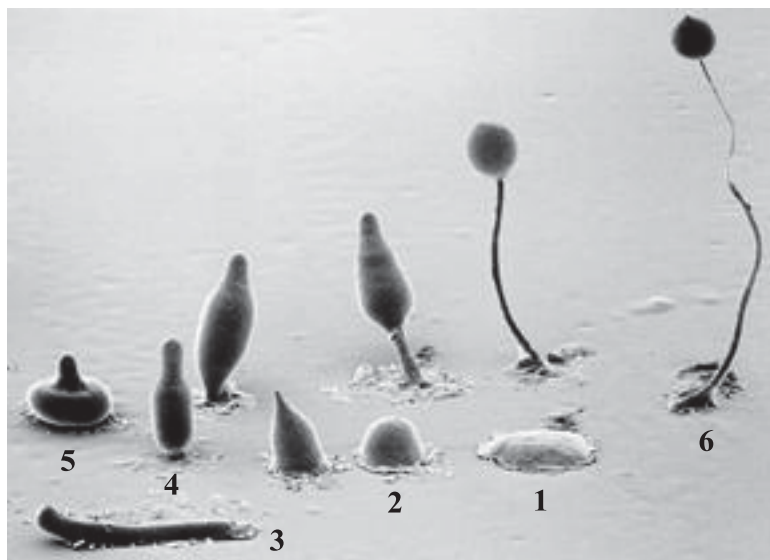


Figure 3. Composite electron micrograph of the developmental stages of *D. discoideum* upon starvation. © M.J. Grimson & R.L. Blanton.

Studies underscoring the key participatory nature of sphingolipids in development and signaling *D. discoideum* are becoming increasingly more common, as well as indications that this organism and its sphingolipids may provide valuable information for other fields of research (16-19). Sphingosine-1-phosphate (S1P, Figure 1) exhibits a significant role in the signal transduction pathways that regulate cell proliferation and cell death, as well as in growth and

multicellular development (17). Disruption of expression of S1P lyase in *Dictyostelium* that is responsible for degradation of S1P resulted in abnormal morphogenesis. The absence of sphingosine-1-phosphate lyase affected multiple stages of development; the aggregation of cells, the ability to form migrating slugs, the control of developmental gene expression, terminal spore differentiation, and the ability to complete morphogenesis (17).

Dictyostelium sphingolipid metabolism has been used as a model in cancer research (18, 20). Researchers have identified potential means of increasing the efficacy of a commonly used chemotherapy drug, cisplatin, using *D. discoideum* as a model organism. The performance of this drug is often only short-term, due to a resistance that develops over time. A *D. discoideum* mutant defective in the sphingosine-1-phosphate lyase gene was found with increased resistance to the drug, uncovering that elevated levels of sphingosine-1-phosphate correlated to increased resistance to cisplatin. Treatment of *D. discoideum* cell lines with varying levels of overexpression of sphingosine-1-phosphate lyase (to increase S1P degradation) with cisplatin resulted in an increase in sensitivity to the drug as monitored by assessing cell viability (18). This work suggested that blocking sphingolipid production could increase the sensitivity to cisplatin, and presented points of pharmacological intervention that could increase the clinical effectiveness of the drug (18).

The unique characteristics of this organism provide an opportunity to probe the distinctive (or redundant) properties of each elongase, specifically the role of its products in sphingolipids. Prior to examination of the modes of elongation in *D. discoideum* and interpreting the roles of elongated fatty acids and sphingolipids in its biological processes, it is essential to establish the fatty acid biosynthetic pathways by which these species are produced, as well as the sphingolipid profile of *D. discoideum*. As such, this research focuses upon characterizing the fatty acids of *D. discoideum*, elucidating their metabolism, and identifying the *D. discoideum* sphingolipids. The objective of this work was to construct a lipidomic profile of *D. discoideum* that can be used in addressing the

question of whether the identity of a sphingolipid's acyl chain targets it for a specific biological function.

There are several long-term practical applications from this research. As many of these sphingolipids are responsible for such life-altering signaling processes as apoptosis (11), a proper understanding of these pathways may allow for the development of pesticides and/or herbicides that can induce similar effects while maintaining a low environmental impact. Alternatively, this work may aid in the development of methods of artificially increasing the production of specific sphingolipids, such as ceramides, which are becoming popular ingredients in therapeutic products such as lotions and creams for skin disorders, chiefly eczema (21, 22).

1.2. Fatty acid biosynthesis and degradation

Fatty acids are long hydrocarbon chains terminated by a carboxylic acid. They are almost exclusively referenced in shorthand. For example, the monounsaturated fatty acid seen in Figure 1, oleic acid, is abbreviated as 18:1⁹, conveying that it contains 18 carbons, has one point of unsaturation, located at the 9th carbon (Δ^9 ; counting from the carboxyl group). Similarly, a 16:2^{5,9} FA describes a C₁₆ chain with double bonds at the 5 and 9 positions. While fatty acids encompass a large class of lipids, the biological functions of FAs can be generalized into four basic categories: 1) the building blocks of glycolipids, phospholipids and sphingolipids that comprise biomembranes; 2) a major storage form of metabolic fuel in the form of triacylglycerols; 3) as hormones and secondary messengers upon specific modification; and 4) as modifying agents in membrane-bound proteins.

1.2.1. Fatty Acid Biosynthesis

Plants and animals synthesize a wide array of fatty acids although only a very few of these lipids are major and common cellular constituents (9). *De novo* fatty acid biosynthesis occurs in the cytosol of animals and the plastids of plants, where the lipids are constructed from acetyl coenzyme A (CoA) units and assembled via acetyl-CoA carboxylase (ACC) and fatty acid synthase (FAS). The primary end product of this iterative process is palmitate (16:0), and to a lesser extent myristate (14:0) and stearate (18:0). Odd chain length fatty acids can be constructed in the same fashion by condensation with propionyl-CoA, or through an oxidative pathway known as α -oxidation (3).

Two physically distinct forms of the acetyl-CoA carboxylase enzyme are found in nature. In plants, it is a three subunit enzyme, while a higher efficiency form exists in mammals with the three subunits fused into a single polypeptide chain and an additional allosteric regulatory subunit activated by citrate to control FA production. Fatty acid synthase also exists in two forms: it occurs as a multifunctional homodimer in eukaryotes (Type I), while the more primitive FA synthase (Type II; prokaryotes) can be separated into individual subunits (3, 23).

Acetyl-CoA carboxylase catalyzes the first committed step of fatty acid synthesis, the carboxylation of acetyl-CoA to malonyl-CoA. The biosynthetic intermediates are then transferred from coenzyme A-derivatives to an acyl carrier protein (ACP) of FA synthase (by acetyl/malonyl transacylases-Figure 4a), and acetyl-ACP binds to 3-ketoacyl-ACP synthase (KS; Figure 4b) (3). Malonyl-ACP is equipped for coupling to an acetyl-KS primer; it is decarboxylated to form an enolate, which nucleophilically attacks the carbonyl of an acetyl-KAS, displacing the acetyl group from the KS unit, and yielding an acetoacyl-ACP (4 carbon chain) (3). Acetoacyl-ACP then undergoes reduction, dehydration, and a second reduction catalyzed by 3-ketoacyl-ACP-reductase, 3-hydroxyacyl-ACP-dehydrase, and enoyl-ACP reductase (Figure 4c,d,e, respectively), to yield butyryl-ACP, at which point the process repeats by condensing another malonyl-ACP with butyryl-ACP to continue building the fatty acid (3). After seven rounds

of elongation, the palmitoyl-ACP product is hydrolyzed from the enzyme by palmitoyl thioesterase (Figure 4f), and the 16:0 free fatty acid is quickly sequestered again in the form of palmitoyl-CoA, becoming available for incorporation into complex lipids and subjected to desaturation, elongation, and hydroxylation enzymatic modifications. However, depending upon the modification, it may take place after the fatty acid has been esterified/N-acylated to a complex lipid.

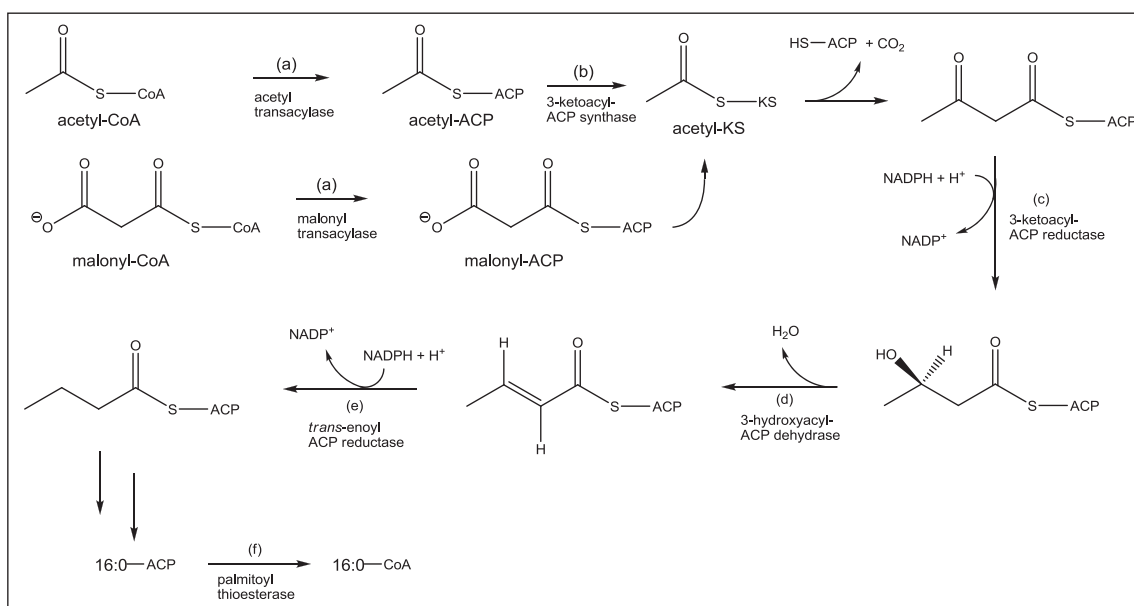


Figure 4. The synthesis of saturated fatty acids in plants and mammals.

Elongation of fatty acids beyond the palmitate product of FA synthase to long and very long chain fatty acids is a common modification, with the products acting as signaling metabolites and components for waxes and sphingolipids. The process involves four enzymes, an acyl-CoA substrate, malonyl-CoA, and NADPH (Figure 5) (3). Unlike acetyl-CoA carboxylase and fatty acid synthase, which are soluble enzymes, the elongases are membrane-bound and sited in the endoplasmic reticulum (ER), where elongation takes place (24). Elongation can occur not only with *de novo* saturated and unsaturated fatty acid substrates, but also with those obtained through dietary sources (25). A significant distinction

from fatty acids produced during elongation is that the substrates remain esterified to Coenzyme A. Malonyl-CoA continues to serve as the 2-carbon unit donor in a reaction sequence similar to standard FA biosynthesis. The first step in FA elongation, the condensation of a C₂ unit from malonyl-CoA with a fatty acyl-CoA substrate, is catalyzed by a 3-ketoacyl-CoA synthase (Figure 5a; KCS or ELO), with liberation of CO₂ and CoA. Next, a 3-ketoacyl-CoA reductase (Figure 5b) reduces the resulting ketone to a hydroxyl group, which is dehydrated by a 3-hydroxyacyl-CoA dehydratase (Figure 5c) to produce a *trans* alkene. Finally, a second reduction of the alkene is catalyzed by *trans*-2,3-enoyl-CoA reductase (Figure 5d) to form the acyl-CoA (3). The elongation of acyl-CoA precursors can be extensive. The waxes of plant leaves have been found to contain even numbered FA chains up to 36 carbons in length (8) while the majority of sphingolipid acyl chains range from C₂₀ to C₃₀ (4).

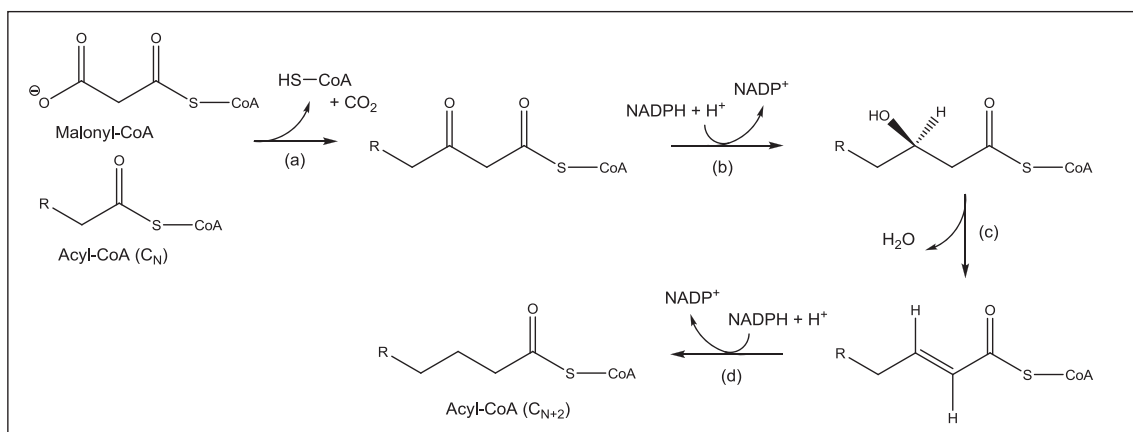


Figure 5. The primary fatty acid elongation pathway of eukaryotes.

A second common form of FA modification is desaturation. Iron-dependent enzymes known as desaturases introduce double bonds (usually with the *cis* configuration) at regiospecific positions along a fatty acid chain. Unsaturated fatty acid chains serve an important function in the structural organization of cellular membranes as a proper ratio of saturated to unsaturated FAs helps regulate membrane fluidity (3). They also have bioactive roles, acting

as signaling metabolites both in the free fatty acid state as well as when incorporated into more complex lipids (3, 4, 26).

FA desaturases can be sorted into two groups: the soluble acyl carrier protein desaturases and the membrane-bound desaturases. The soluble ACP desaturases introduce double bonds into ACP-linked fatty acids, and are located in the stroma of plant plastids (26). In terms of the membrane-bound enzymes, the acyl-lipid desaturases responsible for desaturation of glycerolipid acyl chains are sited within the endoplasmic reticulum in mammals and the chloroplast membrane in plants. The acyl-CoA desaturases, which insert double bonds into CoA-derivatized fatty acids, are located within the ER of animals and fungi (26).

The insertion of an alkene in an acyl-CoA is an electron-transfer reaction that is accomplished with three membrane proteins of the ER in eukaryotic cells: a desaturase, cytochrome b_5 and NADH-cytochrome b_5 reductase (3, 26). Two protons are extracted from the FA hydrocarbon chain as the double bond is formed (Figure 6) by reducing molecular oxygen to form two molecules of water. The arrows of Figure 6 outline the flow of electrons from NADH to the desaturase via the FAD-containing reductase and cytochrome b_5 (26).

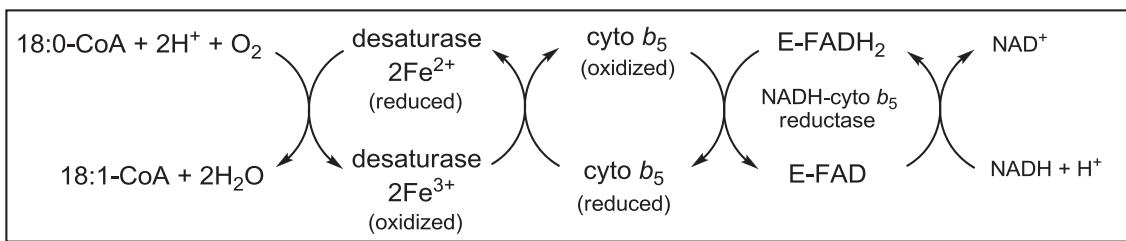


Figure 6. Desaturation of stearoyl-CoA (3).

Hydroxylated fatty acids are commonly incorporated into sphingolipids and are believed to offer stabilizing effects in the form of hydrogen bonding (5), imparting greater structural integrity to membranes (27, 28). The SL acyl groups are normally saturated and, while the hydroxyl group most commonly located at the α -position, there are examples of ω -hydroxy (5) and dihydroxy FAs that have

been observed in sphingolipids (4, 6). FA hydroxylation reactions often take place succeeding this incorporation, as there are fatty acid hydroxylases (also referred to as ceramide hydroxylases) with specificity for complex lipid substrates such as ceramides (4, 29). Hydroxylases share a high degree of homology with desaturases (30). In some cases, a substitution of as few as four amino acids can differentiate between desaturation or hydroxylation activity (30, 31).

1.2.2. Fatty Acid Degradation

Degradation of fatty acids is commonly referred to as β -oxidation, and is the sequential 2-carbon unit breakdown of fatty acids over four enzymatic reactions, producing acetyl-CoA units, which can be utilized as metabolic fuel or for the biosynthesis of new fatty acids. Prior to undergoing β -oxidation, free fatty acids are released from complex lipids (such as stored or dietary triacylglycerols (TAGs) and phospholipids) via lipase enzymes and esterified to Coenzyme A (3). Once an acyl-CoA species, β -oxidation of saturated chains begins with the acyl-CoA dehydrogenase-catalyzed oxidation of the β -carbon of the acyl-CoA to generate a *trans* alkene (enoyl-CoA; Figure 7) (3). Step 2 involves the stereospecific hydration of the double bond to create 3-hydroxyacyl-CoA, followed by a second oxidation with NAD^+ to yield a 3-ketoacyl-CoA. The fourth and final step utilizes β -ketothiolase, which breaks the diketone bond between carbons 2 and 3 via nucleophilic attack of the carbon 3 carbonyl with S-CoA , thioesterifying the new two-carbon shorter acyl chain and yielding acetyl-CoA. The cycle repeats until the fatty acid has been completely degraded, with the final round of degradation yielding two acetyl-CoA species (or acetyl-CoA and propionyl-CoA during β -oxidation of odd-numbered chains) (3).

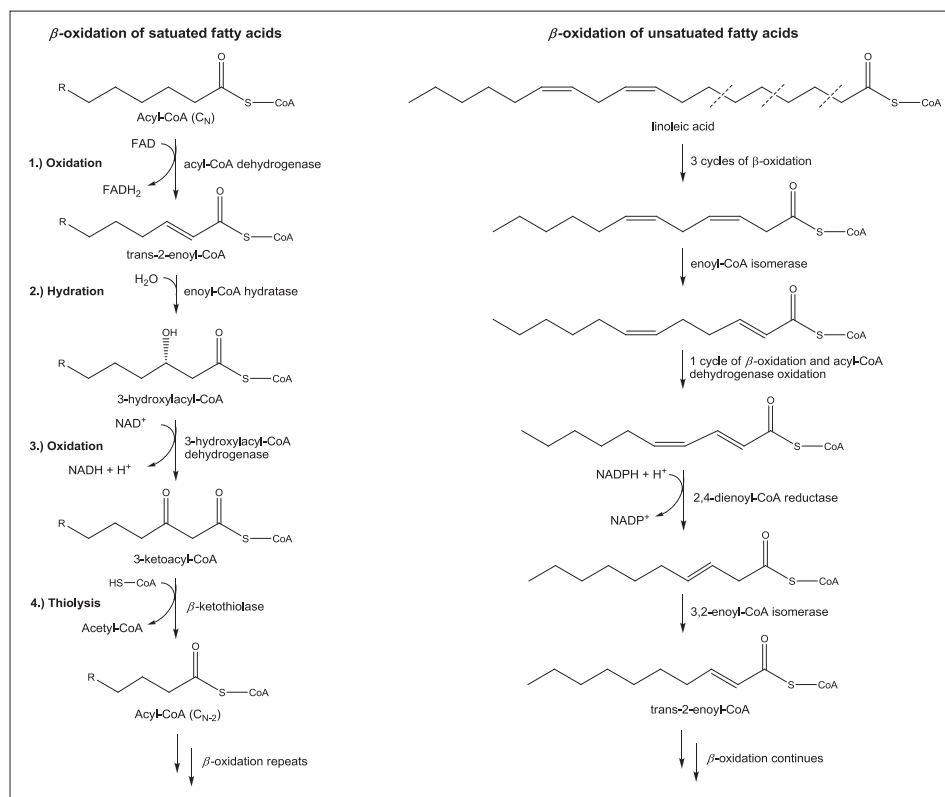


Figure 7. Examples of β -oxidation for saturated and unsaturated fatty acids.

The oxidation of unsaturated fatty acids proceeds in much the same fashion as saturated FAs, but requires additional enzymes to facilitate degradation of the alkenes. As most unsaturated FAs do not have double bonds closer to the carbonyl than the Δ^5 position, one or more cycles of “normal” β -oxidation will occur until an alkene is encountered. The *cis* double bonds of most FAs create an obstacle for the enoyl-CoA hydratase enzyme, which stereospecifically hydrates a *trans* alkene (Figure 7). An enoyl-CoA isomerase is therefore employed to convert the alkene to the *trans* confirmation, and β -oxidation continues (3). Another problematic situation is illustrated in Figure 7, where the oxidation product of acyl-CoA dehydrogenase yields a *trans* bond at carbon 2, but if there is a point of unsaturation at carbon 4, enoyl-CoA hydratase cannot hydrate the alkene at carbon 2 halting β -oxidation. Reductases reduce the diene and shift the 2-alkene to a 3-alkene. This enoyl-CoA is then

isomerized to generate a *trans*-2-enoyl-CoA, the desired substrate for β -oxidation (3).

The degradation of odd chain length fatty acids proceeds in precisely the same manner, with the final thiolysis step yielding acetyl-CoA and propionyl-CoA (3). Propionyl-CoA is decarboxylated and subjected to a cascade of reactions that converts it to pyruvate (and ultimately acetyl-CoA). In terms of biosynthesis, odd chains can be produced via an oxidative pathway known as α -oxidation, which shortens the overall chain length by a single carbon unit. α -Oxidation is not employed strictly for biosynthetic means, it is also widely utilized to breakdown FAs that cannot undergo β -oxidation, specifically those containing modifications at the β -carbon. An illustration of this pivotal process shown in Figure 8. This breakdown begins with hydroxylation at the α -carbon, followed by removal of the thioester, and decarboxylation in the form of formyl-CoA. The resulting aldehyde with one fewer carbon atoms can then be oxidized to the carboxylic acid by aldehyde dehydrogenase and esterified to CoA, such that standard β -oxidation can recommence (3).

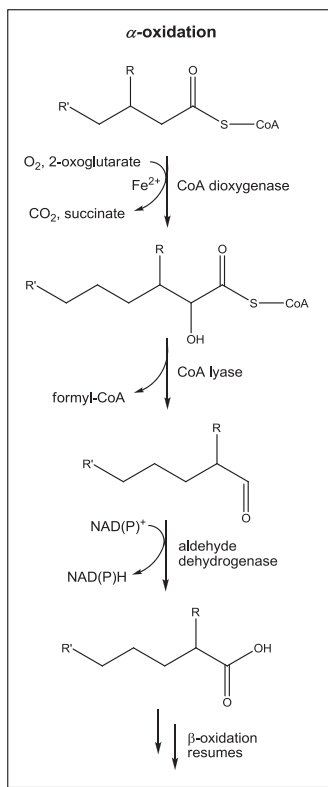


Figure 8. α -Oxidation of a β -substituted fatty acid.

1.3. Sphingolipids

Sphingolipids are essential for eukaryotic life (5). They comprise an amazingly diverse class of bioactive lipids and until recently were thought to be merely structural components of biological membranes. However, within the past decade and a half, these unique lipids have been implicated in an array of cellular processes, including cell structure, regulation and metabolism (4, 32). Intrinsic to eukaryotes as well as some prokaryotes and viruses, sphingolipids have been shown to be active signal transduction mediators: regulating cell growth, differentiation, proliferation, and stress responses, and influencing cell motility (5). They also act in the formation of specialized structures (such as lipid rafts), mediate cell-cell interactions, and regulate the activity of intracellular proteins (5, 6). As structural components, they constitute an average of 30% of the total lipid found in the plasma membranes of eukaryotes (5).

In simplistic terms, sphingolipids are derived from a variety of structurally similar long chain bases (LCBs-see Figure 9), also referred to as sphingoid bases. An LCB is the defining structural scaffold or “backbone” upon which the various classes of sphingolipids are constructed (7). They are aliphatic amines, typically 18 carbons in length, containing two or three hydroxyl groups near the amino terminus, and often equipped with a *trans* alkene at C-4. In Figure 9, note the (2*S*,3*R*)-*erythro* stereochemistry, consistent among all LCBs. Standard fatty acid nomenclature applies, and the italicized prefixes “*d*” and “*l*” denote di- and trihydroxylation respectively, while *Z* or *E* designates a cis or trans alkene configuration, respectively.

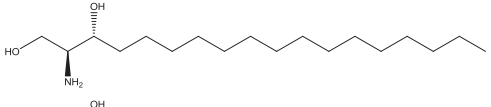
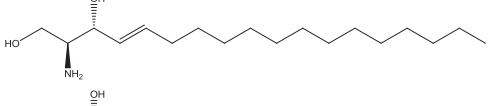
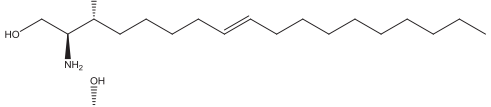
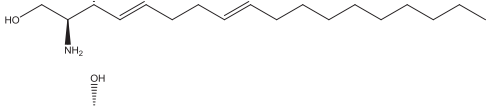
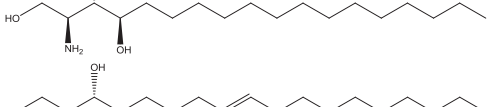
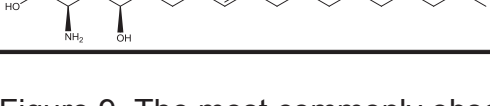
	Name	Shorthand	Organism
	sphinganine/dihydrosphingosine	<i>d</i> 18:0	plants/animals
	(<i>E</i>)-sphing-4-enine/sphingosine	<i>d</i> 18:1 ^{<i>E</i>}	plants/animals
	(<i>E</i>)-sphing-8-enine	<i>d</i> 18:1 ^{<i>E</i>}	plants
	(4 <i>E</i> ,8 <i>E</i>)-sphinga-4,8-dienine	<i>d</i> 18:2 ^{4<i>E</i>,8<i>E</i>}	plants
	4-hydroxysphinganine/ phytosphingosine	<i>l</i> 18:0	yeast/plants
	(<i>E</i>)-4-hydroxysphing-8-enine	<i>l</i> 18:1 ^{<i>E</i>}	plants

Figure 9. The most commonly observed sphingolipid long chain bases in plants, animals, and yeast (4, 33).

Mammalian tissues are found to contain almost exclusively sphingosine, while phytosphingosine is the most prevalent LCB identified in plants and yeast (4, 5, 33). Alternatively, insects are often found to contain shorter long chain bases: the fruit fly *Drosophila melanogaster*, commonly used in genetic research, has a C₁₄ sphingoid base as its main component (34). Trace amounts of

hundreds of sphingoid bases have been isolated from various organisms and characterized (35). These backbones are distinguished by chain lengths, points of unsaturation and hydroxylation, stereochemistry, and even such chain modifications as methylations, cyclic rings and the presence of alkynes (35). These highly specialized LCBs are usually produced for incorporation into a specific class of sphingolipid. For example, eicosasphingosine (*d*20:1) is only found in the gangliosides extracted from brain (36) and intestinal tissues (35, 37).

While it may be commonly perceived that only the complex sphingolipids are responsible for the bioactivity observed in organisms, this is far from the case. Sphingoid bases exhibit a vast range of structural diversity, and many of the known bases have been shown to display important biological functionality in their free states, typically in the form of cell signaling (35). Potent signaling properties include the phosphorylated form of sphingosine (sphingosine-1-phosphate) and other LCB phosphates that have been implicated in the abscisic acid-mediated stomatal closure in *Arabidopsis* (38). In the fungus *Aspergillus nidulans*, the free LCB forms of *d*18:0 and *t*18:0 induce apoptosis (39). Many of the more unique sphingoid natural products have exhibited toxicity towards cancer cells and pathogens, giving rise to their further investigation as potential chemotherapy leads (35).

The first instance along the sphingolipid metabolic pathway where long chain bases are modified into more specialized sphingolipids occurs when they are *N*-acylated to form the SL subgroup known as ceramides; an example is shown in Figure 1. An acyl chain can range from C₁₄ to upwards of C₄₀ in some tissues (4). They are usually saturated but have been observed to contain up to two points of unsaturation; other modifications to the fatty acid include hydroxylation (usually at the α -position) and amination (4, 5). Ceramides are very active signaling agents that require tight regulation, as they have been shown to mediate such processes as cell growth, differentiation, secretion and apoptosis (22).

While ceramides are the crucial intermediate for all complex sphingolipids, they rarely accumulate in any quantity in tissues other than skin (22). Due to their potentially lethal signaling capacities, they are quickly utilized as precursors for more complex lipids, via linkage at the terminal primary hydroxyl group to moieties such as phosphates and carbohydrates (Figure 1).

1.3.1. Sphingolipid Biosynthesis

De novo sphingoid base synthesis begins with the condensation of palmitoyl-CoA and serine to form 3-keto-sphinganine via serine palmitoyltransferase (Figure 10). Similarly, less common bases are formed using varying acyl-CoAs. For example, C₂₀ bases are synthesized by condensation with stearoyl-CoA. This first step is thought to be the rate-determining step of ceramide biosynthesis (22). The resulting ketone is reduced by 3-ketosphinganine reductase, yielding a hydroxyl group at position 3 and the product sphinganine (*d*18:0, dihydrosphingosine), the saturated form of sphingosine. At this point, the fate of sphinganine diverges: its hydroxylation via sphinganine hydroxylase yields phytosphingosine (*t*18:0), or dihydroceramides (or phytoceramides) can be generated by ceramide synthase N-acylation of sphinganine (or phytosphingosine) (7, 22). The enzyme dedicated to the acylation of LCB is generically labeled as dihydroceramide synthase, but various isoforms of this enzyme exist among plants and animals, each with specificities for both the long chain base and the acyl-CoA substrates (22).

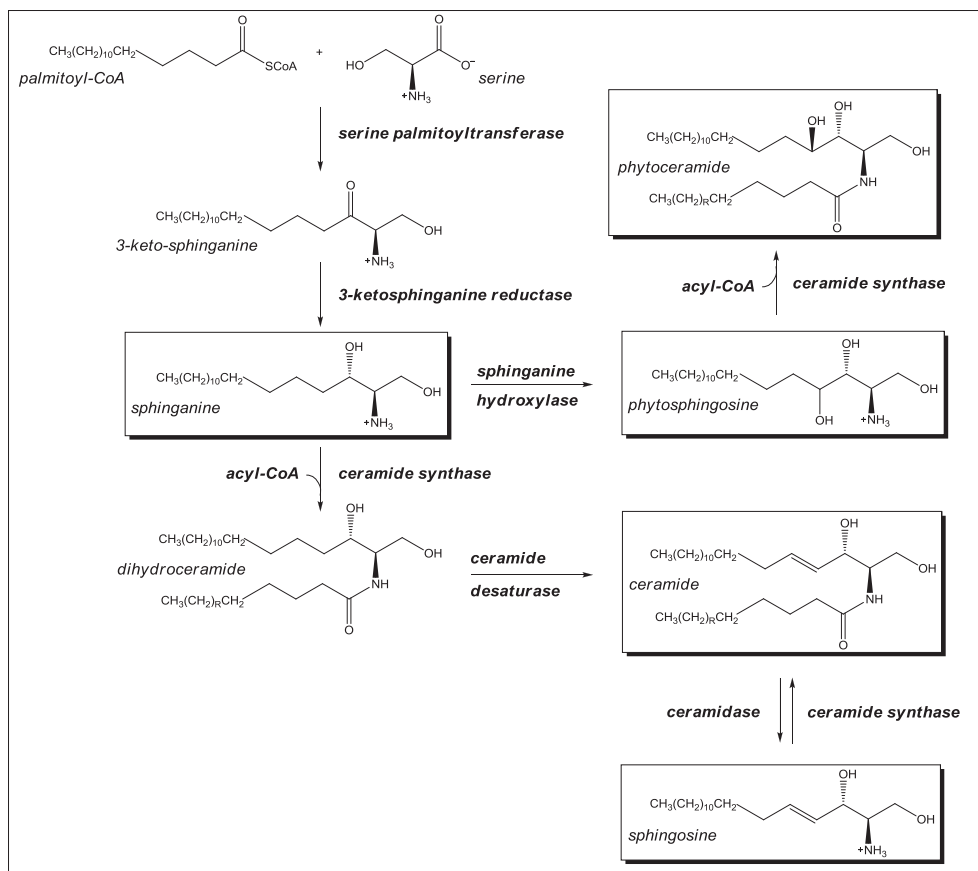


Figure 10. The biosynthesis of long chain bases and ceramides (22).

While it may seem counterintuitive, sphingosine is not formed in its free long chain base state. After sphinganine is coupled with an acyl-CoA to form a dihydroceramide, a ceramide desaturase enzyme inserts a *trans* double bond at the 4-position of the sphingoid backbone, to yield sphingosine (and the designation changes to ceramide) (22). This is the only pathway with which this LCB can be produced, but sphingosine is a bioactive contributor as the free base as well. An additional enzyme is active in regulating the appropriate concentrations of sphingosine and ceramide: a ceramidase cleaves the amide linkage to liberate the free LCB as needed, and ceramide synthase sequesters sphingosine back into ceramide form. Once at the ceramide platform, a large host of enzymes are available to convert this pivotal precursor into more

specialized sphingolipids, such as ceramide-1-phosphates, phosphoinositols and glycosphingolipids (22). The particular enzymes that are present and the modifications that take place are specific to each organism.

Ceramide-1-phosphates (C1P; Figure 11) are produced when ceramide kinase phosphorylates a ceramide at the terminal (1-position) hydroxyl group of the long chain base. In animals, a specific pool of ceramides is phosphorylated by ceramide kinase (22, 40). However, there is evidence that other means of generating ceramide-1-phosphate must exist, as mice in which the ceramide kinase gene has been disrupted still demonstrate normal levels of C1P and the metabolite cannot be produced via acylation of sphingosine-1-phosphate (41). While C1P appears characteristic of animal tissues, a ceramide kinase has also been observed in *Arabidopsis* and other higher plants, but not in yeast (42, 43). The enzyme's function has not been fully elucidated, but as C1P has been implicated in defense mechanisms, it may act to remove excess ceramide and make the plant more resilient to environmental stresses (44). Additionally, it appears that an equilibrium between ceramide and ceramide-1-phosphate may regulate apoptosis (45).

Another prominent SL class is the inositolphosphoryl ceramides (IPCs; Figure 11), which are essentially the sphingolipid analogue of phosphatidylinositol. IPCs constitute a vital component of the sphingolipids in many eukaryotic species but are not, however, found in animals (5, 46). These SLs are biosynthesized via ceramide phosphorylinositol synthase, which catalyzes the transfer of an inositol phosphate moiety from phosphatidylinositol to a ceramide (4). They are generally comprised of phytosphingosine backbones, have been observed in both plants and fungi, and primarily contain saturated fatty acid chains, which may be α -hydroxylated (5).

While only a few plant species have been examined, their IPCs primarily contain phytosphingosine bases with 24:0 acyl chains (4, 47). In the case of fungi, in *S. cerevisiae*, the only sphingolipid class that contains polar head groups is derived from phosphoinositol (IPC and mannosyl inositol

phosphorylceramides-MIPC) with phytosphingosine backbones (1, 5, 48). *P. pastoris* contains SL classes in addition to IPCs such as glucosylceramides and sphinganine-containing species (49).

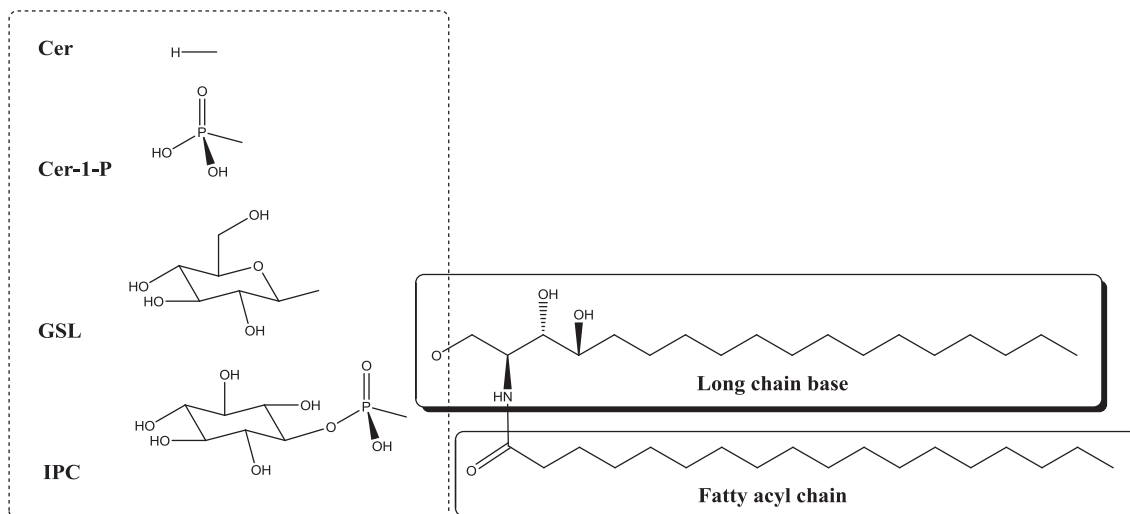


Figure 11. The building blocks of ceramide, ceramide-1-phosphate, glycosylceramide, and inositolphosphoryl ceramide complex sphingolipids (4).

Glycosphingolipids (GSLs; Figure 11) consist of a saccharide coupled via a β -glycosidic linkage to the terminal hydroxyl group of the LCB. This linkage is achieved through the enzyme-catalyzed transfer of a uridine 5-diphosphate-coupled sugar directly to the ceramide of interest (7, 22). Some of the most common GSLs are glucosylceramide, which is a major constituent of the outer leaflet of plasma membranes, and galactosylceramide, the largest single component in myelin sheaths (22). The addition of a carbohydrate head group is typically classified as acidic (gangliosides) or neutral (oligoglycosylceramides), further diversifying this class of complex sphingolipid. Over 500 different carbohydrate structures have been identified in GSLs, with the most prominent sugars being glucose, galactose, fucose, *N*-acetylglucosamine (GlcNAc), *N*-acetylgalactosamine (GalNAc) and sialic acids (Figure 12) (7). The number of sugar head groups ranges from one to upwards of twenty monosaccharide units in some animals (7).

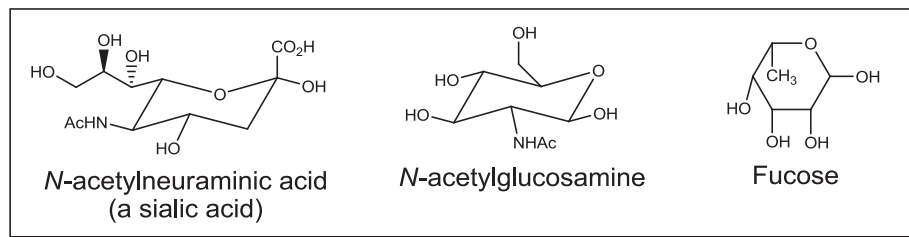


Figure 12. Common GSL carbohydrate head groups.

Research Objectives

In order to understand the roles of elongated fatty acids and sphingolipids in *D. discoideum*, the identification of the lipids present in a cell is essential. The endogenous FAs must be identified and their metabolic pathways elucidated in order to understand the roles of FAs in the organism. In the current work, fatty acids were first identified using commercial and synthetic standards. Once a fatty acid profile was developed, the focus shifted toward elucidating the metabolic pathway by which the FAs are biosynthesized and degraded. This work was pursued with particular interest in identifying the source of 18:2^{5,11} and 18:1¹¹ that constitutes the majority of the FAs in *Dictyostelium*. Finally, the sphingolipids were analyzed. SL research has evolved from classical TLC to HPLC and mass spectrometry-based analysis. With the innovations of instrumentation design that have taken place in the past decade, tandem mass spectrometry (MS/MS) combined with electrospray ionization (ESI) has proven to be an exceptionally robust and efficient method of analyzing this vast lipid class (32, 50). These analytical techniques are discussed in detail in Chapter 4.

CHAPTER 2. FATTY ACID PROFILING OF *DICTYOSTELIUM DISCOIDEUM*

2.1. Introduction

To begin to uncover the products of the two condensing enzyme families and available desaturases, it was necessary to correctly identify the fatty acids produced by *D. discoideum*, specifically the chain length and positioning of double bonds within the aliphatic chains. Preliminary determination of the fatty acids of *D. discoideum* was performed with fatty acid methyl esters (FAMES) prepared from axenic cells grown in shaking culture and analyzed by gas chromatography-mass spectrometer (GC-MS). FAMES are employed because the acidic conditions by which they are prepared will cleave the ester bonds that link fatty acids to the backbones of complex lipids and converts them to methyl esters. Ester derivatives are preferred over free fatty acids for their ease of analysis; they chromatograph and analyze substantially better on a GC-MS (51, 52).

Comparisons of GC retention time and MS fragmentation upon ionization of FAMES prepared from cells with the commercial standards 16:0, 16:1⁹, 18:0, 18:1⁹, and 18:1¹¹ allowed for the identification of a number of FAs. For the remaining unidentified FAs, preliminary identifications were made with fatty acid pyrrolidine (FAPys) derivatives, which exhibit diagnostic fragmentation patterns upon ionization in an electron impact (EI) source.

The attractiveness of pyrrolidine derivatives is found in their unique display of ion fragments that allow for the placement of double bonds deduced from the diagnostic fragment ions observed in MS analysis (51). This is illustrated in Figure 13. Beginning with the molecular ion (m/z 333) and comparing daughter ion pairs until a difference of 12 m/z is denoted, a double bond's position can be

ascertained, based upon the number of methylene groups that are between the molecular ion and the point at which a difference of 12 mass units is observed (51).

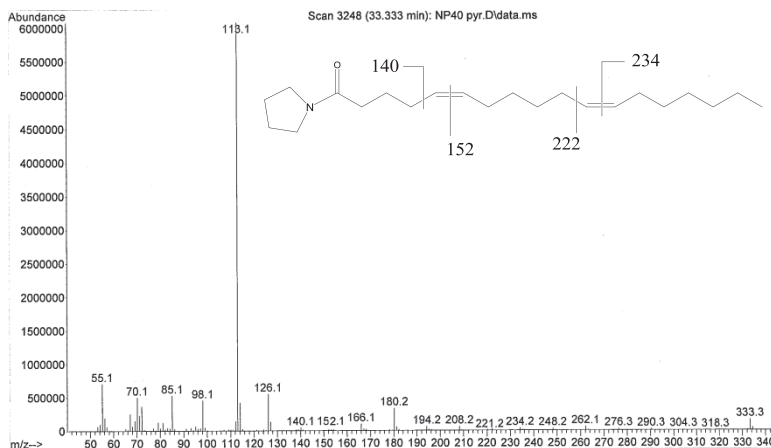


Figure 13. The mass spectrum of the pyrrolidine derivative of 18:2^{5c,11c}.

This mathematical approach to locating the alkenyl groups was verified using FAPYs of standards. Using this methodology, the Blacklock lab preliminarily identified the remaining uncharacterized FAs in *D. discoideum*. As no commercial standards exist for many of the preliminarily identified FAs, unambiguous identification required the direct synthesis of several compounds in order to establish a profile. The candidate list of fatty acids included 16:1^{5c}, 16:2^{5c,9c}, 17:2^{5c,9c}, 18:2^{5c,11c}, and 18:2^{7c,11c} (10). In addition to the FAs outlined by Blacklock *et al.* (10), two FAs were discussed in the profile of *Dictyostelium* by Saito *et al.*: 18:1^{5c} and 18:2^{5c,9c} (53). To resolve this discrepancy, these two FAs were also slated for synthetic production and a strategy was formulated to produce these commercially unavailable compounds.

2.2. Methods and materials

All manipulations were performed in glass conical vials unless otherwise mentioned. Fatty acid standards were obtained from Sigma Aldrich. All solvents

used were of HPLC grade. The components used to make HL5 media and penicillin-G potassium were obtained from Fisher Scientific, and streptomycin sulfate and *N,O*-bis(trimethylsilyl) trifluoroacetamide (BSTFA) were supplied by Sigma Aldrich. AX4 *D. discoideum* was obtained from the dictyBase Stock Center and was maintained on 100 x 20 mm BD Falcon polystyrene tissue culture dishes (catalog number 353003).

2.2.1. Maintenance and growth of *Dictyostelium discoideum*

D. discoideum was maintained axenically at 22 °C in liquid HL5 media (components in Appendix) and penicillin/streptomycin (pen/strep; 100 µg/mL) on tissue culture plates. Passage of cells (150 µL of media from the expiring plate) into 15 mL fresh media was performed every 4-6 days. As living AX4 cells adhere to the plastic surface of the plate and dead cells float in the media, the plate bottom was flushed with the residing media to suspend living cells into solution prior to inoculation of the new plate.

For analysis of *D. discoideum* fatty acids, 50-mL cultures were set in 250-mL autoclaved flasks containing HL5 and pen/strep, and inoculated with 1.0 mL of media from a well-established plate of *Dictyostelium* (grown to the time of passage). Cells were grown at 22 °C with shaking (180 RPM) to a density of $\sim 3.0 \times 10^7$ cells/mL measured under a microscope using a hemocytometer.

2.2.2. Preparation and Analysis of Derivatives

Fatty acid methyl esters were prepared from cells collected by centrifugation of cultures (50-mL culture of $\sim 3.0 \times 10^7$ cells/mL) at 450g to remove media, and washed by vortexing with nanopure H₂O and centrifugation at 450g (repeated 3x). The resulting cellular pellet was incubated for 1 h at 80 °C with 1 mL of 2% H₂SO₄ in MeOH. FAMES were isolated upon the addition of 1 mL of H₂O and extraction with 3x with 2 mL of hexane, followed by evaporation of hexane to dryness under a stream of nitrogen.

Fatty acid pyrrolidines were prepared by incubating a dry sample of fatty acid methyl esters from a 50-mL culture of $\sim 3.0 \times 10^7$ cells/mL with 250 μ L of pyrrolidine and 25 μ L of glacial acetic acid at 100 °C for 1 h. The product was isolated upon addition of 1 mL of H₂O and extraction with 3 mL of 1:1 diethyl ether/hexane, then washing the organic extracts 2x with 1 mL of H₂O. The diethyl ether/hexane solution was evaporated under a stream of nitrogen.

Trimethylsilyl (TMS) derivatives of hydroxy fatty acids were prepared by dissolving a neat FAME sample from 50-mL culture of $\sim 3.0 \times 10^7$ cells/mL in 1 mL of acetonitrile (ACN) and 70 μ L of BSTFA and incubating at 70 °C for 30 min. The silylating agent and ACN were evaporated under a stream of nitrogen.

FAME, FAPy, and TMS-FAME samples were resuspended in 0.5 mL of hexane for GC-MS analysis, but volumes were often adjusted to suit the particular sample concentration after initial analysis. Derivatized samples were analyzed on an Agilent 7890A GC/5975C MS with a 30 m HP-5 column using the GC oven methods outlined in Figure 14 and injection volumes of 1 μ L. The ionization efficiencies among all fatty acids were assumed to be equal.

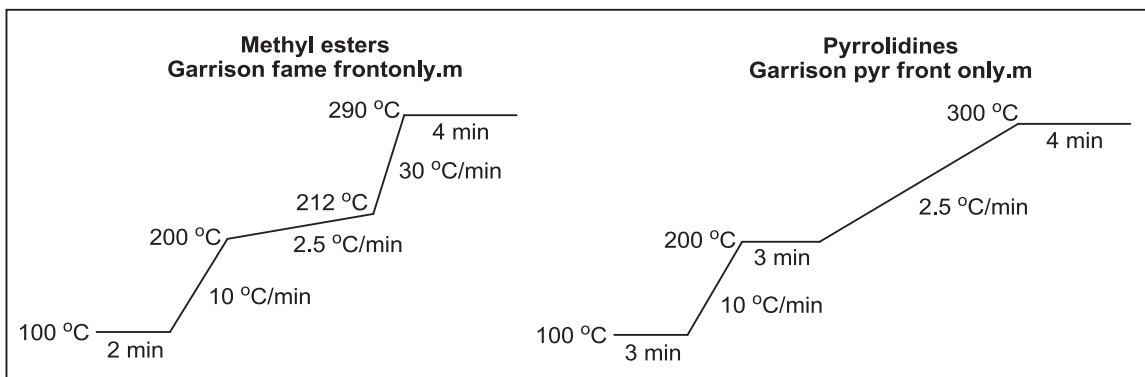


Figure 14. The GC oven methods for FAME and FAPY analysis.

esters to the aldehyde oxidation state, initial experimentation showed a considerable amount of this ethyl ester was being over-reduced to the alcohol. It was suspected that, while the reaction runs in dichloromethane (DCM) at $-78\text{ }^{\circ}\text{C}$, localized heating readily occurs upon addition of DIBAL and that this increase in thermodynamic energy is sufficient to cause over-reduction if the reducing agent is introduced too quickly. The issue was resolved by employing a syringe pump with addition at 1 mL/min , allowing for **1** to be quantitatively produced. Despite the fact that the reaction was essentially quantitative by $^1\text{H NMR}$, the overall yield for compound **1** was extremely variable, largely due to the low molecular weight and boiling point of the compound. Even upon gentle rotary evaporation, the material easily entered the vapor phase.

The aldehyde **1** was then protected from nucleophilic attack in subsequent *n*-BuLi reactions using ethylene glycol and catalytic amounts of *p*-toluenesulfonic acid (*p*-TsOH) (**54**). Upon refluxing the mixture in benzene with a Dean-Stark apparatus for 3 h, approximately 90% of the aldehyde had been converted to the 1,3-dioxolane. The remaining low boiling point **1** was removed from **2** under high vacuum. To complete the preparation of **3**, the alkyl bromide **2** was converted to an alkyl iodide via reflux with acetone and sodium iodide, also known as the Finkelstein reaction (**55**). The crude material was subjected to purification on a silica gel column to remove any ester and aldehyde materials that may have remained affording a 78% yield. To preserve the material from degradation by spontaneous HI formation, **3** was stabilized by storage over K_2CO_3 .

A 6-carbon version of this protected dioxolane (**6**; Figure 16, the precursor necessary to position alkenes at the 7th and 11th carbons for production of the 18:2^{7,11} fatty acid) was produced through the same synthetic manipulations using ethyl 6-bromohexanoate.

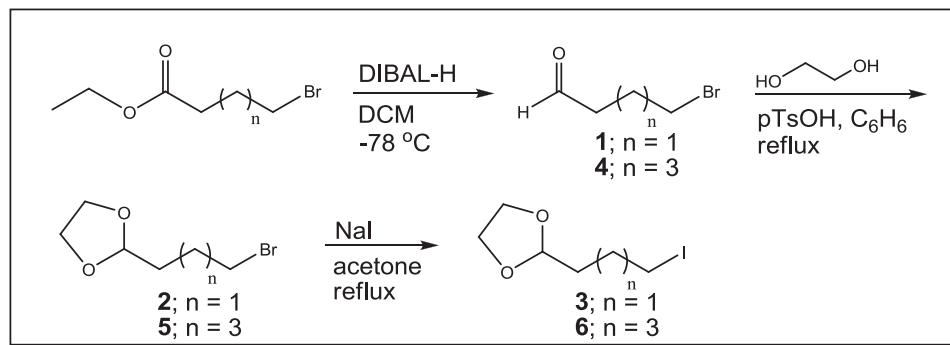


Figure 16. The synthesis of dioxolanes **3** and **6**.

The selection of an alkyne for the next step pivoted around the desired location(s) of the double bonds in the product FA. For example, in order to produce 18:2^{5,11}, the 4-carbon unit **3** needed to be attached to the diacetylene 1,7-octadiyne, placing the alkynyl groups at positions 5 and 11. Once the positions of the acetylenes were locked in place, a second alkylation with an alkyl halide (1-iodohexane) of appropriate length to complete the overall chain was carried out.

The deprotonation of acetylenes by *n*-BuLi took place in THF at -78 °C with the addition of a co-solvent, hexamethylphosphoramide (HMPA), which assists by coordinating Li⁺ and activating the *n*-Bu anion. Deprotonation of a single terminal alkyne was achieved by addition of 1.2 equivalent units of the base with respect to the alkyne. After stirring for 30 min at -78 °C, deprotonation was complete and the reaction was allowed to warm to room temperature, at which time the alkyl halide was added, and the mixture refluxed for 18 h. Upon silica-gel purification, the yields for diacetylene reactions (compounds **7**, **8**, **9**) hovered around 50%, because ~50% of the diacetylene material is deprotonated once, while ~25% is deprotonated twice, and ~25% remains protonated.

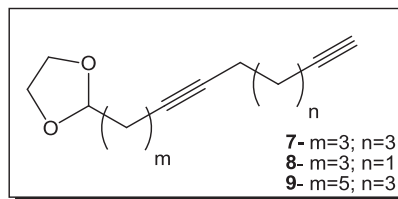


Figure 17. The intermediary diacetylenes **7**, **8** and **9**.

Secondary couplings that involved a single site of deprotonation were obtained in much greater efficiency, with yields approaching 90%. The monounsaturated compounds were completed first (16:1⁵ and 18:1⁵); their low yields relative to the others stemmed from a substandard bottle of *n*-BuLi. Table 1 summarizes the various reagents used to afford a particular end product.

Table 1. Summary of alkylations and the resulting products.

Starting Material	Alkylating material	Product	Yield
3	1-dodecyne	16:1 ⁵ (10)	54%
3	1-tetradecyne	18:1 ⁵ (11)	62%
7	1-iodohexane	18:2 ^{5,11} (12)	80%
8	1-iodohexane	16:2 ^{5,9} (13)	85%
8	1-iodooctane	18:2 ^{5,9} (14)	74%
8	1-iodoheptane	17:2 ^{5,9} (15)	76%
9	1-iodohexane	18:2 ^{7,11} (16)	91%

With the aliphatic backbone of each fatty acid assembled, the acetylenes were hydrogenated using Lindlar's catalyst (5% Pd on CaCO₃). The catalyst, poisoned with lead, selectively reduces an alkyne to a *cis* alkene. This reaction was performed in 100% ethanol, with the addition of quinoline, to further poison

the reaction, and exposed to H₂ atmosphere provided by a balloon (56). The initial reduction test was allowed to react for 24 h, which yielded a mixture of over-reduced alkane and the desired product. In troubleshooting this issue, a reaction was set and monitored hly by gas chromatography. Analysis confirmed reduction of the acetylenes after 1 h and ¹H NMR verified formation of the desired *cis* alkene in quantitative yield. Quinoline was removed from the crude material by passage through a silica-gel column prior to deprotection. Removal of the dioxolane protecting group was accomplished in 90% yield by refluxing in wet acetone (15% H₂O) (57). Lingering dioxolane material was not separated from the aldehyde, as its presence did not hinder the final oxidation step and it could be more readily purified away from the carboxylic acid than the aldehyde. The conversion of the aldehyde to the carboxylic acid was achieved at room temperature via an NaH₂PO₄-buffered water/DMSO solution containing sodium chlorite (NaClO₂) as the oxidant (58). The conditions were conducive to consumption of virtually all aldehyde starting material. Following flash chromatography, the final compounds were separated from any remaining dioxolane species in an 80-90% yield. An overall summary of this synthetic scheme, including yields, is provided in Figure 18. In addition, Section 5.2 contains experimental details for each reaction, using the synthesis of 18:2^{5,9} as a template.

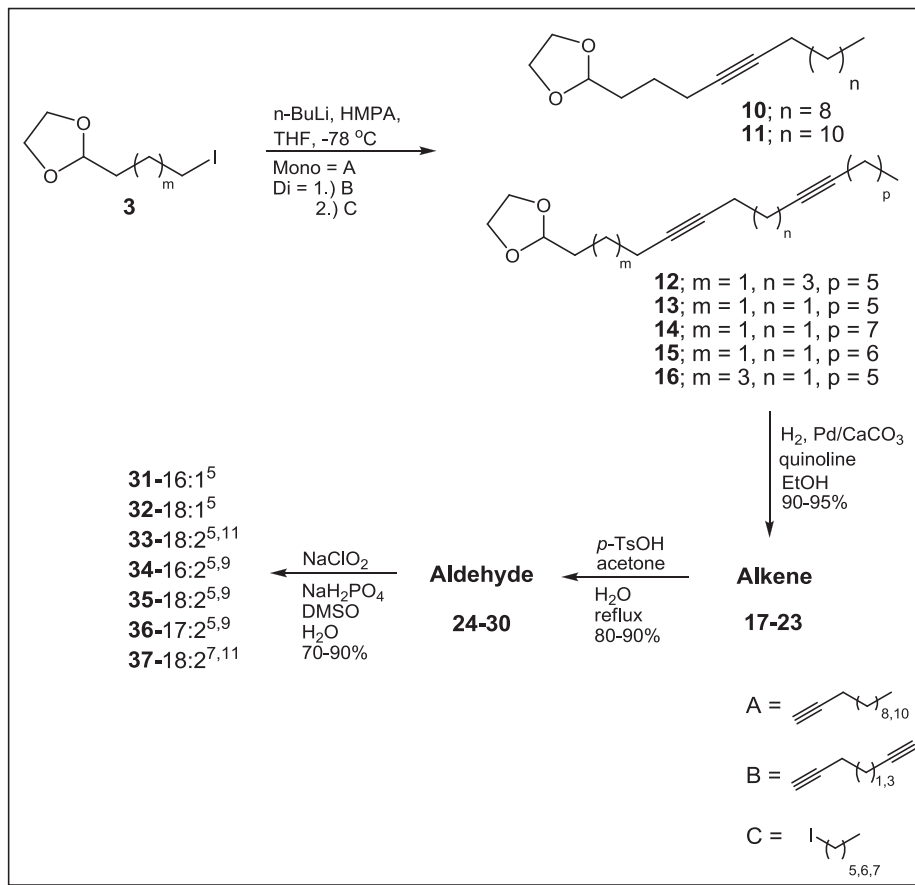


Figure 18. Synthesis of specialized fatty acids.

2.3.2. The fatty acid profile of *D. discoideum*

Upon completion of the synthesis of the fatty acid standards, the endogenous FAs of *D. discoideum* were identified by comparison of the retention time and fragmentation pattern of their derivatized forms (FAMES and FAPys) with the synthesized standards. A representative total ion chromatogram (TIC) from the analysis of FAMES is shown in Figure 19.

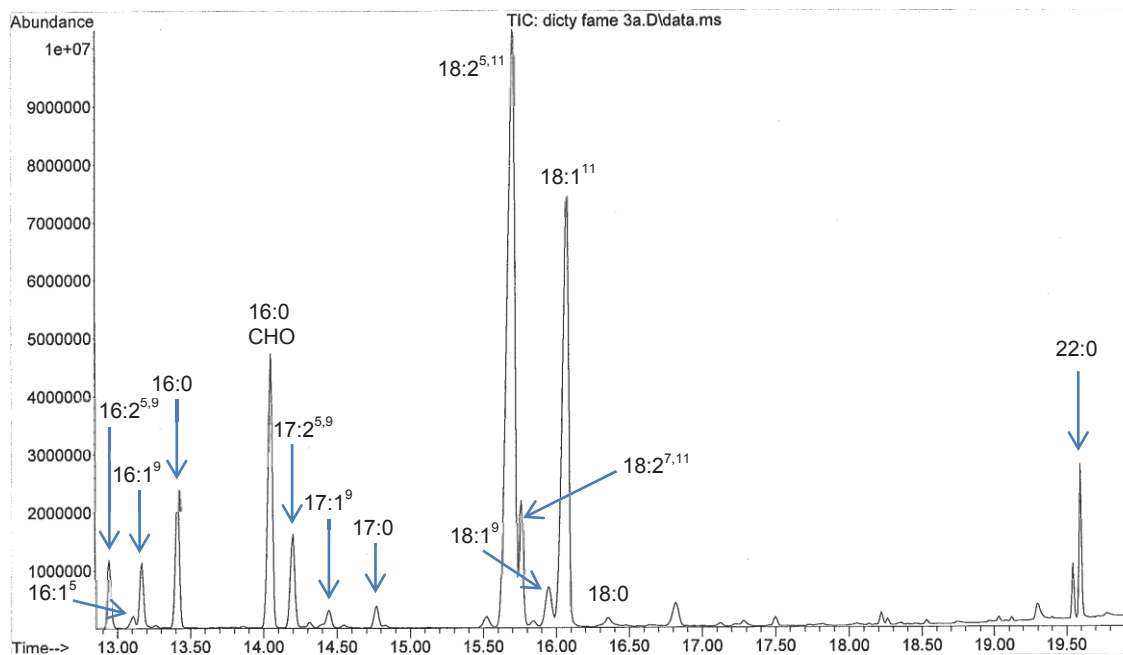


Figure 19. The TIC of the FAMES of *D. discoideum*.

A retention time comparison to synthetic standards is made in Table 2, comprised of the FAs determined to be present in *D. discoideum*. The two standards listed at the bottom denote FAs not found in the profile: 18:1⁵ and 18:2^{5,9}.

Table 2. GC-MS retention time comparison of methyl ester and pyrrolidine derivatized synthetic standards to the FAs found in AX4 *D. discoideum*.

Fatty Acid	FAMES		Pyrrolidines	
	Std RT	D.d. RT	Std RT	D.d. RT
16:2 ^{5,9}	12.964	12.956	27.540	27.530
16:1 ⁵	13.107	13.115	27.892	27.898
17:2 ^{5,9}	14.205	14.205	30.187	30.191
18:2 ^{5,11}	15.657	15.662	32.868	32.874
18:2 ^{7,11}	15.751	15.749	33.430	33.435
18:2 ^{5,9}	15.665	-	32.893	-
18:1 ⁵	15.934	-	33.356	-

As the pyrrolidine derivative provides a more rigorous examination of structural characteristics by mass spectrometry, a comparison of the fragmentation patterns of endogenous and standard FAPys removed any ambiguity presented by slight variances in retention time. Figure 20 underscores the ability to distinguish between isomers by contrasting the fragmentation observed in 18:2^{5,11} and 18:2^{7,11} pyrrolidines.

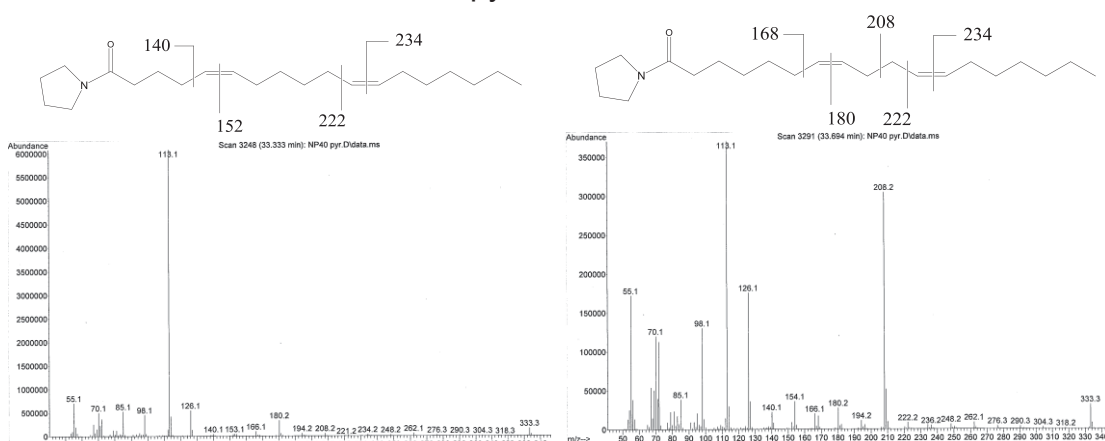


Figure 20. The investigative power of FAPYs in fragmentation-based analysis: contrasting 18:2^{5,11} (left) and 18:2^{7,11} (right).

Generating the fatty acid profile using two separate techniques provided unequivocal characterization, and definitively ruled out the presence of 18:1⁵ and 18:2^{5,9}. The identities of each FA and their percent compositions are presented in Figure 21. The profile was created using the previous work of Blacklock *et al.* (10) and the comparison of synthetic standards. The percent compositions were derived from cell cultures grown axenically to 3.0x10⁷ cells/mL. The percent composition was calculated by obtaining the areas under each peak by integration performed by ChemStation to determine the abundance of each FA. The area of each FA was then divided by the sum of the areas of all FAs (see Equation 1).

$$\frac{\text{Area of FA}}{\text{Sum of areas of all FAs}} \times 100 = \% \text{ composition} \quad (1)$$

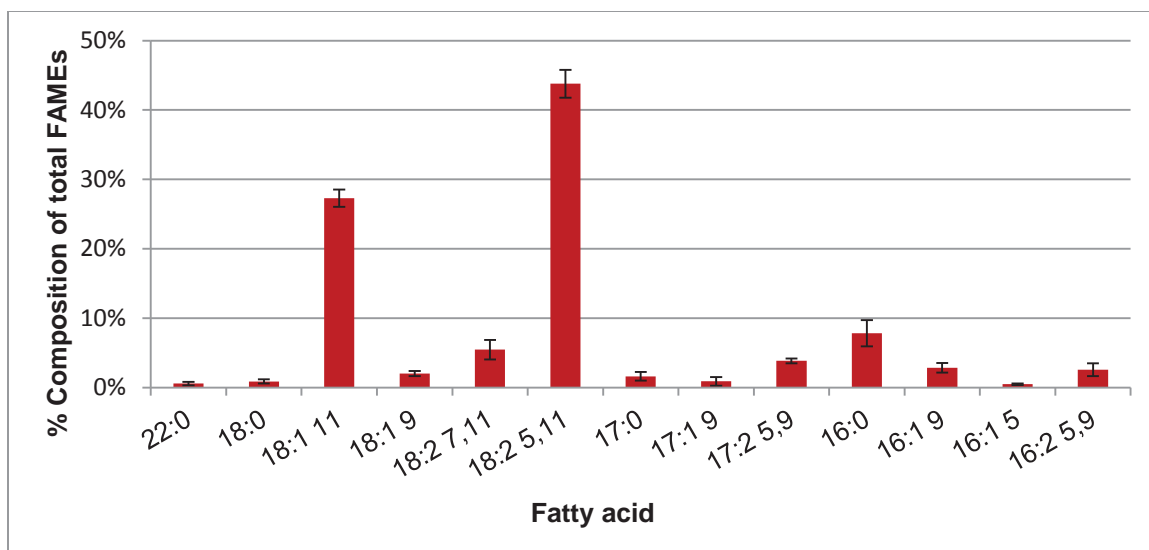


Figure 21. The percent composition of fatty acids of *D. discoideum*.

The vast majority (~70%) of all observed fatty acids is comprised of 18:2^{5,11} and 18:1¹¹. The overall profile of FAs observed in *Dictyostelium discoideum* is as follows: 16:0, 16:1⁵, 16:1⁹, 16:2^{5,9}, 17:0, 17:1⁹, 17:2^{5,9}, 18:2^{5,11}, 18:2^{7,11}, 18:1⁹, 18:1¹¹, 18:0, and 22:0, with trace levels of 20:0 (not shown).

In addition to the collection of saturated and unsaturated FAs, hydroxylated fatty acids were also detected in *Dictyostelium*. Gas chromatographic analysis of these lipids is difficult due to the presence of the hydroxyl group. To reduce the polarity of these compounds, the hydroxyl groups can be silylated to form the corresponding TMS derivative (59). The mass spectrum of a TMS-derivatized hydroxylated C₂₀ FA is shown in Figure 22, representing the most abundant hydroxy FA observed in *D. discoideum*. The molecular ion itself is presented as a relatively weak signal (m/z 414), but two additional pieces of information make this hydroxylated species readily identifiable; strong signals represent the loss of one methyl group of the TMS moiety (m/z 399) and the cleavage between carbons 1 and 2 (m/z 355).

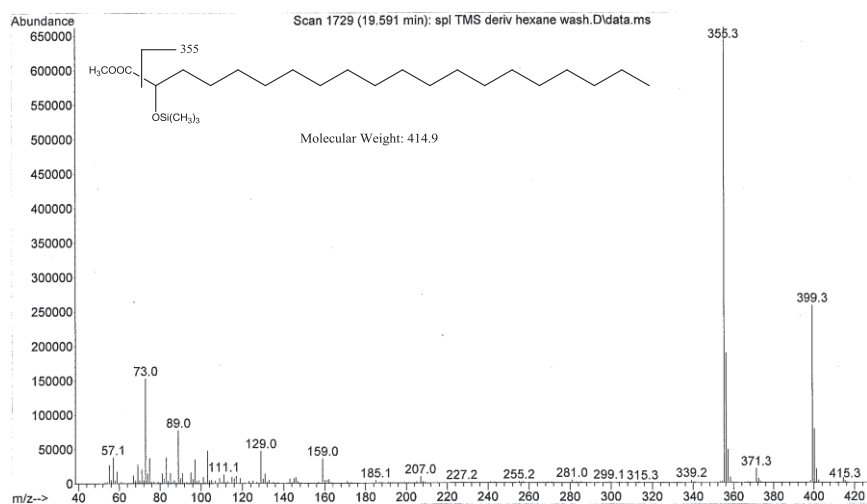


Figure 22. The mass spectrum of TMS-derivatized 2-hydroxy eicosanoic acid (*h20:0*) from *Dictyostelium*.

There were also four α -hydroxy fatty acids detected in much lower abundances than *h20:0*. Comparable concentrations of *h18:0*, *h19:0*, *h21:0* and *h22:0* were observed, which cumulatively accounted for approximately the same amount as *h20:0* alone.

The final component observed in the TIC of *Dictyostelium* FAMES was difficult to identify. This unknown peak eluted between the C_{16} and C_{17} fatty acids at 15.1 min, and its molecular weight did not correspond to any possible FAME. It was not until it began to exhibit incorporation in the feeding experiments of Section 3.3.2. that it became apparent it was potentially a product of fatty acid metabolism. While saturated and monounsaturated fatty acids have an m/z 74 base peak ion, corresponding to a McClafferty rearrangement, the unknown species exhibited a m/z 75 base peak (Figure 23). The weak molecular ion of this species (m/z 285) was only observable when very high sample concentrations were injected, and as a result, the initial characterization of this compound began under the impression that the m/z 255 signal was the molecular ion.

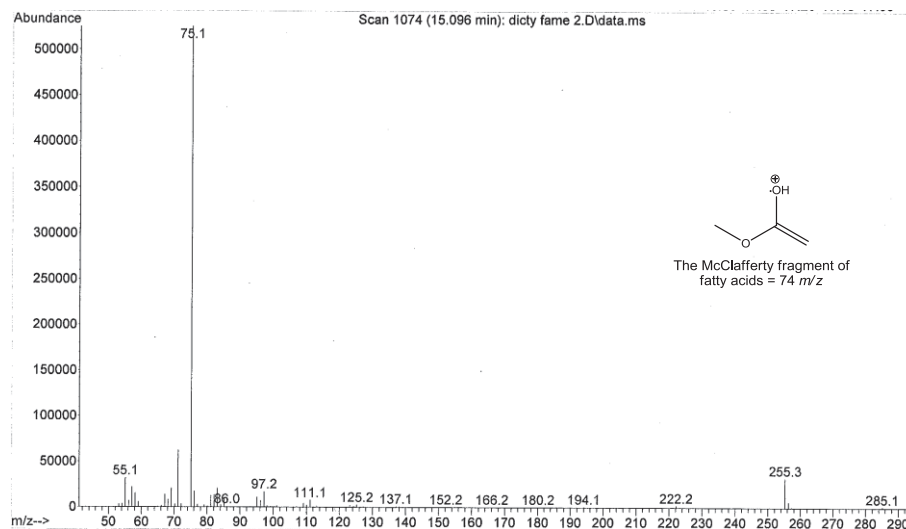


Figure 23. The mass spectrum of the unknown species of *D. discoideum*.

Without knowing the correct molecular ion, no feasible identifications emerged from the data in hand, so a different strategy was employed to provide new information. It was unclear whether the strong base peak was the product of a McLafferty rearrangement (inset Figure 23). If it was, outside of a nitrogen substitution, there was no plausible explanation for a single mass unit difference from the classical m/z 74 McLafferty fragment intrinsic to FAMEs. The methoxy end of a McLafferty fragment derives from the acidic methanol incubation that transesterifies the fatty acid. It was reasonable to suspect that if this m/z 75 base peak was a McLafferty rearrangement product, it also would contain this methoxy group in some fashion. To test whether it was incorporating the methanol-derived methoxy group, the FAME derivatization was modified by substituting deuterated methanol (CD_3OD) as the reacting solvent in 2% d_2 -sulfuric acid. If the base peak was derived from the transesterification reaction, addition of three deuterium should shift it to m/z 78. The results however, were quite perplexing, as the base peak shifted to m/z 81, while the 255 signal only increased to m/z 259 (Figure 24).

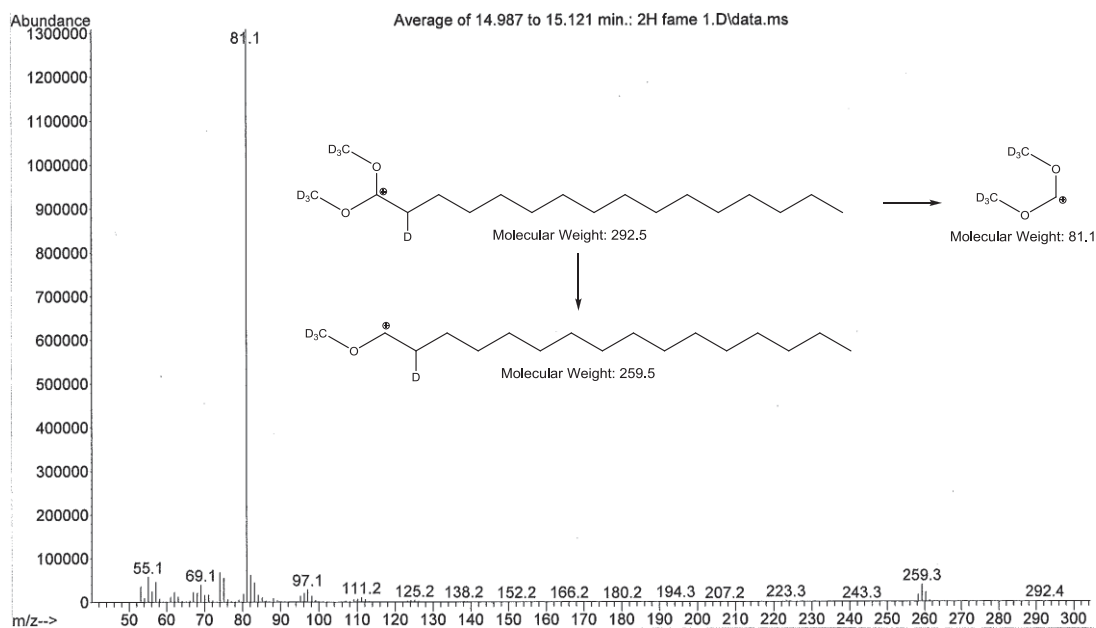


Figure 24. The mass spectrum of the unknown species with CD_3OD reacting solvent.

While the outcome was unexpected, it indicated that this was not a McClafferty product, as somehow two methyl groups were found in the base peak, and if the 255 ion did not increase by m/z 6 as well, then one of the methyl groups must be lost, signifying that it was not in fact the molecular ion. After close examination of the CD_3OD experiment, a m/z 292 ion could be seen, which correlated to a m/z 285 ion in the standard FAME analysis. The cations that correspond to the observed fragments are shown in Figure 25.

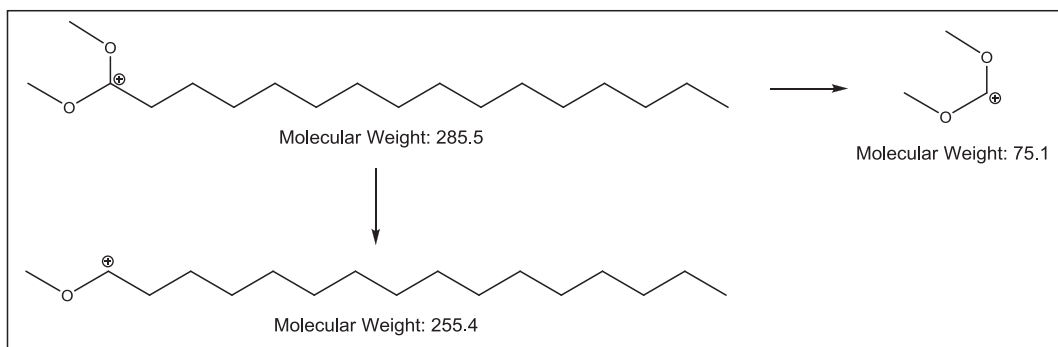


Figure 25. The 16:0 acetal fragments.

Upon reflecting on the possible reactions that could be occurring to form this as the molecular ion, it was determined that the results were consistent with a 16:0 aldehyde. The actual molecule that is being observed upon GC-MS analysis was essentially a “protected” aldehyde, or acetal. The mechanism in Figure 26 contrasts how the acetal seen in Figure 25 is produced upon incubation with acidic methanol, with the fatty acid methyl ester that is released from a complex lipid.

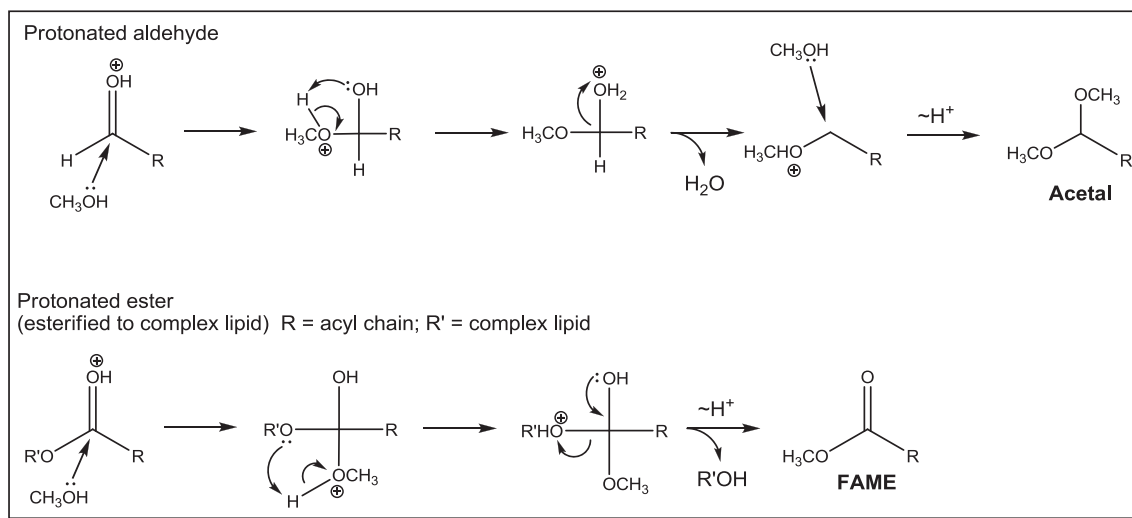


Figure 26. The mechanisms of FAME and acetal formation.

The reactions proceed in much the same manner except that only one esterification occurs when FAMEs are generated because the complex lipid acts as a good leaving group. As the aldehyde has no such leaving group, the hemiacetal is susceptible to a second nucleophilic attack by methanol, generating the acetal. The presence of aldehydes is a curious discovery in biological terms. Free aldehydes have been described in the waxes which cover the organs of plants (60), but it may be more plausible to suspect that the aldehyde is formed as the result of cleavage of a vinyl ether from a complex lipid (structure in Figure 27).

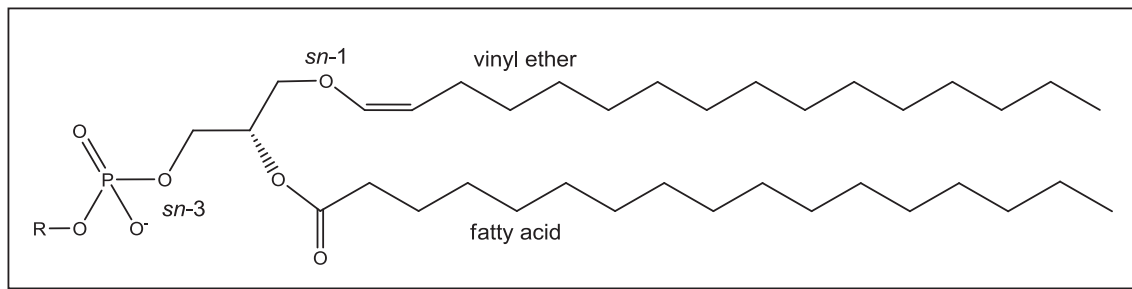


Figure 27. Example of an ether lipid.

Ether lipids are a form of complex lipid with a polar head group attached to a glycerol backbone with either *O*-alkyl or *O*-alk-1-enyl ether attachments (as well as fatty acids). Those possessing the alkene moiety have a *cis* double bond at carbon 1 (adjacent to the ether linkage) and are referred to as vinyl ethers (61). Typically, only the *sn*-1 position is ether linked, commonly with 16:0, 18:0, and 18:1 chains. Furthermore, vinyl ethers are known to yield aldehydes during acidic transesterifications, and such lipids are found in animals and are minor components in several higher plants (61). This is a plausible complex lipid structure that would result in the release of an aldehyde upon incubation in acidic methanol, and a mechanistic reasoning to support this statement can be seen in Figure 28.

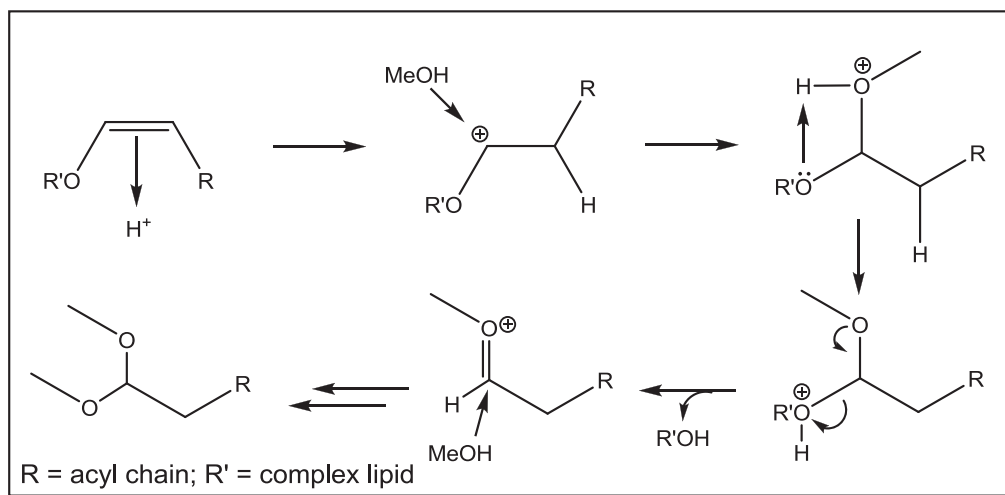


Figure 28. The mechanism of aldehyde release from a vinyl ether.

In summary, five α -hydroxy fatty acids were detected in the AX4 strain *D. discoideum*. Comparable concentrations of *h18:0*, *h19:0*, *h21:0* and *h22:0* were observed, accounting for approximately 50% of the hydroxy FAs, while *h20:0* encompassed the remaining 50%. Three aldehydes were also found in their dimethoxy acetal forms, likely originating from vinyl ethers. The 16:0 species was present in comparable levels to that of the 16:0 FAME, along with traces of 18:0 and 18:1. The remainder of the FA profile was composed of the fatty acids 16:0, 16:1⁵, 16:1⁹, 17:0, 17:1⁹, 16:2^{5,9}, 17:2^{5,9}, 18:2^{5,11}, 18:2^{7,11}, 18:1⁹, 18:1¹¹, 18:0, 20:0 (trace) and 22:0, with 18:2^{5,11} and 18:1¹¹ comprising approximately 70% of the content.

CHAPTER 3. FATTY ACID METABOLISM IN *DICTYOSTELIUM DISCOIDEUM*

3.1. Introduction

With a fatty acid profile in place, the focus of research shifted towards elucidating the metabolic pathway by which *D. discoideum* FAs are biosynthesized by supplementing cultures with deuterium-labeled fatty acids. This work was pursued with particular interest in the generation of 18:2^{5,11} and 18:1¹¹, which make up the majority of the FAs in *Dictyostelium*. This profile differs from plants, which have high levels of Δ^9 and Δ^{12} unsaturated FAs (62, 63). The process of developing a fatty acid metabolic pathway for *Dictyostelium* involved deducing the possible cascade(s) of enzymatic reactions that could generate the array of fatty acid products observed in the profile from 16:0 and 18:0. A hypothetical metabolic pathway was conceived based upon the FA profile and known *Dictyostelium* enzymes (10, 13, 53, 64, 65), in order to begin to limit the number of practical paths and provide a general outline for how these products may be formed (Figure 29). The inclusion of the Δ^{11} desaturase pathway was purely hypothetical; however, the extremely high levels of Δ^{11} unsaturated fatty acids in the profile begs the question of whether a portion of these pools could be attributed to such an enzyme.

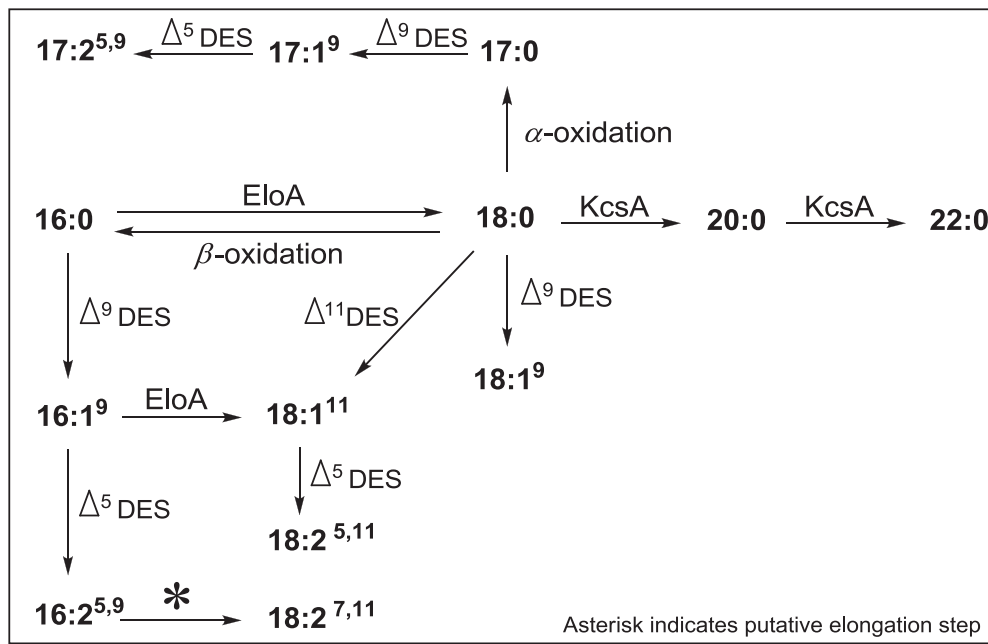


Figure 29. The hypothetical fatty acid metabolic pathway for *D. discoideum*.

To test this hypothetical metabolic pathway, several deuterium-labeled fatty acids were synthesized. It has become common to use deuterated lipids as stable isotopically labeled precursors for metabolic studies (66). The deuterium label is easier to analyze than spin labels used in NMR experiments or fluorescent handles, whose properties may change as they travel through biological processes or are incorporated into other lipids (66). By engineering fatty acids substituted with strategically placed deuterium atoms for supplementation to *D. discoideum* in culture, *in vivo* studies could be performed, and the host of enzymatic modifications that yield the FA profile could be observed via mass spectrometry. Three saturated fatty acids were designed for synthesis: stearate- d_5 (**49**) and palmitate- d_5 (**50**), with five deuterium substitutions at the methyl end of the molecule; and a stearate- d_4 (**55**) containing substitutions at the β and γ carbons respective to the carbonyl. In addition, two unsaturated FAs were generated: 18:1⁵- d_7 (**74**) and 18:1¹¹- d_7 (**81**), with deuterium substitutions at carbons 16-18. The various locations of deuterium on the

aliphatic chains allowed us to investigate specific events that may take place in fatty acid metabolism in *D. discoideum*. The synthetic scheme for developing d_5 -stearate and d_5 -palmitate paralleled the syntheses of the unlabeled fatty acids that were utilized as standards, with modifications to the precursor chain length to accommodate alkylation by a d_5 -labeled alkyl bromide chain.

3.2. Methods and materials

In vivo feeding studies were conducted using 50-mL shaking cultures set in 250-mL autoclaved flasks containing HL5 and pen/strep, with the inclusion of 0.5-mM labeled FA substrate and 1% NP40 (tergitol) detergent. Feeding stocks were heated to solubilize the FA and then filter sterilized (25mm/0.2 μ m). Inoculations were made from a starter culture such that all experiments were inoculated at 1.0×10^6 cells/mL and shaken (180 rpm) at 22 °C for the prescribed time period (6, 12, 24, 48, 72 h). Upon completion, cells from the 50-mL cultures were isolated by centrifugation at 450g to remove media, and washed by vortexing with three 1% NP40 washes and centrifugation at 450g (repeated 3x), followed by a 4th wash with nanopure H₂O. FAMES were prepared from the cellular pellet and analyzed as described. Cultures were set in triplicate and analyzed at 6, 12, 24, 48 and 72 h of incubation, for a total of 15 cultures per compound. Experimental protocols for the synthesis of deuterium-labeled fatty acids can be found in Section 5.3.

3.2.1. Calculation of incorporation levels

Data obtained by GC-MS was processed in two ways. The first examined the results in terms of the ratio between ion abundances of deuterium labeled products relative to non-labeled materials (percent incorporation-Equation 2), while the second expresses the results in terms of the percent composition of labeled compounds (Equation 4).

$$\frac{\text{Abundance of } (d_5 \times CF) \text{ FA}}{\text{Abundance of } d_0 + (d_5 \times CF) \text{ FAs}} = \% d_5 \text{ incorporation} \quad (2)$$

To compensate for the lack of isotopic specificity in the d_5 compounds, a correction factor (CF) was derived from the subtraction of the M+1 and M+2 ion counts for the natural abundance values from the summation of the entire range of isotopic products from GC-MS analysis of the fed synthetic fatty acids to define the d_5 ion abundance had scrambling not occurred. Using the results from GC-MS analysis of 18:0- d_5 and 16:0- d_5 FAMES, the 18:0- d_5 experiment required a correction factor of 4.36 to offset the deuterium scrambling while the 16:0- d_5 experiments employed a correction factor of 3.30.

$$\frac{(d_1+d_2+d_3+d_4+d_5+d_6+d_7+d_8)-[M+1]-[M+2]}{d_5} = CF \quad (3)$$

The second method in which the GC-MS data was analyzed expresses the results in terms of the percent composition of labeled compounds, which was calculated by taking the percent incorporation value obtained via Equation 2 and multiplying it by the sum of the areas under the curve of both labeled and unlabeled species (Equation 4). The analysis must be done in this manner because in many cases the labeled species coelute with the endogenous FAs such that the two peaks cannot be individually integrated. The result of this calculation is the percent composition of labeled material with respect to the total of each fatty acid product.

$$\% d_5 \text{ incorporation} \times (\text{areas of } d_5 + d_0 \text{ FA}) = \% \text{ composition of } d_5 \text{ FA} \quad (4)$$

The d_4 product percent incorporations were calculated in a manner analogous to the d_5 experiments, with one exception. As in this experiment both d_2 and d_4 products were observed, the abundance of both products was included in the denominator of the equation to attain the percent incorporation of d_4 label. Additionally, as the [M+2] natural abundance of ^{13}C isotope originating from

endogenous fatty acids contributes to the abundance of any d_2 ions, it must be subtracted, respective of the number of carbons, as seen in Equation 5. The [M+2] natural abundance varies based upon the number of carbons in the chain. For example, a C_{18} chain has an [M+2] value that is 1.8% the abundance of the molecular ion, while a C_{16} compound has a value of 1.4%. It was not necessary to account for deuterium scrambling in this experiment.

$$\frac{\text{Abundance of } d_4 \text{ FA}}{\text{Abundance of } d_0 + (d_2\text{-natural abundance}) + d_4 \text{ FAs}} = \% d_4 \text{ incorporation} \quad (5)$$

The calculation for d_2 percent incorporation analysis was conducted in a similar fashion (Equation 6).

$$\frac{(\text{Abundance of } d_2\text{-natural abundance}) \text{ FA}}{\text{Abundance of } d_0 + (d_2\text{-natural abundance}) + d_4 \text{ FAs}} = \% d_2 \text{ incorporation} \quad (6)$$

3.2.2. Statistical analysis

A rigorous statistical evaluation of the incorporation results was performed (student t-test) in order to determine the statistical significance of incorporation trends. This statistical test takes two sets of data (two incubation periods), calculates the average, variance and standard deviation between them to determine whether the mean average of two sets of data are statistically different. For this analysis, the t-test helped to distinguish the actual trends in the incorporation results by determining which changes in percent incorporation were truly significant. A null hypothesis must be selected to weigh the incorporation values against; this analysis assumed there was no difference exists between the two sets. A p-value describes the probability that the null hypothesis is true; this value was selected as $p < 0.05$ (less than a 5% chance that it is true). This value sets the threshold for determining whether two data sets are statistically different or not.

3.3. Results and discussion

3.3.1. Synthesis of deuterium-labeled fatty acids

In the synthesis of 16:0 and 18:0 d_5 -labeled molecules, a dioxolane-protected alkyl iodide precursor was alkynylated and alkylated with a deuterated precursor producing the target chain length. First, the C₈ dioxolane (**40**) was alkynylated with either 1,7-octadiyne or 1,5-hexadiyne, leading to **41** and **42** respectively (Figure 30). The corresponding C₁₄ and C₁₆ diacetylenes were then alkylated with ethyl bromide- d_5 in the presence of NaI to complete the C₁₆ and C₁₈ chains. To generate the saturated chains for palmitate and stearate, the alkynes were fully reduced with palladium on carbon under a hydrogen atmosphere followed by deprotection and oxidation, as previously described.

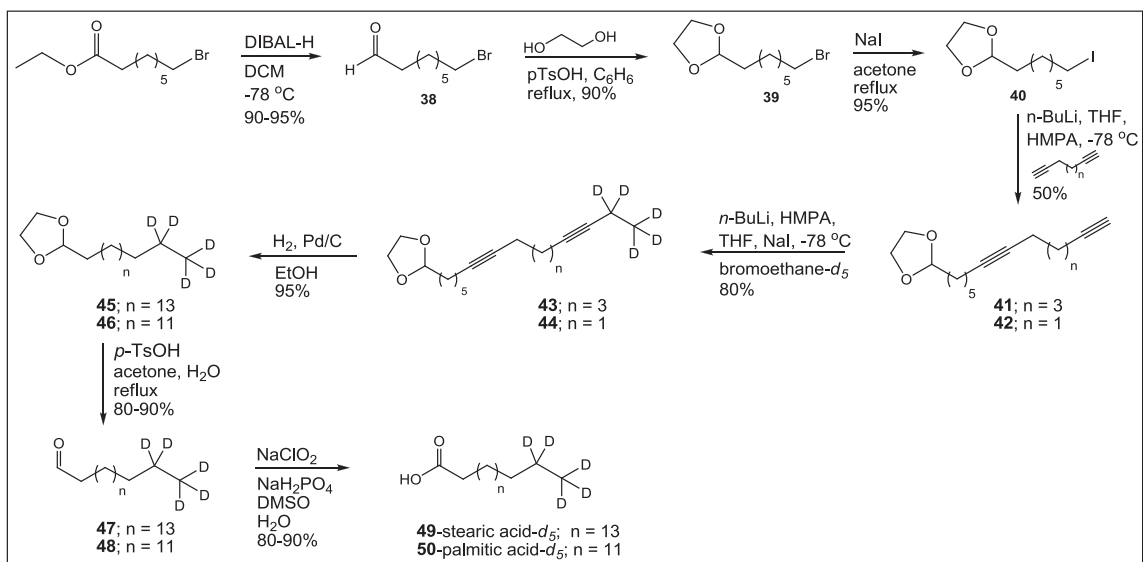


Figure 30. The synthetic pathway for producing stearic acid- d_5 (**49**) and palmitic acid- d_5 (**50**).

The synthetic pathway (Figure 31) that was developed to generate d_4 -stearate (**55**) was distinct from the previous approaches. While a malonate-mediated strategy was initially considered, a pathway was chosen that combined the acetylide coupling methodology of previous FA syntheses with a

methoxymethyl (MOM) ether protected alkyne (**51**) that had been previously synthesized by Michael Shepard of the Minto research group to generate an 18 carbon alkyl chain.

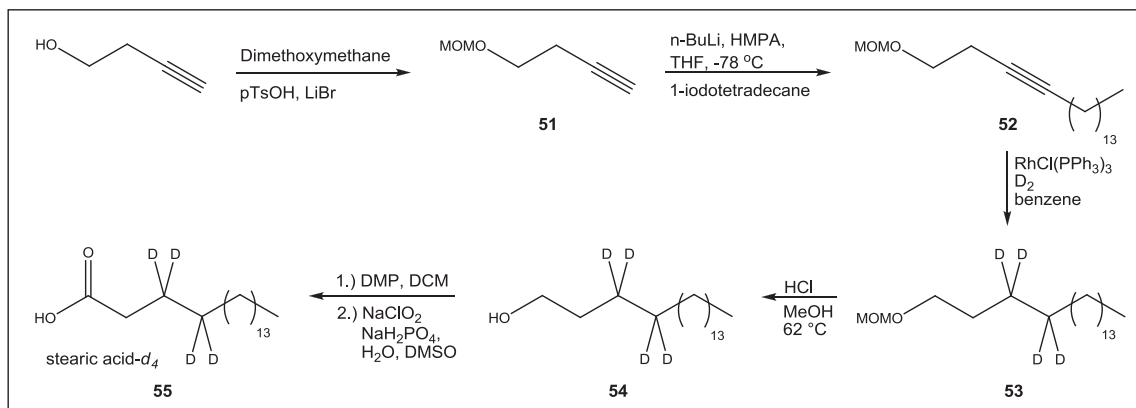


Figure 31. The synthetic scheme of [3,3,4,4- d_4] stearic acid (**55**).

In the synthesis of **55**, **51** served to place an alkyne between the β and γ carbons, which could be alkylated with a long alkyl halide to create an 18 carbon chain. The premise of this approach was that a β , γ -alkynyl group at this position could be catalytically reduced with deuterium gas, inserting the label at the desired 3 and 4 positions without scrambling. The protection and alkylation steps were straightforward and **52** was readily obtained in high yield (Figure 31). However, it was considerably more challenging to selectively add deuterium across the alkyne during reduction to its corresponding alkane.

As the d_5 -compounds were synthesized first, this lack of isotopic purity (scattering) was observed during GC-MS analysis as well, but was initially dismissed as ionization-induced rearrangement upon exposure to the harsh environment of an electron impact source. However, upon realization that this Boltzmann-like distribution of masses (Figure 32) would not allow the interpretation of the results of the d_4 experiment, work commenced to determine if this was indeed the product of source-induced deuterium scrambling. A previously synthesized deuterium labeled fatty acid, 18:2 9c,15c (**56**; Section 5.4),

which had been reduced by Lindlar's catalyst was analyzed by GC-MS, with the surprising result that a single molecular ion was observed. This indicated that the problems lay within the synthesis, not the ionization source.

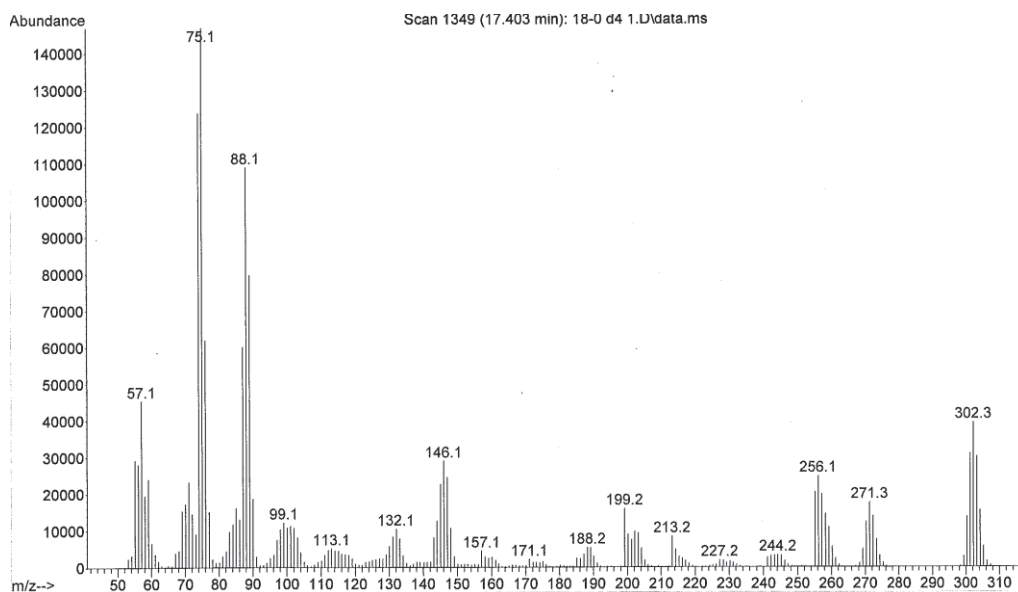


Figure 32. Mass spectrum of the 18:0- d_4 (**55**) FAME derivative using 10% palladium on carbon and D_2 for alkyne reduction; $[M^+]$ m/z 302.

It was discovered that the catalyst for the reduction step used to generate **49** and **50** (palladium on carbon) was not capable of yielding an alkane with the degree of isotopic purity necessary to be able to interpret the results of the feeding study. Metal catalysts for hydrogenation reactions such as palladium and platinum have the propensity to locally redistribute hydrogen (and deuterium) within a molecule by 1,3-hydride shifts (67, 68). While this is imperceptible in alkyne reductions with H_2 , attempting to label a protonated compound with deuterium yields a considerable amount of scrambling, as can be seen in Figure 32. The mass spectrum illustrates the various isotopic products that were formed. Although the desired d_4 product (m/z 302) is the most abundant, isomeric products ranged from d_0 (m/z 298) all the way to d_8 (m/z 306).

An improved strategy for reducing the alkyne **52** used Wilkinson's catalyst, as outlined by Rakoff and Rohwedder (68). Their work demonstrated that this rhodium-based catalyst could selectively introduce deuterium to an alkyne resulting in an isotopic purity of up to 96%. In contrast to Figure 32, the resulting mass spectrum in Figure 33 shows considerably less scattering in the final 18:0- d_4 fatty acid.

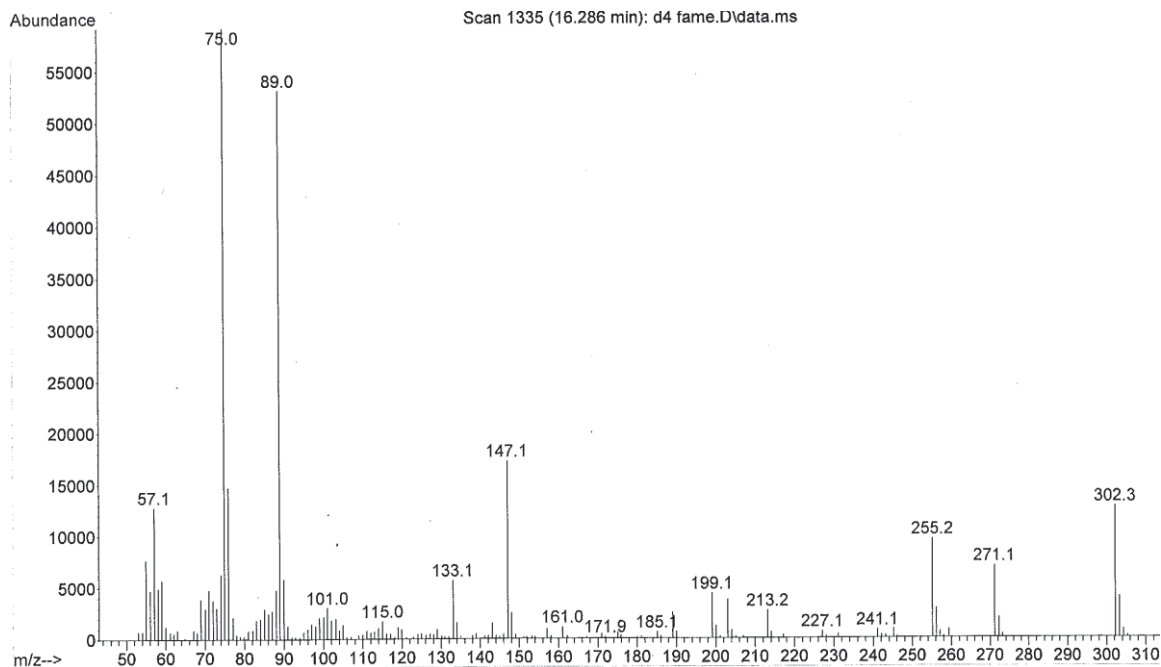


Figure 33. Mass spectrum of the 18:0- d_4 (**55**) FAME derivative using Wilkinson's catalyst and D_2 for alkyne reduction; $[M^+] = 302$ m/z .

While these conditions allowed for the synthesis of **53** with an isotopic purity of approximately 97% d_4 -product (2% d_3 -product, 1% d_5 -product), the reaction did not reach full conversion within 48-72 h (~80% alkane), despite the 3 h reaction time denoted by Rakoff and Rohwedder (68). After isolating the material and subjecting it to a second reaction, the remaining alkyne was consumed in 2 h. The yield of **53** was reduced to 81% as a result of performing two workups and purifications. However, during the silica-gel purification, an inseparable contaminant was discovered by GC-MS that paralleled the R_f of **53**.

The impurity was carried forward in the expectation that it would become separable once the desired material had been converted to the final carboxylic acid. Upon hydrolysis by heating in methanol and 2% HCl (**57**), conversion to the aldehyde using Dess-Martin periodinane (**69**), and sodium chlorite oxidation (**58**), the final oxidation yielded **55**. After flash chromatography, the impurity from the Wilkinson's catalyst reduction was concentrated to an oily yellow substance, and identified by Chemstation software as methyl 6,8-dodecadienyl ether (NIST 08 Mass Spectral Library), presumably a rearranged side-product resulting from the dimethoxymethane protection group falling off during the reduction. The low yield of **55** (43% yield) is not a result of poor NaClO₂ oxidation, which has consistently generated 80-90% yields, but a reflection of the side reaction during the reduction.

The final pair of labeled species that was developed were the unsaturated FAs 18:1⁵-*d*₇ and 18:1¹¹-*d*₇. Outlines of the manipulations that were employed to yield these two fatty acids are depicted in Figures 34 and 35. 18:1⁵-*d*₇ was stitched together with three 6-carbon units. First, 5-hexyn-1-ol was protected with dimethoxymethane to yield **65**. This protected alkyne was coupled to the commercially available halide, bromohexane-4,4,5,5,6,6,6-*d*₇, in the customary fashion. The internal acetylene of this twelve carbon product was reduced by Wilkinson's catalyst and hydrogen gas to yield **67**. The reaction halted at about 80% conversion and it was necessary to resubject the material to a second reaction to complete the reduction. The saturated intermediate **67** was subsequently deprotected and converted to the alkyl bromide **69** through exposure to triphenylphosphine and bromine, in preparation for its coupling to a second **65** molecule. The resulting C₁₈ chain **70** was reduced again, this time with Lindlar's catalyst and H₂ to afford a *cis* alkene at carbon 5. The MOM group of **71** was then hydrolyzed and the primary alcohol converted to the carboxylic acid under the previously described Dess-Martin periodinane and sodium chlorite oxidative conditions, to yield 18:1⁵-*d*₇ (**74**).

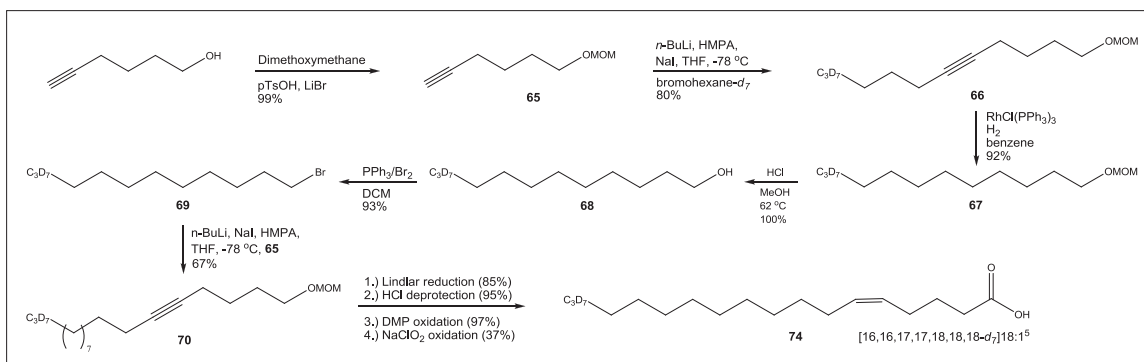


Figure 34. The synthetic approach utilized to afford 18:1⁵-d₇.

To procure 18:1¹¹-d₇, groundwork began with the MOM protection of bromodecanol (Figure 35). In preparation for coupling the resulting alkyl bromide with bromohexane-*d*₇, **75** was alkynylated with a TMS-acetylene, followed by cleavage of the TMS group with TBAF to yield **76**. After alkylation of the labeled chain, **77** was reduced with Lindlar's catalyst, leading to a Δ¹¹ *Z*-alkene. The alkene **78** was deprotected and oxidized to complete the 18:1¹¹-d₇ fatty acid.

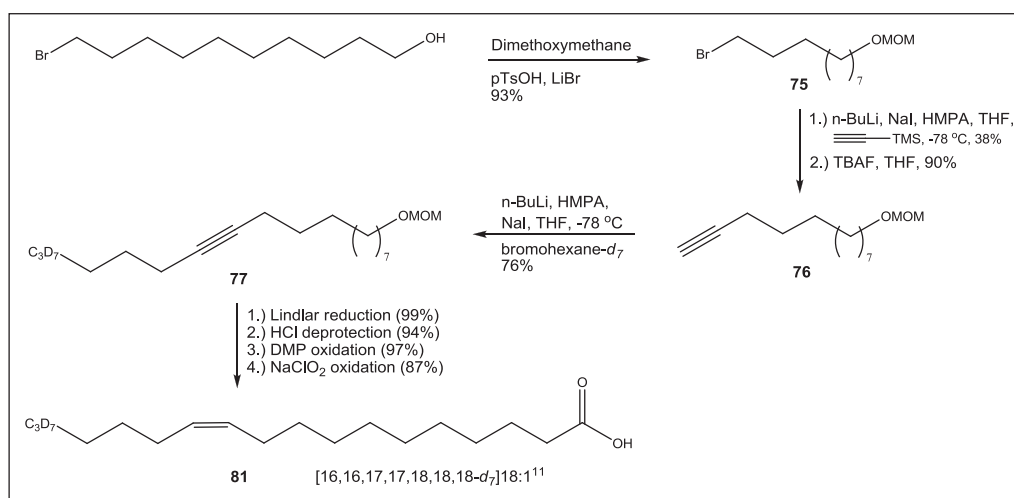


Figure 35. The synthetic methodology of producing 18:1¹¹-d₇.

3.3.2. *In vivo* feeding studies

The five deuterium-labeled fatty acids were supplemented to *D. discoideum* cultures, in which they were incorporated into the endogenous FA pools, and became substrates for elongation, oxidation, and desaturation. The labeled metabolic products from *Dictyostelium* were analyzed by preparing FAMES from cell cultures and calculating the percentage of each labeled FA relative to its endogenous counterpart. By monitoring the incubations at specific intervals, the flux of the labeled substrate through FA metabolism was observed.

3.3.2.1. *In vivo* studies: stearate- d_5 and palmitate- d_5

By feeding 16:0- d_5 and 18:0- d_5 , the ensuing reactions could be monitored from both the 16:0 perspective, as well as through the 18:0 channel. The experiments relied on the difference of 5 m/z units between the deuterium-labeled supplemented FAs and endogenous unlabeled FAs to follow the newly biosynthesized products by GC-MS analysis. An example of the GC-MS results of the 18:0- d_5 supplementation for 24 h is shown in Figure 36, displaying the total ion chromatogram (A) with mass data from the 16:0 peak between 14.36 and 14.52 min (B). The mass spectrum shows the endogenous 16:0 FAME (m/z 270) and the isotopic distribution associated with the d_5 labeled 16:0 product (β -oxidized from 18:0- d_5). The d_5 -products elute slightly before the endogenous FAs, as observed in the split 18:2^{5,11} peak.

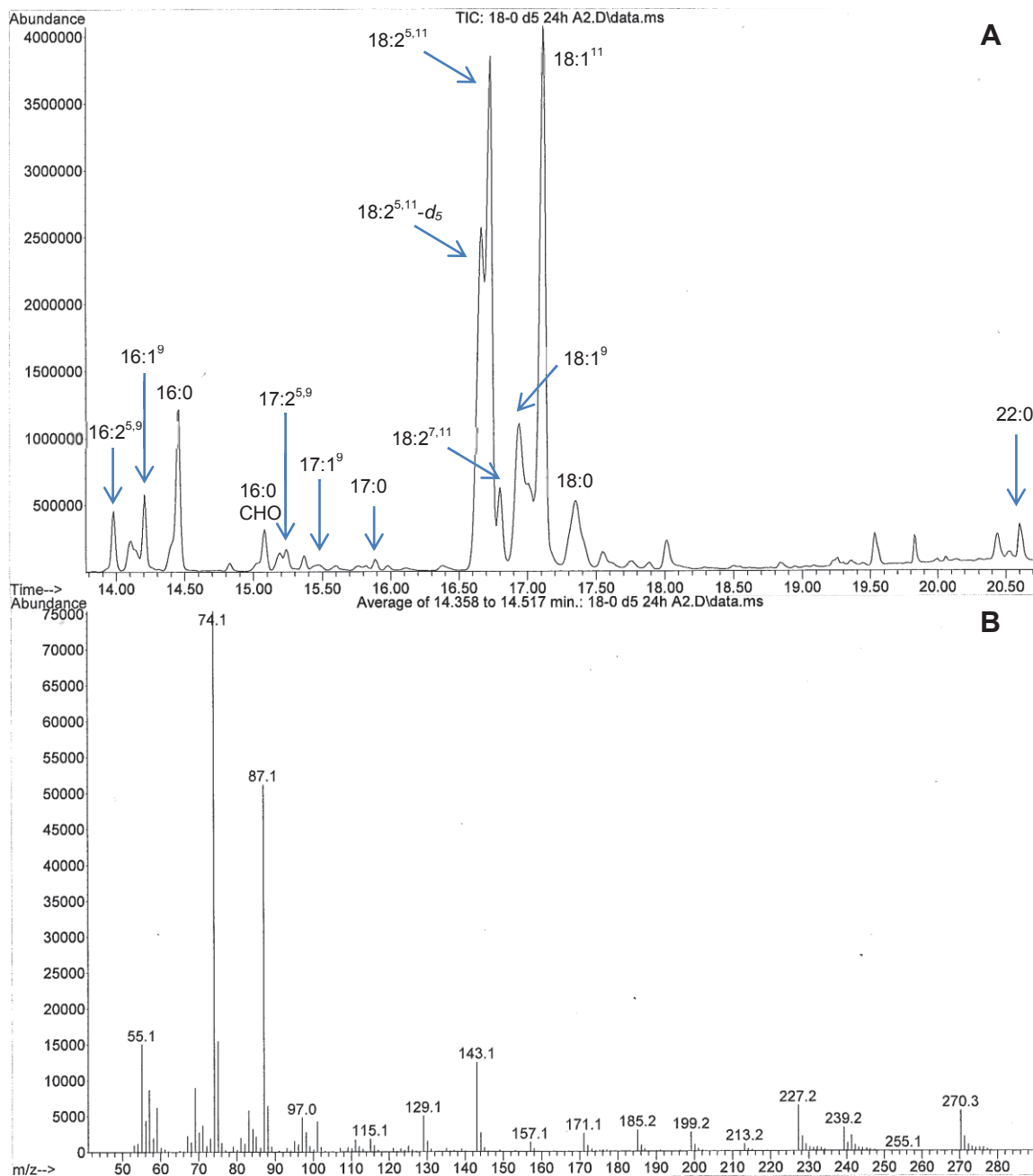


Figure 36. The total ion chromatogram (A) from supplementation with 18:0-*d*₅ and the mass spectrum of the resulting 16:0 FAME product (B).

The data obtained by GC-MS was processed in two ways. The first examined the results in terms of the ratio between ion abundances of deuterium labeled products relative to non-labeled materials (percent incorporation-

Equation 2), while the second expresses the results in terms of the percent composition of labeled compounds (Equation 4). The percent incorporation method illustrates the order and efficiency in which the processes of elongation, desaturation and oxidation occurred with the supplemented FA. Figures 37 and 40 summarize the percent incorporation results of stearate- d_5 and palmitate- d_5 feeding studies.

In the figures that describe percent incorporation (Figures 37, 40, 45 and 47), asterisks that are located below the percent incorporation bars indicate a p-value of 0.05 or less. Therefore, the time periods marked with asterisks designate those that have incorporation results with greater than a 95% probability of being different than those of the previous time period. For example, if an asterisk is present below the 24 h incubation period, it can be said with 95% confidence that its percent incorporation was statistically different from the 12 h results.

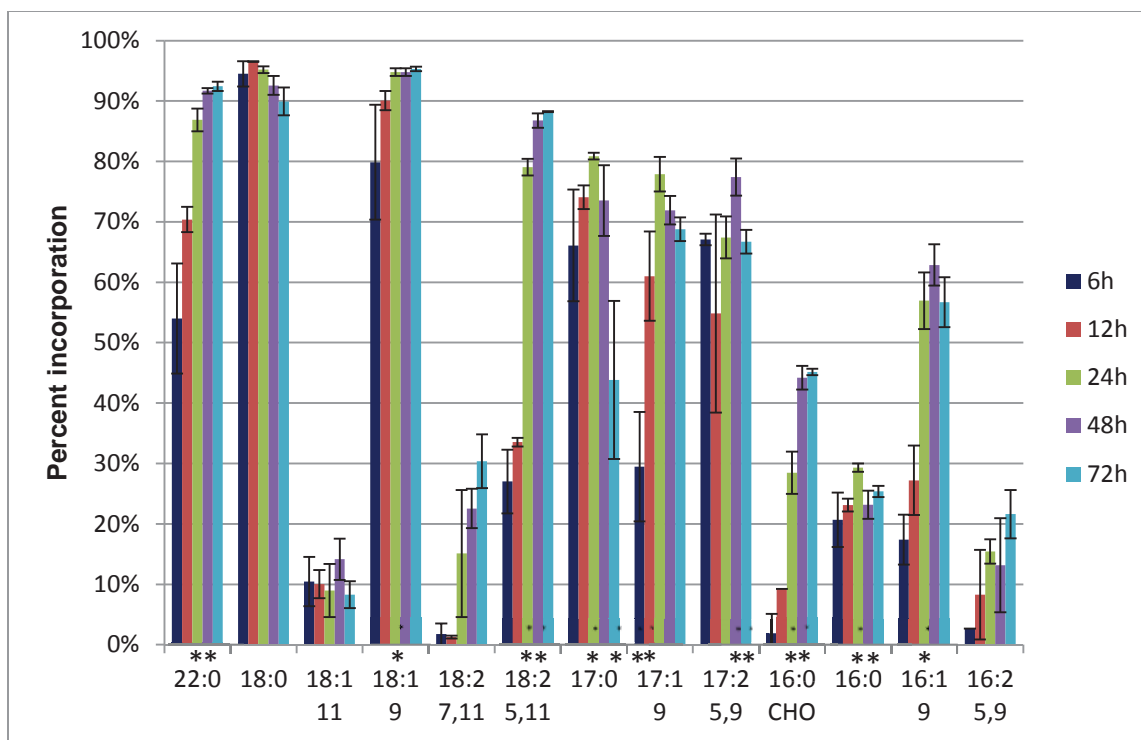


Figure 37. Time course of the percent incorporation of d_5 label into FA products after supplementation with 18:0- d_5 and 1% NP-40.¹

The analysis of the percent incorporation of d_5 label from supplementation with 18:0- d_5 supplied a large abundance of information regarding the fatty acid metabolism in *D. discoideum*. As Figure 37 demonstrates, the labeled substrate was quickly taken up by the cells, as the introduction of label into newly synthesized fatty acids was observed after 6 h, with several of those labeled products having already achieved greater than 50% incorporation (22:0, 18:1⁹, 17:0, 17:2^{5,9}). It was apparent that the elongation of 18:0 to VLCFAs in *D. discoideum* was quite active. Within the initial 6 h incubation interval, the 18:0- d_5 substrate had been elongated to such a degree that labeled material comprised over 50% of the total 22:0 composition. While trace quantities of 20:0 exist in *D. discoideum*, it appears the 20:0 elongation product was almost immediately

¹ Data is presented as the mean percent incorporation of labeled fatty acids \pm standard deviation; n=3. Asterisks located below the percent incorporation bars indicate a p-value of 0.05 or less.

subjected to a second elongation, as incorporation into 20:0 was below the detection limits of the GC-MS. The Δ^9 desaturase enzyme of *D. discoideum* was also active, as it converted 18:0- d_5 to 18:1⁹- d_5 at a rate that rendered nearly 80% of all 18:1⁹ FAs as the d_5 -product after only 6 h incubation. It appeared that α -oxidation of the 18:0 substrate also occurred, as the 17:0 species contained approximately 70% of the d_5 label at the 6 h interval.

β -Oxidation, as determined by the formation of 16:0- d_5 , appeared to take place more gradually, as the percent incorporation did not greatly deviate over 72 h from the 20% incorporation observed at 6 h incubation, to ~30% between 24 and 72 h. This may be interpreted as *Dictyostelium* funneling regulated quantities of stearate down the β -oxidation pathway to maintain a 16:0 pool as the precursor for other reactions. Following the initial reactions that take place directly from the 18:0- d_5 substrate, it was evident that a large portion of the newly formed 16:0- d_5 was a substrate for a Δ^9 desaturase, as demonstrated by the increasing levels of 16:1⁹- d_5 over 72 h. Upon further incubation, 16:2^{5,9}- d_5 (the apparent product of Δ^5 desaturation of 16:1⁹) began to rise notably at the 12 and 24 h marks. Following the initiation of 16:2^{5,9}- d_5 production, the abundance of its elongation product, 18:2^{7,11}- d_5 , could be seen growing in at the 24 and 48 h marks.

While 18:1¹¹ has been demonstrated to be the EloA-catalyzed elongation product of 16:1⁹ (10), there was no clear labeling pathway that outlines its formation in *Dictyostelium*. Based on Figure 37, its incorporation of 18:0- d_5 into 18:1¹¹- d_5 behaved similarly to 16:0 in that it is present at a rather consistent ~10% incorporation of the total 18:1¹¹ fatty acid content throughout the time course, despite the fact that incorporation 18:2^{5,11} approached 90%. It is possible that 18:1¹¹ is an excellent substrate for a Δ^5 desaturase (FadA or FadB), and is immediately converted into 18:2^{5,11}. Alternatively, these results may suggest that the pool of 18:1¹¹ is being directly produced from 18:0 (at least in part) through a Δ^{11} desaturase. If such a desaturase exists, it could be

responsible for the production of one of these fatty acids, while the other may be produced via a separate pathway.

The gradual incorporation of d_5 label into the 16:0 aldehyde did not give any clear indication of its origins. A plausible scenario is that *D. discoideum* contains some form of a carboxylic acid reductase that converts the 16:0 fatty acid to its reduced aldehyde state (only observed in bacteria (70)), or from incorporation into a C₁₆ vinyl ether lipid. No additional information could be derived regarding the formation of 17:1⁹ and 17:2^{5,9}. These FAs are presumed to be the products of Δ^5 and Δ^9 desaturases, but the d_5 -labeling strategy cannot unequivocally confirm the substrate that gives rise to them. Finally, while 16:1⁵ is likely produced from 16:0 via a Δ^5 desaturase (53, 64, 71), it was not included in the analysis because any incorporation of the d_5 label was below the detection limits of the GC-MS. The 16:1 d_5 incorporation product was identified as 16:1⁹ by analysis of fatty acid pyrrolidines from the supplemented cultures (Figure 38).

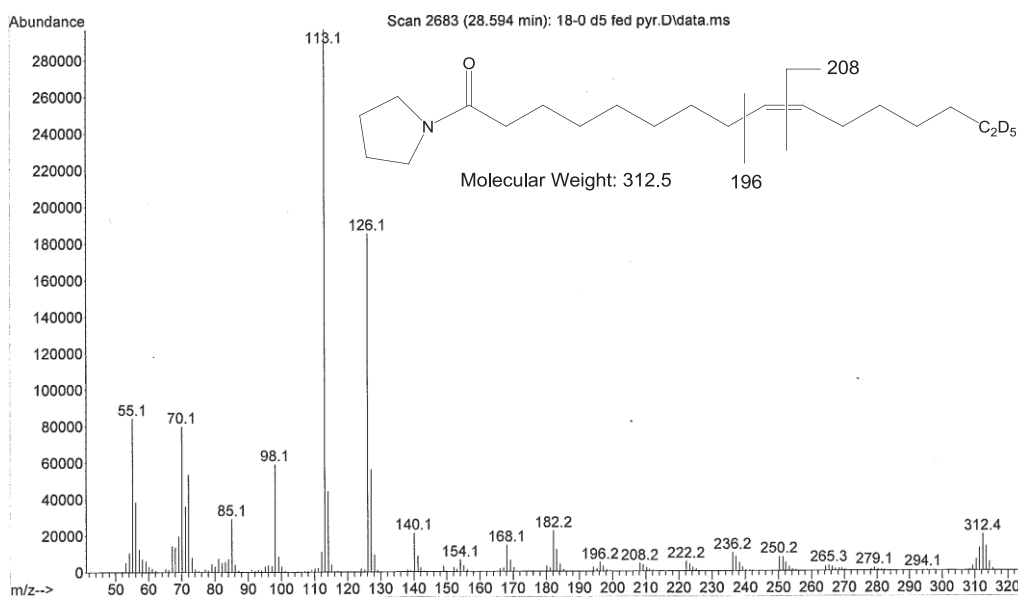


Figure 38. The mass spectrum of 16:1⁹- d_5 FAPy.

The second method in which the GC-MS data was analyzed expressed the results in terms of the percent composition of labeled compounds (Figure 39).

This representation highlights the overall proportions of each new labeled fatty acid that is produced by the enzymatic pathways. For example, all three of the C₁₇ FAs show high incorporation levels of the *d*₅ label (Figure 37). However, the percent composition of the three C₁₇ labeled FA products combined for under 5% of the total labeled products observed, suggesting that they are turned over at a rapid pace.

In addition, the percent composition underscores the decreasing levels of the labeled fatty acid that was available to *D. discoideum* over time. In the 18:0-*d*₅ experiment, the percent composition of the supplemented FA remained quite high during the initial h of incubation, decreasing over time as the organism gradually consumes it. This also supplied evidence that the 1% NP40 washes applied prior to the preparation of FAMES were effective in removing supplemented fatty acid not taken up by the cells, as the labeled substrate would vanish beyond 72 h of incubation, indicative that it had all been incorporated into other FAs by that point.

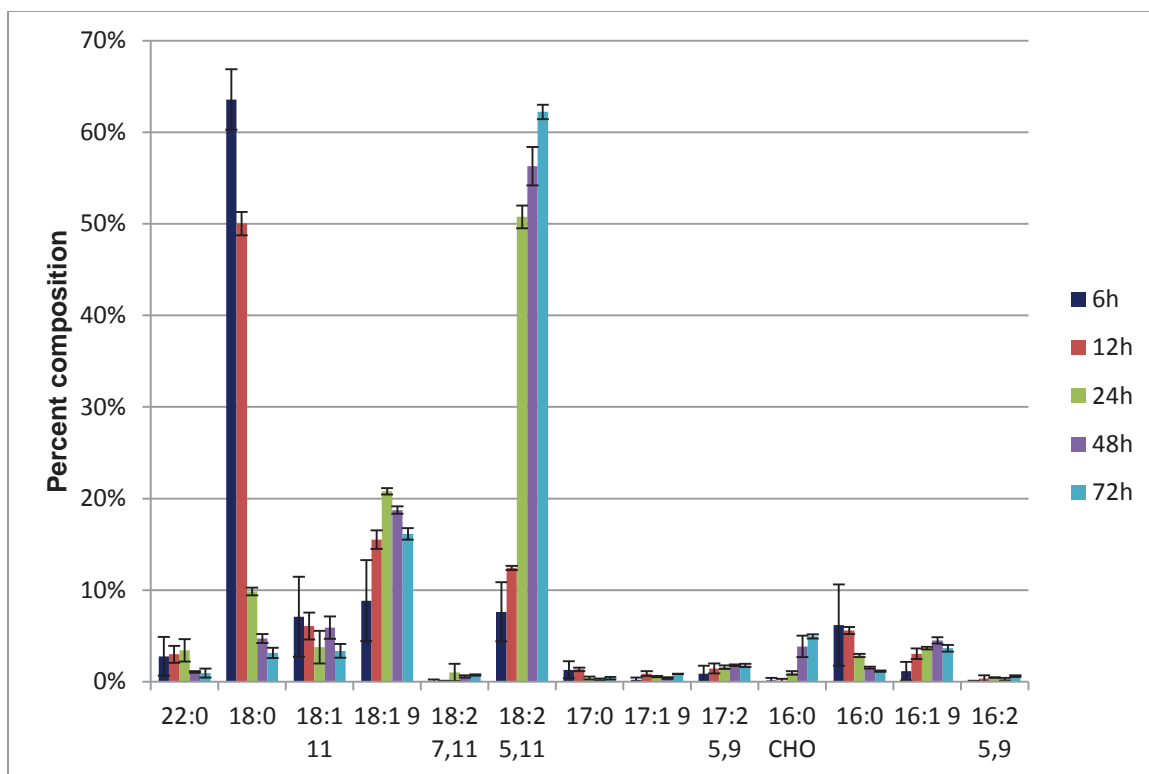


Figure 39. The percent composition of all d_5 -labeled fatty acids observed upon supplementation with $18:0-d_5$.²

The percent composition results showed that $18:1^9$ and $18:2^{5,11}$ had the highest incorporation of $18:0$ -derived d_5 label, raising the question of why $18:1^{11}$ is not a majority product as observed in the FA profile. The amount of products will differ based upon the point along the metabolic thoroughfare at which a synthesized substrate was supplemented. From the hypothetical FA metabolism scheme (Figure 29), it is not surprising that $18:1^9$ appears artificially high in comparison to the fatty acid profile. Since $18:0-d_5$ was fed, $18:1^9$ only has to pass through one Δ^9 desaturation reaction, whereas $18:1^{11}$ must be β -oxidized, Δ^9 desaturated, and elongated if only a Δ^9 desaturase, and not a Δ^{11} -specific enzyme is available. However, by that reasoning, $18:2^{5,11}$ also has to travel through the same pathway as $18:1^{11}$ (plus an additional desaturation). The

² Data is presented as the mean percent composition of labeled fatty acids \pm standard deviation; n=3.

overwhelming dominance of 18:2^{5,11} together with low deuterium incorporation into 18:1¹¹ suggests that these two majority FAs may be produced via separate pathways.

In the palmitate-*d*₅ experiments, the substrate did not appear to be incorporated into fatty acids with nearly the efficiency of the stearate-*d*₅ (Figure 40). While this may have been due to a higher rate of cellular uptake of 18:0 versus 16:0, 16:0-*d*₅ may have also been used at a slower pace by the enzymes downstream of 16:0. While unanticipated, the 16:0-*d*₅ data allowed for a more interpretable picture of the fatty acid metabolism, because the flow of new products were generated at a more gradual rate than seen in the stearate-*d*₅ feeding experiment.

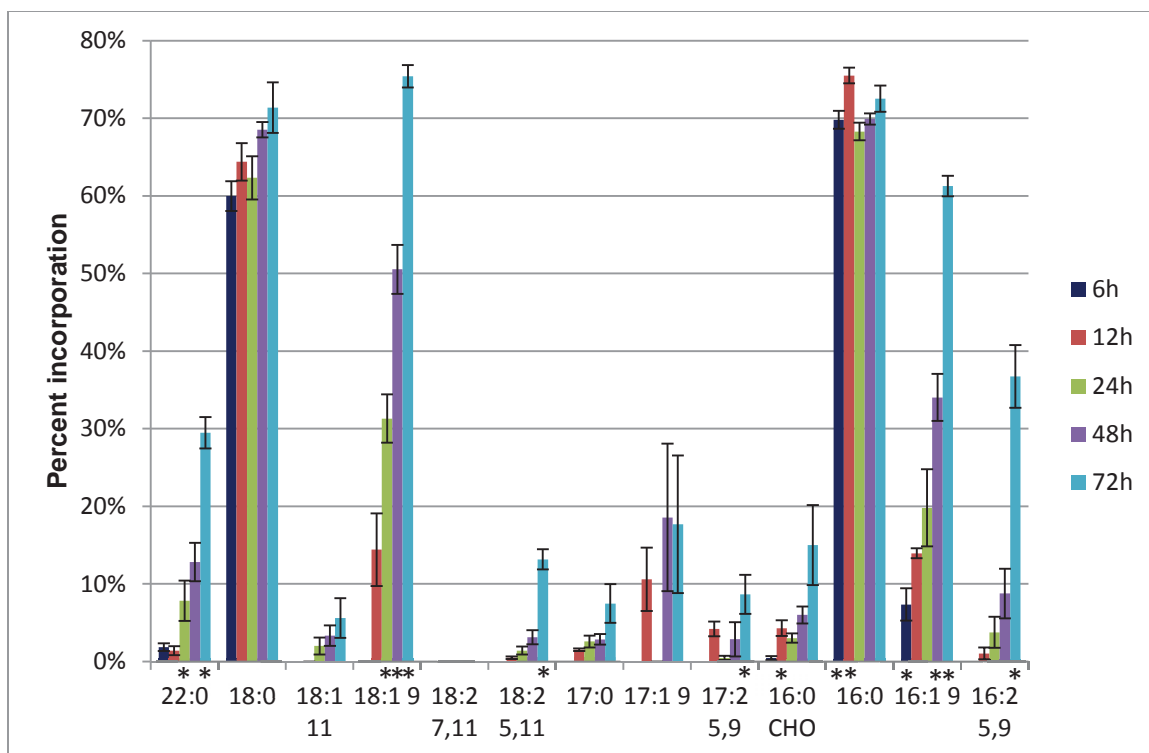


Figure 40. Time course of the percent incorporation of d_5 label into FA products after supplementation with 16:0- d_5 and 1% NP-40.³

The 16:0- d_5 was readily elongated, as the d_5 label was present in 60% of the total 18:0 FA content at 6 h, and 22:0- d_5 was observed at nearly 30% incorporation at 72 h (Figure 40). Beyond the propensity for elongation, the only other product generated in 6 h was that of 16:1⁹. More deuterium-labeled products were detected at the 12 and 24 h intervals, with increased formation of 16:1⁹- d_5 , the emergence of 16:2^{5,9} and particularly 18:1⁹, which ascended to over 30% incorporation at 24 h. Incorporation into 18:2^{7,11} was not observed in this experiment. In the 18:0- d_5 labeling experiments, the d_5 label did not emerge in 18:2^{7,11} until 16:2^{5,9} reached incorporation levels nearing 20%. However, in the 16:0- d_5 experiments, the incorporation levels of 16:2^{5,9}- d_5 did not exceed 10%

³ Data is presented as the mean percent incorporation of labeled fatty acids \pm standard deviation; n=3. Asterisks located below the percent incorporation bars indicate a p-value of 0.05 or less.

until 72 h. Therefore, if the 16:0- d_5 experiment had been allowed to proceed another 24 h, 18:2^{7,11}- d_5 may have been detected.

The 16:0- d_5 incorporation into 18:1¹¹ progressed in a similar manner to the 18:0- d_5 experiments, as it exhibited incorporation in only modest amounts and remained consistent within the error bars ($p > 0.15$) throughout the experiments, despite an increase in the 18:2^{5,11}- d_5 product over 72 h. The very dissimilar behavior of 18:1¹¹ and 18:2^{5,11} again suggested they may be made via separate pathways and it became clear that the 18:0- d_5 and 16:0- d_5 FAs would not suffice to answer the question of how 18:1¹¹ and 18:2^{5,11} were being made.

Incorporation of the d_5 label into the C₁₇ carbon FAs occurred at lower percentages than in the 18:0- d_5 experiments and no definitive information was obtained regarding the 16:0 aldehyde, since the d_5 aldehyde incorporation product was not produced in large abundance (15% incorporation at 72 h). In comparison to other products, its incorporation behavior does not follow that of 16:1⁹- d_5 , which is produced directly from 16:0- d_5 .

The percent composition of labeled FAs (Figure 41) illustrates the slow rate of 16:0- d_5 incorporation into other FAs versus 18:0- d_5 (Figure 39). During the 18:0- d_5 experiment, nearly all of the supplemented material had been metabolized by 72 h; whereas 16:0- d_5 still accounted for ~40% of the total d_5 labeled fatty acids.

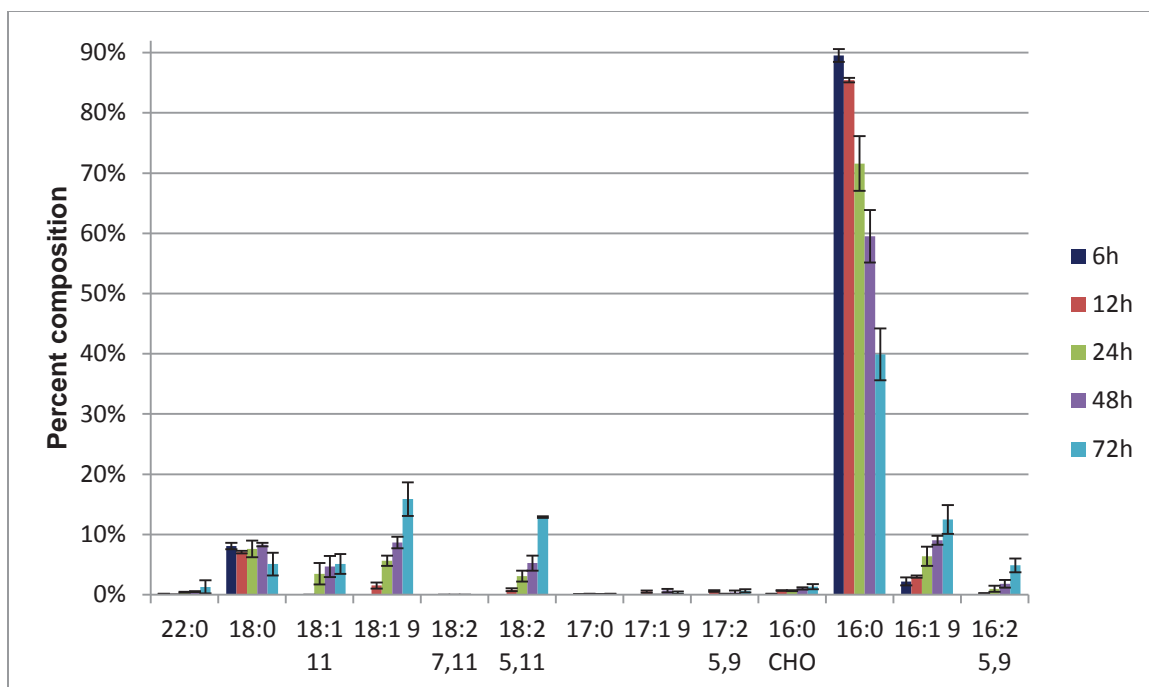


Figure 41. The percent composition of all d_5 -labeled fatty acids observed upon supplementation with $16:0-d_5$.⁴

In summary, the supplementation of $18:0-d_5$ and $16:0-d_5$ was successful in confirming *D. discoideum* has active elongation, desaturation, and β -oxidative pathways, and also suggested that the C_{17} fatty acids of *Dictyostelium* may be produced via α -oxidation. However, these labeled FAs could not explicitly explain the high abundance and behavior of $18:1^{11}$ and $18:2^{5,11}$ or if a Δ^{11} desaturase contributes to either of these FA pools. To address this, an $18:0-d_4$ feeding substrate was designed.

3.3.2.2. *In vivo* studies: stearate- d_4

The premise for developing the stearate- d_4 feeding strategy was distinct from that of the d_5 -compounds. While the d_5 FAs were employed to observe the

⁴ Data is presented as the mean percent composition of labeled fatty acids \pm standard deviation; n=3.

entire metabolic pathway, and incorporation of label into both $18:1^{11}$ and $18:2^{5,11}$ was observed, the d_4 -compound was engineered to gain insight into how the large proportions of $18:1^{11}$ and $18:2^{5,11}$ are produced, and to test for the existence of a Δ^{11} desaturase activity in *D. discoideum*. Figure 42 outlines the two potential pathways by which $18:1^{11}$ and $18:2^{5,11}$ could be produced from $18:0$ and the premise upon which the stearate- d_4 feeding experiment can clarify the issue.

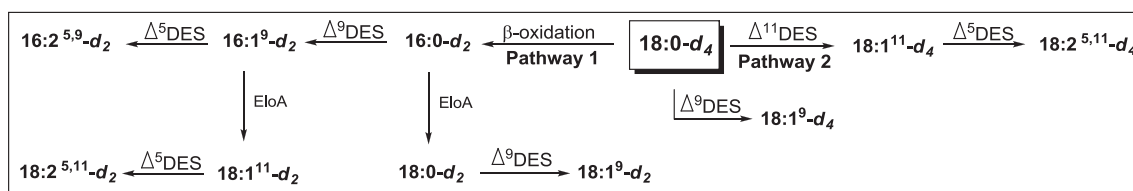


Figure 42. The potential products of stearate- d_4 metabolism.

Upon supplementation with the labeled stearate, the substrate could undergo β -oxidation (Pathway 1) and ultimately arrive at $18:1^{11}$ and $18:2^{5,11}$ after three or four transformations, respectively. Alternatively, if there is Δ^{11} desaturation activity, $18:0$ could be directly converted into the $18:1^{11}$ and $18:2^{5,11}$ products (Pathway 2). The key to this experiment relied on the ability to observe the effects of β -oxidation upon stearate- d_4 labeled in the β and γ positions. Figure 43 below underscores the process by which two deuterium are lost during β -oxidation to form d_2 products. While d_2 products would be observed regardless of the presence or absence of a Δ^{11} desaturase, if the experiments yielded any $18:1^{11}-d_4$ or $18:2^{5,11}-d_4$ products, they would provide evidence that a pathway exists for making these FAs that is composed solely of desaturases (no β -oxidation).

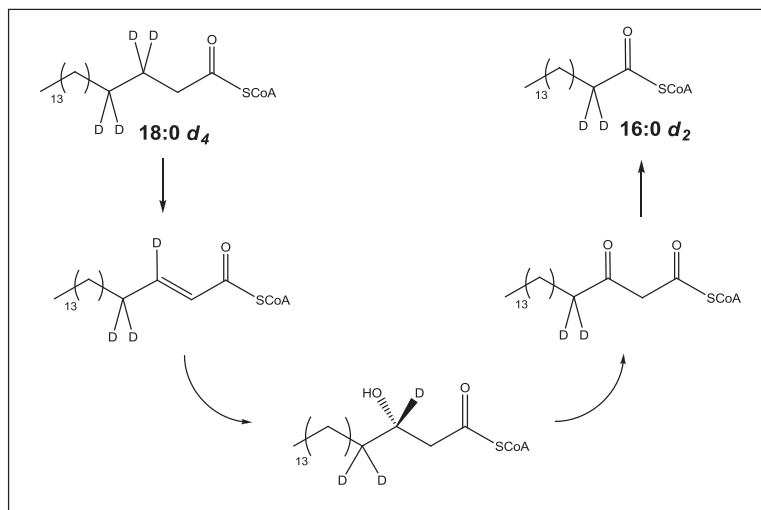


Figure 43. The loss of deuterium during β -oxidation of stearate- d_4 .

The results of this experiment were extremely clear and provided strong evidence to support the existence of a Δ^{11} desaturase in *D. discoideum*; 18:2^{5,11} was observed as the d_4 -product by GC-MS. GC-MS results from the 18:0- d_4 supplementation at 24 h is shown in Figure 44, displaying the total ion chromatogram (A), with mass data from the 18:2^{5,11} peak between 15.55 and 15.72 min (B). The mass spectrum shows the endogenous 18:2^{5,11} FAME (m/z 294) and the d_4 -labeled product (m/z 298). Significantly, a d_2 -labeled 18:2^{5,11} species (m/z 296) was only observed in an approximate 2% incorporation, indicating that 18:2^{5,11} is produced from 18:0 almost exclusively via a Δ^{11} desaturase pathway.

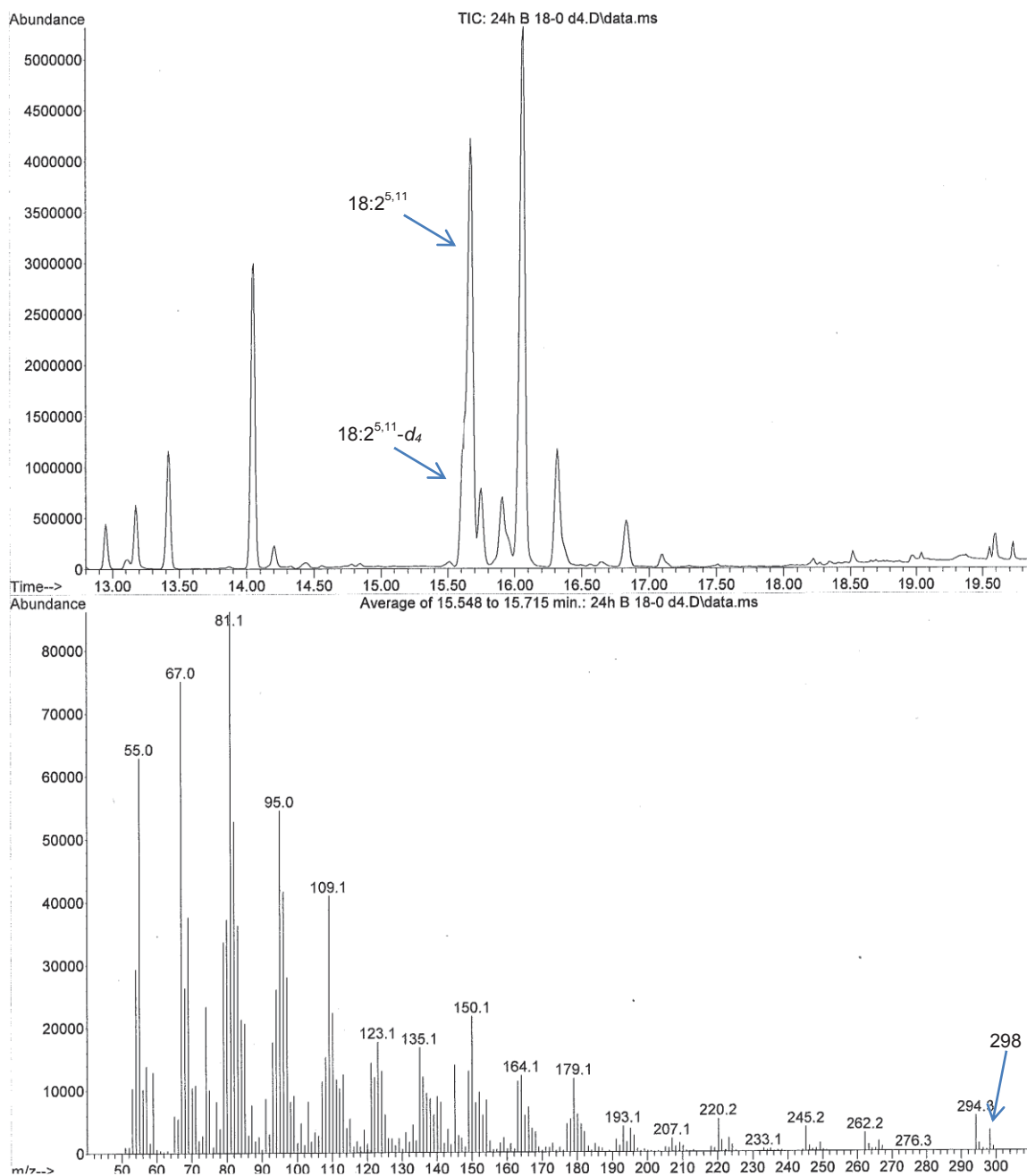


Figure 44. The total ion chromatogram (A) from 24-h supplementation with 18:0- d_4 and the mass spectrum of the resulting 18:2^{5,11} FAME product (B).

In the FAME analysis of cultures from the initial 6 h of incubation, the presence of 18:2^{5,11}- d_4 , indicated that the supplemented 18:0- d_4 material was quickly converted to this product directly without β -oxidation (Figure 45). Longer

intervals of incubation produced a large quantity of the 18:2^{5,11}- d_4 product (50% incorporation).

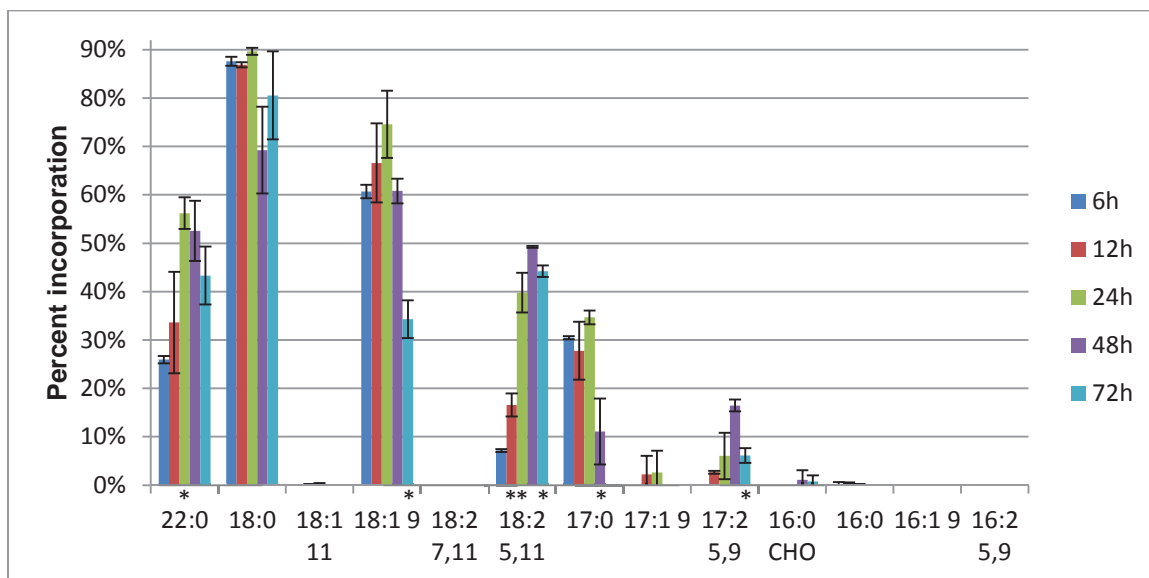


Figure 45. Time course of the percent incorporation of d_4 label into FA products after supplementation with 18:0- d_4 and 1% NP-40.⁵

The results of this experiment allowed for consistent interpretations with the conclusions derived from the palmitate- d_5 and stearate- d_5 studies. For example, 18:1⁹- d_4 was produced rapidly, approaching 60% incorporation within 6 h of incubation, again demonstrating that 18:0 is a substrate for the $\Delta 9$ desaturase in *D. discoideum*. Additionally, 18:0- d_4 was readily elongated to 22:0- d_4 , achieving 25% incorporation at 6 h and peaking with 55% at 24 h. β -oxidation of 18:0 to 16:0 followed by desaturation to form 16:1⁹ and 16:2^{5,9} was further affirmed by the absence of any d_4 -labeled C_{16} species. The trace of 16:0- d_4 seen in Figure 45 was believed to be a background ion sharing the same m/z value (mass spectrum of ion in Figure 46).

⁵ Data is presented as the mean percent incorporation of d_4 -labeled fatty acids \pm standard deviation; $n=3$. Asterisks located below the percent incorporation bars indicate a p -value of 0.05 or less.

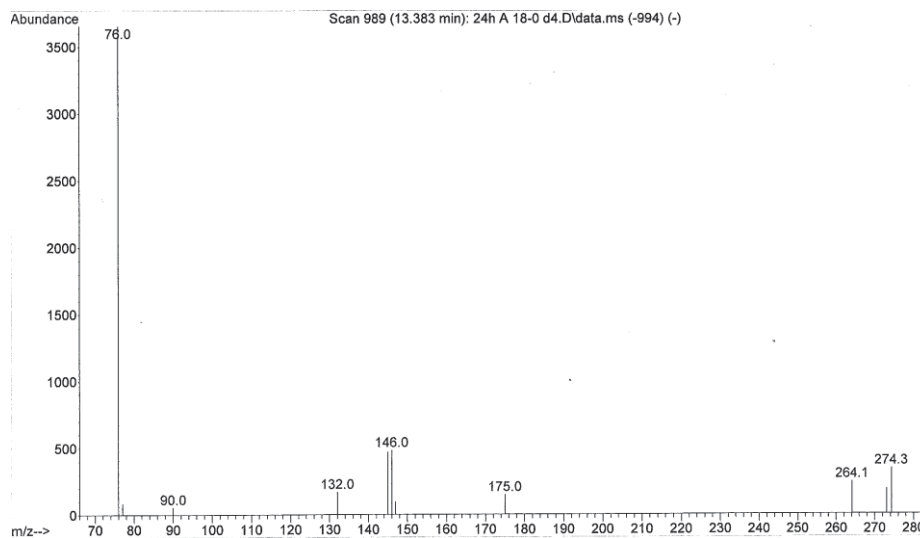


Figure 46. Mass spectrum of a background compound sharing the molecular weight of the 16:0- d_4 product (m/z 274).

Further evidence that 17:0 is formed from the α -oxidation of 18:0 was provided by the presence of 17:0- d_4 (40% incorporation at 24 h). The 17:2- d_4 FA observed in the profile could be the α -oxidation product (17:2^{4,10} or 17:2^{6,10}) of an 18:2- d_4 FA in *D. discoideum*, but comparison of the pyrrolidine derivative with that of a 17:2^{5,9} synthetic standard was consistent with its identity as 17:2^{5,9} (data not shown). Furthermore, as an 18:2^{6,10} FA would need to be present in order to generate an 17:2^{5,9} α -oxidation product, it is most likely formed from α -oxidation of 18:0, followed by two desaturation steps. While the pathway could be arranged such that a Δ^5 desaturase first acts on 17:0 followed by Δ^9 desaturation, it was confirmed by FAPys and Lipid Library's collection of FAPy mass spectra that the only desaturation product of 17:0 is 17:1⁹. It is again possible that this 17:1 FA could originate from the α -oxidation of 18:1⁹, but the confirmation of the alkene's location at position 9 precludes this. Palmitoyl-CoA and stearoyl-CoA are known to be preferred substrates of the Δ^9 desaturase (stearoyl-CoA desaturase) (72), although it has also been shown to accept other chain lengths (73, 74). In *Dictyostelium*, the Δ^9 desaturase appears to have the same specificity for saturated substrates, as evidenced by the production of 16:1⁹ from

16:0, 17:1⁹ from 17:0, and 18:1⁹ from 18:0. And while it has been shown that the Δ^5 desaturases in *D. discoideum* are active toward both saturated and unsaturated FAs (53, 64), the results presented here suggest that the Δ^5 desaturase(s) has a strong preference for monounsaturated substrates, as shown in the conversion of 16:2^{5,9} from 16:1⁹, 17:2^{5,9} from 17:1⁹, and potentially 18:2^{5,11} from 18:1¹¹. The compiled results of the d_2 percent incorporation are available in Figure 47.

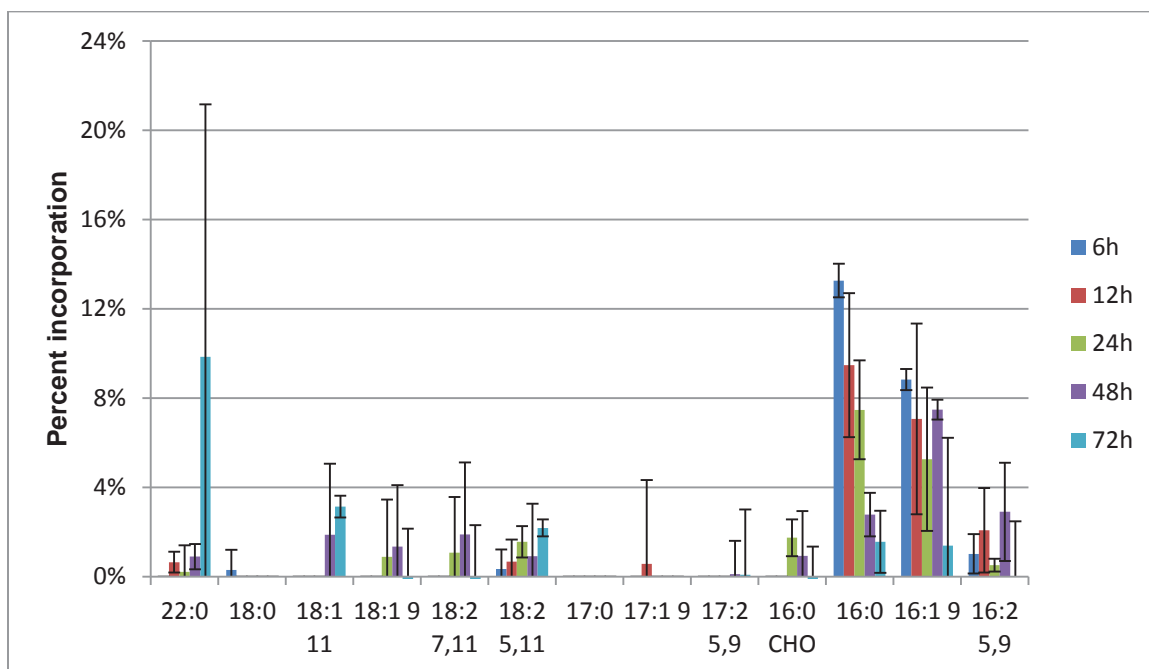


Figure 47. Time course of the percent incorporation of d_2 label into FA products after supplementation with 18:0- d_4 and 1% NP-40.⁶

Another remark about this experiment lies in the apparent strain that the 18:0- d_4 feeding placed on *D. discoideum*'s long-term health. All of the feeding experiments had lower growth rates than the control (1% NP40 only). The growth curves in Figure 48 illustrate how the 16:0- d_5 and 18:0- d_5 experiments exhibited very similar growth patterns, at a consistently slower rate than the control. However, the 18:0- d_4 experiments portrayed similar initial growth

⁶ Data is presented as the mean percent incorporation of d_2 -labeled fatty acids \pm standard deviation; n=3.

patterns to the other feeding studies, but began to diverge at the 24/48 h mark, after which the rate of growth slowed.

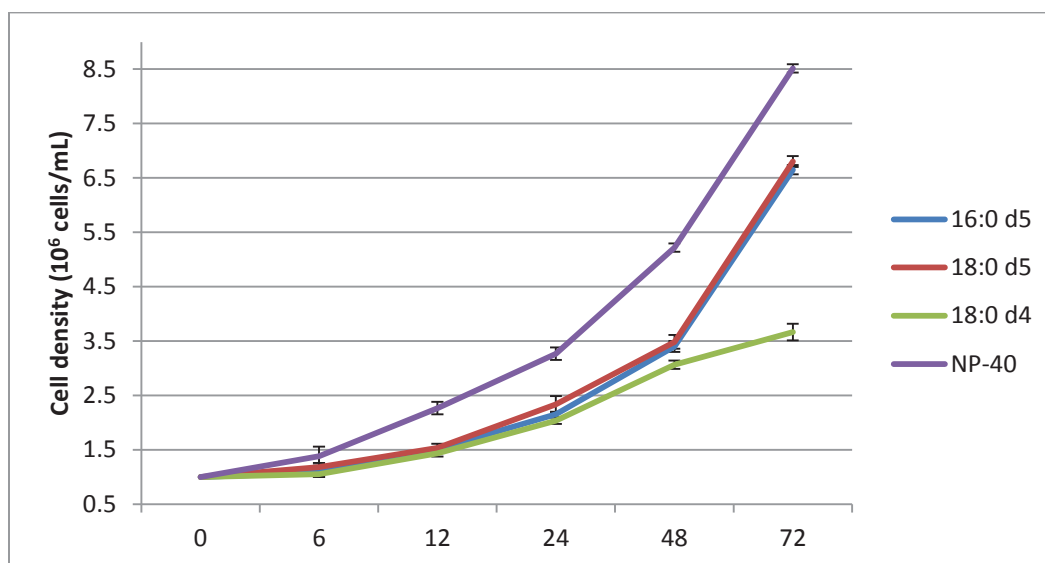


Figure 48. The cell growth curves of the 16:0- d_5 , 18:0- d_5 , 18:0- d_4 , and control (NP-40) cultures during time courses.⁷

This decreased growth rate was reflected in the d_2 and d_4 percent incorporation results. The maximal levels of incorporation did not occur at the longest incubation period, as was observed in the d_5 experiments. In fact, they occurred at 24 h for the d_4 products (the same time when the growth rate began to slow), and the d_2 products showed a decrease between each time period following 6 h. Since the cells did not continue to incorporate labeled material at the same rate during longer incubations, percent incorporation did not climb to the same levels as observed in the 18:0- d_5 experiments. A specific culprit of this stunted growth could not be determined. However, it was evident from the d_2 data that *D. discoideum*'s ability to convert 18:0- d_4 to 16:0- d_2 was diminished compared to the d_5 experiments suggested that the positioning of deuterium at the β and γ carbons hindered β -oxidation. The percent incorporation of 16:0- d_2 was roughly 13% at its highest point (6 h), while in the 18:0 d_5 -experiments 16:0

⁷ Data is presented as the mean growth density in 10⁶ cells/mL \pm standard deviation; n=3.

d_5 consistently maintained incorporation levels between 20% and 30%. The elongation from 18:0- d_4 to 22:0- d_4 occurred more slowly than in the 18:0- d_5 experiments.

While the rapid production of 18:2^{5,11}- d_4 provides concrete evidence of Δ^{11} desaturase activity, it is curious that little, if any, d_4 label was incorporated into 18:1¹¹. It is clear that the pathway from 18:0- d_4 to 18:2^{5,11}- d_4 does not pass through β -oxidation, and as such, the only combination of enzymes capable of affording such a product is a Δ^5 and Δ^{11} desaturase. *D. discoideum* has been shown to contain at least two Δ^5 desaturases-FadA and FadB (53, 64). *D. discoideum* was demonstrated by comparison of FAPys fragments of a synthetic standard to the endogenous FAs to have undetectable levels of 18:1⁵, making it unlikely that 18:2^{5,11} is produced by a Δ^5 desaturase followed by Δ^{11} desaturation. A second plausible path to 18:2^{5,11} is that the Δ^{11} desaturase acts first, and the 18:1¹¹- d_4 product is immediately transferred to a Δ^5 desaturase with such proficiency that it does not enter the 18:1¹¹ FA pool. Additional support for this notion stems from the low levels of 18:1¹¹- d_2 that are produced at longer incubation periods, after having passing through the enzymatic machinery of Pathway 1 (Figure 42). A *Dictyostelium* ELO elongates 16:1⁹ to 18:1¹¹ (10), suggesting that 18:1¹¹ could be generated through Pathway 1. Therefore, it is postulated that the majority of 18:2^{5,11} is produced via Pathway 2, and 18:1¹¹ through Pathway 1.

A method by which the pathway to 18:2^{5,11} may be elucidated resided with the synthesis and supplementation of two additional fatty acids, 18:1⁵- d_7 and 18:1¹¹- d_7 with deuterium labeling at the methyl ends. Upon supplementation, one of the two fatty acids was expected to be converted into 18:2^{5,11} with the deuterium label present while the other would not, allowing the order of installation of Δ^5 and Δ^{11} double bonds to be determined. Preliminary results from supplementation with these two fatty acids suggest that 18:1⁵ is produced first and is subsequently acted on by a Δ^{11} desaturase, as demonstrated by the formation of 18:2^{5,11}- d_7 from 18:1⁵- d_7 but not 18:1¹¹- d_7 . As the 18:1⁵ FA is not

observed in *D. discoideum*'s FA profile, the Δ^{11} desaturase must act very quickly. Taking into consideration the $18:0-d_4$, $18:1^5-d_7$, and $18:1^{11}-d_7$ incorporation results, evidence of a Δ^{11} desaturase, and the detection of α -oxidative pathways, a current proposal of the fatty acid metabolic pathways of *D. discoideum* is presented in Figure 49.

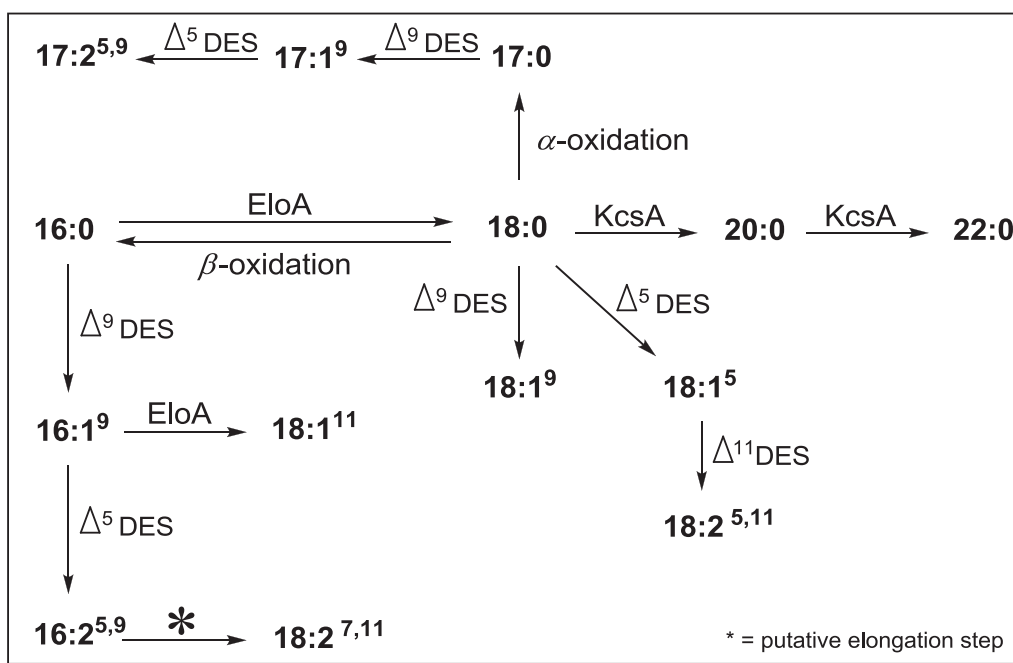


Figure 49. The summarized metabolic processes that yield the observed fatty acid profile in *D. discoideum*.

The pathway does not include the aldehydes observed in *D. discoideum*, as it is still unclear if they are truly metabolic products, such as cleavage products from vinyl ether lipids, or degradation products. Also, $16:1^5$ was not included in the pathway in Figure 49 because any incorporation of deuterium label was below the detection limits of the GC-MS. It is still unclear from these experiments why the large quantities of $18:1^{11}$ observed in the FA profile were not reflected in the incorporation results.

Examination of the sequencing work of Eichinger *et al.* (13) reinforced the hypothesis that a Δ^{11} desaturase is active in the fatty acid metabolism of

Dictyostelium: a tBLASTn search of the genome revealed a potential Δ^{11} desaturase. This is particularly intriguing because such enzymes are primarily found in insects to date. A search for Δ^{11} fatty acid desaturases in BRENDA, the Comprehensive Enzyme Information System, output 12 organisms: 11 insects (moths) and 1 diatom (*Thalassiosira pseudonana*) (70). The possibility of demonstrating the presence of such an atypical fatty acid desaturase in this organism is an alluring prospect. The putative gene has been cloned (B. Blacklock, personal communication) and will be functionally characterized by heterologous expression in *S. cerevisiae*.

CHAPTER 4. SPHINGOLIPID CHARACTERIZATION IN *DICTYOSTELIUM DISCOIDEUM*

4.1. Introduction

As a preface to understanding the roles of elongated fatty acids and sphingolipids in *D. discoideum*, a characterization of those lipids is was undertaken. The first objective was to characterize the long chain bases that comprise the backbones of these complex lipids. Harsh basic conditions for isolating the LCBs from cells and tandem MS methods were developed using commercial sphingolipid standards and *Saccharomyces cerevisiae* as a model. Complex lipid extraction from cells (total lipid extraction), isolation of SLs from other lipids (mild alkaline hydrolysis), and conditions for tandem MS analysis of sphingolipids were developed using commercial sphingolipid standards and *S. cerevisiae*. The *D. discoideum* LCB profile was generated and used during the characterization of the intact sphingolipids using the developed techniques.

4.2. Methods and materials

All manipulations were performed in glass conical vials unless otherwise mentioned. All solvents used were of HPLC grade. 1-Fluoro-2,4-dinitrobenzene, 1,4-dioxane, 33% methylamine in absolute ethanol, and barium hydroxide octahydrate were obtained from Sigma Aldrich. Commercial sphingolipids were procured from Avanti Polar Lipids. *S. cerevisiae* InvSc1 was obtained from Invitrogen. Total lipid extractions were performed using 0.5-mm soda-lime beads and a Mini-Beadbeater, both supplied by Biospec Products, Inc. HPLC separations and tandem mass spectrometry was performed on an Agilent 1200 series LC system and 6410 triple quadrupole (QQQ) MS equipped with

electrospray ionization (ESI). Chromatographic separations were conducted on an Agilent 4.6 x 50 mm, 1.8 μm Zorbax Eclipse XBD-C₁₈ column. High-resolution MS data was obtained on an Agilent 6520 quadrupole time-of-flight (QTOF) mass spectrometer equipped with ESI and a 1200 series capillary LC system.

4.2.1. Culturing of *D. discoideum* and *S. cerevisiae*

For analysis of *D. discoideum* SLs, 50-mL cultures were set in 250-mL autoclaved flasks containing HL5 media and 500 μL pen/strep, and inoculated with 1.0 mL of media from a well-established plate of *Dictyostelium* (grown to the time of passage). Cells were then grown at 22 °C with shaking (180 rpm) for 4 days (density of $\sim 1.0 \times 10^7$ cells/mL), then the entire culture was transferred to a 2 L autoclaved flask containing HL5 media (450 mL) and 5 mL pen/strep. After shaking at 22 °C for 4 days (density of $\sim 3.0 \times 10^7$ cells/mL), the culture was centrifuged at 450g to remove media, followed by vortexing with nanopure H₂O and centrifugation at 450g (repeated 3x) and cells lyophilized to dryness (1-1.5 g).

For analysis of *S. cerevisiae* SLs, 50-mL cultures were set in 250-mL autoclaved flasks containing yeast peptone dextrose (YPD; recipe in Appendix) media, and inoculated with 5.0 mL of media from a starter culture (5 mL) set from freezer stock of InvSc1. Cells were then grown at 30 °C with shaking (250 rpm) overnight, then the entire culture was transferred to a 2 L autoclaved flask containing YPD media (450 mL). After shaking for 3 days (to saturation), the culture was centrifuged at 450g to remove media, followed by vortexing with nanopure H₂O and centrifugation at 450g (repeated 3x) and cells lyophilized to dryness (3-4 g).

4.2.2. Ba(OH)₂ hydrolysis

Acyl chains were hydrolyzed from sphingolipids in the methods described by Markham *et al.* (75) and Valentin *et al.* (76) with modifications to the reaction

time as discussed. Sphingolipid standards (100 μg) or lyophilized cells (100 mg) were combined with 1 mL 1,4-dioxane and 1 mL 10% barium hydroxide octahydrate (w/v) in water ($\text{Ba}(\text{OH})_2$ solution heated to 60 $^\circ\text{C}$ prior to aliquoting) and reacted in a sealed conical vial for 24 h at 110 $^\circ\text{C}$. Long chain bases were isolated by introduction of 6 mL of chloroform/dioxane/ H_2O (6:1:5), vortexing and removal of the organic layer (bottom). The extracts were washed with 0.1 M KOH (5 mL) and 0.5 M KCl (5 mL), then evaporated under a stream of nitrogen. Samples were dissolved in 0.5 mL 1:1 MeOH/ CHCl_3 for mass spectrometric analysis. For conversion to the dinitrophenyl (DNP) derivative, the dried LCB residue was taken directly to the next step.

4.2.3. Dinitrophenyl derivatization of LCBs

DNP derivatives were formed via the method outlined by Valentin *et al.* (76) and Heinz *et al.* (77). LCB standards (50 μg) or those generated from $\text{Ba}(\text{OH})_2$ hydrolysis were dissolved in 1 mL of MeOH to which 4 mL of 2.0 M potassium borate buffer (pH 10.5) was slowly added, along with 5 μL of 1-fluoro-2,4-dinitrobenzene. The resulting lime-green mixture was vortexed and incubated for 30 min at 60 $^\circ\text{C}$. Following the reaction, DNP-LCBs were isolated by introduction of 7.5 mL of chloroform/methanol/ H_2O (8:4:3), vortexing, separation of the CHCl_3 layer, and extraction of the aqueous phase a second time with 4 mL CHCl_3 . The organic phases were pooled and solvent removed under a stream of nitrogen. Samples were dissolved in 0.5 mL of 1:1 ACN/MeOH for chromatographic separation and LC-MS analysis.

4.2.4. Total lipid extraction

Complex lipids (phospholipids and sphingolipids) were extracted from lyophilized cells by the method described by Markham *et al.* (75) with slight alteration to the incubation procedure. Lyophilized cells (100-400 mg) were combined in a 5-mL bead beater vial (plastic) with glass beads (0.5 mm, 3x the

mass of cells) and 5 mL of Solvent A (bottom layer of isopropanol/hexane/H₂O; 55:20:25) and beat for 3 min. The homogenized mixture was then incubated for 20 min at 60 °C, followed by centrifugation at 250g and removal of the supernatant. These steps were repeated two more times, with substitution of bead beating with vortexing (1 min), and the solvent evaporated under a stream of nitrogen from the pooled supernatants. For LC-MS analysis of phospholipids, the total lipid extract (TLE) was redissolved in 0.5 mL of Solvent A. For methylamine hydrolysis, this crude mixture was taken on directly.

4.2.5. Mild alkaline hydrolysis

The phospholipids of the total lipid extract were degraded in accordance with the protocol described by Markham *et al.* (78). The residue obtained from the TLE procedure was combined with 1 mL of a solution containing 33% methylamine in absolute ethanol/water (7:3 v/v) and heated at 50 °C for 1 h, yielding an enriched sphingolipid sample free of phospholipids after evaporation of solvent and methylamine under a stream of nitrogen. The concentrated product was resuspended in 0.5 mL of Solvent A, vortexed, centrifuged at 250 g for 2 min, and the supernatant was transferred to an LC-MS vial for QQQ and QTOF analysis.

4.2.6. Lithiation of sphingolipids

Lithium adducts of biological and commercial sphingolipids were generated by addition of lithium hydroxide (dissolved in methanol) to sample vials at a final solution concentration of 2.0 µmol/mL (79). Standards were prepared at concentrations of approximately 1 nmol/mL in 1:1 MeOH/CHCl₃ or Solvent A, while biological products of mild alkaline hydrolysis were lithiated directly. Samples were immediately analyzed on the QQQ following exposure to LiOH via direct injection (no chromatography) (79).

4.2.7. LC-MS analysis of lipids

With the exception of the DNP derivatives and the quantification of long chain bases, all experiments were performed without the aid of chromatography. Samples were directly injected into the source via the system autosampler. Listed below are the acquisition methods used on the QTOF and QQQ MS to analyze various types of biological samples with descriptions of the solvents, polarities, and ionization conditions. All standards used in optimizations were prepared as 100 µg/mL in 1:1 CHCl₃/MeOH. Source parameters were set as follows:

- Gas temp: 350 °C
- Gas flow: 10 L/min
- Nebulizer: 45 psi
- Capillary: +/- 4000 V

Agilent 6520 Quadrupole Time-of-Flight MS

Spl LCBs pos.m

- A full scan MS method designed to obtain the accurate mass of long chain bases following Ba(OH)₂ hydrolysis.
- Fragmentor: +140 V
- Solvent A: 20% H₂O + 5 mM NH₄OAc. Solvent B: 80% 10:3:1 MeOH/ACN/IPA + 0.1% formic acid. (76) or Solvent A: 20% H₂O + 5 mM NH₄OAc. Solvent B: 80% 1:1 CHCl₃/MeOH (1)

Spl neg.m

- A full scan MS method utilized to obtain exact mass data from a methylamine hydrolysate containing SLs.
- Fragmentor: -180 V
- Solvent A: 20% H₂O + 5 mM NH₄OAc. Solvent B: 80% 1:1 CHCl₃/MeOH (1)

Agilent 6410 Triple Quadrupole MS

DNP derivatives.m

- MS2 full scan method used to analyze DNP-derivatized long chain bases.
- Diode array detector: 350 nm
- Fragmentor: -105 V
- Solvent A: H₂O + 5 mM NH₄OAc. Solvent B: 10:3:1 MeOH/ACN/IPA + 0.1% formic acid. (76)
- Flow: 0.5 mL/min; 80 → 90% organic over 15 min, then 95% until run ends
- Run time: 23 min
- Post time: 7 min

LCB loop positive.m

- MS2 full scan method used to analyze long chain bases following Ba(OH)₂ hydrolysis (direct injection).
- Fragmentor: +140 V
- Solvent A: 20% H₂O + 5 mM NH₄OAc. Solvent B: 80% 10:3:1 MeOH/ACN/IPA + 0.1% formic acid. (76)

LCB MRM1.m

- Multiple reaction monitoring method (with chromatography) for the quantitation of *t*18:0 (318→300→282→264 *m/z*), *d*18:0 (302→284→266 *m/z*) and *d*18:1 (300→282→264 *m/z*) in *D. discoideum*. *d*17:0 (288→270→252 *m/z*) was employed as the internal standard (10 µg/mL).
 - All fragmentor voltages and collision energies were established by Optimizer analysis of standards (Table 3).
- Solvent A: H₂O + 5 mM NH₄OAc. Solvent B: 10:3:1 MeOH/ACN/IPA + 0.1% formic acid. (76)
- Flow: 0.5 mL/min; 80 → 84% organic over 4 min, then 95% until run ends
- Run time: 10 min
- Post time: 5 min

Table 3. Optimizer defined conditions for MRM.

Standard	Precursor Ion	Product Ion	Dwell	Fragmentor	Collision Energy
phytosphingosine	318.3	300.3	200	144	10
phytosphingosine	318.3	282.3	200	144	14
phytosphingosine	318.3	60.1	200	144	18
phytosphingosine	318.3	55.1	200	144	42
dihydrosphingosine	302.3	284.3	200	114	10
dihydrosphingosine	302.3	67.1	200	114	34
dihydrosphingosine	302.3	60.1	200	114	14
dihydrosphingosine	302.3	55.1	200	114	38
sphingosine	300.3	282.3	200	100	6
sphingosine	300.3	69.1	200	100	26
sphingosine	300.3	67.1	200	100	30
sphingosine	300.3	55.1	200	100	34
C ₁₇ sphinganine	288.3	270.3	200	126	9
C ₁₇ sphinganine	288.3	60.1	200	126	13
C ₁₇ sphinganine	288.3	55.1	200	126	37

Optimizer.m

- Template scanning method designed to be resaved as a new name prior to being used in Optimizer. Only the pump conditions are applicable. All other information is selected and derived by Optimizer.
- Solvent A: 20% H₂O + 5 mM NH₄OAc. Solvent B: 80% 10:3:1 MeOH/ACN/IPA + 0.1% formic acid. (76) or Solvent A: 20% H₂O + 5 mM NH₄OAc. Solvent B: 80% 1:1 CHCl₃/MeOH (1)

LCB pdt ion loop.m

- Product ion scanning method designed as a template for the collision-induced dissociation of long chain bases. Molecular ions of interest in the Ba(OH)₂ hydrolysate were used as precursor ions.

- Solvent A: 20% H₂O + 5 mM NH₄OAc. Solvent B: 80% 10:3:1 MeOH/ACN/IPA + 0.1% formic acid. (76) or Solvent A: 20% H₂O + 5 mM NH₄OAc. Solvent B: 80% 1:1 CHCl₃/MeOH (1)

Optimal C1P conditions.m

- The method used during the analysis of C1P and lithiated C1P species in *D. discoideum*. Source and collision cell conditions were optimized from the d18:1/18:0 C1P standard.
- Fragmentor: -180 V; collision energy: 50 eV
- Solvent A: H₂O + 10% 5 mM NH₄OAc. Solvent B: 90% 1:1 CHCl₃/MeOH (1)

Optimal IPC conditions.m

- The method used during the analysis of IPC and lithiated IPC species in *D. discoideum*. Source and collision cell conditions were optimized from the IPCs in *S. cerevisiae*.
- Fragmentor: -180 V; collision energy: 50 eV
- Solvent A: H₂O + 10% 5 mM NH₄OAc. Solvent B: 90% 1:1 CHCl₃/MeOH (1)

Optimal MIPC conditions.m

- The method used during the analysis of MIPC species in *S. cerevisiae* unknown SLs (1064, 1078, 1092 and 1328 *m/z*) and their lithiated adducts in *D. discoideum*.
- Fragmentor: -180 V; collision energy: 75 eV
- Solvent A: H₂O + 10% 5 mM NH₄OAc. Solvent B: 90% 1:1 CHCl₃/MeOH (1)

Cerebroside loop neg.m

- The standard MS2 method utilized to analyze a methylamine hydrolysate of SLs, lithiated SLs or phospholipids.
- Fragmentor: -180 V
- Solvent A: H₂O + 10% 5 mM NH₄OAc. Solvent B: 90% 1:1 CHCl₃/MeOH (1)

Cerebroside loop.m

- The standard MS2 method utilized to analyze phospholipids (total lipid extracts) prior to methylamine hydrolysis.
- Fragmentor: +200 V
- Solvent A: H₂O + 10% 5 mM NH₄OAc. Solvent B: 90% 1:1 CHCl₃/MeOH (1)

4.3. Results and discussion

4.3.1. Identification of sphingolipid long chain bases in *D. discoideum*

The first step to effectively analyzing the composition of sphingolipids in *D. discoideum* involved identifying the long chain bases that comprise the backbone of sphingolipids. This was approached by direct harsh alkaline hydrolysis (1:1 10% w/v Ba(OH)₂/1,4-dioxane; 110 °C) (75, 76) of *D. discoideum* cells to hydrolyze the amide bonds of SLs liberating the acyl chain from the LCB backbone (Figure 50).

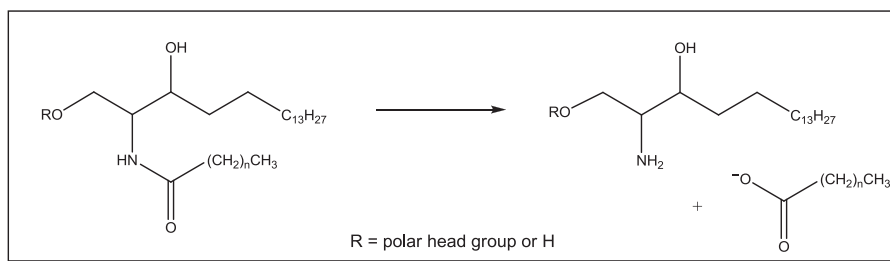


Figure 50. Hydrolysis of N-acyl lipids with Ba(OH)₂.

The development of the barium hydroxide hydrolysis procedure for *Dictyostelium* sphingolipids required considerable effort and multiple experiments, including varying reaction times to determine optimal acyl chain cleavage conditions, as monitored by LC-MS. Initial test reactions were conducted with a single C₁₂ glucoceramide (D-glucosyl-β1-1'-N-dodecanoyl-D-erythro-sphingosine) in order to determine the optimal hydrolysis time for complete acyl chain removal. However, hydrolysis of the standard resulted in partial loss of the sugar head group in addition to varying degrees of N-acyl group cleavage. As such head group cleavage was expected to be the result of the presence of some proton donor (acid), the 1,4-dioxane was investigated as a possible source. A mock reaction of lipid and dioxane only revealed head group loss upon heating, suggesting that peroxides had formed in the aged bottle of dioxane capable of removing some of the sugar head groups from the LCB. New solvent eliminated the majority of head group cleavage, yet complete hydrolysis of the acyl chain remained variable, even among replicate experiments.

While published methods reported a 16 h hydrolysis time for quantitative acyl chain cleavage (75), the reaction continued to produce increasing amounts of long chain base at incubation times to 72 h. Additionally, despite the absence of any acidic component, varying amounts of sugar head group cleavage were still observed, as can be seen in the comparison of two replicate Ba(OH)₂ time courses (Figure 51). In these replicate time courses, 100 μg of a C₁₂ glucoceramide standard was reacted for 0, 0.5, 2, 6, 24 and 48 h to determine

the optimal reaction time. The graphs illustrate two points: that identical reactions produce varying amounts of psychosine (deacylated glucoceramide), as reaction A generated roughly 15% more than reaction B; and that sphingolipid deacylation is complete by 24 h, with head group cleavage (or psychosine degradation) beginning to occur beyond 24 h. Despite observing a maximum psychosine production at a hydrolysis time of 24 h, the variation in psychosine concentration between the replicates showed that the reaction was not consistent enough for use in quantitating LCBs, psychosines and related compounds.

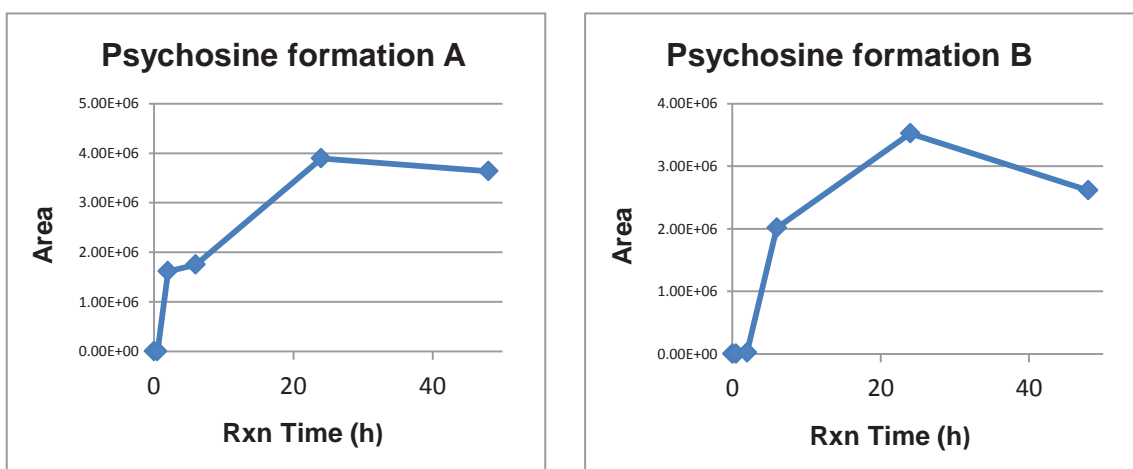


Figure 51. The psychosine formation from $\text{Ba}(\text{OH})_2$ hydrolysis of a C_{12} GlcCer standard performed in replicate under identical conditions.

Putting the reproducibility issue aside, upon obtaining the free amine from $\text{Ba}(\text{OH})_2$ hydrolysis, the free LCBs could either be analyzed directly by LC-MS or be subjected to an additional derivatization. Introducing a DNP handle (inset, Figure 52B) with diagnostic absorption at 350nm (76) allowed for the rapid screening of complex biological mixtures for LCBs by UV detection. This methodology was validated using *S. cerevisiae* by testing our ability to identify the LCBs observed in literature (76). The signals from the diode array detector at 350 nm are displayed in Figure 52.

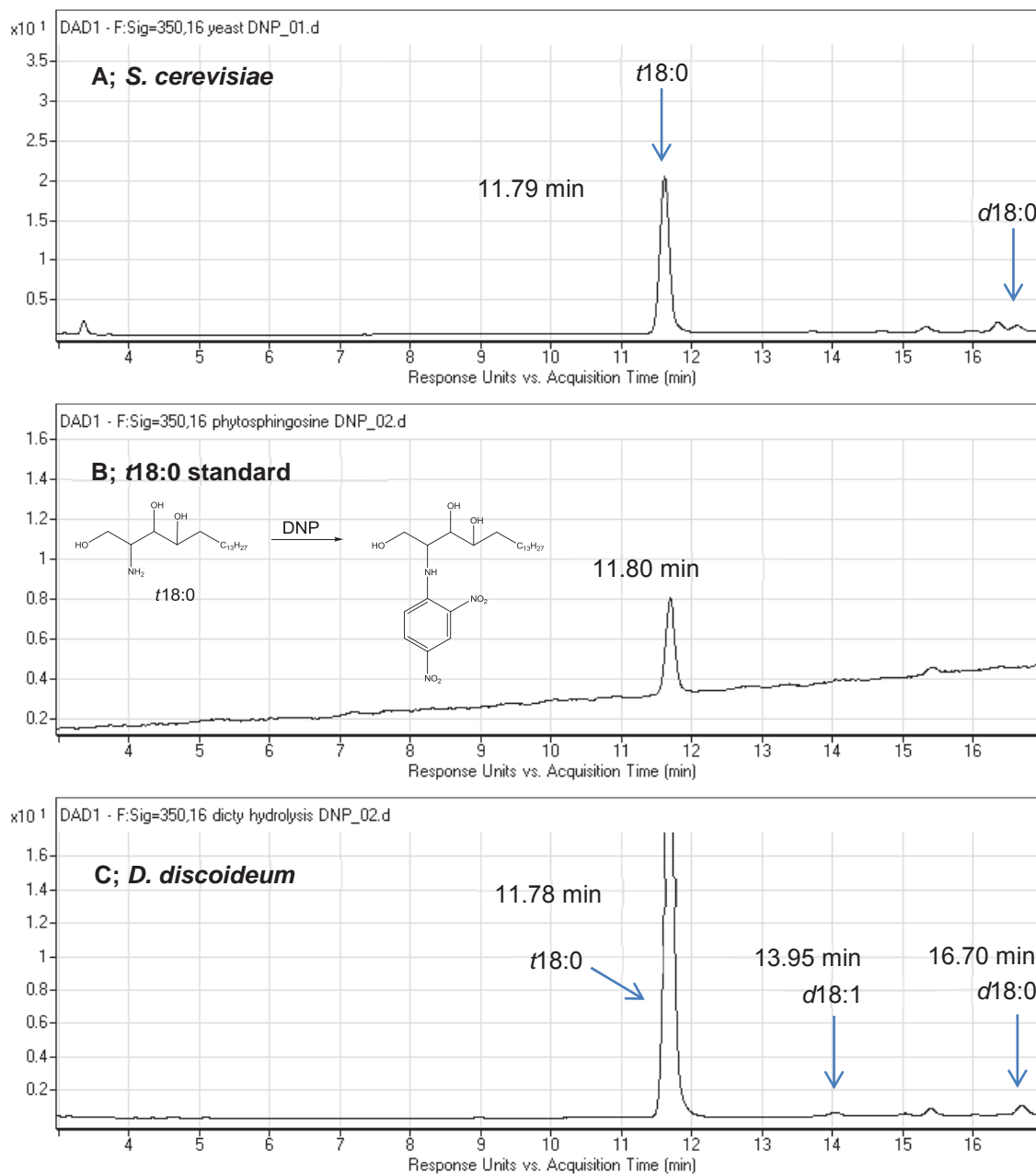


Figure 52. HPLC-UV chromatograms of DNP-derivatized LCB standards and biological samples.

S. cerevisiae chiefly contains $t_{18:0}$ LCB with small quantities of $d_{18:0}$ (identified by standard, not shown) (76) as demonstrated in Figure 52 (A/B). *D.*

discoideum was found by analysis of DNP derivatives from Ba(OH)₂ hydrolysate and comparison of UV absorption and retention time to DNP-derivatized standards to contain three LCBs; phytosphingosine (*t*18:0), sphinganine (*d*18:0) and sphingosine (*d*18:1) (Figure 52 (C)). Figure 52 (B) corresponds to the DNP-derivatized standard phytosphingosine, while sphinganine, and sphingosine were similarly identified and compared to *Dictyostelium* (not shown).

The DNP derivatives were very helpful in determining the presence of a number of LCBs in *D. discoideum*. A mass spectrometry approach was then taken to provide a more concrete identification of the long chain bases, without derivatization following the barium hydroxide hydrolysis. The non-derivatized LCB species proved to be very stable and provided consistent and valuable fragmentation patterns for identification. A triple quadrupole mass spectrometer is particularly useful for such analyses because of its ability to ionize and dissociate a large range of compounds. It utilizes a soft ionization technique (such as ESI) to produce charged molecules whose masses can be detected directly (MS scan), or fragmented into smaller components by collision-induced dissociation (CID). The fragmentation pattern or “fingerprint” of a molecule is unique to that molecule (or class of molecules) and is crucial to compound identification and accurate quantitation of biological samples. The structural fragments of *t*18:0 are illustrated in Figure 53, with a CID spectrum of the *t*18:0 standard.

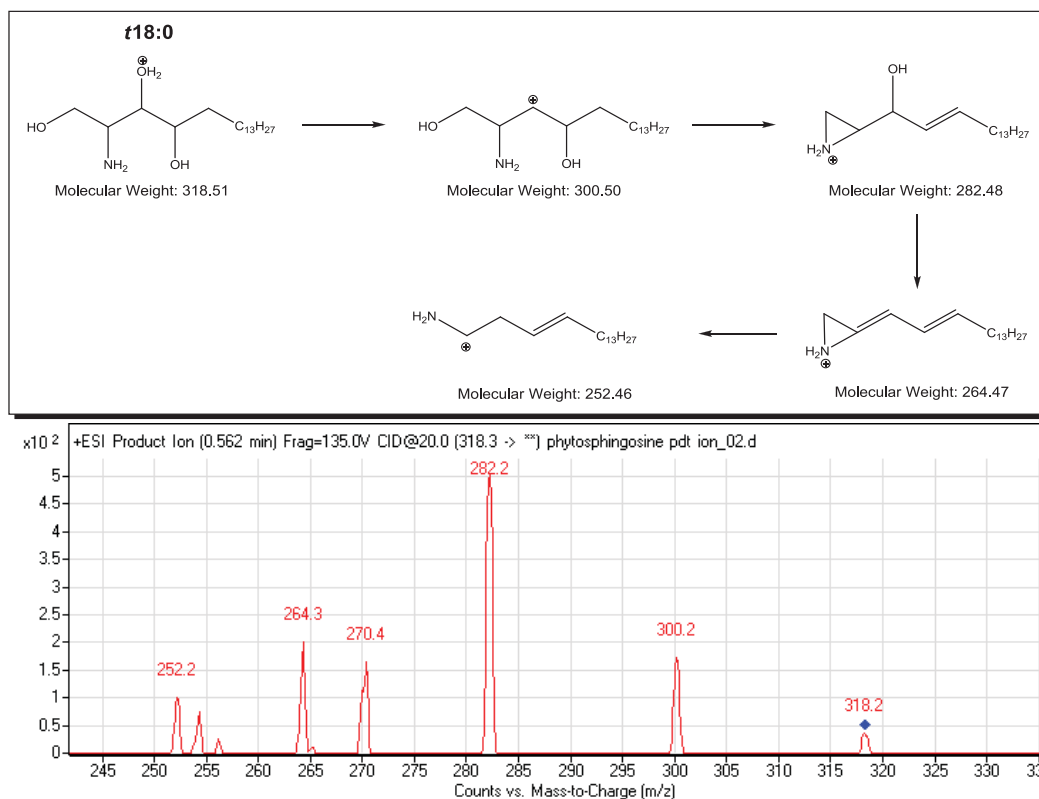


Figure 53. The structural fragmentation of the phytosphingosine backbone upon CID (80).

The three LCB standards (*t*18:0, *d*18:0, *d*18:1) were analyzed by Agilent's Optimizer software, a program designed for the QQQ to derive the best conditions of ionization and fragmentation. Optimizer uses a series of MS-MS experiments to find the conditions that most efficiently produce fragments that can be used to identify a compound. Quantitation of the three LCBs identified in *D. discoideum* was achieved via multiple reaction monitoring (MRM), a tandem MS technique that screens for the specified molecular weights of target analytes in a mixture then applies the optimal collision energies needed to afford fragments. This method matches the fragments defined by Optimizer analysis of standards to those observed in a biological sample to unambiguously confirm the presence of a molecule, and quantify it based on a response curve. In this quantification, calibration curves were generated by MRM for LCBs using *t*18:0, *d*18:0 and *d*18:1 standards (10 concentrations; 40 µg/mL → 0.078 µg/mL) and the

data was normalized to an unnatural *d*17:0 sphinganine internal standard (10 µg/mL) added to the dilution solvent. *D. discoideum* Ba(OH)₂ hydrolysis reactions (25 mg dry cell mass) were run for 24 and 48 h with 10 µg/mL *d*17:0 internal standard. Quantities of long chain bases in the hydrolysates at the two reaction times are shown in Table 4, where data is presented as the mean concentration (µg/mL) of replicate injections ± standard deviation; n=3. The increase in concentration of each LCB from 24 to 48 h indicates that LCBs were still being released from SLs after 24 h, despite the experiments that showed the C₁₂ glucoceramide standard gave optimal acyl cleavage at 24 h (Figure 51).

Table 4. Three long chain bases quantified by MRM as free LCBs.

	<i>t</i> 18:0 (µg/mL)	<i>d</i> 18:0 (µg/mL)	<i>d</i> 18:1 (µg/mL)
24 h hydrolysis	13.5 ± 0.3	0.6 ± 0.0	0.0 ± 0.0
48 h hydrolysis	18.0 ± 0.4	0.6 ± 0.0	0.0 ± 0.0

The above results were initially believed to describe the complete long chain base profile in *D. discoideum*, but as our methods for analyzing sphingolipids improved and our LC-MS techniques evolved largely towards employing direct injections (no chromatography) which allowed for heightened sensitivity and ease of interpretation, the existing profile was reassessed. To improve the chances of detecting new LCBs, the barium hydroxide hydrolysis preparation was performed on a larger quantity of cells (100 mg dry cell mass for 24 and 48 h). Using the 6410 QQQ in scanning mode, the ions of the hydrolysate were determined, followed by product ion scanning of each ion. The ions [M+H⁺] = 332, 344, 346, 358, 372 *m/z* in the sample each revealed a fragmentation pattern similar to that of previously identified phytosphingosine species indicating that they too may be long chain bases (Figure 54).

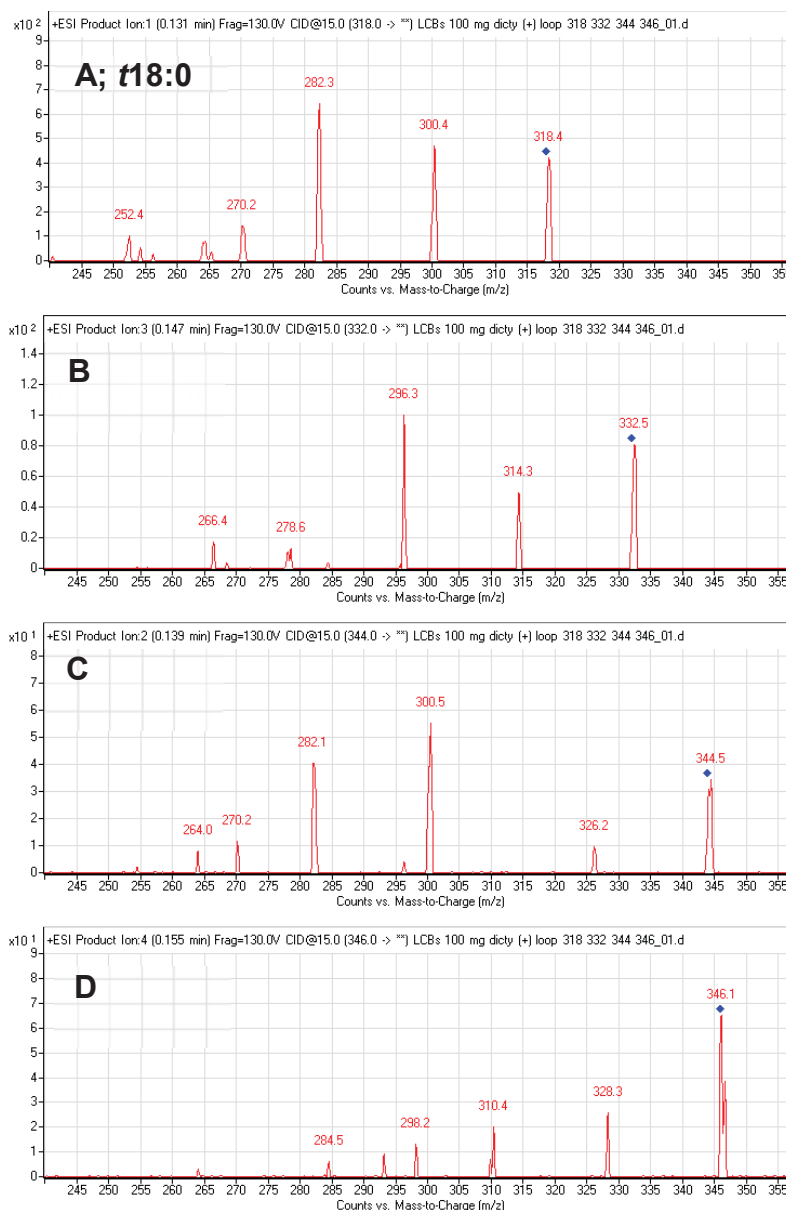


Figure 54. Fragmentation patterns of additional *D. discoideum* long chain bases from Ba(OH)₂ hydrolysate.

Figure 54 (A) illustrates the fragmentation pattern of biologically derived t18:0, which follows with the fragmentation scheme presented in Figure 53. Upon collision-induced dissociation, [M+H⁺] = 332, 344, 346, 358, 372 ions were found to produce nearly identical fragmentation patterns to t18:0, differing only by integers of *m/z* 14 indicating increasing number of methylene groups and/or by

one unit of unsaturation. While the fragmentation patterns strongly suggested that these ions corresponded to longer chain length trihydroxy LCBs, without the availability of other authentic standards, the only available method of verifying their identities lay in obtaining the accurate masses of each. The Ba(OH)₂ hydrolysate was therefore analyzed on an Agilent 6520 QTOF under the same conditions used on the QQQ. The MassHunter qualitative analysis software generated formulae consistent with *t*19:0 (*m/z* 332), *t*20:0 (*m/z* 346), *t*20:1 (*m/z* 344), *t*21:1 (*m/z* 358) and *t*22:1 (*m/z* 372) long chain bases (Figure 55). *t*18:0 (*m/z* 318) was excluded from this window, because its significantly higher abundance (1×10^6) made it more difficult to view the lower intensity LCBs (full spectrum inset in Figure 55). The two signals at *m/z* 334 and *m/z* 337 represent background ions. As discussed above, given the variability associated with the Ba(OH)₂ hydrolysis, the exact concentrations of these newly discovered LCBs were not pursued.

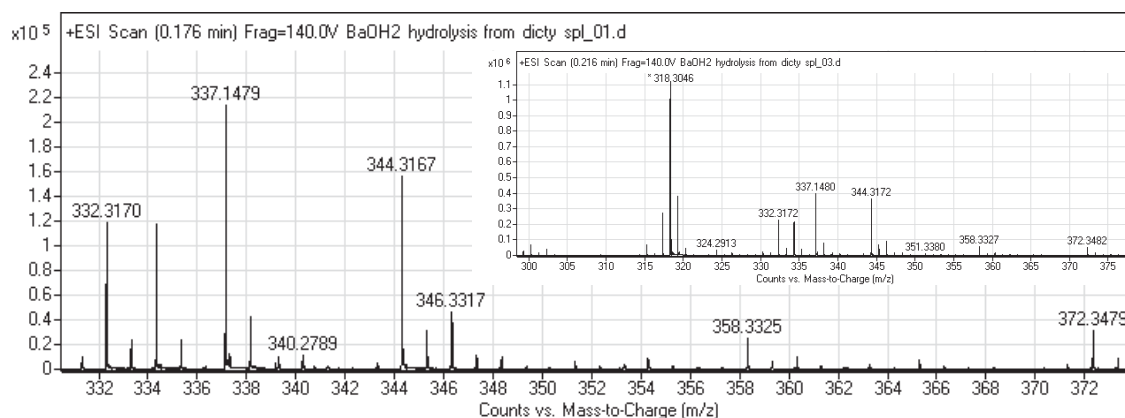


Figure 55. The exact masses of long chain bases obtained via a quadrupole time-of-flight mass spectrometer.

Ultimately, it seemed that while the DNP approach was sound in principle, it did not allow for the full characterization of long chain bases due to the lack of sensitivity, which was a particular drawback of having to perform chromatography in order to visualize individual LCBs. The derivatization also greatly decreased sample lifetimes. By shifting to direct injection, Ba(OH)₂ hydrolysis to liberate

acyl chains from LCBs, and combining the fragmentation patterns obtained from the QQQ with the resolving power of the QTOF, eight long chain bases were identified in total. The majority of the LCB content is derived of *t*18:0, *t*19:0, *t*20:0 and *t*20:1, with lower abundances of *t*21:1 and *t*22:1, followed lastly by *d*18:0 and *d*18:1. A percent composition of LCBs representative of the Ba(OH)₂ hydrolysis reaction is displayed in Figure 56, derived from [M+H⁺] ion abundances (QTOF data).

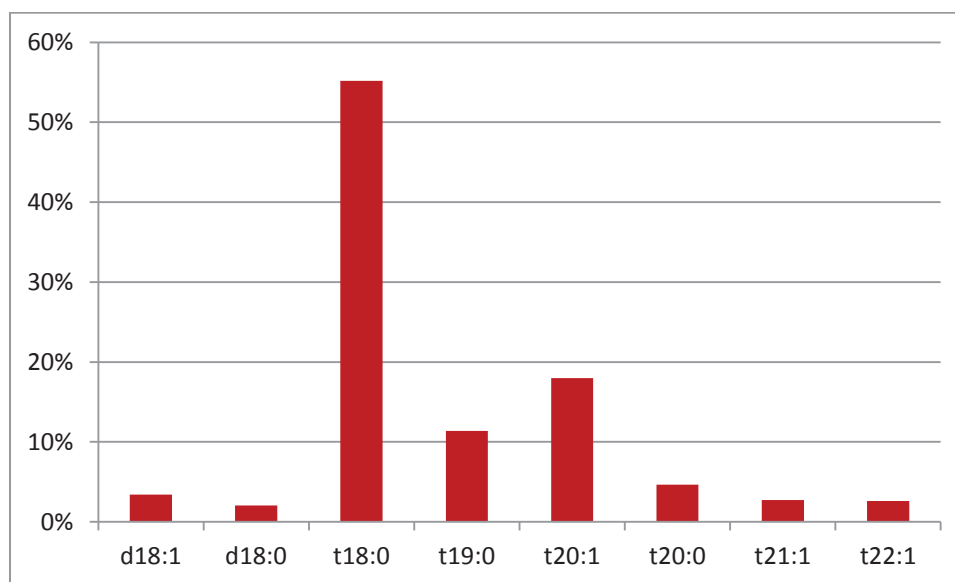


Figure 56. Percent composition of *D. discoideum* LCBs.

This phytosphingosine-based LCB profile coincides with those usually associated with plants (*t*18:0 and *d*18:0) and yeast (*t*18:0 and other trihydroxy LCBs) (4, 33). The dominance of phytosphingosine in *Dictyostelium* is interesting. Given the corresponding scarcity of sphingosine, it is reasonable to suggest that previous work examining of the signaling properties of sphingosine-1-phosphates (16-20) may have in fact been observing the effects of phytosphingosine-1-phosphates. Misinterpretations such as this have been addressed in the past; Corso *et al.* (81) challenged the commonly accepted viewpoint that S1P is essential for signaling in plants due to the fact that

sphingosine is rarely present in detectable amounts. The signaling metabolite for stomatal closure in *Arabidopsis* was initially characterized as S1P, but it was shown that this signaling was not specific to S1P, as phytosphingosine-1-phosphate promoted stomatal closure as well. Additionally, the sphingosine kinase of *Arabidopsis* (the enzyme that phosphorylates sphingosine to yield S1P) is not specific to sphingosine, but can also phosphorylate other LCBs (38). While publications regarding S1P signaling in *Dictyostelium* relied on the assumption that sphingosine-1-phosphate is the long chain base phosphate, without fully characterizing the LCBs of *D. discoideum* as we have, they may have assumed incorrectly. Phytosphingosine-1-phosphate has also been shown to have bioactivity in *S. cerevisiae* (82) and two genes encoding LCB kinases (*LCB4* and *LCB5*) that can use sphingosine, dihydrosphingosine, or phytosphingosine have been described (83).

However, there is no evidence that directly challenges S1P's activity as described. It is also possible that sphingosine acts as a signaling molecule in *D. discoideum*, as suggested by the very low concentrations in our profile, but it may be more plausible that the bioactive form is phosphorylated. Two homologues of the sphingosine kinase gene (termed *sgkA* and *sgkB*) have been described in *Dictyostelium* (84) and there appears to be no literature precedent to support signaling by free sphingosine nor have sphingosine receptors been described in *Dictyostelium*. Furthermore, mammals, which predominantly have sphingosine LCBs, use sphingosine-1-phosphate as a bioactive agent in processes such as inflammation (45). Therefore, experiments could be performed in *D. discoideum* to determine if phytosphingosine-1-phosphate also has activity as shown in *Arabidopsis* (81), and whether the kinases discussed by Alexander *et al.* (84) will phosphorylate other LCBs (38). Additionally, in terms of the work on sphingosine-1-phosphate effects on cisplatin resistance and *Dictyostelium* development (17, 18), an experiment could be performed to determine whether sphingosine-1-phosphate lyase is capable of degrading other LCBPs.

4.3.2. Isolation of sphingolipids for characterization

Once a library of long chain bases was created for *D. discoideum*, the focus shifted toward developing protocols for isolating the intact sphingolipids. A generic scheme for how this was accomplished is portrayed in Figure 57 and is similar to that of Markham *et al.* (75). A polar extraction solvent (Solvent A) and bead beating for three min provided sufficient force to break cell membranes and allow for the solubilization of complex lipids. After centrifugation, the supernatant of this total lipid extraction contains the sphingolipids, phospholipids, triacylglycerols and other lipids of the organism, with phospholipids comprising the vast majority of the extract.

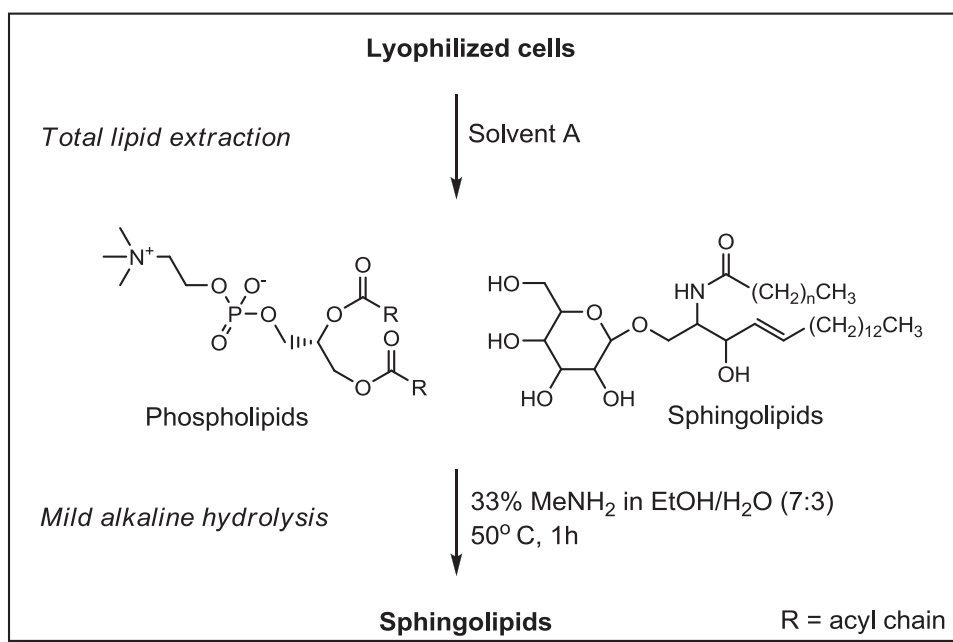


Figure 57. Approach to obtaining and isolating complex lipids from cells.

Mass spectrometry of a cellular TLE demonstrates that the phospholipid abundance is several orders of magnitude greater than that of the sphingolipids (1). Therefore, in order to analyze SLs by mass spectrometry, further preparation is required. Luckily, the carboxyl ester groups of phospholipids are much more susceptible to attack by a nucleophile than their amide counterparts

in SLs. By exposure to low concentrations of base, the fatty acids of phospholipids can be preferentially hydrolyzed, while sphingolipids remain intact as they will not succumb unless subjected to much stronger alkaline conditions such as barium hydroxide. Conditions for this mild alkaline hydrolysis of ester bonds in phospholipids have included incubations in low concentrations of NaOH in methanol or ethanol (85), but the optimal conditions employ methylamine as the base (86). The reaction is very effective at 50 °C under conditions of 33% methylamine in absolute ethanol/water, at a ratio of 7:3 (v/v) for 1 h (78) yielding an enriched sphingolipid sample devoid of phospholipids. The presence of hydrolyzed free fatty acids from this degradation is not of great consequence due to their low molecular weight relative to SLs; they can be ignored or excluded from the scan range in MS.

The efficiency of the total lipid extraction was tested by including two sphingolipid standards, a C₁₂ glucoceramide and a C₁₈ ceramide (100 µg), in a mixture with the extraction solvent and 100 mg lyophilized *Dictyostelium* cells, to simulate any matrix effects that may be present, and monitored by MS analysis of consecutive extraction fractions. The procedure from literature (75, 78) stated that the sample should be incubated to 60 °C for 20 min prior to centrifugation in the first of three extractions, and while the results from repeating this method were acceptable, sphingolipid standards were still being found in extractions from the cellular mixture after four rounds of extraction. The protocol was therefore modified to include incubations between each extraction. Figure 58 indicates the abundance of sphingolipid standard present in each of four extractions and demonstrates that under these conditions, two extractions removed greater than 90% of the sphingolipid material from the mixture, and with three extractions, all SLs were removed.

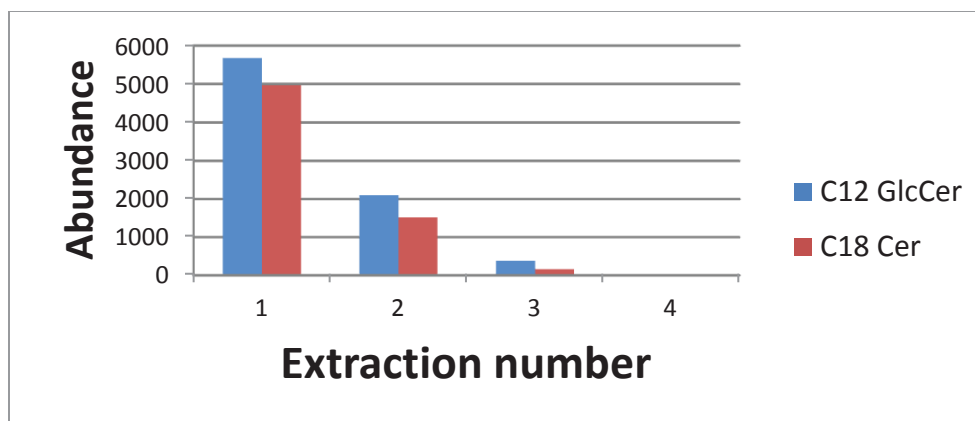


Figure 58. Efficiency of optimized total lipid extraction procedure, as illustrated with SL standards.

A mock total lipid extract with the phospholipid, 1-oleoyl-2-stearoyl-*sn*-glycero-3-phosphocholine (OSPC), C₁₂ GlcCer and C₁₈ Cer standards was used to test the efficacy of the mild alkaline hydrolysis in degrading the OSPC while leaving the sphingolipids intact throughout the reaction. A solution of 33% methylamine in absolute ethanol as a 7:3 mixture in H₂O provided swift decomposition of the OSPC species in one h with no apparent decrease in the concentrations of the sphingolipid standards.

To challenge these protocols further, they were also compared to published results. Cells of *S. cerevisiae* (InvSc1) were grown in shaking cultures, lyophilized, subjected to total lipid extraction and mild alkaline hydrolysis, and analyzed by ESI-MS. The results were compared to the work of Wenk *et al.* (1) and Schneider *et al.* (87), who characterized the phospholipid and sphingolipid profile of *S. cerevisiae* using similar mass spectrometry-based techniques to those we employed. After some optimization of solvent conditions (1:1 MeOH/CHCl₃ (1)), comparable profiles were obtained for phospholipids and sphingolipids. The spectra obtained of the total lipid extract (A) and sphingolipid (B) are provided in Figure 59. The prominent phospholipids in the TLE are phosphatidylinositol (PI) and phosphatidylethanolamine (PE) (1).

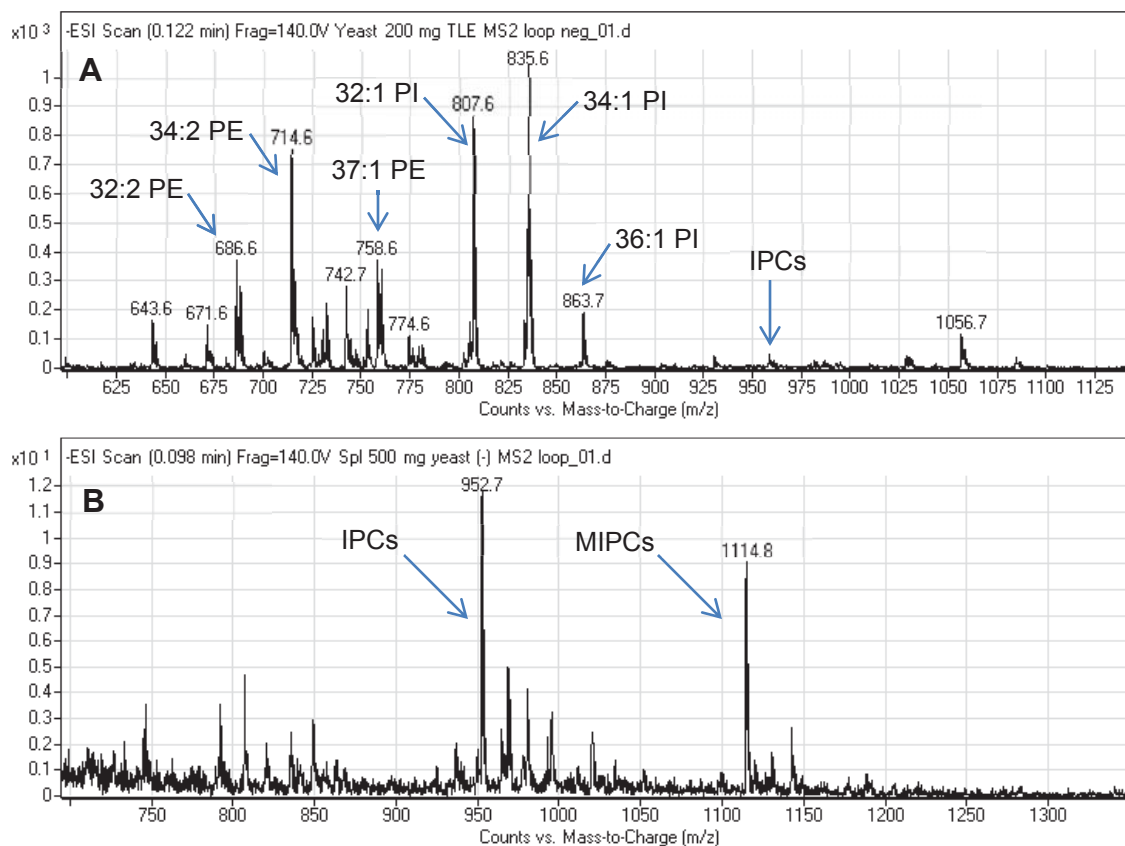


Figure 59. The complex lipids of *S. cerevisiae* following total lipid extraction (A) and sphingolipids following methylamine hydrolysis (B).

The ions of m/z 936, 952 and 968 (Figure 59; B) constitute a $t18:0/26:0$ inositol phosphorylceramide (IPC) series of SLs, with zero, one and two hydroxylations on the C_{26} fatty acyl chain (1, 88). Similarly, the ions 1098, 1114 and 1130 m/z are indicative of $t18:0/26:0$ mannosyl inositol phosphorylceramides (MIPC) SLs, again with zero, one and two hydroxylations to the C_{26} chain (1, 88) (structures in Figure 60).

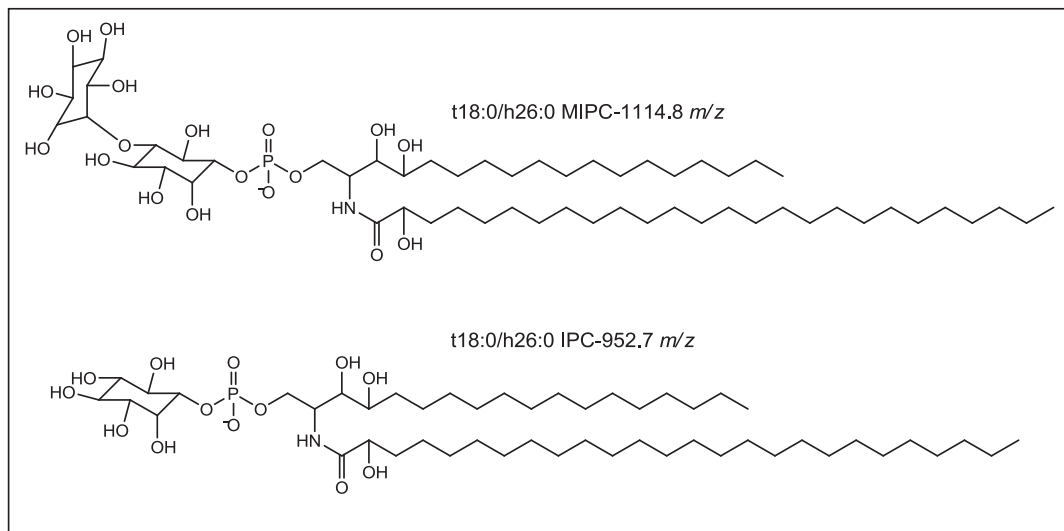


Figure 60. Examples of the IPC and MIPC SLs in *S. cerevisiae*.

Both classes were readily analyzed by ESI/MS/MS (-140 V) and yielded noteworthy fragmentation patterns upon collision-induced dissociation at 50 eV (IPC) and 75 eV (MIPC). The IPC class of sphingolipid exhibited exceptionally diagnostic fragmentation patterns upon CID, as can be seen in Figure 61. Upon selection of the 952.7 ion for dissociation, losses of the phosphoinositol head group can be observed as m/z 259 (phosphate+sugar), and its dehydration product at m/z 241. Additionally, while the particular spectra included here were obtained in scan ranges of 200-1200 m/z units, a prominent ion of m/z 78.9 is also observed when scanning the lower end of the mass range. This ion is the dehydration product of phosphate, signifying the presence of a phosphate group. All fragments were confirmed by literature (1, 89).

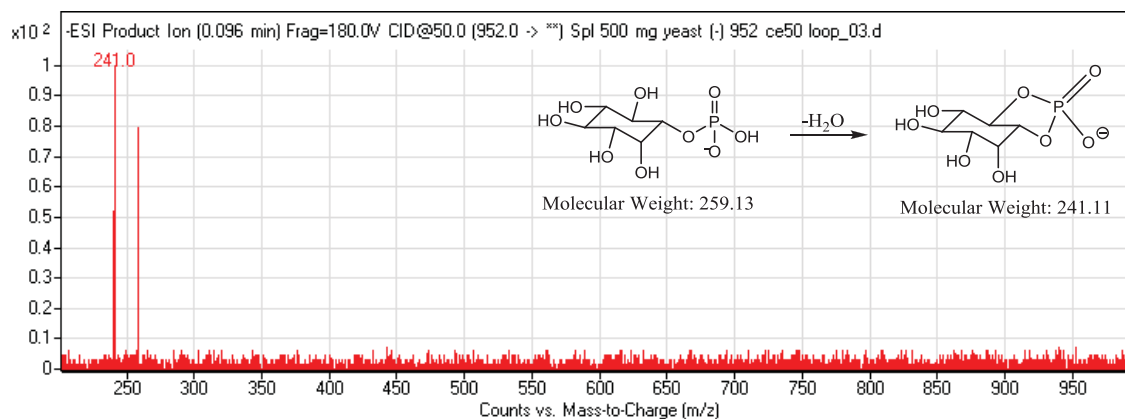


Figure 61. The fragments resulting from CID at 50 eV of a prominent inositolphosphorylceramide (m/z 952.7) in yeast.

In a similar fashion, the most prominent MIPC (m/z 1114.8) dissociates to masses of m/z 421 and 403, which correspond to the same phosphate+inositol species as IPC, with the inclusion of a second mannosyl sugar. With protocols and procedures of analysis in place, the research moved to characterizing the sphingolipids in *D. discoideum*.

4.3.3. Sphingolipid characterization for *D. discoideum*

Using the optimized total lipid extraction procedure, *Dictyostelium* cell membranes were broken and the complex lipids obtained. Upon analysis of the extract by tandem MS, the organism was found to contain high concentrations of three phosphatidylcholines (PC), with m/z values of 782 (36:4), 754 (34:4) and 730 (32:2), and a phosphatidylserine (PS 32:1; m/z 704).

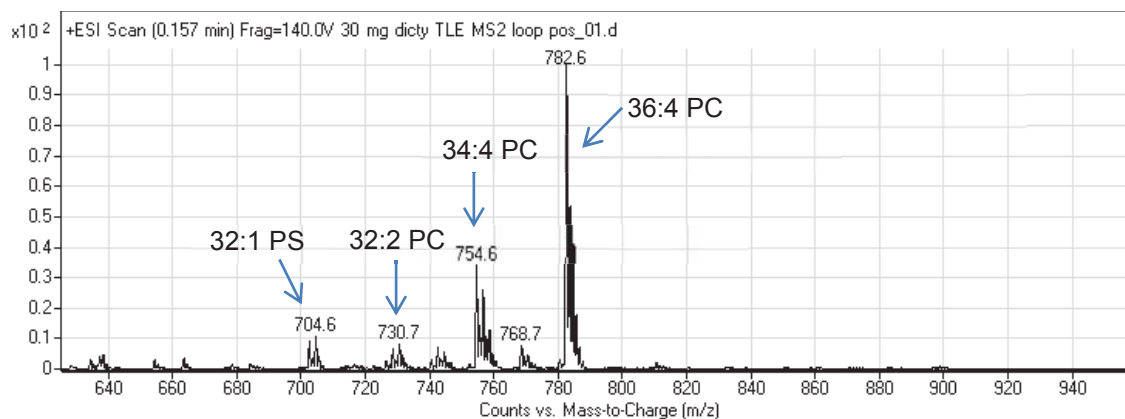


Figure 62. MS2 scan of the *D. discoideum* total lipid extract (phospholipids).

Phosphatidylcholines are particularly straightforward to distinguish by tandem mass spectrometry. Upon direct injection into the ESI source and collision-induced dissociation, the phosphocholine head group dissociates from the remainder of the molecule, producing an intense, diagnostic $m/z = 184$ fragment. The product ion scan in Figure 63 illustrates the ease with which PCs can be distinguished from other lipids. The spectrum portrays CID at 30eV of the 754 m/z ion seen in Figure 62, and exhibits a strong 184 m/z signal for the head group. While the characterization of all the components of the total lipid extract was not the goal, it was advantageous to have an idea of what the phospholipids were, specifically so that their disappearance could be confirmed following the methylamine reaction.

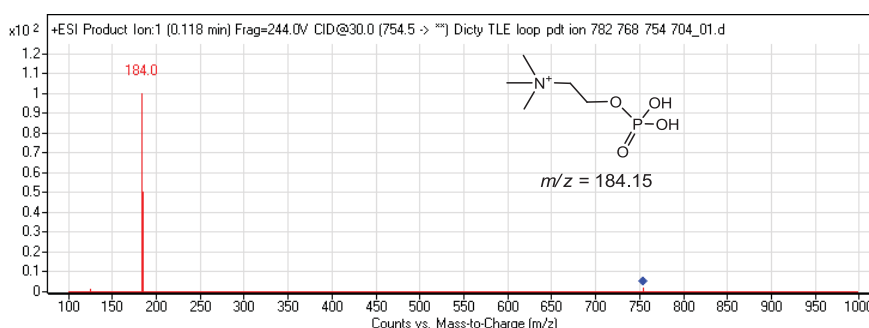


Figure 63. The collision-induced dissociation spectrum of 34:4 PC via tandem mass spectrometry.

The direct injection MS scan results of the SL-enriched mild alkaline hydrolysis product of the total lipid extract are shown in Figure 64.

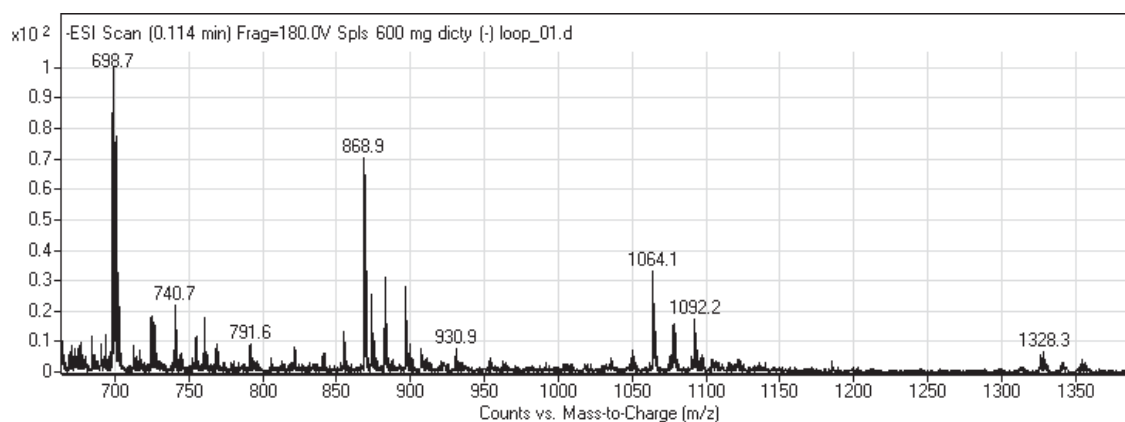


Figure 64. Mass spectrum of the enriched sphingolipid sample of *D. discoideum* following methylamine hydrolysis of phospholipids.

While the results vary slightly from sample to sample in terms of background ions and contaminants, the consistent signals presumed to be sphingolipids are as follows: 698, 700, 868, 882, 896, 1064, 1078, 1092, and 1328 m/z . Using QQQ and QTOF tandem mass spectrometers, attempts were made to identify these potential SLs.

The fatty acid profile generated in Section 2.3.2. represents the FAs from all complex lipids. To better understand the fatty acids in *D. discoideum* sphingolipids, fatty acid methyl esters were prepared from the sphingolipid mild alkaline hydrolysate. Analysis of FAMES prepared directly from the hydrolysate revealed a near identical distribution of FAMES to those seen in whole cells, with a duplicate set of 18:2 peaks differing by 1 m/z unit, corresponding to methyl amides (Figure 65).

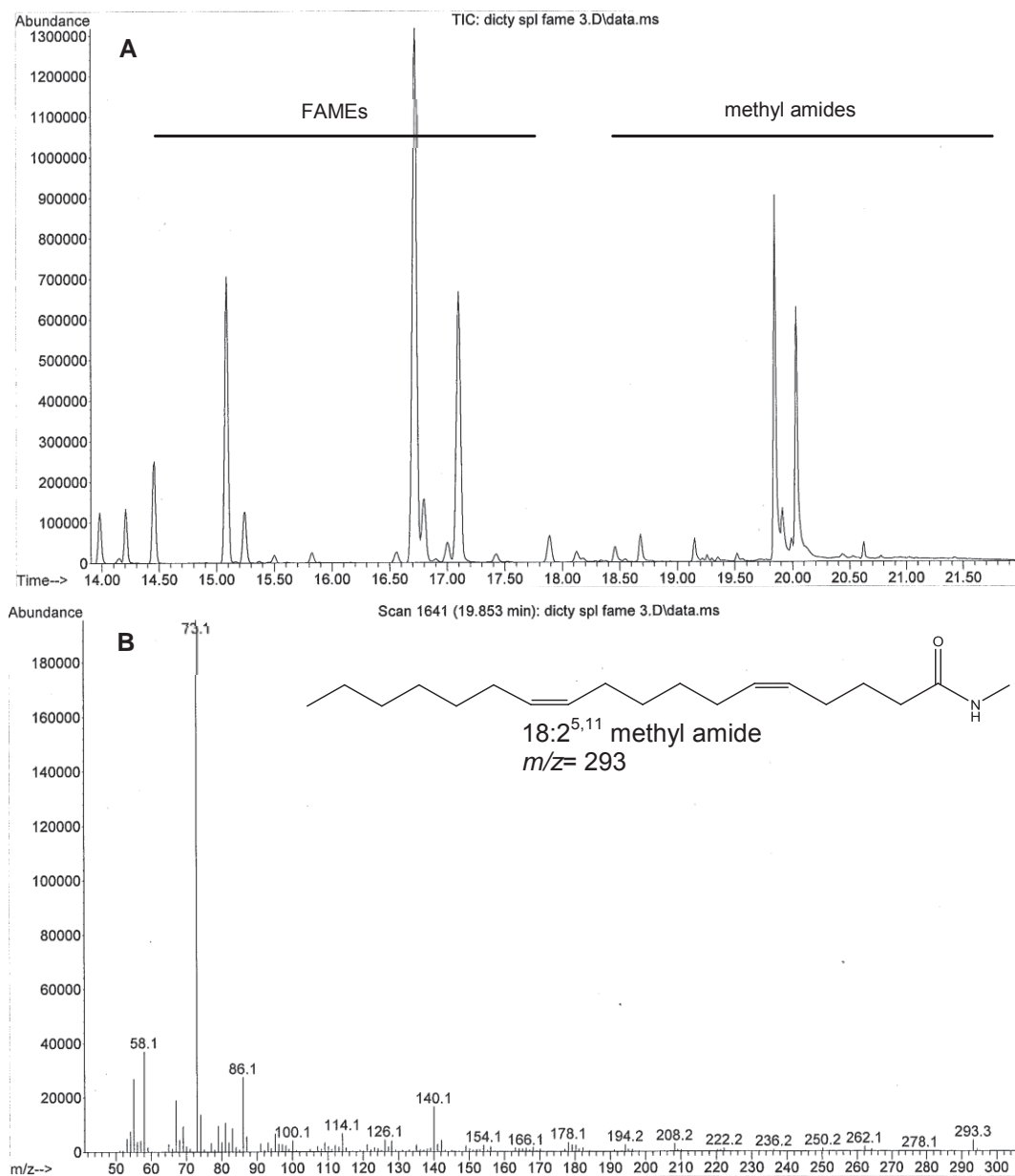


Figure 65. The total ion chromatogram (A) from FAME analysis of a mild alkaline hydrolysate and the mass spectrum of an 18:2^{5,11} methyl amide (B).

These amides are the direct products of the methylamine hydrolysis. As the ester bonds of phospholipids are hydrolyzed by nucleophilic attack of hydroxide and free carboxylate forms of the fatty acids are released (which are later converted to FAMES during derivatization), methylamine can also attack the

carboxyl group, generating the methyl amide derivative of the fatty acid. In order to obtain an accurate assessment of the sphingolipid fatty acids, the sphingolipid sample was dissolved in Solvent A and washed with hexane to remove protonated free fatty acids/amides prior to the FAME derivatization. The GC-MS results are shown in Figure 66.

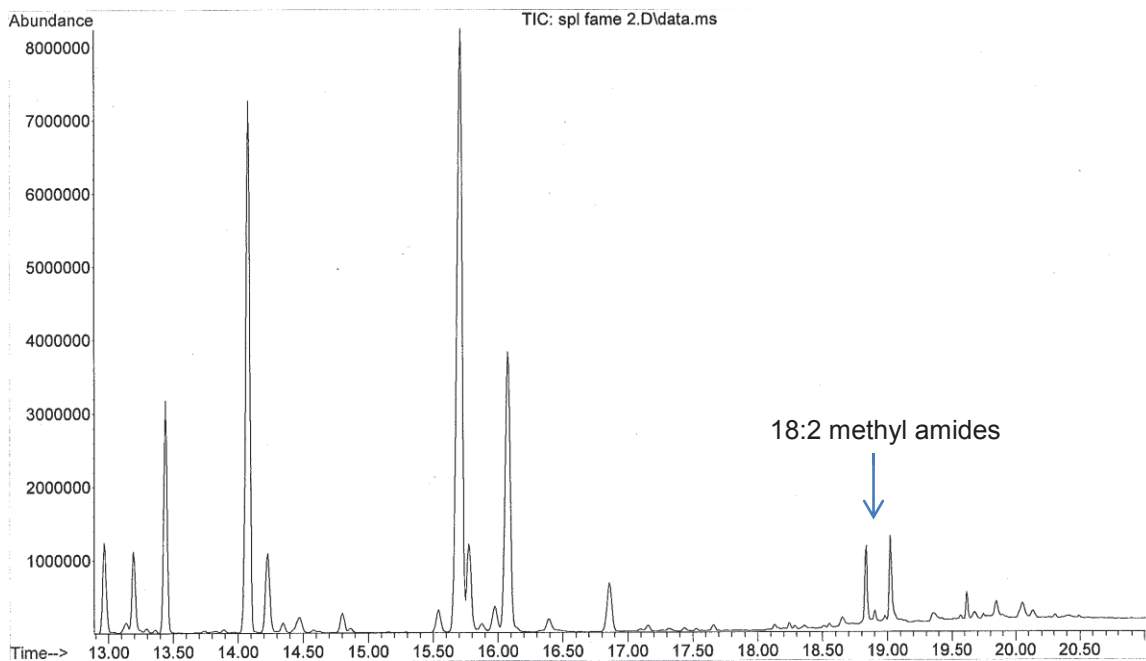


Figure 66. TIC of FAME analysis of a mild alkaline hydrolysate following hexane wash.

While the results showed a significant drop in the methyl amides, this only implies that the hexane wash was effective in removing the majority of that species but indicates nothing about the removal of free fatty acids from the mixture. The abundance of FAMES did not appear to decrease, and enrichment in VLCFA content was not observed suggesting that the free fatty acids were not removed. As many sphingolipid acylations are hydroxy FAs, TMS derivatives were prepared as well, but *h18:0-h22:0* were observed in comparable ratios to the total FA profile (Figure 67). It is probable that the FFAs remained in carboxylate form following the methylamine hydrolysis, and were therefore not removed by the hexane wash. However, the FAME results from an attempted

acidification of the hexane wash experiment contained no detectable fatty acids. In short, the experiments were not successful in supplying a sphingolipid-specific FA profile.

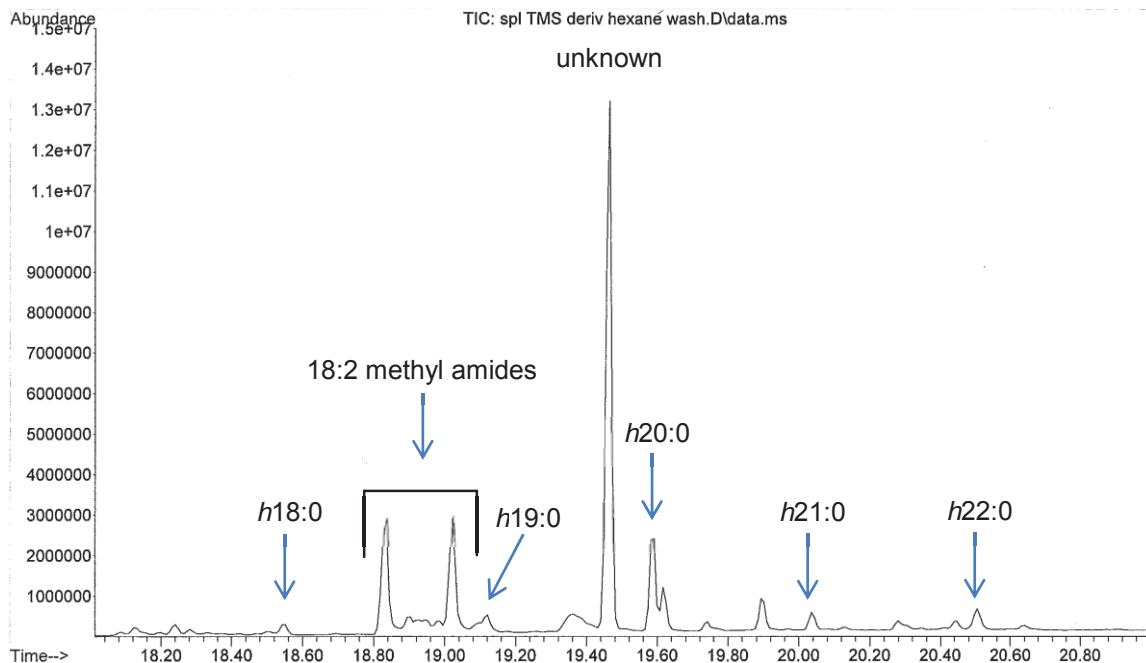


Figure 67. TIC of TMS-FAME analysis of a mild alkaline hydrolysate following hexane wash.

4.3.3.1. Ceramide-1-phosphates

The characterization of the potential sphingolipids in Figure 64 began with the collision-induced dissociation and formulae generation from accurate mass determination of the 698 and 700 ions, suggesting that they represented ceramide-1-phosphates differing by one unit of unsaturation. The fragmentation patterns observed for the $[M-H]^+$ 698 and 700 ions are shown in Figure 68.

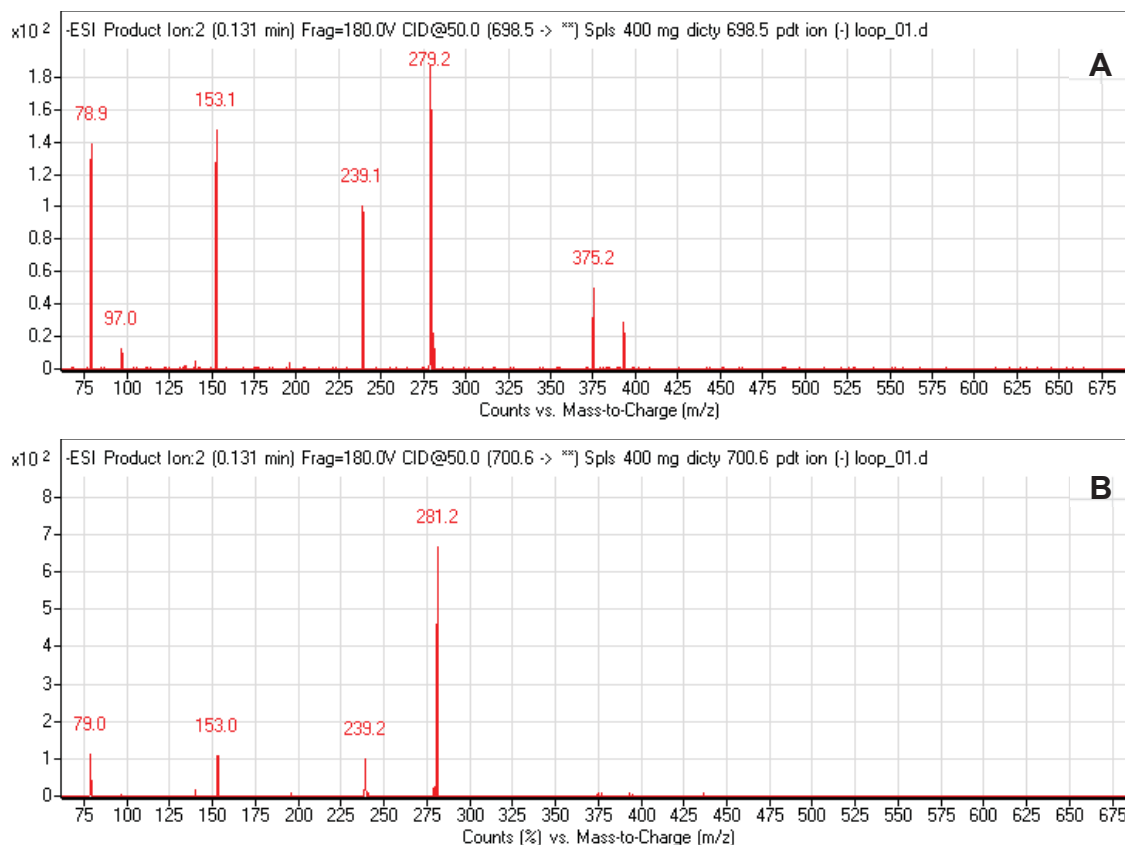


Figure 68. The CID mass spectrum of probable ceramide-1-phosphates in *D. discoideum*; $[M-H^+]$ 698 (A) and 700 (B).

The m/z 78.8 peak is a signature signal of a dehydrated phosphate group. Additionally, signals of m/z 279 and m/z 281 correspond to losses of 18:1 and 18:2 fatty acid chains from the 698 and 700 m/z parent ions, respectively. Exact mass data of $[M-H^+] = 698.5152$ and 700.5306 m/z was obtained for these ions by ESI-QTOF. MassHunter qualitative software generated formulae for these masses corresponding to $C_{39}H_{73}NO_7P^-$ and $C_{39}H_{75}NO_7P^-$; suggesting similar structures, differing by one unit of unsaturation. The presence of 39 carbons in each molecule indicates that either the LCB or the FA must be of an odd chain length. The proposed structures of $\ell 21:1^8$ LCB, with $18:2^{5,11}$ and $18:1^{11}$ FAs shown are shown in Figure 69 are supported by the FA and LCB profiles (the double bonds of the LCB and FA have been arbitrarily placed). Alternatively,

these structures could have been portrayed as *t*22:1/17:2 and *t*22:1/17:1, as *D. discoideum* has been shown to contain such C₁₇ fatty acids and a *t*22:1 LCB. However, given the losses of fragments consistent with 18:1 and 18:2 acyl chains during dissociation, the structures in Figure 69 are the most reasonable. These C1Ps are present in nearly a 1:1 ratio, as 54% of the composition is *t*21:1/18:2, while 46% is *t*21:1/18:1.

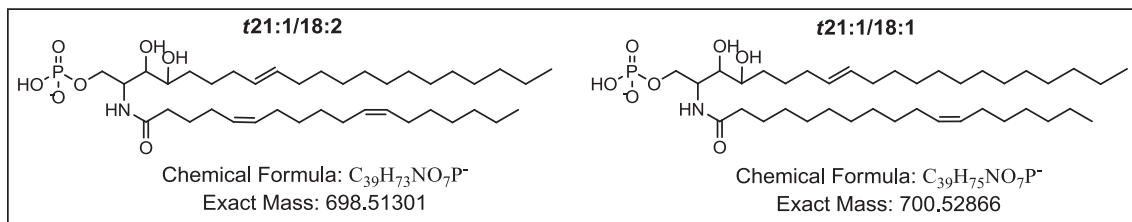


Figure 69. The proposed structures of the ceramide-1-phosphates of *Dictyostelium*. [M-H⁺] 698 and [M-H⁺] 700.

Inconsistencies in fragmentation between the *d*18:1/16:0 C1P standard (Figure 70) and the *Dictyostelium* C1Ps were observed. The losses of 18:1 and 18:2 FA from *Dictyostelium* C1Ps allowed for the assignment of the acyl chain while this fragment was not observed for *d*18:1/16:0 C1P. Differences may stem from the number and location of double bonds and additional hydroxyl group in the biological LCB, making the *Dictyostelium* species more susceptible to dissociation in a collision cell. Unfortunately, this is difficult to confirm, as neither phytosphingosine-derived C1Ps nor any C1P standards with greater than one unit of unsaturation in the acyl chain are readily available. Literature data is not available that would aid in the structural assignment of the proposed ceramide-1-phosphates. In ESI mass spectrometry, sphingolipids are commonly analyzed in the presence of cationic species (usually lithiated), affording adducts that create diagnostic fragments useful in structural determination (79, 89, 90). However, no information could be located in literature regarding structural determination of ceramide-1-phosphates as lithiated adducts. Additionally, the in-house testing of

a ceramide-1-phosphate standard only resulted in the decomposition of the SL, no lithiated species emerged that could be dissociated.

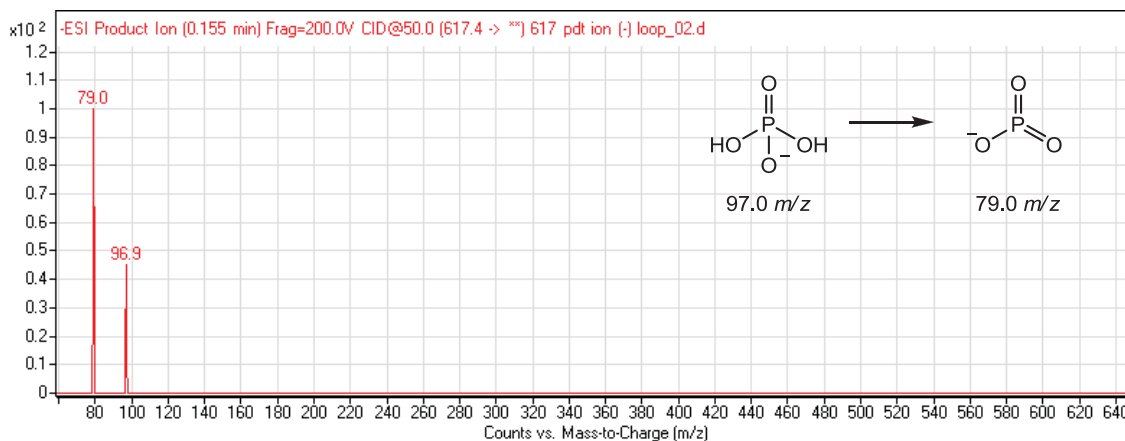


Figure 70. Collision-induced dissociation of *d*18:1/16:0 ceramide-1-phosphate standard.

In comparing *Dictyostelium* to other organisms, no clear ceramide kinase homologues have been observed in yeast (42, 43), but a gene encoding for ceramide kinase activity has been reported in *Arabidopsis* (44), and C1Ps have been shown to regulate cellular processes in plants (45, 47).

4.3.3.2. Inositol phosphorylceramides

The IPC series of sphingolipids in *S. cerevisiae* proved particularly useful as standards during the profiling of *D. discoideum* since there are no commercial standards available for these SLs. A series of ions in the SL-enriched *D. discoideum* extract with $m/z = 868, 882$ and 896 (Figure 64) suggested the presence of SLs varying by one methylene unit (m/z 14) within an SL species. CID of the most abundant ion (m/z 868) revealed a fragmentation pattern (m/z 868 \rightarrow 259 \rightarrow 241; Figure 71) reminiscent of that observed for the IPC sphingolipids in *S. cerevisiae* (Figure 61).

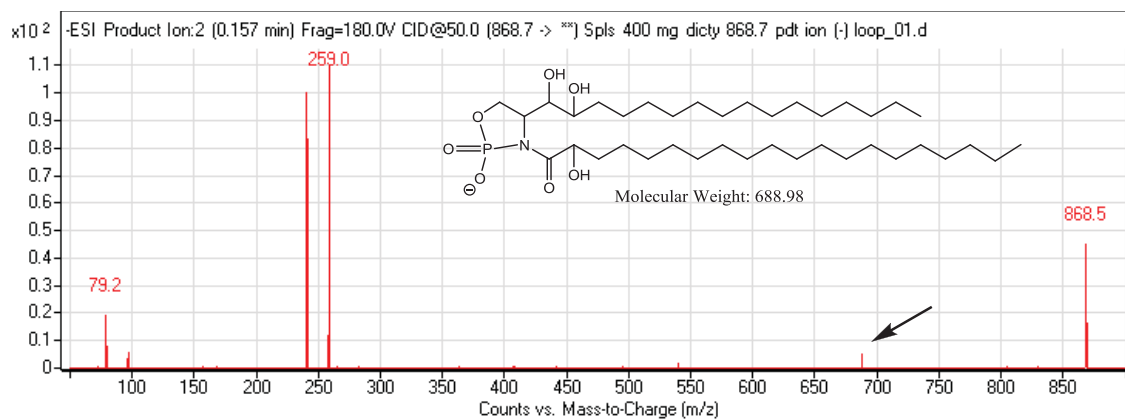


Figure 71. The mass fragmentation of most prominent IPC sphingolipid of *D. discoideum* ($[M-H]^+$ m/z 868).

Confident in the assignment of the signals (m/z 259 and 241) to an IPC head group, the sample was injected into the ESI source of the QTOF to obtain its exact mass (868.5959) and formula ($C_{44}H_{87}NO_{13}P^-$). This data is consistent with $t18:0/h20:0$ (Figure 72). The low abundance fragment at m/z 688.7 (arrow; Figure 71) likely results from the rearrangement product shown in the inset in the figure, as described by Hsu *et al.* (89). An alternative structure for this molecule is $t20:0/h18:0$. However, the presence in *D. discoideum* of 2-hydroxy 20:0 combined with the high concentrations of $t18:0$ LCB supports this classification. Upon analysis by ESI-QTOF, which has greater sensitivity than the QQQ, the presence of $t18:0/h18:0$ and $t18:0/h19:0$ (m/z 840 and 854) was revealed and verified by fragmentation. While this method could not definitively identify the specific chain length of the LCB in these SLs, there is potential to determine them by generation of lithiated SL species (89). However, further structural information could not be gathered for these IPCs. The percent composition of total *Dictyostelium* IPCs of the $t18:0/h18:0$ IPC is approximately 4%, while $t18:0/h19:0$ is twice as abundant. Including the more abundant IPCs $t18:0/h20:0$ (50%), $t18:0/h21:0$ (19%) and $t18:0/h22:0$ (18%), these discoveries brought the total number of IPC sphingolipids in *Dictyostelium* to five.

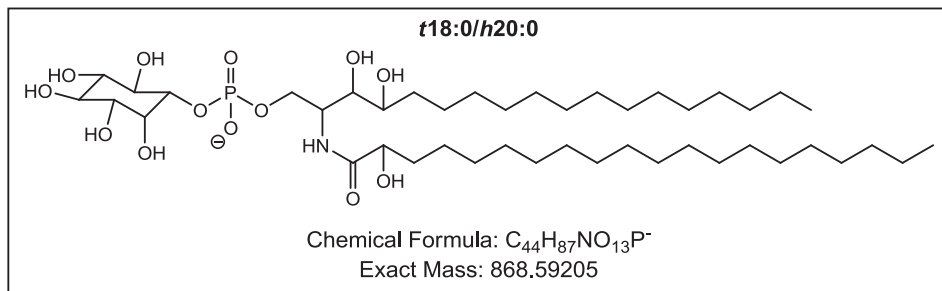


Figure 72. *t18:0/h20:0* IPC, the most prominent inositolphosphoryl ceramide of *D. discoideum*.

IPCs constitute a large proportion of the complement of sphingolipids in many eukaryotic species, but are not, however, found in animals (5, 46). As such, it is not surprising to find a large abundance of this SL class in *D. discoideum*. While in some aspects, it may appear to possess more animal-like qualities, in this instance, the prominence of IPCs in its sphingolipid profile reinforces its placement in the phylogenetic tree between plants and animals.

4.3.3.3. Unknown sphingolipids

The group of sphingolipid molecules in the enriched fraction from *Dictyostelium* with *m/z* values of 1064, 1078 and 1092 could not be correlated to any commercial or biological SL standards but exhibited variation by *m/z* 14, indicating that they likely differ by one methylene group. The ions *m/z* 1064, 1078 and 1092 were present in a 51:27:22 ratio, respectively. A product ion scan of the most abundant ion (*m/z* 1064) is shown in Figure 73. The only truly diagnostic piece of information that could be derived from the CID data was that these molecules contain a phosphate group, as indicated by the signal at *m/z* 78.8.

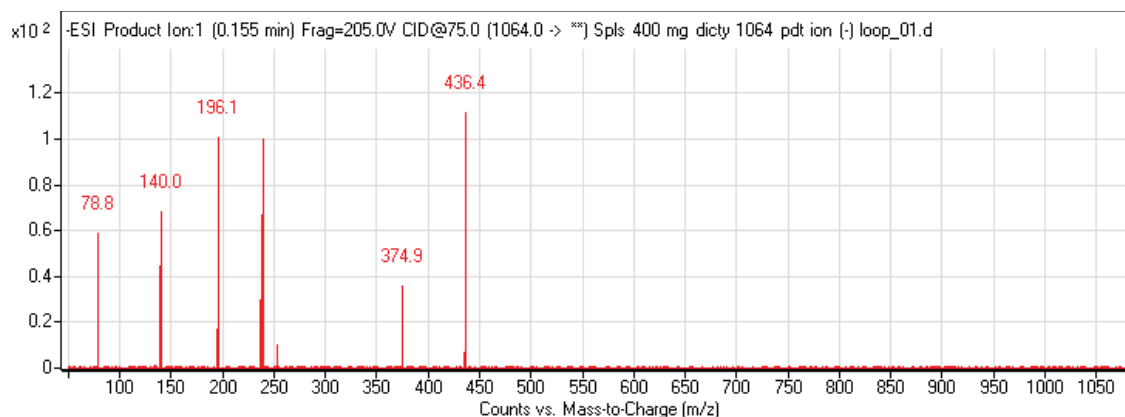


Figure 73. Product ion scan of a sphingolipid of *D. discoideum* ($[M-H]^+$ m/z 1064).

Preliminary work with *S. cerevisiae* sphingolipids suggested that the strong 436 fragment was in a mass range associated with some form of an MIPC head group. However, the collision-induced dissociation patterns of the unknown *Dictyostelium* molecules (Figure 73) did not match with that observed with the yeast MIPC (Figure 74).

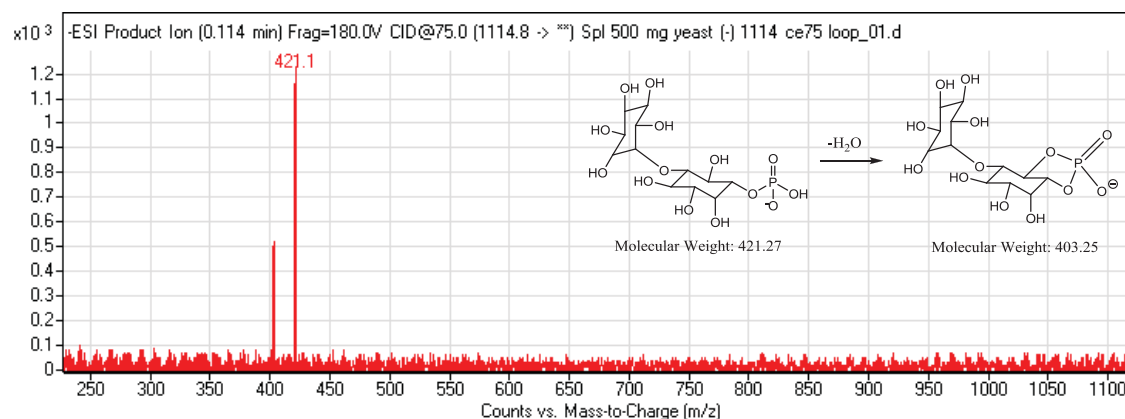


Figure 74. Product ion scan of an MIPC from yeast ($[M-H]^+$ m/z 1064) (1, 2).

The exact masses of the unknown sphingolipids did not provide assistance either. A mass of $[M-H]^+$ 1063.8670 was obtained for the most abundant ion; however, the MassHunter qualitative software could not generate

plausible formulae for any of the three unknown ions. The software produced formulae with such anomalous suggestions as 10.5 units of unsaturation, indicating the ion may be part of a dimer. While a sphingolipid in the m/z 2200 range was improbable, this result could also point to some form of an adduct, for example with cationic species such as lithium, sodium or potassium (79, 89, 90). There were no such monovalent metal ion species in the LC solvents that could contribute to such adducts, however, sodium adducts were observed by Hsu et al. (89) during the characterization of IPCs, despite the lack of added sodium ions. Unfortunately, inclusion of these cationic species into the formula generation parameters of the MassHunter software did not provide any new developments.

The exact mass of the largest fragment of the $[M-H^+]$ 1064 ion (m/z 436; Figure 73) was also obtained with the rationale that it represented the sphingolipid head group and may be more straightforward to identify. Unfortunately, the accurate mass, $[M-H^+]$ 436.2849, was not easily converted into a formula by the MassHunter software or by non-automated trial and error of possible structures. There is no evidence to suggest that this signal is even for an intact head group, and may be more likely a rearranged fragment. Possible head group and complete sphingolipid structures that correspond to similar exact masses are shown in Figure 75. The sphingolipid shown is an MIPC with a sodium sequestered somewhere on the molecule and a ι 22:1 LCB. However, given the relative abundances of each LCB as demonstrated in Figure 56, it is unlikely that the ι 22:1 LCB could be the sole contributor to such an abundant class of SL. A second reasonable assignment categorizes the LCB as ι 20:1, which was observed in high abundance (~20% composition) with a 20:0 fatty acid. However, the head group that would dissociate from either of these long chain base + fatty acid configurations does not correlate to the m/z 436.2849 obtained, or to any other fragment observed in Figure 73, and the accurate mass of either proposed structure is outside the range that determines a reasonable

match ($m/z = 1063.6548$ vs 1063.8670 observed). Further examination must be conducted to unequivocally characterize this *Dictyostelium* sphingolipid class.

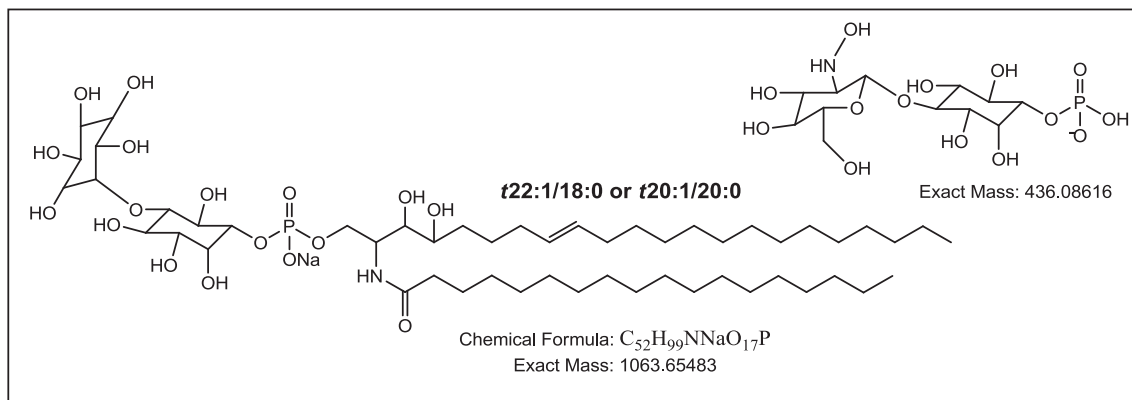


Figure 75. The proposed structure for the sphingolipid of *D. discoideum*, $[M-H^+]$ m/z 1064.

An analogous approach was used to attempt to determine the identity of the signal at m/z 1328 (product ion in Figure 76). This species may be a larger derivative (possibly containing an additional sugar moiety on the head group) of the 1064 series of SLs, however, neither the molecular ion nor the m/z 700 ion (Figure 76) was amenable to formula generation via accurate mass acquisition, which again suggested some sort of adduct formation. The strong signal of 281 m/z correlates to an 18:1 fatty acid. At sufficiently high collision energy (100 eV) the dehydration product of phosphate can be observed as well (m/z 78.9, data not shown). With such limited pieces of structural information, no theoretical structures could be generated that correlated to the observed exact mass of $[M-H^+]$ 1328.1102 m/z .

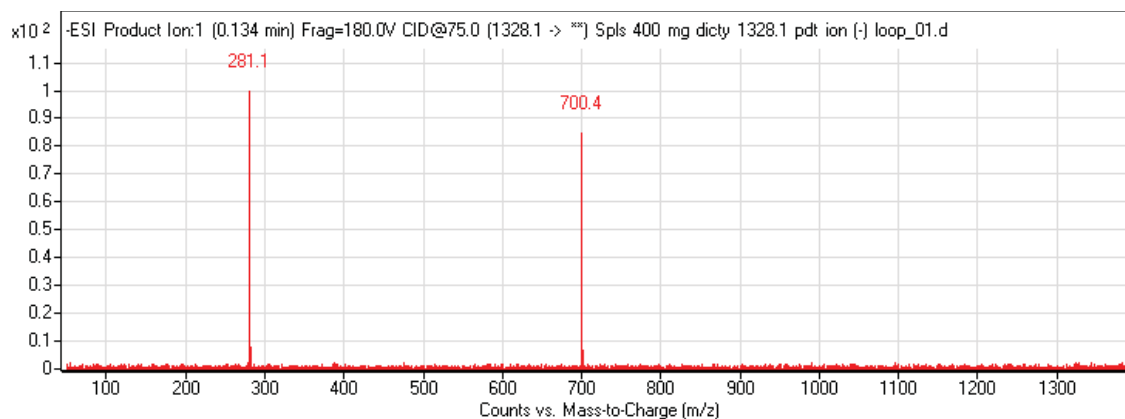


Figure 76. Product ion scan of a sphingolipid of *D. discoideum* ($[M-H]^+$ m/z 1328).

Attempts were also made to lithiate the sphingolipids of *D. discoideum* in order to gain additional structural information, particularly for the m/z 1064 series and the signal at m/z 1328. However, very limited information was derived from these experiments. Lithium adduct experiments that have been helpful in SL structural determination are typically performed on multistage ion-trap (IT) mass spectrometers (79, 89-91). These instruments have high sensitivity as well as the ability to generate a more extensive array of fragments through an MS technique that allows fragments to be “re-fragmented” multiple times. The effectiveness of using a triple quadrupole instrument (such as in our studies) in lithiated SL experiments was compared to that of an ion-trap by Hsu *et al.* (89). They concluded that while a QQQ could be effective in generating some fragments from lithiated species, the degree of sensitivity and extensiveness of fragments produced via the multistage experiments of an ion-trap is vital for obtaining structural identification of such complex sphingolipids as IPCs, GSLs, and ceramides (89). As such, it is doubtful that our instrument is capable of detecting the necessary fragments for structural identification of the SLs in the 1064 and 1328 series. To obtain these structures, it is likely that they will need to be analyzed on an IT-MS.

4.3.4. Closing Remarks

In summary, the sphingolipid profile of *D. discoideum* was partially elucidated. While the precise LCB+fatty acid combinations of the ceramide-1-phosphates and IPCs still need to be confirmed via the generation of lithiated adducts and analysis on an ion-trap MS, most of the LCB components can be accounted for in our preliminary analysis of the SL profile. The *t*18:0 (and possibly some *t*20:0) LCBs are the backbone for the majority of IPCs, and *t*21:1 (and *t*22:1) comprise the bulk of the LCBs of the ceramide-1-phosphate population. This leaves the *t*20:1 LCB with the second largest abundance unaccounted for, and may constitute the backbone for the 1064 series of uncharacterized SLs in *Dictyostelium*.

Sufficient evidence was uncovered to positively identify the most prominent sphingolipid class in the organism as inositol phosphorylceramides. Five members of this SL class were observed, each differing by one methylene unit. The most abundant IPC was that of a *t*18:0/*h*20:0, followed by *t*18:0/*h*21:0 and *t*18:0/*h*22:0, with lower levels of *t*18:0/*h*18:0 and *t*18:0/*h*19:0. As discussed, the exact combinations of long chain base and acyl chains may vary from the designations given. The arrangement of acyl chains and LCBs in the ceramide-1-phosphates, the second most abundant class of SL observed in *Dictyostelium*, were less subject to interchangeable combinations, and were classified as *t*21:1/*h*18:2 and *t*21:1/*h*18:1. Four potential sphingolipids will require additional experimental analysis (*m/z* 1064, 1078, 1092 and 1328) by generating lithiated adducts and analyzing on an ion-trap mass spectrometer. A final overview of the sphingolipid profile of *D. discoideum* is displayed in Table 5.

Table 5. The sphingolipids of *Dictyostelium discoideum*.

<i>m/z</i> Detected	Sphingolipid	Percent Composition
698.5	<i>t</i> 21:1/ <i>h</i> 18:2 C1P	54%
700.5	<i>t</i> 21:1/ <i>h</i> 18:1 C1P	46%
840.5	<i>t</i> 18:0/ <i>h</i> 18:0 IPC	4%
854.6	<i>t</i> 18:0/ <i>h</i> 19:0 IPC	8%
868.6	<i>t</i> 18:0/ <i>h</i> 20:0 IPC	50%
882.6	<i>t</i> 18:0/ <i>h</i> 21:0 IPC	19%
896.6	<i>t</i> 18:0/ <i>h</i> 22:0 IPC	18%
1063.8		51%
1077.8		27%
1091.8		22%
1328.1		

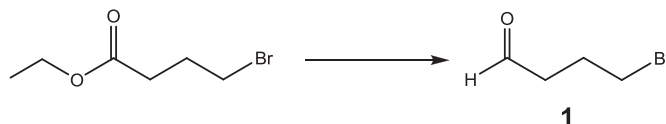
CHAPTER 5. EXPERIMENTAL DETAILS OF THE SYNTHESIS OF FATTY ACIDS

5.1. General experimental information

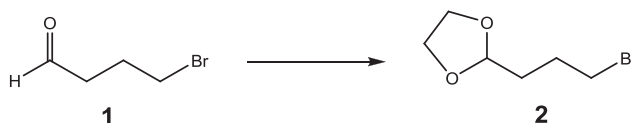
All manipulations were performed in oven-dried glassware under an argon atmosphere unless otherwise mentioned. All solvents were dried and were distilled freshly before use. THF was dried and deoxygenated by distillation under Ar from sodium-benzophenone ketyl. Methylene chloride (DCM) was dried over CaH_2 , and hexamethylphosphoramide (HMPA) was vacuum distilled from CaH_2 . Other reagents were purchased from Sigma-Aldrich or Fisher Scientific/ACROS and used without purification. Silica gel for chromatography was procured from Dynamic Absorbents (32-63 micron, #02826), using the indicated solvent. ^1H -NMR and ^{13}C -NMR spectra were recorded on a Bruker Avance-III NMR spectrometer using CDCl_3 as solvent; residual CHCl_3 (^1H , δ 7.26; 500 MHz) and CDCl_3 (^{13}C , δ 77.0; 125 MHz) were used as internal references. Peak multiplicities were given as follows: s, singlet; d, doublet; t, triplet; q, quartet; qn, quintet; m, multiplet; br, broad. IR spectra were determined as neat films (using NaCl plate) or by KBr pellets on a Thermo Nicolet Avatar 330 FT-IR spectrophotometer. High-resolution MS spectra (HRMS) were obtained on an Agilent 6520 quadrupole time-of-flight mass spectrometer equipped with ESI and atmospheric pressure chemical ionization (APCI), and through the Indiana University Chemistry Department Mass Spectrometry Facility in Bloomington, IN for compounds analyzed by chemical ionization (CI)-MS.

5.2. Synthetic standards for characterization of fatty acid profile

5.2.1. Synthesis of 18:2^{5,9} (**35**)



3-Bromobutanal (1). Ethyl 4-bromobutanoate (9.75 g, 50.00 mmol) was dissolved in DCM (90 mL) and cooled to -78 °C under argon, to which diisobutylaluminum hydride (50 mL, 1.0 M solution in hexanes, 50.00 mmol) was added dropwise at 1 mL/min. A slow rate of addition is required to reproduce the reported yield. The clear solution stirred at -78 °C for 1 h, then was allowed to warm to -60 °C for 1 h. HCl (20 mL, 10%) was added at 0 °C and a gray precipitate swiftly formed. After 1 h stirring, the product was extracted 3x with DCM, and organic extracts were washed with water and brine, then dried with MgSO₄. Careful evaporation under reduced pressure resulted in a minimal loss of the low mw product **1**, which was a light yellow oil (6.51 g, 86.1%). The aldehyde, whose NMR was consistent with literature data (**54**) was used in the preparation of **2** without further purification.

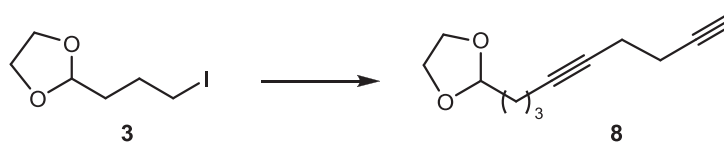


2-(3-Bromopropyl)-1,3-dioxolane (2). In a round-bottom flask, the crude residue of **1** (6.51 g, 43.10 mmol) was dissolved in benzene (175 mL), and ethylene glycol (17.8 mL, 322.50 mmol) and para-toluenesulfonic acid (0.380 g, 2.00 mmol) were added under argon. After attaching a Dean-Stark apparatus filled with 3Å molecular sieves to the flask, the heterogeneous mixture was stirred and refluxed for 3 h. NaHCO₃ (1.575 g, 18.75 mmol) was introduced and the reaction mixture was stirred for 10 min prior to being washed 2x with sat. aq.

NaHCO₃, and dried with MgSO₄. Concentration of the organic phase with a rotary evaporator yielded **2** as a light yellow oil (7.352 g, 87.5%). The dioxolane, whose NMR was consistent with literature data (54) was used in the preparation of **3** without further purification.

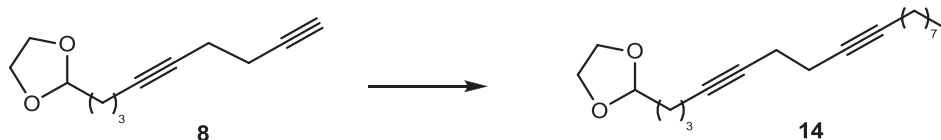


2-(3-Iodopropyl)-1,3-dioxolane (3). To a stirred solution of the crude product **2** (5.00 g, 25.60 mmol) in HPLC-grade acetone (25 mL) was added sodium iodide (4.80 g, 32.00 mmol). The solution was heated to reflux under an inert atmosphere for 3 h. The mixture was allowed to cool then DI water (25 mL) was added and the reaction mixture was stirred for 10 min. After passing the acetone solution through a sintered glass funnel packed with Celite, the filtrate was extracted 3x with DCM and dried with MgSO₄. The crude product was subjected to flash silica gel chromatography (hexanes-EtOAc gradient, 0-10% EtOAc) to yield the yellow product **3** (4.850 g, 78.2%) which was stabilized by storing over K₂CO₃. The iodide, whose NMR was consistent with literature data (92), was used in the preparation of acetylenic derivatives without further purification.



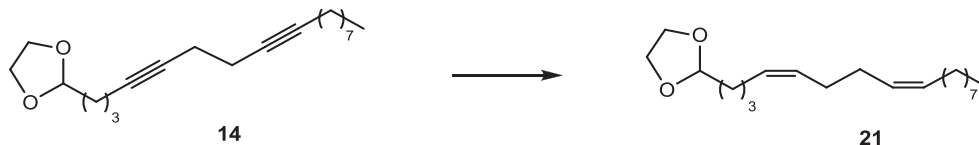
2-(Nona-4,8-diynyl)-1,3-dioxolane (8). 1,6-Hexadiyne (0.645 g, 6.20 mmol, 75% in pentane), HMPA (1.08 mL, 9.30 mmol) and dry THF (20 mL) were combined in a round-bottom flask that was then cooled to -78 °C in a dry-ice acetone bath. *n*-Butyllithium (2.55 mL, 2.43 M in hexanes, 7.44 mmol) was added dropwise over 10 min and the reaction mixture was stirred for 30 min at -78 °C. The cooling bath was removed and **3** (1.000 g, 4.13 mmol) was added in THF (5 mL). The light yellow mixture was then refluxed for 18 h, producing a dark yellow solution. Sat. NH₄Cl (~50 mL) was added to the round-bottom flask and the mixture was

stirred for 5 min and then extracted 3x with Et₂O, dried with MgSO₄ and the solvent evaporated with the use of a rotary evaporator. The yellow residue was separated by silica gel column chromatography (hexane-EtOAc gradient, 0-5% EtOAc) to afford alkyne **8** as a yellow oil (0.330 g, 41.7% yield). ¹H NMR (500 MHz, CDCl₃) δ 4.89 (t, *J* = 4.8 Hz, 1H), 3.98 (m, 2H), 3.86 (m, 2H), 2.39 (s, 4H), 2.24 (t, *J* = 7.0 Hz, 2H), 2.03 (t, *J* = 2.7 Hz, 1H), 1.78 (m, 2H) 1.64 (m, 2H); ¹³C NMR (125 MHz, CDCl₃) δ 104.28, 83.04, 80.86, 78.67, 69.06, 64.90 (2C), 32.89, 23.38, 19.11, 18.88, 18.63; IR (neat film) ν_{max} 3289, 2953, 2883, 2119, 1457, 1436, 1410, 1135, 1035, 940 cm⁻¹; HRMS (CI⁺) *m/z* [M+H⁺] calcd C₁₂H₁₇O₂ 191.1067, found 191.1069.



2-(Heptadeca-4,8-diyne)-1,3-dioxolane (14). Alkyne **8** (0.310 g, 1.61 mmol), HMPA (0.421 mL, 2.41 mmol) and dry THF (13 mL) were combined in a round-bottom flask and cooled to -78 °C. *n*-Butyllithium (0.797 mL, 2.43 M in hexanes, 1.93 mmol) was added dropwise over 10 min and the solution was then stirred for 30 min at -78 °C. The cold bath was removed and iodoctane (0.465 g, 1.93 mmol) was added in 5 mL of THF. The light yellow mixture was then refluxed for 18 h, resulting in a dark yellow solution. The reaction was quenched with sat. NH₄Cl (~25 mL) and allowed to stir for 5 min. The mixture was extracted 3x with Et₂O, dried with MgSO₄ and the solvent removed with the aid of a rotary evaporator. The yellow crude product was purified by silica gel column chromatography (hexane-EtOAc gradient, 0-5% EtOAc) to afford **14** as a yellow oil (0.330 g, 74% yield). ¹H NMR (500 MHz, CDCl₃) δ 4.88 (t, *J* = 4.8 Hz, 1H), 3.98 (m, 2H), 3.86 (m, 2H), 2.34 (s, 4H), 2.22 (t, *J* = 7.0 Hz, 2H), 2.15 (t, *J* = 7.0 Hz, 2H), 1.77 (m, 2H), 1.62 (m, 2H), 1.48 (qn, *J* = 7.5 Hz, 2H), 1.38 (m, 2H), 1.29 (s, 10H), 0.90 (t, *J* = 7.0 Hz, 3H); ¹³C NMR (125 MHz, CDCl₃) δ 104.30, 81.17, 80.41, 79.30, 78.68, 64.83 (2C), 32.87, 31.87, 29.20, 29.12, 29.00, 28.84, 23.42,

22.64, 19.49, 19.47, 18.70, 18.63, 14.08; IR (neat film) ν_{\max} 2927, 2856, 1457, 1436, 1142, 1037, 941 cm^{-1} ; HRMS (Cl^+) m/z $[\text{M}+\text{H}^+]$ calcd $\text{C}_{20}\text{H}_{35}\text{O}_2$ 305.2475, found 305.2470.

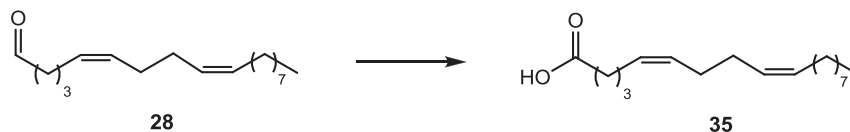


2-((4Z,8Z)-Heptadeca-4,8-dienyl)-1,3-dioxolane (21). A round-bottom flask was charged with Pd on CaCO_3 (0.104 g, 0.96 mmol, 3.5% Pb, 5.0% Pd), quinoline (0.026 mL, 0.22 mmol), **14** (0.243 g, 0.80 mmol) and absolute ethanol (3.5 mL). The mixture was flushed with H_2 provided by a balloon for 1 min, then stirred for 1 h, at which time GC analysis confirmed reduction of the acetylenic groups (56). The reaction mixture was passed through a sintered glass funnel packed with Celite to remove Pd, washed copiously with Et_2O , and concentrated under reduced pressure by a rotary evaporator. The residue was subjected to silica gel column chromatography (hexane-EtOAc gradient, 0-5% EtOAc) to remove quinoline, obtaining 0.245 g (99%) as a clear oil. ^1H NMR (500 MHz, CDCl_3) δ 5.40 (m, 4H), 4.87 (t, $J = 4.8$ Hz, 1H), 4.00 (m, 2H), 3.87 (m, 2H), 2.10 (t, $J = 2.6$ Hz, 4H), 2.04 (dt, $J = 7.0$ Hz, 4H), 1.68 (m, 2H), 1.51 (m, 2H), 1.30 (m, 12H), 0.91 (t, $J = 7.0$ Hz, 3H); ^{13}C NMR (125 MHz, CDCl_3) δ 130.46, 129.79, 129.61, 129.07, 104.58, 64.86 (2C), 33.46, 31.91, 29.75, 29.62, 29.54, 29.33, 27.44, 27.36, 27.28, 27.08, 24.09, 22.69, 14.13; IR (neat film) ν_{\max} 2925, 2854, 1653, 1457, 1141 cm^{-1} ; HRMS (Cl^+) m/z $[\text{M}+\text{H}^+]$ calcd $\text{C}_{20}\text{H}_{37}\text{O}_2$ 309.2788, found 309.2787.



(5Z,9Z)-Octadeca-5,9-dienal (28). The dioxolane **21** (0.200 g, 0.66 mmol) was combined with *p*-TsOH (0.020 g, 0.100 mmol), acetone (6.5 mL) and H_2O (1.0 mL) in a round-bottom flask equipped with a condenser, and heated to reflux

(57). After reacting for 3 h, acetone was evaporated, pTsOH was quenched with sat. NaHCO_3 , and the aldehyde product was extracted 3x with DCM and dried with MgSO_4 . The crude mixture of **28** (0.163 g, 94% yield) was used in the next step without further preparation.



(5Z,9Z)-Octadeca-5,9-dienoic acid (35). The aldehyde **28** (0.291 g, 0.96 mmol) and DMSO (6.0 mL) were combined in a round-bottom flask to which NaH_2PO_4 (0.266 g, 1.92 mmol) was slowly added in H_2O (3.0 mL, exothermic). Once the solution had cooled to room temperature, aqueous NaClO_2 (0.483 g, 4.80 mmol in 3.0 mL H_2O) was added dropwise over 5 min. The resulting yellow solution was stirred under an inert atmosphere for 4 h (92). To isolate the product, the reaction mixture was poured into ice-cold HCl (10%), extracted 4x with hexane, and dried with MgSO_4 . After rotary evaporation of the organic phase, the yellow residue was purified by silica gel column chromatography (hexane-EtOAc gradient with 0.1% acetic acid, 0-5% EtOAc) to elute the clear oil **35** (0.264 g, 86% yield). ^1H NMR (500 MHz, CDCl_3) δ 10.85 (br, 1H), 5.36 (m, 4H), 2.38 (t, $J = 7.5$ Hz, 2H), 2.09 (t, $J = 2.6$ Hz, 4H), 2.05 (dt, $J = 7.0$ Hz, 4H), 1.74 (qn, $J = 7.5$ Hz, 2H), 1.29 (m, 12H), 0.91 (t, $J = 7.0$ Hz, 3H); ^{13}C NMR (125 MHz, CDCl_3) δ 180.10, 130.63, 130.56, 128.91, 128.60, 33.44, 31.91 (2C), 29.74, 29.54, 29.35 (2C), 27.41, 27.29, 26.49, 24.58, 22.69, 14.11; IR (neat film) ν_{max} 3007, 2925, 2854, 1710, 1457 cm^{-1} ; HRMS (ESI $^-$) m/z $[\text{M}-\text{H}^+]$ calcd $\text{C}_{18}\text{H}_{31}\text{O}_2$ 279.2330, found 279.2335.

Compounds **31-37** were prepared by an analogous series of alkynylation, reduction, deprotonation, and oxidation reactions. The spectroscopic data for the final products **31-37** are as follows:

(Z)-Hexadec-5-enoic acid (31). ^1H NMR (500 MHz, CDCl_3) δ 5.35 (m, 1H), 5.25 (m, 1H), 2.29 (t, $J = 7.5$ Hz, 2H), 2.02 (q, $J = 7.5$ Hz, 2H), 1.94 (q, $J = 7.5$ Hz, 2H), 1.63 (qn, $J = 7.5$ Hz, 2H) (s, 16H), 0.81 (t, $J = 7.5$ Hz, 3H); ^{13}C NMR (125 MHz, CDCl_3) δ 179.72, 131.39, 128.13, 33.39, 31.98, 29.73, 29.69, 29.65, 29.57, 29.37, 29.34, 27.26, 26.44, 24.68, 22.73, 14.18; IR (neat film) ν_{max} 3006, 2923, 2854, 1710, 1457, 1413, 1241, 935 cm^{-1} ; HRMS (ESI $^-$) m/z $[\text{M}-\text{H}^+]$ calcd $\text{C}_{16}\text{H}_{29}\text{O}_2$ 253.2173, found 253.2175.

(Z)-Octadec-5-enoic acid (32). ^1H NMR (500 MHz, CDCl_3) δ 5.34 (m, 1H), 5.26 (m, 1H), 2.30 (t, $J = 7.5$ Hz, 2H), 2.03 (q, $J = 7.5$ Hz, 2H), 1.96 (q, $J = 7.5$ Hz, 2H), 1.65 (qn, $J = 7.5$ Hz, 2H), 1.20 (s, 16H), 0.80 (t, $J = 7.5$ Hz, 3H); ^{13}C NMR (125 MHz, CDCl_3) δ 179.82, 130.59, 129.17, 33.39, 31.98, 29.73, 29.70, 29.69, 29.66, 29.57, 29.37, 29.34, 29.33, 27.25, 26.44, 24.61, 22.71, 14.13; IR (neat film) ν_{max} 3006, 2923, 2854, 1711, 1457, 1413, 1262, 1105 cm^{-1} ; HRMS (ESI $^-$) m/z $[\text{M}-\text{H}^+]$ calcd $\text{C}_{16}\text{H}_{29}\text{O}_2$ 281.2486, found 281.2489.

(5Z,11Z)-Octadeca-5,11-dienoic acid (33). ^1H NMR (500 MHz, CDCl_3) δ 10.56 (br, 1H) 5.37 (m, 4H), 2.38 (t, $J = 7.0$ Hz, 2H), 2.00 (m, $J = 2.6$ Hz, 8H), 1.73 (t, $J = 7.5$ Hz, 2H), 1.32 (m, 12H), 0.89 (t, $J = 7.0$ Hz, 3H); ^{13}C NMR (125 MHz, CDCl_3) δ 179.89, 131.19, 130.13, 129.63, 128.25, 31.84 (2C), 29.76, 29.41, 29.29, 29.05, 29.28, 27.14, 27.10, 26.43, 24.62, 22.75, 14.13; IR (neat film) ν_{max} 3005, 2926, 2855, 1710, 1457 cm^{-1} ; HRMS (ESI $^-$) m/z $[\text{M}-\text{H}^+]$ calcd $\text{C}_{18}\text{H}_{31}\text{O}_2$ 279.2330, found 279.2331.

(5Z,9Z)-Hexadeca-5,9-dienoic acid (34). ^1H NMR (500 MHz, CDCl_3) δ 11.21 (br, 1H), 5.38 (m, 4H), 2.36 (t, $J = 7.5$ Hz, 2H), 2.03 (m, 8H), 1.76 (t, $J = 7.5$ Hz, 2H), 1.36 (m, 8H), 0.92 (t, $J = 7.0$ Hz, 3H); ^{13}C NMR (125 MHz, CDCl_3) δ 179.40, 130.63, 130.56, 128.92, 128.61, 33.31, 31.79, 29.70, 29.56, 28.99, 27.41, 27.28, 26.49, 24.58, 22.66, 14.10; IR (neat film) ν_{max} 3007, 2926, 2855, 1710, cm^{-1} ; HRMS (ESI $^-$) m/z $[\text{M}-\text{H}^+]$ calcd $\text{C}_{16}\text{H}_{27}\text{O}_2$ 251.2017, found 252.2020.

(5Z,9Z)-Heptadeca-5,9-dienoic acid (36). ^1H NMR (500 MHz, CDCl_3) δ 5.31 (m, 4H), 2.29 (t, $J = 7.5$ Hz, 2H), 2.00 (m, 8H), 1.63 (qn, $J = 7.5$ Hz, 2H), 1.19 (m, 10H), 0.89 (t, $J = 7.0$ Hz, 3H); ^{13}C NMR (125 MHz, CDCl_3) δ 179.65, 130.64, 130.53, 128.94, 128.64, 33.42, 32.62, 31.89, 29.76, 29.28, 29.23, 27.40, 27.27, 26.49, 24.58, 22.67, 14.11; IR (neat film) ν_{max} 2926, 2670, 1709, 1457, 1413, 1242, 967, 937, 723 cm^{-1} ; HRMS (ESI $^-$) m/z [M-H $^+$] calcd $\text{C}_{17}\text{H}_{29}\text{O}_2$ 265.2173, found 265.2176.

(7Z,11Z)-Octadeca-7,11-dienoic acid (37). ^1H NMR (500 MHz, CDCl_3) δ 10.90 (br, 1H) 5.39 (m, 4H), 2.38 (t, $J = 7.0$ Hz, 2H), 2.05 (m, 8H), 1.68 (t, $J = 7.5$ Hz, 2H), 1.37 (m, 12H), 0.90 (t, $J = 7.0$ Hz, 3H); ^{13}C NMR (125 MHz, CDCl_3) δ 180.16, 130.44, 129.87, 129.52, 129.07, 34.04, 31.79, 29.71, 29.32, 29.00, 28.71, 27.42, 27.37, 27.28, 27.03, 24.58, 22.66, 14.10; IR (neat film) ν_{max} 3006, 2927, 2855, 2668, 1711, 1457, 1412, 1279, 1236, 938, 725 cm^{-1} ; HRMS (ESI $^-$) m/z [M-H $^+$] calcd $\text{C}_{18}\text{H}_{31}\text{O}_2$ 279.2330, found 279.2332.

5.3. Production of ^2H -labeled fatty acids for *in vivo* studies

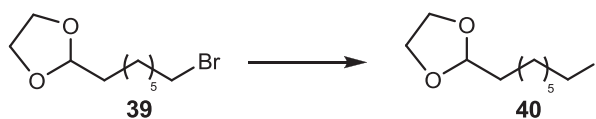
This section provides the experimental protocols employed during the generation of deuterium-labeled fatty acids for the *in vivo* studies of *D. discoideum*, split into four subsections. The first segment discusses the pathway of making d_5 -labeled FAs using stearic acid- d_5 as the template; the latter portions describe the pathways by which d_4 and d_7 -labeled FAs were produced.

5.3.1. Synthesis of stearic acid-17,17,18,18,18- d_5 (**49**)

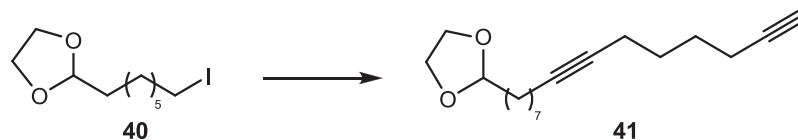
8-Bromooctanal (38). Methyl 8-bromooctanoate (5.000 g, 21.1 mmol) was dissolved in DCM (38 mL) and cooled to $-78\text{ }^{\circ}\text{C}$ under argon, to which diisobutylaluminum hydride (21.1 mL, 1.0 M solution in hexanes, 21.1 mmol) was added by syringe pump at 1 mL/min. A slow rate of addition is required to reproduce the reported yield. The clear solution stirred at $-78\text{ }^{\circ}\text{C}$ for 1 h, then allowed to warm to $-60\text{ }^{\circ}\text{C}$ for 1 h. HCl (20 mL, 10%) was added at $0\text{ }^{\circ}\text{C}$ and gray precipitate swiftly formed. After 1 h stirring, the product was extracted 3x with DCM, and organic extracts were washed with water and brine, then dried with MgSO_4 . Evaporation under reduced pressure resulted in product **38** as a light yellow oil (4.225 g, 97%). The aldehyde, whose NMR was consistent with literature data (54), was used in the preparation of **39** without further purification.



2-(7-Bromoheptyl)-1,3-dioxolane (39). In a round-bottom flask, the crude residue of **38** (4.225 g, 20.4 mmol) was dissolved with stirring in benzene (80 mL), and ethylene glycol (10.6 mL, 153 mmol) and para-toluenesulfonic acid (0.155 g, 0.82 mmol) were added under argon. After attaching a Dean-Stark apparatus filled with 3- Å molecular sieves to the flask, the heterogeneous mixture was stirred and refluxed for 3 h. NaHCO_3 (1.35 g, 16.2 mmol) was introduced and the reaction mixture was stirred for 10 min prior to being washed 2x with sat. aq. NaHCO_3 , and dried with MgSO_4 . Concentration of the organic phase with a rotary evaporator yielded **39** as a light yellow oil (5.100 g, 100%). The dioxolane, whose NMR was consistent with literature data (54), was used in the preparation of **40** without further purification.

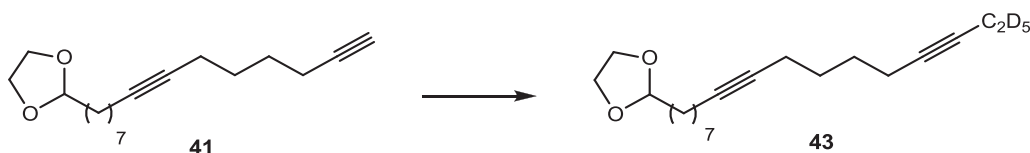


2-(2-Iodoheptyl)-1,3-dioxolane (40). To a stirred solution of the crude bromide **39** (5.10 g, 20.3 mmol) in HPLC-grade acetone (21 mL) was added sodium iodide (3.81 g, 25.4 mmol). The solution was heated to reflux under an inert atmosphere for 3 h. The mixture was allowed to cool then deionized (DI) water (25 mL) was added and the reaction mixture was stirred for 10 min. After passing the acetone solution through a sintered glass funnel packed with Celite, the filtrate was extracted 3x with DCM and dried with MgSO_4 . Upon concentration under reduced pressure yellow product **40** (5.703 g, 94%) was obtained, which was stabilized by storing over K_2CO_3 . The iodide, whose NMR was consistent with literature data (92), was used in the preparation of acetylenic derivatives without further purification.

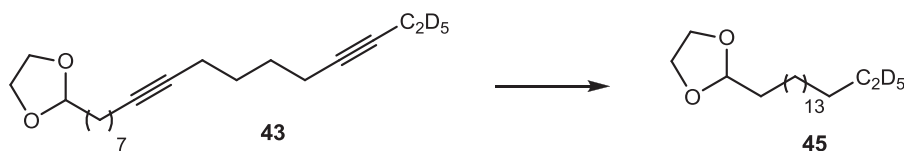


2-(Pentadeca-8,14-diyne-1-yl)-1,3-dioxolane (41). 1,8-Octadiyne (1.062 g, 10.0 mmol), HMPA (2.60 mL, 15.0 mmol) and dry THF (50 mL) were combined in a round-bottom flask that was then cooled to $-78\text{ }^\circ\text{C}$ in a dry-ice acetone bath. *n*-Butyllithium (4.84 mL, 2.48 M in hexanes, 12.0 mmol) was added dropwise over 10 min and the reaction mixture was stirred for 30 min at $-78\text{ }^\circ\text{C}$. The cooling bath was removed and **40** (1.997 g, 8.25 mmol) was added in THF (2 mL). The light yellow mixture was then refluxed for 18 h, producing a dark yellow solution. Sat. NH_4Cl (~75 mL) was added to the round bottom flask and the mixture was stirred for 5 min and then extracted 3x with Et_2O , dried with MgSO_4 and the solvent evaporated with the use of a rotary evaporator. The yellow residue was separated by silica gel column chromatography (hexane-EtOAc gradient, 0-5% EtOAc) to afford alkyne **41** as a yellow oil (0.967 g 52.1% yield). ^1H NMR (500 MHz, CDCl_3) δ 4.88 (t, $J = 4.8$ Hz, 1H), 3.99 (m, 2H), 3.87 (m, 2H), 2.25 (m, 4H),

2.16 (m, 2H), 1.98 (t, $J = 2.7$ Hz, 1H), 1.70-1.58 (m, 6H) 1.49-1.34 (m, 10H); ^{13}C NMR (125 MHz, CDCl_3) δ 104.67, 84.30, 80.63, 79.53, 68.35, 64.83 (2C), 33.89, 29.44, 29.07, 29.05, 28.73, 28.05, 27.53, 24.04, 18.74, 18.30, 18.01; IR (neat film) ν_{max} 3291, 2932, 2858, 2117, 1461, 1434, 1410, 1140, 1037, 943 cm^{-1} ; HRMS (CI) m/z $[\text{M}+\text{H}^+]$ calcd $\text{C}_{18}\text{H}_{29}\text{O}_2$ 277.2162, found 277.2149.



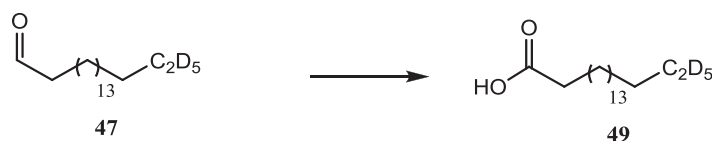
2-(Heptadeca-8,14-diyne-1-yl)-1,3-dioxolane-17,17,18,18,18- d_5 (43). Alkyne **41** (0.500 g, 1.810 mmol), HMPA (0.482 mL, 2.714 mmol) and dry THF (30 mL) were combined in a round-bottom flask and cooled to -78 $^{\circ}\text{C}$. *n*-Butyllithium (0.924 mL, 2.354 M in hexanes, 2.173 mmol) was added dropwise over 10 min and the solution was then stirred for 30 min at -78 $^{\circ}\text{C}$. The cold bath was removed and ethyl bromide- d_5 (0.168 mL, 2.173 mmol), and NaI (0.029 g, 0.173 mmol) were added. The light yellow mixture was then refluxed for 18 h, resulting in a dark yellow solution. The reaction was quenched with sat. NH_4Cl (~ 50 mL) and allowed to stir for 5 min. The mixture was extracted 3x with Et_2O , dried with MgSO_4 and the solvent removed with the aid of a rotary evaporator. The yellow crude product was purified by silica gel column chromatography (hexane-EtOAc gradient, 0-5% EtOAc) to afford **43** as a yellow oil (0.485 g, 87% yield). ^1H NMR (500 MHz, CDCl_3) δ 4.87 (t, $J = 4.8$ Hz, 1H), 3.99 (m, 2H), 3.87 (m, 2H), 2.19 (m, 6H), 1.67 (m, 2H), 1.60 (m, 4H), 1.42 (m, 10H); ^{13}C NMR (125 MHz, CDCl_3) δ 104.69, 80.46 (2C), 79.80, 79.13, 64.84 (2C), 33.90, 29.44, 29.11 (2C), 29.06, 28.75, 28.26, 24.06, 18.74, 18.35, 18.31; IR (neat film) ν_{max} 2932, 2858, 2231, 1457, 1140, 1037 cm^{-1} ; HRMS (ESI $^+$) m/z $[\text{M}+\text{H}^+]$ calcd $\text{C}_{20}\text{H}_{28}\text{D}_5\text{O}_2$ 310.2789, found 310.2790.



2-Heptadecyl-1,3-dioxolane-17,17,18,18,18- d_5 (45). A round-bottom flask was charged with 10% Pd on carbon (0.350 g), **43** (0.350 g, 1.129 mmol) and absolute ethanol (10 mL). The mixture was flushed with H_2 atmosphere provided by a balloon for 1 min, then stirred for 1 h, at which time GC analysis confirmed reduction of the acetylenes. The reaction mixture was passed through a sintered glass funnel packed with Celite to remove Pd, washed copiously with Et_2O , and concentrated under reduced pressure by a rotary evaporator. Dioxolane **45** was obtained 0.350 g (98%) as a white solid, and the residue was deprotected without further preparation.



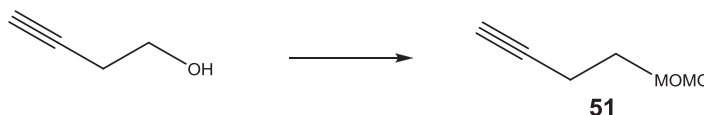
Stearaldehyde-17,17,18,18,18- d_5 (47). The dioxolane **45** (0.350 g, 1.104 mmol) was combined with *p*-TsOH (0.032 g, 0.166 mmol), acetone (12 mL) and H_2O (1.8 mL) in a round-bottom flask equipped with a condenser, and heated to reflux (57). After reacting for 3 h, acetone was evaporated, *p*-TsOH was quenched with sat. $NaHCO_3$, and the aldehyde product was extracted 3x with DCM and dried with $MgSO_4$. The crude mixture of **47** (0.270 g, 92% yield) was used in the next step without further preparation.



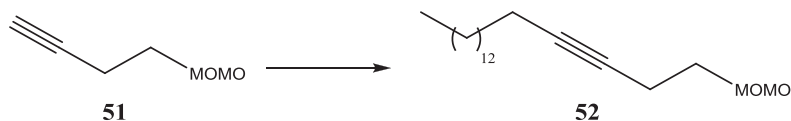
Stearic acid-17,17,18,18,18- d_5 (49). The aldehyde **47** (0.270 g, 1.012 mmol) and DMSO (7.0 mL) were combined in a round-bottom flask to which NaH_2PO_4

(0.281 g, 2.037 mmol) was slowly added in H₂O (1.0 mL, exothermic). Once the solution had cooled to room temperature, NaClO₂ (0.461 g, 5.094 mmol) was added dropwise in H₂O (1.0 mL). The resulting yellow solution was stirred under an inert atmosphere for 4 h (58). To isolate the product, the reaction mixture was poured into ice-cold HCl (10%), extracted 4x with hexane, and dried with MgSO₄. After rotary evaporation of the organic phase, the yellow residue was purified by silica gel column chromatography (hexane-EtOAc gradient with 0.1% acetic acid, 0-5% EtOAc) to elute the crystalline white solid **49** (0.233 g, 79% yield) upon evaporation of solvents under reduced pressure. ¹H NMR (500 MHz, CDCl₃) δ 11.46 (br, 1H), 2.37 (t, *J* = 7.5 Hz, 2H), 1.66 (quint, *J* = 7.5 Hz, 2H), 1.29 (m, 26H). ¹³C NMR (125 MHz, CDCl₃) δ 180.08, 34.04, 31.64, 29.70, 29.68, 29.65, 29.60 (3C), 29.50, 29.44, 29.37, 29.34, 29.25, 29.07, 24.68. IR (KBr pellet) ν_{max} 2917, 2949, 1700, 1679; HRMS (ESI⁻) *m/z* [M-H⁺] calcd C₁₈H₃₀D₅O₂ 289.3029, found 289.2956.

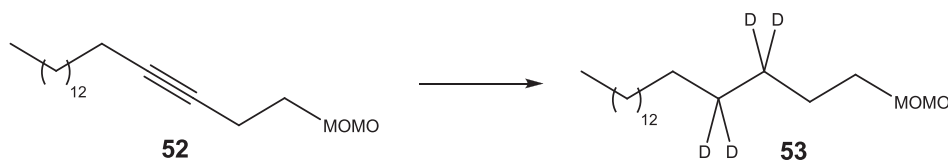
5.3.2. Synthesis of stearic acid-3,3,4,4-*d*₄ (**55**)



4-(Methoxymethoxy)but-1-yne (51). 3-Butyn-1-ol (7.500 g, 0.107 mol) was dissolved in dimethoxymethane (175 mL) to which para-toluenesulfonic acid (2.033 g, 0.011 mol) and lithium bromide (1.858 g, 0.021 mol) were added, and the resulting white solution was allowed to stir at rt for 18 h under Ar (57). The reaction mixture was washed with sat. aq. NaHCO₃, and the organics dried with MgSO₄. Concentration of the organic phase with a rotary evaporator yielded **51** as a clear oil (10.100 g, 82.0%). ¹H NMR (500 MHz, CDCl₃) δ 4.63 (s, 2H), 3.63 (t, *J* = 7.0 Hz, 2H), 3.35 (s, 3H), 2.46 (dt, *J* = 1.3, 3.5 Hz, 2H), 1.98 (d, *J* = 3.0 Hz, 1H); ¹³C NMR (125 MHz, CDCl₃) δ 96.31, 81.23, 69.24, 65.65, 55.19 19.90.



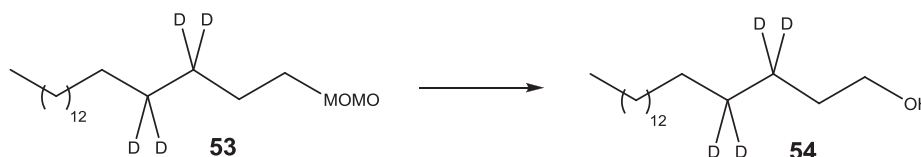
1-(methoxymethoxy)octadec-3-yne (52). Alkyne **51** (1.250 g, 10.950 mmol), HMPA (2.86 mL, 16.448 mmol) and dry THF (60 mL) were combined in a round-bottom flask and cooled to $-78\text{ }^{\circ}\text{C}$. *n*-Butyllithium (6.625 mL, 2.485 M in hexanes, 13.158 mmol) was added dropwise over 10 min and the solution was then stirred for 30 min at $-78\text{ }^{\circ}\text{C}$. The cold bath was removed and bromotetradecane (3.645, 13.158 mmol), and NaI (0.081 g, 1.096 mmol) were added. The light yellow mixture was then refluxed for 18 h, resulting in a dark yellow solution. The reaction was quenched with sat. NH_4Cl ($\sim 75\text{ mL}$) and allowed to stir for 5 min. The mixture was extracted 3x with Et_2O , dried with MgSO_4 and the solvent removed with the aid of a rotary evaporator. The yellow crude product was purified by silica gel column chromatography (hexane-EtOAc gradient, 0-5% EtOAc) to afford **52** as a light yellow oil (2.750 g, 82% yield). ^1H NMR (500 MHz, CDCl_3) δ 4.64 (s, 2H), 3.61 (t, $J = 7.0\text{ Hz}$, 2H), 3.36 (s, 3H), 2.45 (tt, $J = 2.5, 4.5\text{ Hz}$, 2H), 2.13 (tt, $J = 2.5, 4.5\text{ Hz}$, 2H), 1.46 (qn, $J = 7.5\text{ Hz}$, 2H), 1.25 (s, 22H), 0.85 (t, $J = 7.0\text{ Hz}$, 3H); ^{13}C NMR (125 MHz, CDCl_3) δ 96.50, 81.65, 66.65, 55.32, 32.06, 29.83, 29.81, 29.79, 29.75, 29.69, 29.50, 29.32, 29.14, 29.02, 22.83, 20.43, 18.89, 14.25. IR (neat film) ν_{max} 2925, 2854, 2215, 1466, 1457, 1151, 1112, 1074, 1030, 920 cm^{-1} ; HRMS (CI^+) m/z $[\text{M}+\text{H}^+]$ calcd $\text{C}_{20}\text{H}_{39}\text{O}_2$ 311.2945, found 311.2939.



1-(Methoxymethoxy)octadecane-3,3,4,4- d_4 (53). A round-bottom flask was charged with $\text{RhCl}(\text{PPh}_3)_3$ (0.072 g, 0.077 mmol) and dry benzene (5 mL) under an inert atmosphere. The stirring mixture was flushed with D_2 provided by a balloon for 1 min, producing a red solution upon exposure, to which **52** (0.400 g, 1.290 mmol) was added in 1 mL benzene and allowed to stir for 18 h (68).

Benzene was evaporated from the reaction mixture, and the residue was redissolved in hexane and passed through a sintered glass funnel packed with Celite, and concentrated under reduced pressure by a rotary evaporator. The material was resubjected to a second reduction of 3 h succeeding the first workup, at which time GC analysis confirmed complete reduction of the acetylene. The crude product was purified by silica gel column chromatography (hexane-EtOAc gradient, 0-3% EtOAc) to afford **53** as a white solid (0.335 g, 81% yield*). ^1H NMR (500 MHz, CDCl_3) δ 4.62 (s, 2H), 3.51 (t, $J = 7.0$ Hz, 2H), 3.36 (s, 3H), 1.58 (m, $J = 7.0$ Hz, 2H), 1.25 (s, 26H), 0.85 (t, $J = 7.0$ Hz, 3H); ^{13}C NMR (125 MHz, CDCl_3) δ 96.53, 68.03, 55.21, 32.07, 29.84 (8C), 29.81, 29.76, 29.65, 29.51, 22.83, 14.26. IR (neat film) ν_{max} 2923, 2854, 1457, 1153, 1113, 1047 cm^{-1} ; HRMS (CI^+) m/z [(M-OCH₃) H⁺] calcd $\text{C}_{19}\text{H}_{35}\text{D}_4\text{O}_2$ 287.3246, found 287.3260.

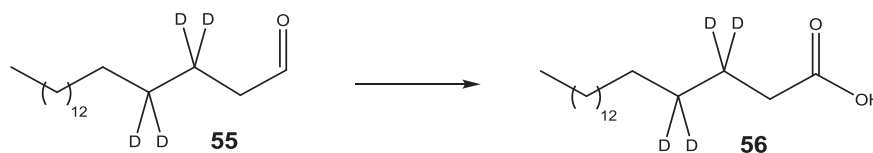
*A contaminant was produced during this reduction step that was carried on because it was not separable by silica gel chromatography. It may have originated from a partial loss of the dimethoxymethyl protecting group.



Octadecan-1-ol-3,3,4,4-*d*₄ (54). The methoxymethane-protected **53** (0.500 g, 1.577 mmol) was solvated in 2% HCl (12 M) in methanol (20 mL) in a round-bottom flask equipped with a condenser, and heated to 62 °C for 45 min (**57**), at which time HCl was quenched with sat. NaHCO_3 . The primary alcohol product was extracted 3x with hexane and dried with MgSO_4 . The crude mixture of **54** (0.420 g, 97% yield) was used in the next step without further preparation.



Stearaldehyde-3,3,4,4- d_4 (55). To a mixture of **54** (0.420 g, 1.53 mmol) and DCM (10 mL) at 0 °C was added Dess-Martin periodinane (0.908 g, 2.15 mmol). The ice bath was removed and the translucent clear solution stirred for 2h, at which time cold pentane (25 mL) was added and stirred for 10 min to precipitate DMP-derived side products. After filtration through a sintered glass funnel packed with Celite, the eluent was washed with saturated $\text{NaHCO}_3/\text{Na}_2\text{S}_2\text{O}_3$ (1:1) (69). The organics were dried with MgSO_4 and concentrated under reduced pressure by a rotary evaporator. The crude aldehyde (0.420 g, 99% yield) was taken to the next step without further preparation.

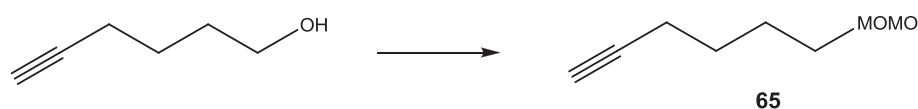


Stearic acid-3,3,4,4- d_4 (56). The aldehyde **55** (0.420 g, 1.544 mmol) and DMSO (9.0 mL) were combined in a round-bottom flask to which NaH_2PO_4 (0.420 g, 3.09 mmol) was slowly added in H_2O (2.0 mL, exothermic). Once the solution had cooled to room temperature, NaClO_2 (0.688 g, 7.72 mmol) was added dropwise over 5 min in H_2O (2.0 mL). The resulting yellow solution was stirred under an inert atmosphere for 4 h (58). To isolate the product, the reaction mixture was poured into ice-cold HCl (10%), extracted 4x with hexane, and dried with MgSO_4 . After rotary evaporation of the organic phase, the yellow residue was purified by silica gel column chromatography (hexane-EtOAc gradient with 0.1% acetic acid, 0-5% EtOAc) to elute the crystalline white solid **56** (0.190 g, 43% yield*). ^1H NMR (500 MHz, CDCl_3) δ 2.34 (qn, $J = 7.5$ Hz, 2H), 1.64 (qn, $J = 7.0$ Hz, 2H), 1.25 (s, 24H), 0.88 (t, $J = 7.0$ Hz, 3H); ^{13}C NMR (125 MHz, CDCl_3) δ 180.39, 32.07, 29.84 (8C), 29.81, 29.79, 29.74, 29.51, 22.84 14.26; IR (KBr

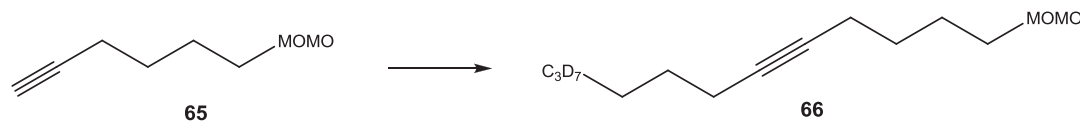
pellet) ν_{\max} 3004, 2926, 2854, 2222, 1710 cm^{-1} ; HRMS (ESI⁻) m/z [M-H⁺] calcd C₁₈H₃₁D₄O₂ 287.2894, found 287.2898.

*The contaminant discussed during the Wilkinson reduction step emerged as an oil following purification. The low yield is the result of this impurity comprising approximately half of the mass that was carried through.

5.3.3. Synthesis of octadec-5-enoic acid-16,16,17,17,18,18,18-*d*₇ (**74**)



6-(Methoxymethoxy)hex-1-yne (65). Hex-5-yn-1-ol (5.000 g, 51.00 mmol) was dissolved in dimethoxymethane (85 mL), to which para-toluenesulfonic acid (0.967 g, 5.10 mmol) and lithium bromide (0.885 g, 1.05 mmol) were added, and the resulting white solution was allowed to stir at rt for 18 h under Ar (**57**). The reaction mixture was washed with sat. aq. NaHCO₃, and the organics dried with MgSO₄. Concentration of the organic phase with a rotary evaporator yielded **65** as a clear oil (7.230 g, 99%).

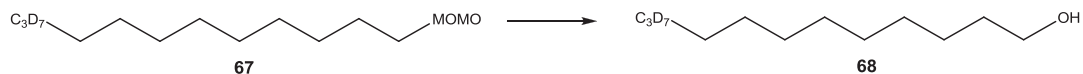


1-(Methoxymethoxy)dodec-5-yne-16,16,17,17,18,18,18-*d*₇ (66). Alkyne **65** (0.689 g, 4.84 mmol), HMPA (1.264 mL, 7.27 mmol) and dry THF (35 mL) were combined in a round-bottom flask and cooled to -78 °C. *n*-Butyllithium (2.340 mL, 2.485 M in hexanes, 5.81 mmol) was added dropwise over 10 min and the solution was then stirred for 30 min at -78 °C. The cold bath was removed and bromohexane-4,4,5,5,6,6,6-*d*₇ (1.000 g, 5.81 mmol), and NaI (0.073 g, 0.48 mmol) were added. The light yellow mixture was then refluxed for 18 h, resulting in a dark yellow solution. The reaction was quenched with sat. NH₄Cl (~75 mL)

and allowed to stir for 5 min. The mixture was extracted 3x with Et₂O, dried with MgSO₄ and the solvent removed with the aid of a rotary evaporator. The yellow crude product was purified by silica gel column chromatography (hexane-EtOAc gradient, 0-3% EtOAc) to afford **66** as a light clear oil (0.908 g, 80% yield). ¹H NMR (500 MHz, CDCl₃) δ 4.48 (s, 2H), 3.41 (t, *J* = 7.0 Hz, 2H), 3.22 (s, 3H), 2.06 (dt, *J* = 2.5, 4.5 Hz, 2H), 1.99 (dt, *J* = 2.5, 4.5 Hz, 2H), 1.55 (m, *J* = 6.0 Hz, 2H), 1.41 (m, 2H), 1.33 (qn, *J* = 6.5 Hz, 2H), 1.21 (m, 2H); IR (neat film) ν_{\max} 2917, 2851, 2214, 1150, 1116, 1043 cm⁻¹; HRMS (CI⁺) *m/z* [M+H⁺] calcd C₁₄H₂₀D₇O₂ 234.2445, found 234.2445.

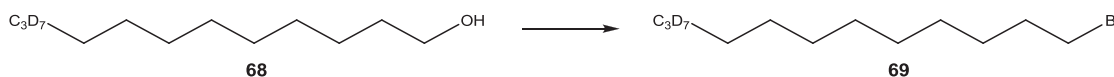


1-(Methoxymethoxy)dodecane-16,16,17,17,18,18,18-d₇ (67). A round-bottom flask was charged with RhCl(PPh₃)₃ (0.214 g, 0.23 mmol) and dry benzene (18 mL) under an inert atmosphere. The stirring mixture was exposed to D₂ atmosphere provided by a balloon, producing a red solution, to which **66** (0.900 g, 3.86 mmol) was added in 2 mL of benzene and allowed to stir for 18 h at rt (68). Benzene was evaporated from the reaction mixture, and the residue was redissolved in hexane and passed through a sintered glass funnel packed with Celite, and concentrated under reduced pressure by a rotary evaporator. The material was resubjected to a second reduction of 3 h succeeding the first workup, at which time GC analysis confirmed complete reduction of the acetylene. The crude product was purified by silica gel column chromatography (hexane-EtOAc gradient, 0-3% EtOAc) to afford **67** as a clear oil (0.820 g, 92% yield).

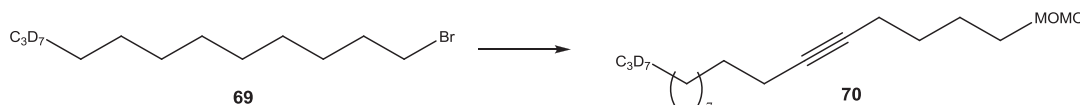


Dodecan-1-ol-16,16,17,17,18,18,18-d₇ (68). The methoxymethane-protected **67** (0.820 g, 3.46 mmol) was solvated with 2% HCl (12 M) in methanol (50 mL) in a

round-bottom flask equipped with a condenser, and heated to 62 °C for 45 min (57), at which time HCl was quenched with sat. NaHCO₃, and the primary alcohol product was extracted 3x with hexane and dried with MgSO₄. The crude mixture of **68** (0.671 g, 100% yield) was used in the next step without further preparation. ¹H NMR (500 MHz, CDCl₃) δ 3.59 (t, *J* = 7.0 Hz, 2H), 1.48 (m, 8H), 1.25 (m, 8H); IR (neat film) ν_{max} 2920, 2851, 1651, 1559, 660 cm⁻¹; HRMS (CI⁺) *m/z* [(M+CH₃CN) H⁺] calcd C₁₄H₂₃D₇NO₂ 235.2761, found 235.2759.

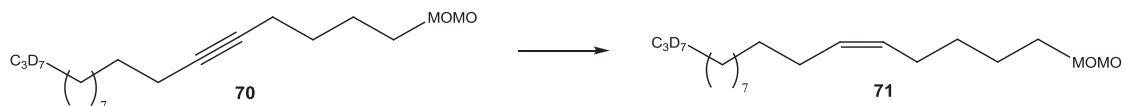


Bromododecan-1-ol-16,16,17,17,18,18,18-d₇ (69). PPh₃ (1.878 g, 7.16 mmol) and dry DCM (18 mL) were combined in a round-bottom flask at 0 °C. Bromine (0.173 mL, 6.82 mmol) was added dropwise to the stirring mixture. The resulting cloudy, light-yellow solution stirred at 0 °C for 30 min, at which time the ice bath was removed and **68** (0.660 g, 3.41 mmol) was added in DCM (2 mL). The clear solution stirred for 2 h at rt. The DCM was evaporated and the residue was redissolved in hexane, passed through a sintered glass funnel packed with Celite, and then concentrated under reduced pressure by a rotary evaporator. The product was isolated by silica gel column chromatography (hexane-EtOAc gradient, 0-1% EtOAc) to afford **69** as a clear, light oil (0.815 g, 93% yield). ¹H NMR (500 MHz, CDCl₃) δ 3.43 (t, *J* = 7.0 Hz, 2H), 1.90 (qn, *J* = 7.5 Hz, 2H), 1.45 (m, 2H), 1.28 (s, 10H); ¹³C NMR (125 MHz, CDCl₃) δ 34.08, 32.86, 29.64, 29.58, 29.56, 29.45, 29.11, 28.79, 28.20.



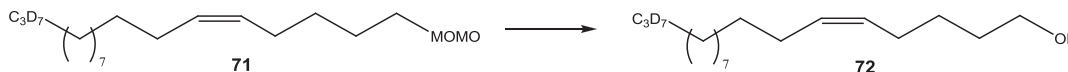
1-(Methoxymethoxy)octadec-5-yne-16,16,17,17,18,18,18-d₇ (70). Alkyne **65** (0.370 g, 2.60 mmol), HMPA (0.679 mL, 3.12 mmol) and dry THF (20 mL) were combined in a round-bottom flask and cooled to -78 °C. *n*-Butyllithium (1.256 mL, 2.485 M in hexanes, 3.12 mmol) was added dropwise over 10 min and the

solution was then stirred for 30 min at $-78\text{ }^{\circ}\text{C}$. The cold bath was removed and **69** (0.800, 3.12 mmol), and NaI (0.047 g, 0.31 mmol) were added. The light yellow mixture was then refluxed for 18 h, resulting in a dark yellow solution. The reaction was quenched with sat. NH_4Cl ($\sim 75\text{ mL}$) and allowed to stir for 5 min. The mixture was extracted 3x with Et_2O , dried with MgSO_4 and the solvent removed with the aid of a rotary evaporator. The yellow crude product was purified by silica gel column chromatography (hexane-EtOAc gradient, 0-4% EtOAc) to afford **70** as a clear oil (0.670 g, 67% yield). ^1H NMR (500 MHz, CDCl_3) δ 4.55 (s, 2H), 3.47 (t, $J = 7.0\text{ Hz}$, 2H), 3.29 (s, 3H), 2.13 (dt, $J = 2.5, 4.5\text{ Hz}$, 2H), 2.06 (dt, $J = 2.5, 4.5\text{ Hz}$, 2H), 1.63 (qn, $J = 7.5\text{ Hz}$, 2H), 1.50 (qn, $J = 7.5\text{ Hz}$, 2H), 1.38 (qn, $J = 7.5\text{ Hz}$, 2H), 1.18 (s, 14H); ^{13}C NMR (125 MHz, CDCl_3) δ 96.39, 80.67, 79.66, 67.32, 55.12, 29.70, 29.65, 29.62, 29.57, 29.18, 29.16, 29.13, 28.90, 28.88, 25.83, 18.76, 18.56; IR (neat film) ν_{max} 2925, 2854, 1648, 1556, 1451, 1149, 1113, 1044, 932 cm^{-1} ; HRMS (Cl^+) m/z $[\text{M}+\text{H}^+]$ calcd $\text{C}_{20}\text{H}_{32}\text{D}_7\text{O}_2$ 318.3384, found 318.3383.

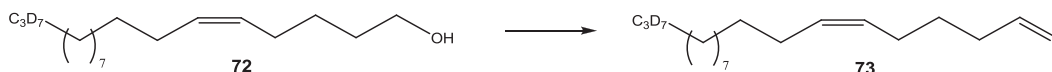


(Z)-1-(Methoxymethoxy)octadec-5-ene-16,16,17,17,18,18,18- d_7 (71). A round-bottom flask was charged with Pd on CaCO_3 (0.279 g, 2.57 mmol, 3.5% Pb, 5.0% Pd), quinoline (0.073 mL, 0.62 mmol), **70** (0.660 g, 2.06 mmol) and absolute ethanol (12 mL). The mixture was exposed to H_2 atmosphere provided by a balloon for 1 h, at which time GC analysis confirmed reduction of the acetylenes (56). The reaction mixture was passed through a sintered glass funnel packed with Celite to remove Pd, washed copiously with Et_2O , and concentrated under reduced pressure by a rotary evaporator. The residue was subjected to silica gel column chromatography (hexane-EtOAc gradient, 0-5% EtOAc) to remove quinoline, obtaining 0.570 g (85%) as a clear oil. ^1H NMR (500 MHz, CDCl_3) δ 5.30 (m, 2H), 4.55 (s, 2H), 3.46 (t, $J = 7.0\text{ Hz}$, 2H), 3.29 (s, 3H), 1.95 (m, 4H), 1.50 (qn, $J = 7.5\text{ Hz}$, 2H), 1.35 (qn, $J = 7.5\text{ Hz}$, 2H), 1.18 (s,

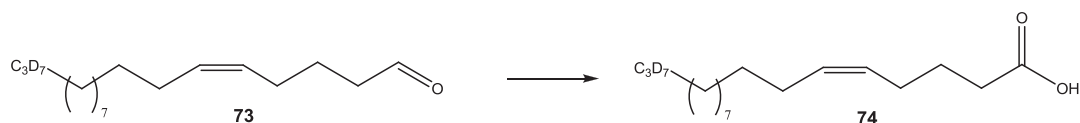
16H); ^{13}C NMR (125 MHz, CDCl_3) δ 130.40, 129.42, 96.37, 67.77, 55.18, 32.60, 32.37, 29.76, 29.72, 29.66, 29.62, 29.54, 29.35, 29.20, 29.12, 27.24, 26.94, 26.37, 26.20; IR (neat film) ν_{max} 2924, 2854, 1647, 1553, 1458, 1147, 1112, 1045, 922 cm^{-1} ; HRMS (Cl^+) m/z $[\text{M}+\text{H}^+]$ calcd $\text{C}_{20}\text{H}_{34}\text{D}_7\text{O}_2$ 320.3540, found 320.3536.



(Z)-Octadec-5-en-1-ol-16,16,17,17,18,18,18- d_7 (72). The methoxymethyl-derivative **71** (0.570 g, 1.77 mmol) was dissolved in 2% HCl (12 M) in methanol (40 mL) in a round-bottom flask equipped with a condenser, and heated to 62 °C for 45 min (**57**), at which time HCl was quenched with sat. aqueous NaHCO_3 , and the primary alcohol product was extracted 3x with hexane and dried with MgSO_4 . The crude mixture of **72** (0.465 g, 95% yield) was used in the next step without further preparation.

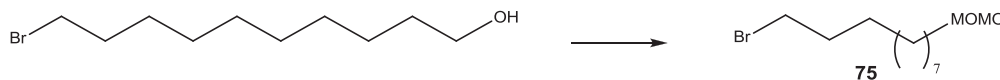


(Z)-Octadec-5-enal-16,16,17,17,18,18,18- d_7 (73). To a mixture of **72** (0.465 g, 1.700 mmol) and DCM (20 mL) at 0 °C was added Dess-Martin periodinane (1.006 g, 2.38 mmol). The ice bath was removed and the translucent clear solution stirred for 2 h, at which time cold pentane (50 mL) was added and stirred for 10 min to precipitate DMP species. After filtration through a sintered glass funnel packed with Celite, the eluent was washed with saturated $\text{NaHCO}_3/\text{Na}_2\text{S}_2\text{O}_3$ (1:1) (**69**). The organics were dried with MgSO_4 and concentrated under reduced pressure by a rotary evaporator. The crude aldehyde (0.460 g, 97% yield) was taken to the next step without further preparation.

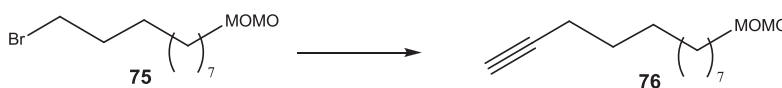


(Z)-Octadec-5-enoic acid-16,16,17,17,18,18,18-d₇ (74). The aldehyde **73** (0.460 g, 1.70 mmol) and DMSO (12 mL) were combined in a round-bottom flask to which NaH₂PO₄ (0.486 g, 3.50 mmol) was slowly added in H₂O (2.0 mL, exothermic). Once the solution had cooled to room temperature, NaClO₂ (0.798 g, 8.50 mmol) was added dropwise over 5 min in H₂O (2.0 mL). The resulting yellow solution was stirred under an inert atmosphere for 4 h (**58**). To isolate the product, the reaction mixture was poured into ice-cold HCl (10%), extracted 4x with hexane, and dried with MgSO₄. After rotary evaporation of the organic phase, the yellow residue was purified by silica gel column chromatography (hexane-EtOAc gradient with 0.1% acetic acid, 0-5% EtOAc) to elute a yellow oil containing the *Z* isomer of **74** (0.175 g, 37% yield*). ¹H NMR (500 MHz, CDCl₃) δ 5.40 (m, 1H), 5.30 (m, 1H), 2.35 (t, *J* = 7.5 Hz, 2H), 2.09 (q, *J* = 7.0 Hz, 2H), 2.00 (q, *J* = 7.0 Hz, 2H), 1.69 (qn, *J* = 7.5 Hz, 2H) 1.24 (s, 16H); ¹³C NMR (125 MHz, CDCl₃) δ 179.23, 131.40, 128.11, 33.27, 29.71, 29.69, 29.66, 29.63, 29.62, 29.57, 29.33, 29.13, 27.25, 26.43, 24.62; IR (neat film) ν_{max} 3004, 2925, 2854, 2675, 2215, 1711, 1458, 1413, 1288, 1236, 938 cm⁻¹; HRMS (ESI) *m/z* [M-H⁺] calcd C₁₈H₂₆D₇O₂ 288.2925, found 288.2921.

*An approximate 1:2 mixture of *cis* and *trans* products was observed following Lindlar catalyst reduction step. Separation of **74** from (*E*)-octadec-5-enoic acid-16,16,17,17,18,18,18-d₇ was required on a 5% AgNO₃ silica chromatotron plate.

5.3.4. Synthesis of octadec-11-enoic acid-16,16,17,17,18,18,18-d₇ (**81**)

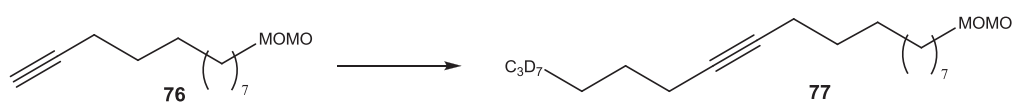
1-Bromo-10-(methoxymethoxy)decane (75). 10-Bromodecan-1-ol (5.000 g, 21.00 mmol) was dissolved in dimethoxymethane (35 mL), to which *para*-toluenesulfonic acid (0.365 g, 2.00 mmol) and lithium bromide (0.398 g, 5.00 mmol) were added, and the resulting white solution was allowed to stir at rt for 18 h under argon (**57**). The reaction mixture was washed with sat. aq. NaHCO₃, and the organics dried with MgSO₄. Concentration of the organic phase with a rotary evaporator yielded **75** as a clear oil (5.500 g, 93%).



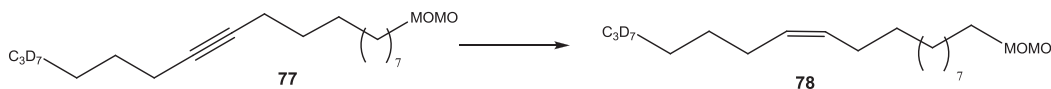
12-(Methoxymethoxy)dodec-1-yne (76). TMS-acetylene (1.571 g, 16.00 mmol), HMPA (2.784 mL, 16.00 mmol) and dry THF (40 mL) were combined in a round-bottom flask and cooled to -78 °C. *n*-Butyllithium (7.725 mL, 2.485 M in hexanes, 19.20 mmol) was added dropwise over 10 min and the solution was then stirred for 30 min at -78 °C. The cold bath was removed and **75** (3.000, 10.67 mmol), and NaI (0.160 g, 1.07 mmol) were added. The light yellow mixture was then refluxed for 18 h, resulting in a dark yellow solution. The reaction was quenched with sat. NH₄Cl (~75 mL) and allowed to stir for 5 min. The mixture was extracted 3x with Et₂O, dried with MgSO₄ and the solvent removed with the aid of a rotary evaporator. The yellow crude product was purified by silica gel column chromatography (hexane-EtOAc gradient, 0-5% EtOAc) to afford the TMS derivative of **76** as a light yellow oil (0.920 g, 38% yield*). The TMS product (0.920 g, 3.09 mmol) was transferred to a round-bottom flask in THF (20 mL) and deprotected by stirring with TBAF (6.170 mL, 1.0 M in THF, 6.17 mmol) for 2 h at room temperature. The reaction was quenched with sat. NH₄Cl (~50 mL) and allowed to stir for 5 min. The mixture was extracted 3x with Et₂O, dried with

MgSO₄ and the solvent removed with the aid of a rotary evaporator, to yield **76** (0.625 g, 90%) as a clear oil. ¹H NMR (500 MHz, CDCl₃) 4.61 (s, 2H), 3.51 (t, *J* = 7.0 Hz, 2H), 3.35 (s, 3H), 2.38 (t, *J* = 6.5 Hz, 2H) 2.17 (dt, *J* = 6.5 Hz, 4H), 1.94 (t, *J* = 3.0 Hz, 1H), 1.53 (m, 4H), 1.26 (s, 8H); ¹³C NMR (125 MHz, CDCl₃) δ 96.39, 84.80, 68.04, 67.88, 55.09, 53.87, 29.74, 29.52, 29.41, 29.08, 28.74, 26.20, 20.81, 18.39.

*Low yield was due to a flask that imploded under vacuum, resulting in significant product loss.

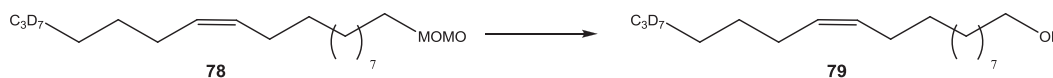


1-(Methoxymethoxy)octadec-11-yne-16,16,17,17,18,18,18-d₇ (77). Alkyne **76** (0.548 g, 2.42 mmol), HMPA (0.632 mL, 3.63 mmol) and dry THF (20 mL) were combined in a round-bottom flask and cooled to -78 °C. *n*-Butyllithium (1.169 mL, 2.485 M in hexanes, 2.90 mmol) was added dropwise over 10 min and the solution was then stirred for 30 min at -78 °C. The cold bath was removed and bromohexane-4,4,5,5,6,6,6-d₇ (0.500 g, 2.90 mmol), and NaI (0.036 g, 0.24 mmol) were added. The light yellow mixture was then refluxed for 18 h, resulting in a dark yellow solution. The reaction was quenched with sat. NH₄Cl (~55 mL) and allowed to stir for 5 min. The mixture was extracted 3x with Et₂O, dried with MgSO₄ and the solvent removed with the aid of a rotary evaporator. The yellow crude product was purified by silica gel column chromatography (hexane-EtOAc gradient, 0-5% EtOAc) to afford **77** as a light yellow oil (0.585 g, 76% yield).

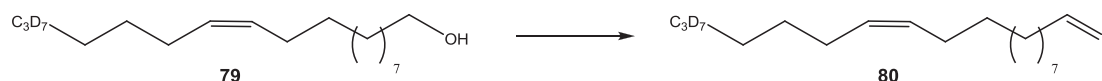


(Z)-1-(Methoxymethoxy)octadec-11-ene-16,16,17,17,18,18,18-d₇ (78). A round bottom flask was charged with Pd on CaCO₃ (0.237 g, 1.812 mmol, 3.5% Pb, 5.0% Pd), quinoline (0.062 mL, 0.52 mmol), **77** (0.570 g, 1.79 mmol) and

absolute ethanol (10 mL). The mixture was exposed to H₂ atmosphere provided by a balloon for 1 h, at which time GC analysis confirmed reduction of the acetylenes (56). The reaction mixture was passed through a sintered glass funnel packed with Celite to remove Pd, washed copiously with Et₂O, and concentrated under reduced pressure by a rotary evaporator. The residue was subjected to silica gel column chromatography (hexane-EtOAc gradient, 0-2% EtOAc) to remove quinoline, obtaining 0.575 g (99%) as a clear oil. ¹H NMR (500 MHz, CDCl₃) δ 5.32 (m, 2H), 4.57 (s, 2H), 3.47 (t, *J* = 7.0 Hz, 2H), 3.29 (s, 3H), 1.94 (q, *J* = 6.5 Hz, 4H), 1.50 (qn, *J* = 7.5 Hz, 2H), 1.23 (s, 18H); ¹³C NMR (125 MHz, CDCl₃) δ 129.95, 129.89, 96.38, 67.91, 55.11, 29.78, 29.76, 29.71, 29.61, 29.58, 29.54, 29.46, 29.31, 28.77, 27.25, 27.21, 26.22; IR (neat film) ν_{max} 2924, 2854, 1653, 1559, 1540, 1457, 1150, 1112, 1046, 919 cm⁻¹; HRMS (CI⁺) *m/z* [M+H⁺] calcd C₂₀H₃₄D₇O₂ 320.3540, found 320.3541.

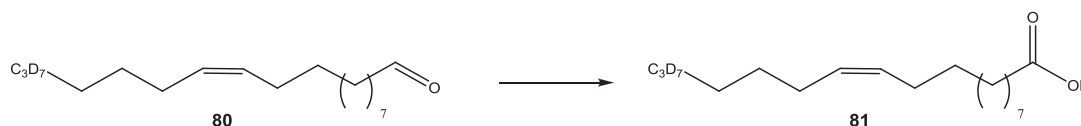


(Z)-Octadec-11-en-1-ol-16,16,17,17,18,18,18-d₇ (79). The protected alcohol **78** (0.570 g, 1.79 mmol) was dissolved in 2% HCl (12 M) in methanol (40 mL) in a round-bottom flask equipped with a condenser, and heated to 62 °C for 45 min (**57**), at which time HCl was quenched with sat. NaHCO₃, and the primary alcohol product was extracted 3x with hexane and dried with MgSO₄. The crude mixture of **79** (0.460 g, 94% yield) was used in the next step without further preparation.



(Z)-Octadec-11-enal-16,16,17,17,18,18,18-d₇ (80). To a mixture of **79** (0.455 g, 1.64 mmol) and DCM (20 mL) at 0 °C was added Dess-Martin periodinane (0.975 g, 2.30 mmol). The ice bath was removed and the translucent clear solution stirred for 2 h, at which time cold pentane (50 mL) was added and stirred for 10 min to precipitate DMP-derived side products. After filtration through a sintered

glass funnel packed with Celite, the eluent was washed with saturated $\text{NaHCO}_3/\text{Na}_2\text{S}_2\text{O}_3$ (1:1) (69). The organics were dried with MgSO_4 and concentrated under reduced pressure by a rotary evaporator. The crude aldehyde (0.438 g, 97% yield) was taken to the next step without further preparation.



(Z)-Octadec-11-enoic acid-16,16,17,17,18,18,18- d_7 (81). The aldehyde **80** (0.438 g, 1.62 mmol) and DMSO (12 mL) were combined in a round-bottom flask to which NaH_2PO_4 (0.388 g, 3.23 mmol) was slowly added in H_2O (2.0 mL, exothermic). Once the solution had cooled to room temperature, NaClO_2 (0.731 g, 8.08 mmol) was added dropwise over 5 min in H_2O (2.0 mL). The resulting yellow solution was stirred under an inert atmosphere for 4 h (58). To isolate the product, the reaction mixture was poured into ice-cold HCl (10%), extracted 4x with hexane, and dried with MgSO_4 . After rotary evaporation of the organic phase, the yellow residue was purified by silica gel column chromatography (hexane-EtOAc gradient with 0.1% acetic acid, 0-5% EtOAc) to elute the yellow oil **81** (0.405 g, 87% yield). ^1H NMR (500 MHz, CDCl_3) δ 5.28 (m, 2H), 2.28 (t, J = 7.0 Hz, 2H), 1.94 (q, J = 7.0 Hz, 4H), 1.58 (qn, J = 7.0 Hz, 2H) 1.24 (s, 16H); ^{13}C NMR (125 MHz, CDCl_3) δ 178.30, 128.93, 128.82, 32.91, 28.73, 28.68, 28.45, 28.38, 28.24, 28.21, 28.04, 27.73, 26.21, 26.17, 23.66; IR (neat film) ν_{max} 3005, 2924, 2854, 2675, 2215, 1713, 1458, 1442, 1288, 1237, 937, 722 cm^{-1} ; HRMS (ESI $^-$) m/z $[\text{M}-\text{H}^+]$ calcd $\text{C}_{18}\text{H}_{26}\text{D}_7\text{O}_2$ 288.2925, found 288.2928.

5.4. Synthesis of ^2H -labeled fatty acid stereoisomers

This discussion pertains to the generation of two specialized fatty acid isomers with deuterium substitutions at the 17 and 18 position carbons: $18:2^{9c,15c}$ and $18:2^{9c,15t}$. The production of these compounds built upon the synthetic scheme created to produce the FA standards that were used to develop the FA

profile of *D. discoideum*. These compounds were produced through a collaboration effort with Dr. Robert Minto in the Department of Chemistry and Chemical Biology at IUPUI. His group transformed a $\Delta 12$ desaturase found in *Phanerochaete chrysosporium* into *S. cerevisiae* for the purpose of determining the catalytic potential of the enzyme. These two compounds were used to elucidate the enzyme's specificity for the *cis* or *trans* substrate (at carbon 15). While this synthetic strategy did not directly impact the research discussed in this manuscript, it does however provide the opportunity to discuss a unique and effective method of making *cis/trans* fatty acids, and it was this approach that inspired the synthetic scheme for making the deuterium labeled FAs used during *in vivo* studies of *D. discoideum*.

This synthesis began as previously discussed, with the preparation of a dioxolane-protected alkyl halide designed to be the electrophile for *n*-butyllithium assisted coupling to a diacetylene. This diacetylene **41** was then taken in two paths to afford the two isomers: the first, more straightforward pathway was that of producing 18:2^{9c,15c}. This was first illustrated in the step to make Compound **43**, whereas a second *n*-BuLi reaction used ethyl bromide-*d*₅ as the alkyl halide, inserting five deuterium to assemble the 18-carbon chain. Upon purification, **43** was equipped for metal-catalyzed hydrogenation with Lindlar's Catalyst, followed by deprotection and oxidation under the conditions discussed in Sections 5.2. and 5.3., to afford the *dicis* carboxylic acid 18:2^{9,15}. Its stereochemical counterpart, 18:2^{9c,15t}, was not so easily obtained.

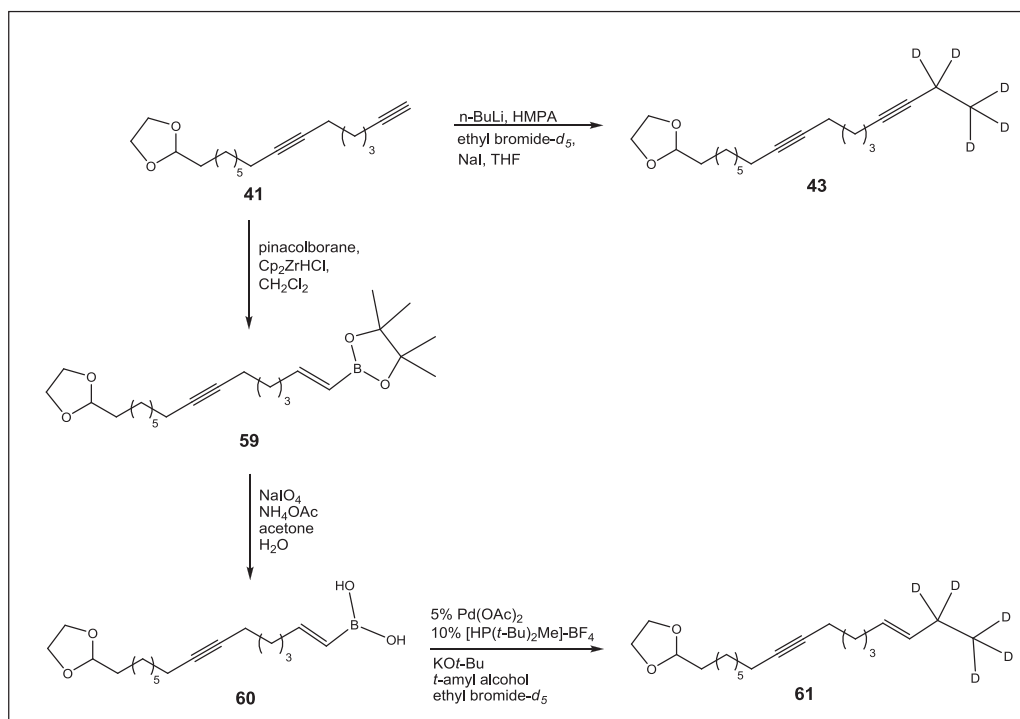


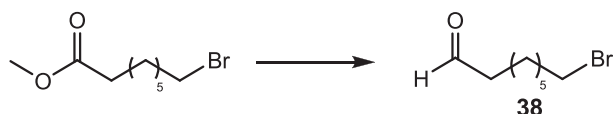
Figure 77. The abbreviated synthesis of 18:2^{9c,15c} and 18:2^{9c,15t}.

The strategy to generate a *trans* double bond at the 15 position was achieved via the hydroboration of **41**. Pereira and Srebni⁴² showed that a terminal alkyne such as this could be hydroborated with pinacolborane in the presence of a catalytic amount of zirconocene chloride hydride (HZrCp₂Cl), also known as Schwartz' Reagent (93). This chemistry allowed for the formation of the boronic ester **59**, as the desired (*E*)-alkene. The rationale in using such a reaction to attain the necessary stereochemistry was that the resulting organoborane would be a prime candidate for a Suzuki-style reaction with bromoethane-*d*₅ to complete the alkyl chain.

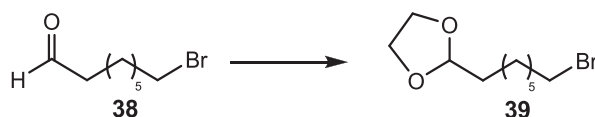
While the traditional palladium-catalyzed Suzuki Coupling was first published as a cross coupling between organoboronic acid and aryl halides, the number of catalysts and reaction partners has since increased tremendously. Once such iteration of the reaction was defined by Gregory Fu *et al.* (94), which detailed the coupling of alkyl bromides to boronic acids at room temperature.

They developed the trialkylphosphine catalyst $[\text{HP}(t\text{-Bu})_2\text{Me}]\text{BF}_4$, which successfully activates Pd(0) for oxidative addition with alkyl halides. Upon refluxing the boronic ester in sodium periodate and ammonium acetate to generate the boronic acid necessary for this coupling (95), the anticipated product **61** was obtained in greater than 90% yield. The remaining internal acetylene was reduced with Lindlar's Catalyst, and the dioxolane was deprotected, then oxidized as discussed previously to afford the $18:2^{9c,15t}$ d_5 -labeled fatty acid (**64**).

Synthesis and spectral data

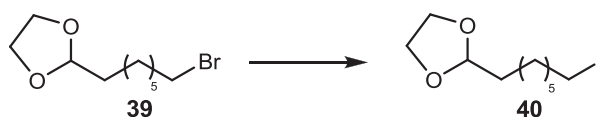


8-Bromooctanal (38). Methyl 8-bromooctanoate (5.000 g, 21.1 mmol) was dissolved in DCM (38 mL) and cooled to $-78\text{ }^\circ\text{C}$ under argon, to which diisobutylaluminum hydride (21.1 mL, 1.0 M solution in hexanes, 21.1 mmol) was added by syringe pump at 1 mL/min. A slow rate of addition is required to reproduce the reported yield. The clear solution stirred at $-78\text{ }^\circ\text{C}$ for 1 h, then allowed to warm to $-60\text{ }^\circ\text{C}$ for 1 h. HCl (20 mL, 10%) was added at $0\text{ }^\circ\text{C}$ and gray precipitate swiftly formed. After 1 h stirring, the product was extracted 3x with DCM, and organic extracts were washed with water and brine, then dried with MgSO_4 . Evaporation under reduced pressure resulted in product **38** as a light yellow oil (4.225 g, 97%). The aldehyde, whose NMR was consistent with literature data (54), was used in the preparation of **39** without further purification.

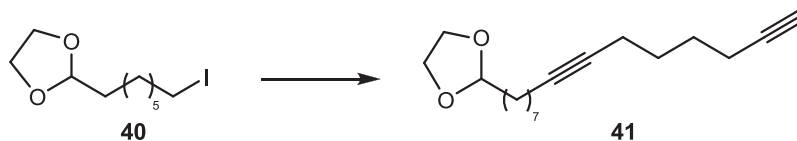


2-(7-Bromoheptyl)-1,3-dioxolane (39). In a round-bottom flask, the crude residue of **38** (4.225 g, 20.4 mmol) was resuspended with stirring in benzene (80 mL), and ethylene glycol (10.6 mL, 153.0 mmol) and para-toluenesulfonic acid

(0.155 g, 0.82 mmol) were added under argon. After attaching a Dean-Stark apparatus filled with 3Å molecular sieves to the flask, the heterogeneous mixture was refluxed for 3 h. NaHCO₃ (1.35 g, 16.2 mmol) was introduced and the reaction mixture was stirred for 10 min prior to being washed 2x with sat. aq. NaHCO₃, and dried with MgSO₄. Concentration of the organic phase with a rotary evaporator yielded **39** as a light yellow oil (5.100 g, 100%). The dioxolane, whose NMR was consistent with literature data (54), was used in the preparation of **40** without further purification.

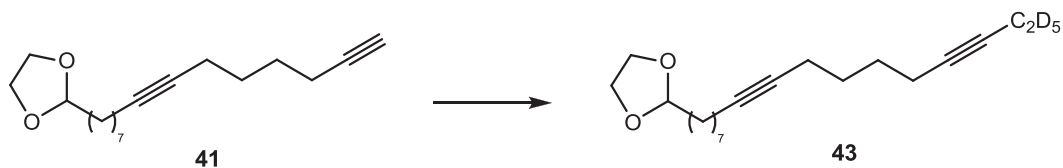


2-(2-Iodoethyl)-1,3-dioxolane (40). To a stirred solution of the crude bromide **39** (5.10 g, 20.3 mmol) in HPLC-grade acetone (21 mL) was added sodium iodide (3.81 g, 25.4 mmol). The solution was heated to reflux under an inert atmosphere for 3 h. The mixture was allowed to cool then deionized water (25 mL) was added and the reaction mixture was stirred for 10 min. After passing the acetone solution through a sintered glass funnel packed with Celite, the filtrate was extracted 3x with DCM and dried with MgSO₄. Upon concentration under reduced pressure yellow product **40** (5.703 g, 94%) was obtained, which was stabilized by storing over K₂CO₃. The iodide, whose NMR was consistent with literature data (92), was used in the preparation of acetylenic derivatives without further purification.



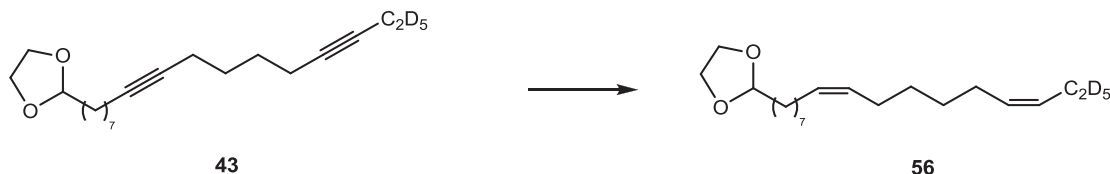
2-(Pentadeca-8,14-diyne-1-yl)-1,3-dioxolane (41). 1,8-Octadiyne (1.062 g, 10.0 mmol), HMPA (2.60 mL, 15.0 mmol) and dry THF (50 mL) were combined in a round-bottom flask that was then cooled to -78 °C in a dry-ice acetone bath. *n*-Butyllithium (4.84 mL, 2.48 M in hexanes, 12.0 mmol) was added dropwise over

10 min and the reaction mixture was stirred for 30 min at $-78\text{ }^{\circ}\text{C}$. The cooling bath was removed and **40** (1.997 g, 8.25 mmol) was added in THF (2 mL). The light yellow mixture was then refluxed for 18 h, producing a dark yellow solution. Sat. NH_4Cl ($\sim 75\text{ mL}$) was added to the round bottom flask and the mixture was stirred for 5 min and then extracted 3x with Et_2O , dried with MgSO_4 and the solvent evaporated with the use of a rotary evaporator. The yellow residue was separated by silica gel column chromatography (hexane-EtOAc gradient, 0-5% EtOAc) to afford alkyne **41** as a yellow oil (0.967 g 52.1% yield). ^1H NMR (500 MHz, CDCl_3) δ 4.88 (t, $J = 4.8\text{ Hz}$, 1H), 3.99 (m, 2H), 3.87 (m, 2H), 2.25 (m, 4H), 2.16 (m, 2H), 1.98 (t, $J = 2.7\text{ Hz}$, 1H), 1.70-1.58 (m, 6H) 1.49-1.34 (m, 10H); ^{13}C NMR (125 MHz, CDCl_3) δ 104.67, 84.30, 80.63, 79.53, 68.35, 64.83 (2C), 33.89, 29.44, 29.07, 29.05, 28.73, 28.05, 27.53, 24.04, 18.74, 18.30, 18.01; IR (neat film) ν_{max} 3291, 2932, 2858, 2117, 1461, 1434, 1410, 1140, 1037, 943 cm^{-1} ; HRMS (CI) m/z $[\text{M}+\text{H}^+]$ calcd $\text{C}_{18}\text{H}_{29}\text{O}_2$ 277.2162, found 277.2149.

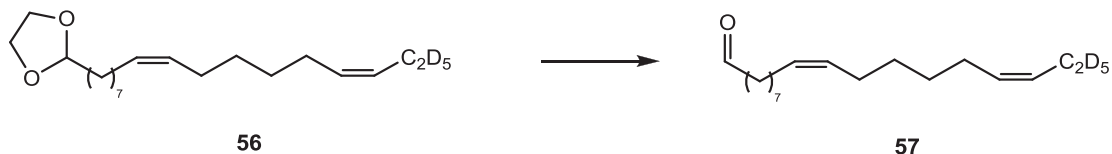


2-(Heptadeca-8,14-diyne-1-yl)-1,3-dioxolane- d_5 (43). Alkyne **41** (0.175 g, 0.633 mmol), HMPA (0.165 mL, 0.950 mmol) and dry THF (10 mL) were combined in a round-bottom flask and cooled to $-78\text{ }^{\circ}\text{C}$. *n*-Butyllithium (0.322 mL, 2.354 M in hexanes, 0.760 mmol) was added dropwise over 10 min and the solution was then stirred for 30 min at $-78\text{ }^{\circ}\text{C}$. The cold bath was removed and ethyl bromide- d_5 (0.056 mL, 0.760 mmol), and NaI (0.010 g, 0.063 mmol) were added. The light yellow mixture was then refluxed for 18 h, resulting in a dark yellow solution. The reaction was quenched with sat. NH_4Cl ($\sim 25\text{ mL}$) and allowed to stir for 5 min. The mixture was extracted 3x with Et_2O , dried with MgSO_4 and the solvent removed with the aid of a rotary evaporator. The yellow crude product was purified by silica gel column chromatography (hexane-EtOAc gradient, 0-5% EtOAc) to afford **43** as a yellow oil (0.170 g, 87% yield). ^1H NMR (500 MHz,

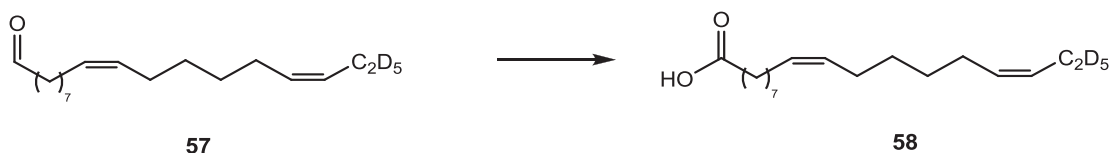
CDCl₃) δ 4.87 (t, J = 4.8 Hz, 1H), 3.99 (m, 2H), 3.87 (m, 2H), 2.19 (m, 6H), 1.67 (m, 2H), 1.60 (m, 4H), 1.42 (m, 10H); ¹³C NMR (125 MHz, CDCl₃) δ 104.69, 80.46 (2C), 79.80, 79.13, 64.84 (2C), 33.90, 29.44, 29.11 (2C), 29.06, 28.75, 28.26 (2C), 24.06, 18.74 (2C), 18.35, 18.31; IR (neat film) ν_{\max} 2932, 2858, 2231, 1457, 1140, 1037 cm⁻¹; HRMS (ESI⁺) m/z [M+H⁺] calcd C₂₀H₂₈D₅O₂ 310.2789, found 310.2790.



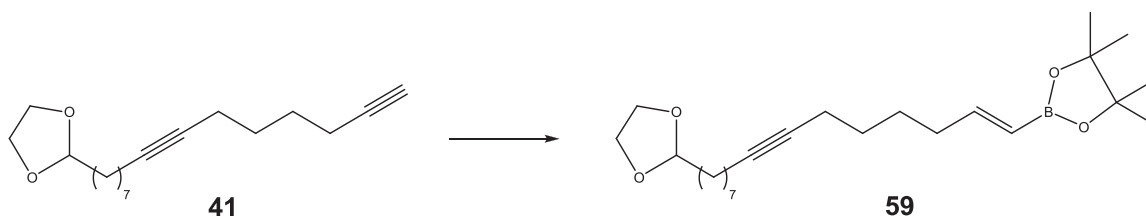
2-((8Z,14Z)-Heptadeca-8,14-dien-1-yl)-1,3-dioxolane-d₅ (56). A round bottom flask was charged with Pd on CaCO₃ (0.083 g, 0.777 mmol, 3.5% Pb, 5.0% Pd), quinoline (0.020 mL, 0.161 mmol), **43** (0.200 g, 0.646 mmol) and absolute ethanol (3.0 mL). The mixture was exposed to H₂ atmosphere provided by a balloon for 1 h, at which time GC analysis confirmed reduction of the acetylenes (**56**). The reaction mixture was passed through a sintered glass funnel packed with Celite to remove Pd, washed copiously with Et₂O, and concentrated under reduced pressure by a rotary evaporator. The residue was subjected to silica gel column chromatography (hexane-EtOAc gradient, 0-5% EtOAc) to remove quinoline, obtaining 0.200 g (99%) as a clear oil. ¹H NMR (500 MHz, CDCl₃) δ 5.37 (m, 4H), 4.88 (t, J = 4.8 Hz, 1H), 3.99 (m, 2H), 3.87 (m, 2H), 2.05 (m, 6H), 1.67 (m, 2H), 1.44-1.21 (m, 14H); ¹³C NMR (125 MHz, CDCl₃) δ 131.54, 130.04, 129.73, 129.25, 104.77, 64.89 (2C), 33.90, 29.76, 29.55, 29.46 (2C), 29.40, 29.35, 29.23 (2C), 27.20, 27.10, 26.99, 24.10; IR (neat film) ν_{\max} 2926, 2855, 1734, 1457, 1141 cm⁻¹; HRMS (CI) m/z [M+H⁺] calcd C₂₀H₃₂D₅O₂ 314.3102, found 314.3117.



(Z,Z)-Octadeca-9,15-dienal-*d*₅ (57). The dioxolane **56** (0.200 g, 0.646 mmol) was combined with pTsOH (0.019 g, 0.100 mmol), acetone (6.5 mL) and H₂O (1.0 mL) in a round-bottom flask equipped with a condenser, and heated to reflux (**57**). After reacting for 3 h, acetone was evaporated, pTsOH was quenched with sat. NaHCO₃, and the aldehyde product was extracted 3x with DCM and dried with MgSO₄. The crude mixture of **57** (0.162 g, 94% yield) was used in the next step without further preparation.

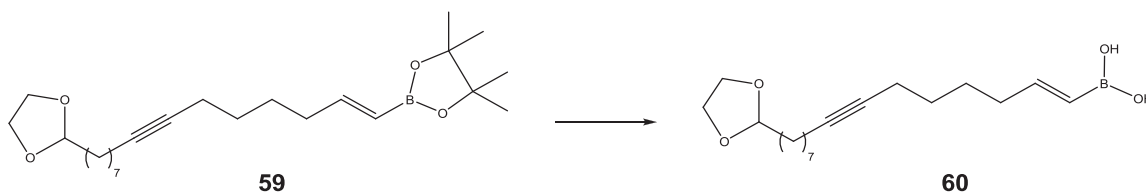


(Z,Z)-Octadeca-9,15-dienoic acid-*d*₅ (58). The aldehyde **57** (0.160 g, 0.592 mmol) and DMSO (3.5 mL) were combined in a round-bottom flask to which NaH₂PO₄ (0.163 g, 1.184 mmol) was slowly added in H₂O (2.5 mL, exothermic). Once the solution had cooled to room temperature, NaClO₂ (0.267 g, 2.960 mmol) was added dropwise over 5 min in H₂O (1.0 mL). The resulting yellow solution was stirred under an inert atmosphere for 4 h (**58**). To isolate the product, the reaction mixture was poured into ice-cold HCl (10%), extracted 4x with hexane, and dried with MgSO₄. After rotary evaporation of the organic phase, the yellow residue was purified by silica gel column chromatography (hexane-EtOAc gradient with 0.1% acetic acid, 0-5% EtOAc) to elute the clear oil **58** (0.145 g, 86% yield). ¹H NMR (500 MHz, CDCl₃) δ 5.37 (m, 4H), 2.38 (t, *J* = 7.5 Hz, 2H), 2.04 (m, 6H), 1.67 (quint, *J* = 7.5 Hz, 2H), 1.34 (m, 12H). ¹³C NMR (125 MHz, CDCl₃) δ 179.30, 131.53, 129.86, 129.83, 129.20, 33.90, 29.67, 29.39, 29.35, 29.25, 29.14, 29.07 (2C), 29.03, 27.17, 27.10, 26.98, 24.67. IR (neat film) ν_{\max} 3004, 2926, 2854, 2222, 1710 cm⁻¹; HRMS (ESI⁻) *m/z* [M-H⁺] calcd C₁₈H₂₆D₅O₂ 284.2643, found 284.2641.

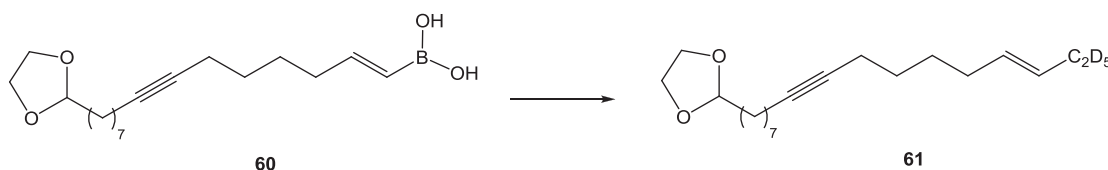


(E)-2-(15-(1,3-Dioxolan-2-yl)pentadec-1-en-7-yn-1-yl)-4,4,5,5-tetramethyl-1,3-dioxo-2-borolane (59). The diacetylene **41** (0.150 g, 0.540 mmol) and DCM (0.5 mL) were combined in a conical vial and cooled to 0 °C. Pinacolborane (0.084 mL, 0.600 mmol) was added dropwise and stirred for 1 min, then the mixture was transferred to a second vacuum purged conical vial at 0 °C containing Schwartz reagent (HZrCp₂Cl) (0.280 g, 0.108 mmol). The heterogeneous mixture was allowed to assume room temperature, at which time the catalyst dissolved to form a clear yellow solution, then was allowed to stir for 16 h. The mixture was transferred to H₂O (5 mL) and extracted 3x with DCM, dried with MgSO₄ and solvents were removed by rotary evaporation (93). The yellow residue was purified by silica gel column chromatography (hexane-EtOAc gradient, 0-4% EtOAc) affording a clear oil **59** (0.133 g, 60% yield). ¹H NMR (500 MHz, CDCl₃) δ 6.44 (dt, *J* = 6.4, 5.0 Hz, 1H), 5.47 (dt, *J* = 16.4, 1.5 Hz, 1H), 4.87 (t, *J* = 4.8 Hz, 1H), 3.99 (m, 2H), 3.869 (m, 2H), 2.17 (m, 6H), 1.68 (m, 2H), 1.52-1.35 (m, 17H), 1.29 (s, 9H); ¹³C NMR (125 MHz, CDCl₃) δ 154.28, 118.10*, 104.70, 83.00 (2C), 80.39, 79.89, 64.83 (2C), 35.27, 33.90, 29.44, 29.13, 29.06, 28.76, 28.61, 27.38, 24.78 (4C), 24.06, 18.74, 18.61; IR (neat film) ν_{\max} 3448, 2974, 2931, 2858, 1739, 1639, 1482, 1398, 1362, 1320, 1146, 971, 850 cm⁻¹; HRMS (ESI⁺) *m/z* [M+NH₄⁺] calcd C₂₄H₄₅BNO₄ 421.3472, found 421.3474.

*118.10 not discernible in ¹³C spectrum, located by HSQC.

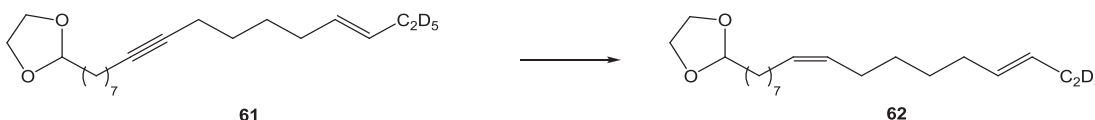


(E)-(15-(1,3-Dioxolan-2-yl)pentadec-1-en-7-yn-1-yl)boronic acid (60). The pinacolborane derivative **59** (0.250 g, 0.620 mmol), NaIO₄ (0.796 g, 3.720 mmol), NH₄OAc (0.287 g, 3.720 mmol), acetone (37 mL), and H₂O (18.5 mL) were combined in a round-bottom flask and warmed to 50 °C for 18 h (95). Subsequently, the acetone was removed by evaporation and the mixture was extracted 3x with Et₂O. Cold 1N HCl washes (3x) removed a set of alkene signals in ¹H NMR likely due to the acetate derivative of boronic acid prior to drying with MgSO₄ and removal of the solvent with a rotary evaporator. The crude product **60** was obtained as a yellow oil (0.195 g, 98% yield) and taken forward without further purification.

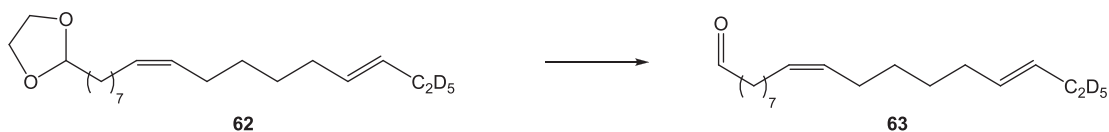


(E)-2-(Heptadec-14-en-8-yn-1-yl)-1,3-dioxolane-d₅ (61). The crude mixture **60** (0.095 g, 0.295 mmol) was combined with Pd(OAc)₂ (0.010 g, 0.045 mmol), [HP(*t*-Bu)₂-Me)-BF₄] (0.011 g, 0.045 mmol), and KO*t*-Bu (0.100 g, 0.885 mmol) in a conical vial and purged with three vacuum-argon cycles. *tert*-Amyl alcohol (0.5 mL) and ethyl bromide-*d*₅ (0.027 mL, 0.369 mmol) were added, and the heterogeneous mixture stirred at ambient temperature for 24 h. The brown reaction mixture was then passed through a sintered glass funnel containing a pad of silica gel, washed copiously with Et₂O, and the solvents were evaporated under reduced pressure (94). The product was isolated by silica gel column chromatography (hexane-EtOAc gradient, 0-5% EtOAc) as a clear oil **61** (0.084 g, 92% yield). ¹H NMR (500 MHz, CDCl₃) δ 5.44 (m, 4H), 4.87 (t, *J* = 4.8 Hz,

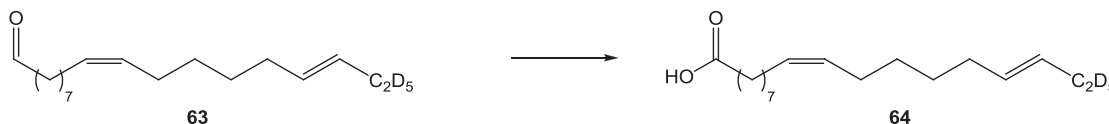
1H), 3.99 (m, 2H), 3.87 (m, 2H), 2.16 (dt, $J=2.2$ Hz, 4H), 2.00 (q, $J=6.7$ Hz, 2H), 1.68 (m, 2H), 1.51-1.35 (m, 12H); ^{13}C NMR (125 MHz, CDCl_3) δ 132.08, 128.99, 104.69, 80.24, 80.14, 64.83 (2C), 33.90, 32.06, 29.45, 29.13 (2C), 29.07 (2C), 28.81, 28.75, 28.64, 24.06, 18.74, 18.65; IR (neat film) ν_{max} 2999, 2925, 2854, 2222.5, 1736, 1462, 1258, 1127, 1020, 801 cm^{-1} ; HRMS (ESI $^+$) m/z $[\text{M}+\text{H}^+]$ calcd $\text{C}_{20}\text{H}_{30}\text{D}_5\text{O}_2$ 312.2945, found 312.2944.



2-((8Z,14E)-Heptadeca-8,14-dien-1-yl)-1,3-dioxolane- d_5 (62). A round-bottom flask was charged with Pd on CaCO_3 (0.068 g, 0.637 mmol, 3.5% Pb, 5.0% Pd), quinoline (0.016 mL, 0.133 mmol), **61** (0.165 g, 0.530 mmol) and absolute ethanol (3.5 mL). The mixture was stirred under 1 atm of H_2 provided by a balloon for 1 h, at which time GC analysis confirmed reduction of the acetylene (**56**). The reaction mixture was passed through a sintered-glass funnel packed with Celite to remove Pd, washed copiously with Et_2O , and concentrated under reduced pressure by a rotary evaporator. The residue was subjected to silica gel column chromatography (hexane-EtOAc gradient, 0-5% EtOAc) to remove the quinoline, affording **62** as a clear oil (0.150 g, 90% yield). ^1H NMR (500 MHz, CDCl_3) δ 5.42 (m, 4H), 4.87 (t, $J=4.8$ Hz, 1H), 3.99 (m, 2H), 3.87 (m, 2H), 2.04 (m, 6H), 1.67 (m, 2H), 1.46-1.31 (m, 14H); ^{13}C NMR (125 MHz, CDCl_3) δ 131.90, 129.94, 129.81, 129.27, 104.72, 64.84 (2C), 33.92, 32.46, 29.74, 29.54, 29.46 (2C), 29.26 (2C), 29.20 (2C), 27.20, 27.08, 24.10; IR (neat film) ν_{max} 3003, 2929, 2852, 1732, 1704, 1458, 1271, 1258, 1189, 1152, 1066 cm^{-1} ; HRMS (CI $^+$) m/z $[\text{M}+\text{H}^+]$ calcd $\text{C}_{20}\text{H}_{32}\text{D}_5\text{O}_2$ 314.3102, found 314.3095.



(9Z,15E)-Octadeca-9,15-dienal-17,17,18,18,18-*d*₅ (63). Dioxolane **62** (0.145 g, 0.463 mmol) was combined with *p*-TsOH (0.013 g, 0.069 mmol), acetone (5.0 mL), and H₂O (0.8 mL) in a round-bottom flask equipped with a condenser and the mixture was brought to reflux (57). After reacting for 3 h, the solvent was evaporated, *p*-TsOH was neutralized with sat. NaHCO₃, and the aldehyde product was extracted 3x with DCM. After drying with MgSO₄ and evaporation of the solvent under reduced pressure, the crude mixture containing **63** (0.120 g, 96% yield) was taken to the next step without further preparation.



(9Z,15E)-Octadeca-9,15-dienoic acid-17,17,18,18,18-*d*₅ (64). Aldehyde **63** (0.120 g, 0.445 mmol) and DMSO (3.0 mL) were combined in a round-bottom flask, to which NaH₂PO₄ (0.123 g, 0.890 mmol) was slowly added in H₂O (1.0 mL, exothermic). Once the mixture had returned to room temperature, a solution of NaClO₂ (0.201 g, 2.23 mmol) in H₂O (1.0 mL) was added dropwise over 5 min. The resulting yellow solution was stirred under an inert atmosphere for 4 h (58). To isolate the product, the reaction mixture was transferred into HCl (10%, cold) and extracted 4x with hexane, and dried with MgSO₄. After rotary evaporation of the organic phase, the yellow residue was purified by silica gel column chromatography (hexane-EtOAc gradient with 0.1% acetic acid, 0-5% EtOAc) to elute a clear oil **64** (0.105 g, 83% yield). ¹H NMR (500 MHz, CDCl₃) δ 10.35 (br, 1H), 5.39 (m, 4H), 2.38 (t, *J* = 7.5 Hz, 2H), 2.02 (m, 6H), 1.66 (quint, *J* = 7.5 Hz, 2H), 1.34 (m, 12H). ¹³C NMR (125 MHz, CDCl₃) δ 179.82, 131.91, 129.89, 129.83, 129.24, 34.06, 32.46, 29.68, 29.27, 29.25, 29.15, 29.08, 29.05, 29.00, 27.23, 27.17, 27.08, 24.70; IR (neat film) ν_{\max} 3006, 2926, 2855, 1712, 1462, 1413, 1285, 966, 910, 735 cm⁻¹; HRMS (ESI⁻) *m/z* [M-H⁺] calcd C₁₈H₂₆D₅O₂ 284.2643, found 284.2647.

REFERENCES

REFERENCES

1. Guan, X. L., and Wenk, M. R. (2006) Mass spectrometry-based profiling of phospholipids and sphingolipids in extracts from *Saccharomyces cerevisiae*, *Yeast* 23, 465-477.
2. Aerts, A. M., Francois, I. E. J. A., Bammens, L., Cammue, B. P. A., Smets, B., Winderickx, J., Accardo, S., De Vos, D. E., and Thevissen, K. (2006) Level of M(IP)₂C sphingolipid affects plant defensin sensitivity, oxidative stress resistance and chronological life-span in yeast, *FEBS Lett.* 580, 1903-1907.
3. Voet, D., and Voet, J. G. (2004) *Biochemistry*, 3rd ed., Wiley, Hoboken, New Jersey.
4. Pata, M. O., Hannun, Y. A., and Ng, C. K. (2010) Plant sphingolipids: decoding the enigma of the Sphinx, *New Phytol.* 185, 611-630.
5. Holthuis, J. C. M., Pomorski, T., Raggars, R. J., Sprong, H., and Van Meer, G. (2001) The organizing potential of sphingolipids in intracellular membrane transport, *Physiol. Rev.* 81, 1689-1723.
6. Futerman, A. H., and Hannun, Y. A. (2004) The complex life of simple sphingolipids, *EMBO Rep.* 5, 777-782.
7. Lahiri, S., and Futerman, A. H. (2007) The metabolism and function of sphingolipids and glycosphingolipids, *Cell. Mol. Life Sci.* 64, 2270-2284.
8. Kunst, L., and Samuels, L. (2009) Plant cuticles shine: advances in wax biosynthesis and export, *Curr. Opin. Plant Biol.* 12, 721-727.
9. Gunstone, F. D., Harwood, J. L., and Dijkstra, A. J. (2007) *The Lipid Handbook*, 3 ed., CRC Press, London, England.

10. Blacklock, B. J., Kelley, D., and Patel, S. (2008) A fatty acid elongase ELO with novel activity from *Dictyostelium discoideum*, *Biochem. Biophys. Res. Co.* 374, 226-230.
11. Parent, C. A., and Devreotes, P. N. (1996) Molecular genetics of signal transduction in *Dictyostelium*, *Annu. Rev. Biochem.* 65, 411-440.
12. Escalante, R., and Vicente, J. J. (2000) *Dictyostelium discoideum*: a model system for differentiation and patterning, *Int. J. Dev. Biol.* 44, 819-835.
13. Eichinger, L., Pachebat, J. A., Glockner, G., Rajandream, M. A., Sucgang, R., Berriman, M., and Song, J. (2005) The genome of the social amoeba *Dictyostelium discoideum*., *Nature* 435, 43-57.
14. Insall, R. (2005) The *Dictyostelium* genome: the private life of a social model revealed?, *Genome Biol.* 6, 222.
15. Gross, J. D. (1994) Developmental decisions in *Dictyostelium discoideum*, *Microbiol. Rev.* 58, 330-351.
16. Alexander, S., Min, J., and Alexander, H. (2006) *Dictyostelium discoideum* to human cells: pharmacogenetic studies demonstrate a role for sphingolipids in chemoresistance, *Biochim. Biophys. Acta.* 1760, 301-309.
17. Li, G., Foote, C., Alexander, S., and Alexander, H. (2001) Sphingosine-1-phosphate lyase has a central role in the development of *Dictyostelium discoideum*, *Development* 128, 3473-3483.
18. Min, J., Stegner, A. L., Alexander, H., and Alexander, S. (2004) Overexpression of sphingosine-1-phosphate lyase or inhibition of sphingosine kinase in *Dictyostelium discoideum* results in a selective increase in sensitivity to platinum-based chemotherapy drugs, *Eukaryot. Cell.* 3, 795-805.

19. Kumar, A., Wessels, D., Daniels, K. J., Alexander, H., Alexander, S., and Soll, D. R. (2004) Sphingosine-1-phosphate plays a role in the suppression of lateral pseudopod formation during *Dictyostelium discoideum* cell migration and chemotaxis, *Cell Motil. Cytoskel.* 59, 227-241.
20. Van Driessche, N., Alexander, H., Min, J., Kuspa, A., Alexander, S., and Shaulsky, G. (2007) Global transcriptional responses to cisplatin in *Dictyostelium discoideum* identify potential drug targets, *Proc. Natl. Acad. Sci. U.S.A.* 104, 15406-15411.
21. Draelos, Z. D. (2008) The effect of ceramide-containing skin care products on eczema resolution duration, *Cutis* 81, 87-91.
22. Zheng, W., Kollmeyer, J., Symolon, H., Momin, A., Munter, E., Wang, E., Kelly, S., Allegood, J. C., Liu, Y., Peng, Q., Ramaraju, H., Sullards, M. C., Cabot, M., and Merrill, A. H., Jr. (2006) Ceramides and other bioactive sphingolipid backbones in health and disease: lipidomic analysis, metabolism and roles in membrane structure, dynamics, signaling and autophagy, *Biochim. Biophys. Acta.* 1758, 1864-1884.
23. Ohlrogge, J. B., and Jaworski, J. G. (1997) Regulation of fatty acid synthesis, *Annu. Rev. Plant Physiol. Plant Mol. Biol.* 48, 109-136.
24. Jump, D. B. (2009) Mammalian fatty acid elongases, *Methods Mol. Biol.* 579, 375-389.
25. Cinti, D. L., Cook, L., Nagi, M. N., and Suneja, S. K. (1992) The fatty acid chain elongation system of mammalian endoplasmic reticulum, *Prog. Lipid Res.* 31, 1-51.
26. Mansilla, M. C., Banchio, C., and Mendoza, D. (2008) Signaling pathways controlling fatty acid desaturation, *Lipids Health Dis.*, 71-99.
27. Shah, J., Atienza, J. M., Rawhgs, A. V., and Shipley, G. G. (1995) Physical properties of ceramides: effect of fatty acid hydroxylation, *J. Lipid Res.* 36, 1945-1955.

28. Hama, H. (2010) Fatty acid 2-hydroxylation in mammalian sphingolipid biology, *Biochim. Biophys. Acta.* 1801, 405-414.
29. Eckhardt, M., Yaghoofam, A., Fewou, S. N., Zoller, I., and Gieselmann, V. (2005) A mammalian fatty acid hydroxylase responsible for the formation of α -hydroxylated galactosylceramide in myelin, *Biochem. J.* 388, 245-254.
30. Broadwater, J. A., Whittle, E., and Shanklin, J. (2002) Desaturation and hydroxylation: residues 148 and 324 of Arabidopsis fad2, in addition to substrate chain length, exert a major influence in partitioning of catalytic specificity, *J. Biol. Chem.* 277, 15613-15620.
31. Broun, P. (1998) Catalytic plasticity of fatty acid modification enzymes underlying chemical diversity of plant lipids, *Science* 282, 1315-1317.
32. Bielawski, J., Szulc, Z. M., Hannun, Y. A., and Bielawska, A. (2006) Simultaneous quantitative analysis of bioactive sphingolipids by high-performance liquid chromatography-tandem mass spectrometry, *Methods* 39, 82-91.
33. Murphy, A. S. (2011) *The Plant Plasma Membrane*, Vol. 19, Springer, New York, New York.
34. Fyrst, H., Zhang, X., Herr, D. R., Byun, H. S., Bittman, R., Phan, V. H., Harris, G. L., and Saba, J. D. (2008) Identification and characterization by electrospray mass spectrometry of endogenous *Drosophila* sphingadienes, *J. Lipid Res.* 49, 597-606.
35. Pruetz, S. T., Bushnev, A., Hagedorn, K., Adiga, M., Haynes, C. A., Sullards, M. C., Liotta, D. C., and Merrill, A. H., Jr. (2008) Biodiversity of sphingoid bases ("sphingosines") and related amino alcohols, *J. Lipid Res.* 49, 1621-1639.
36. Sonnino, S., and Chigorno, V. (2000) Ganglioside molecular species containing C18- and C20-sphingosine in mammalian nervous tissues and neuronal cell cultures, *Biochim. Biophys. Acta.* 1469, 63-77.
37. Keranen, A. (1976) Fatty acids and long-chain bases of gangliosides of human gastrointestinal mucosa, *Chem. Phys. Lipids* 17, 14-21.

38. Lynch, D. V., Chen, M., and Cahoon, E. B. (2009) Lipid signaling in Arabidopsis: no sphingosine? No problem!, *Trends Plant Sci.* 14, 463-466.
39. Cheng, J., Park, T. S., Chio, L. C., Fischl, A. S., and Ye, X. S. (2003) Induction of apoptosis by sphingoid long-chain bases in *Aspergillus nidulans*, *Mol. Cell. Biol.* 23, 163-177.
40. Arana, L., Gangoiti, P., Ouro, A., Trueba, M., and Gomez-Munoz, A. (2010) Ceramide and ceramide 1-phosphate in health and disease, *Lipids Health Dis.* 9, 15.
41. Boath, A., Graf, C., Lidome, E., Ullrich, T., Nussbaumer, P., and Bornancin, F. (2008) Regulation and traffic of ceramide 1-phosphate produced by ceramide kinase: comparative analysis to glucosylceramide and sphingomyelin, *J. Biol. Chem.* 283, 8517-8526.
42. Nitiss, J. L., and Heitman, J. (2007) *Yeast as a tool in cancer research*, Springer, New York, New York.
43. Sugiura, M., Kono, K., Liu, H., Shimizugawa, T., and Minekura, H. (2002) Ceramide kinase, a novel lipid kinase, *J. Biol. Chem.* 277, 23294-23300.
44. Liang, H., Yao, N., Song, J. T., Luo, S., Lu, H., and Greenberg, J. T. (2003) Ceramides modulate programmed cell death in plants, *Genes Dev.* 17, 2636-2641.
45. Chalfant, C. E., and Spiegel, S. (2005) Sphingosine 1-phosphate and ceramide 1-phosphate: expanding roles in cell signaling, *J. Cell Sci.* 118, 4605-4612.
46. Lester, R. L., and Dickson, R. C. (1993) Sphingolipids with inositolphosphate-containing head groups, *Adv. Lipid Res.* 26, 253-274.
47. Lynch, D. V., and Dunn, T. M. (2004) An introduction to plant sphingolipids and a review of recent advances in understanding their metabolism and function, *New Phytol.* 161, 677-702.
48. Lester, R. L., and Dickson, R. C. (1999) Yeast sphingolipids, *Biochim. Biophys. Acta.* 1426, 347-357.

49. Ternes, P., Wobbe, T., Schwarz, M., Albrecht, S., Feussner, K., Riezman, I., Cregg, J. M., Heinz, E., Riezman, H., Feussner, I., and Warnecke, D. (2011) Two pathways of sphingolipid biosynthesis are separated in the yeast *Pichia pastoris*, *J. Biol. Chem.* *286*, 11401-11414.
50. Shaner, R. L., Allegood, J. C., Park, H., Wang, E., Kelly, S., Haynes, C. A., Sullards, M. C., and Merrill, A. H., Jr. (2009) Quantitative analysis of sphingolipids for lipidomics using triple quadrupole and quadrupole linear ion trap mass spectrometers, *J. Lipid Res.* *50*, 1692-1707.
51. Christie, W. W. (2003) *Lipid Analysis: isolation, identification and structural analysis*, 3rd ed., The Oily Press, Bridgewater, UK.
52. Brian, B. L., and Gardner, E. W. (1967) Preparation of bacterial fatty acid methyl esters for rapid characterization by gas-liquid chromatography, *App. Micro.* *15*, 1499-1500.
53. Saito, T., Morio, T., and Ochiai, H. (2000) A second functional delta 5 fatty acid desaturase in the cellular slime mould *Dictyostelium discoideum*, *Eur. J. Biochem.* *267*, 1813-1818.
54. Varseev, G. N., and Maier, M. E. A. (2005) Novel palladium-catalyzed arylation-dehydroaromatization reaction: synthesis of 7-aryltetralones, *Org. Lett.* *18*, 3881-3884.
55. Baughman, T. W., Sworen, J. C., and Wagener, K. B. (2004) The facile preparation of alkenyl metathesis synthons, *Tetrahedron* *60*, 10943-10948.
56. Lindlar, H., and Dubuis, R. (1973) Palladium catalyst for partial reduction of acetylenes, *Org. Synth.* *5*, 880.
57. Greene, T. W., and Wuts, P. G. M. (1991) *Protective Groups in Organic Synthesis*, 2 ed., Wiley, Hoboken, New Jersey.
58. Fang, X., Bandarage, U. K., Wang, T., Schroeder, J. D., and Garvey, D. S. (2003) First examples of oxidizing aldehydes to carboxylic acids in the presence of a tertiary disulfide functional group: synthesis of novel diacid-disulfides, *Synlett.* *4*, 489-492.

59. Woollard, P. M. (1983) Selective silylation using tert-butyldimethylsilyl reagents: Their use in the quantification of fatty acids, *Biol. Mass Spec.* 10, 143-154.
60. Vermeer, C. P., Nastold, P., and Jetter, R. (2003) Homologous very-long-chain 1,3-alkanediols and 3-hydroxyaldehydes in leaf cuticular waxes of *Ricinus communis* L., *Phytochem.* 62, 433-438.
61. Snyder, F., Lee, T., and Wykle, R. L. (2002) Ether-linked lipids and their bioactive species, In *Biochemistry of Lipids, Lipoproteins and Membranes* (Vance, D. E., and Vance, J. E., Eds.) 4th ed., Amsterdam, The Netherlands.
62. Napier, J. A., Michaelson, L. V., and Stobart, A. K. (1999) Plant desaturases: harvesting the fat of the land., *Curr. Opin. Plant Biol.* 2, 123-127.
63. Cook, H. W., and McMaster, C. R. (2002) *Biochemistry of Lipids, Lipoproteins and Membrane*, Vol. 4, Elsevier, Edmonton, Alberta.
64. Saito, T., and Ochiai, H. (1999) Identification of delta 5-fatty acid desaturase from the cellular slime mold Dictyostelium discoideum, *Eur. J. Biochem.* 265, 809-814.
65. Grotenhuis, A., and Blacklock, B. J. Unpublished results.
66. Bragina, N. A., and Chupin, V. V. (1997) Methods of synthesis of deuterium-labelled lipids, *Russian Chem. Rev.* 66, 975-986.
67. Henry, P. M. (1980) *Palladium catalyzed oxidation of hydrocarbons*, D. Reidel Publishing Company, Dordrecht, Holland.
68. Rakoff, H., and Rohwedder, W. K. (1992) Catalytic deuteration of alkynols and their tetrahydropyranyl ethers, *Lipids* 27, 567-569.
69. Dess, D. B., and Martin, J. C. (1983) Readily accessible 12-I-5 oxidant for the conversion of primary and secondary alcohols to aldehydes and ketones, *J. Org. Chem.* 48, 4155-4156.

70. BRENDA, The Comprehensive Enzyme Information System, Berlin Institute of Technology. <http://www.brenda-enzymes.org>. Accessed Aug. 30, 2011.
71. Saito, T., Kato, A., Ochiai, H., and Morita, N. (2005) Temperature adaptation in *Dictyostelium*: role of delta5 fatty acid desaturase, *Microbiol. 151*, 113-119.
72. Ntambi, J. M. (1999) Regulation of stearoyl-CoA desaturase by polyunsaturated fatty acids and cholesterol, *J. Lipid Res. 40*, 1549-1558.
73. Jeffcoat, R., Brawn, P. R., Safford, R., and James, A. T. (1977) Properties of rat liver microsomal stearoyl-Coenzyme A desaturase, *Biochemistry 161*, 431-437.
74. Mahfouz, M. M., Valicenti, A. J., and Holman, R. T. (1980) Desaturation of isomeric trans-octadecenoic acids by rat liver microsomes, *Biochim. Biophys. Acta. 618*, 1-12.
75. Markham, J. E., Li, J., Cahoon, E. B., and Jaworski, J. G. (2006) Separation and identification of major plant sphingolipid classes from leaves, *J. Biol. Chem. 281*, 22684-22694.
76. Sun, D., Froman, B. E., Orth, R. G., MacIsaac, S. A., Larosa, T., Dong, F., and Valentin, H. E. (2009) Identification of plant sphingolipid desaturases using chromatography and mass spectrometry, *J. Chrom. Sci. 47*, 895-901.
77. Michaelson, L. V., Zauner, S., Markham, J. E., Haslam, R. P., Desikan, R., Mugford, S., Albrecht, S., Warnecke, D., Sperling, P., Heinz, E., and Napier, J. A. (2009) Functional characterization of a higher plant sphingolipid delta4-desaturase: defining the role of sphingosine and sphingosine-1-phosphate in *Arabidopsis*, *Plant Physiol. 149*, 487-498.

78. Markham, J. E., and Jaworski, J. G. (2007) Rapid measurement of sphingolipids from *Arabidopsis thaliana* by reversed-phase high-performance liquid chromatography coupled to electrospray ionization tandem mass spectrometry, *Rapid Commun. Mass Spectrom.* 21, 1304-1314.
79. Hsu, F., and Turk, J. (2001) Structural determination of glycosphingolipids as lithiated adducts by electrospray ionization mass spectrometry using low-energy collisional-activated dissociation in a triple stage quadrupole instrument, *J. Am. Soc. Mass Spectr.* 12, 61-79.
80. Lieser, B., Liebisch, G., Drobnik, W., and Schmitz, G. (2003) Quantification of sphingosine and sphinganine from crude lipid extracts by HPLC electrospray ionization tandem mass spectrometry, *J. Lipid Res.* 44, 2209-2216.
81. Curso, S., Stunff, H., Lynch, D. V., Gilroy, S., Assmann, S. M., and Spiegel, S. (2005) *Arabidopsis* sphingosine kinase and the effects of phytosphingosine-1-phosphate on stomatal aperture, *Plant Physiol.* 137, 724-737.
82. Cowart, L. A., Shotwell, M., Worley, M. L., Richards, A. J., Montefusco, D. J., Hannun, Y. A., and Xinghua Lu, X. (2010) Revealing a signaling role of phytosphingosine-1-phosphate in yeast, *Mol. Syst. Biol.* 6, 1-9.
83. Nagiec, M. M., Skrzypek, M., Nagiec, E. E., Lester, R. L., and Dickson, R. C. (1998) The LCB4 (YOR171c) and LCB5 (YLR260w) genes of *Saccharomyces* encode sphingoid long chain base kinases, *J. Biol. Chem.* 273, 19437-19442.
84. Min, J., Traynor, D., Stegner, A. L., Zhang, L., Hanigan, M. H., Alexander, H., and Alexander, S. (2005) Sphingosine kinase regulates the sensitivity of *Dictyostelium discoideum* cells to the anticancer drug cisplatin, *Eukaryot. Cell* 4, 178-189.
85. Brokerhoff, H. (1963) Breakdown of phospholipids in mild alkaline hydrolysis, *J. Lipid Res.* 4, 96-99.

86. Clarke, N. G., and Dawson, R. M. C. (1981) Alkaline O leads to N-transacylation. A new method for the quantitative deacylation of phospholipids, *Biochem. J.*, 301-306.
87. Schneider, R., Brugger, B., Sandhoff, R., Zellnig, G., Leber, A., Lampl, M., Athenstaedt, K., Hrstnik, C., Eder, S., Daum, G., Paltauf, F., Wieland, F. T., and Kohlwein, S. D. (1999) Electrospray ionization tandem mass spectrometry (ESI-MS/MS) analysis of the lipid molecular species composition of yeast subcellular membranes reveals acyl chain-based sorting/remodeling of distinct molecular species en route to the plasma membrane, *J. Cell. Biol.* 146, 741-754.
88. Hechtberger, P., Zinser, E., Saf, R., Hummel, K., Paltauf, F., and Daum, G. (1994) Characterization, quantification and subcellular localization of inositol-containing sphingolipids of the yeast, *Saccharomyces cerevisiae*, *Eur. J. Biochem.* 225, 641-649.
89. Hsu, F., Turk, J., Zhang, K., and Beverley, S. M. (2007) Characterization of inositol phosphorylceramides from *Leishmania major* by tandem mass spectrometry with ESI, *J. Am. Soc. Mass Spectr.* 18, 1591-1604.
90. Olling, A., Breimer, M. E., Peltomaa, E., and Samuelsson, B. E. (1998) Electrospray ionization and collision-induced-dissociation time-of-flight mass spectrometry of neutral glycosphingolipids, *Rapid Commun. Mass Sp.* 12, 637-645.
91. Hsu, F., Turk, J., and Stewart, M. E. (2002) Structural studies on ceramides as lithiated adducts by low energy collisional-activated dissociation tandem mass spectrometry with electrospray ionization, *J. Am. Soc. Mass Spectr.* 13, 680-695.
92. Enders, D., Nolte, B., Raabe, G., and Runsink, J. (2002) Asymmetric synthesis and structural assignment of (-)- α -conhydrine, *Asymmetry* 13, 285-291.
93. Pereira, S., and Srebnik, M. (1995) Hydroboration of alkynes with pinacolborane catalyzed by HZrCp₂Cl, *Organometallics* 14, 3127-3128.

94. Kirchoff, J. H., Netherton, M. R., Hills, I. D., and Fu, G. C. (2002) Boronic acids: new coupling partners in room-temperature Suzuki reactions of alkyl bromides. characterization of an oxidative-addition adduct generated under remarkably mild conditions, *JACS* 124, 13662-13663.
95. Itoh, T., Hirai, K., and Tomioka, H. (2004) Preparation of oligodiazo compounds by using the Suzuki coupling reaction and characterization of their photoproducts, *JACS* 126, 1130-1140.

APPENDIX

APPENDIX

HL5 media: 1.0 L volume.

Prepared the following solutions, autoclaved at 15 psi for 20 min and combined:

- Solution 1: dextrose (14.0 g) in 333 mL of nanopure H₂O
- Solution 2: BD Bacto yeast extract (7.0 g) and Oxoid bacteriological peptone (14.0 g) in 333 mL of nanopure H₂O
- Solution 3: buffer-NaH₂PO₄ (0.520 g) and KH₂PO₄ (0.520 g) in 333 mL of nanopure H₂O, adjusted to pH 6.5 with 1.0 N HCl

Penicillin/streptomycin (pen/strep) antibiotics

Dissolved penicillin-G potassium (0.300 g) and streptomycin sulfate (0.500 g) in 50 mL of nanopure H₂O and sterile filtered (25 mm/0.2 µm) into a sterile 50-mL BD Falcon tube.

YPD media: 500 mL volume.

Dissolved the following components in 500 mL nanopure H₂O and autoclaved at 15 psi for 20 min:

- Dextrose: 10.0 g
- BD Bacto yeast extract: 5.0 g
- Oxoid bacteriological peptone: 10.0 g